Sulfidogenesis at low pH and its application for treatment of metalliferous wastewaters

Charlotte M. van der Graaf

Propositions

1. "Strength in numbers" does not hold for polysulfides at acidic pH.
   (this thesis)

2. Elemental sulfur precedes sulfate reduction in the establishment of biosulfidogenesis in acid mine drainage.
   (this thesis)

3. The sum is greater than its parts when it comes to interdisciplinary scientific research.

4. In science, the excessive emphasis on output stifles exploration and discovery.

5. Societal mistrust of mining jeopardizes the energy transition.

6. Daily-news outlets entertain under the guise of informing.

Propositions belonging to the thesis, entitled

Sulfidogenesis at low pH and its application for treatment of metalliferous wastewaters

Charlotte M. van der Graaf
Wageningen, 5 July 2022

Sulfidogenesis at low pH and its application for treatment of metalliferous wastewaters

Charlotte M. van der Graaf

Thesis committee

Promotor
Prof. Dr A.J.M. Stams
Emeritus Professor, Laboratory of Microbiology
Wageningen University & Research

Co-promotors
Dr I. Sánchez-Andrea
Assistant Professor, Laboratory of Microbiology
Wageningen University & Research

Dr J. Sánchez-España
Senior Scientist and Director, Department of Geological Resources
National Center Institute of Geology and Mining, Spanish Research Council
(CN IGME-CSIC), Madrid, Spain

Other members
Prof. R. Amils, Universidad Autónoma de Madrid, Spain
Prof. R. Boom, Wageningen University & Research
Dr H. King, Utrecht University, The Netherlands
Dr S. Hedrich, TU Bergakademie Freiberg, Germany

This research was conducted under the auspices of the Graduate School
for Socio-Economic and Natural Sciences of the Environment (SENSE).

Sulfidogenesis at low pH and its application for treatment of metalliferous wastewaters

Charlotte M. van der Graaf

Thesis
submitted in fulfilment of the requirements for the degree of doctor
at Wageningen University
by the authority of the Rector Magnificus
Prof. Dr A.P.J. Mol,
in presence of the
Thesis Committee appointed by the Academic Board
to be defended in public

on Tuesday 5 July 2022
at 11 a.m. in the Omnia Auditorium

Charlotte M. van der Graaf
Sulfidogenesis at low pH and its application for treatment of metalliferous wastewaters
250 pages.

PhD thesis, Wageningen University, Wageningen, The Netherlands (2022)
With references, with summaries in English and Dutch.

ISBN: 9978-94-6447-157-1
DOI: https://doi.org/10.18174/567077

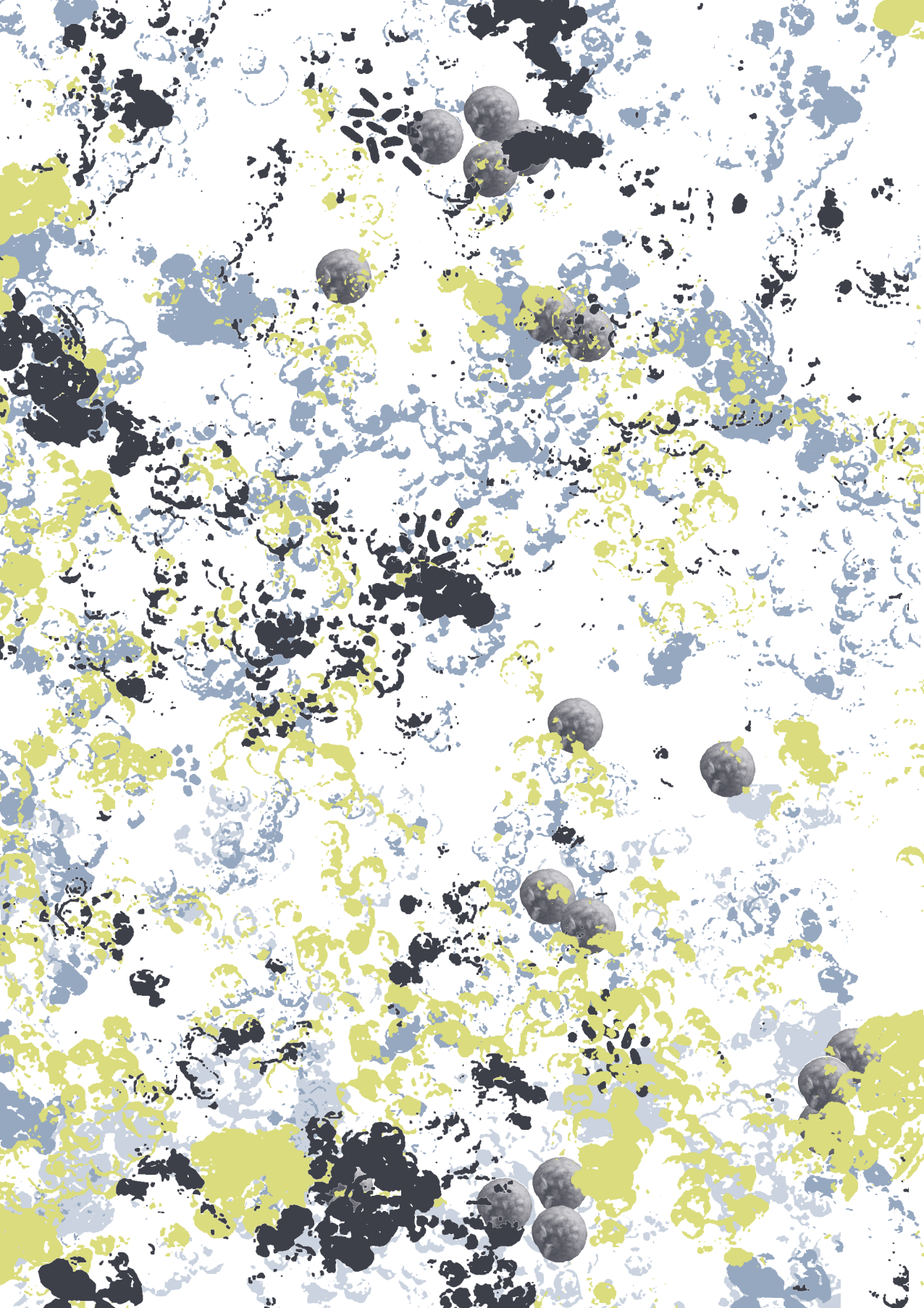

Table of contents

General Introduction and Thesis outline

The sulfur cycle – a geological and microbiological perspective

Sulfur plays an important role in both biological and geological processes (Canfield and Raiswell, 1999; Canfield and Farquhar, 2012). It exists in a range of oxidation states between +6 and -2 (Steudel, 2020b), of which sulfate (SO_4^{2-}, +6), elemental sulfur (S_8^0, 0) and sulfide (H_2S, -2), are probably best known. From a geological perspective, sulfur cycles between the Earth's mantle, crust, and surface environments, and the fluxes between these reservoirs have changed strongly over geologic time (Canfield, 2004). The main routes for transport of sulfur from the mantle, where it accounts for approximately 6 % of elements (McDonough and Sun, 1995), to surface environments is through volcanic outgassing, hydrothermal circulation in deep-sea volcanic areas, and the weathering of oceanic crust (Canfield, 2004) (Figure 1).

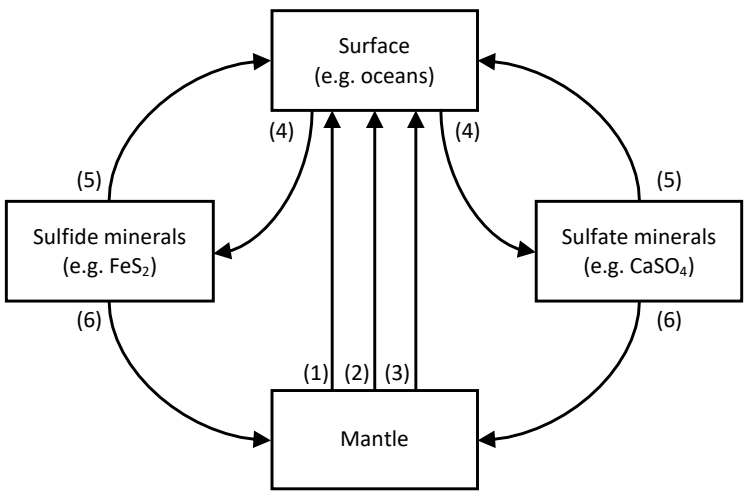

Figure 1: Simplified representation of the global geological sulfur cycle. Sulfur is transported from the the mantle to surface environments via (1) hydrothermal circulation, (2) volcanic gases, and (3) weathering of the ocean crust. Sulfur is cycled back from surface environments, predominantly the ocean, to the crust via (4) the formation and burial of sulfide and sulfate minerals. From these mineral reservoirs sulfur can (5) cycle back into surface environments through weathering, or (6) back into the mantle via subduction in subduction zones. Adapted from Canfield 2004.

In volcanic gases sulfur occurs as sulfur dioxide (SO_2) and H_2S, of which SO_2 disproportionates with water to sulfuric acid and H_2S upon cooling (Doukas and Gerlach, 1995; Nordstrom et al., 2009) (equation 1), or condensates with H_2S to form elemental sulfur (S_8^0) (equation 2), forming sulfur deposits (Johnson and Aguilera, 2015; Amenabar and Boyd, 2019). Sulfur is cycled between surface environments and the crust through the formation and weathering of sulfide and sulfate minerals, and reenters the mantle by subduction of sulfur-containing crust.

$$4\ H_2O(l) + 4\ SO_2(aq) \rightarrow H_2S(aq) + 3\ H^+(aq) + 3\ HSO_4^-(aq) \quad (1)$$

$$2\ H_2S(g) + SO_2(g) \rightarrow 3\ S^0(s) + 2\ H_2O(l) \quad (2)$$

While the cycling of sulfur between the mantle and the Earth surface is governed by geological processes, the cycling of sulfur in surface environments and between the surface and the crust is strongly influenced by microbial activity. Inorganic sulfur compounds (ISC) are used by many microorganisms in their dissimilatory energy metabolism, serving as electron donors or acceptors for respiration or disproportionation (Figure 2) (Kletzin et al., 2004; Rabus et al., 2006a; Finster, 2008). Microbial oxidation of reduced sulfur compounds such as H_2S and S_8^0, for example with oxygen as electron acceptor, results in SO_4^{2-} as the final product. In turn, SO_4^{2-} and other oxidized sulfur compounds can serve as electron acceptors in anaerobic respiration, using organic compounds or H_2 as electron donors, ultimately resulting in the production of H_2S (biosulfidogenesis). Both SO_4^{2-} and H_2S can again serve as electron acceptor and donor, respectively, for microbial respiration, but they also react with other elements to form sulfate and sulfide minerals such as anhydrite ($CaSO_4$) and pyrite (FeS_2), whose burial constitutes the main route for sulfur compounds from surface environments to the crust (Canfield, 2004).

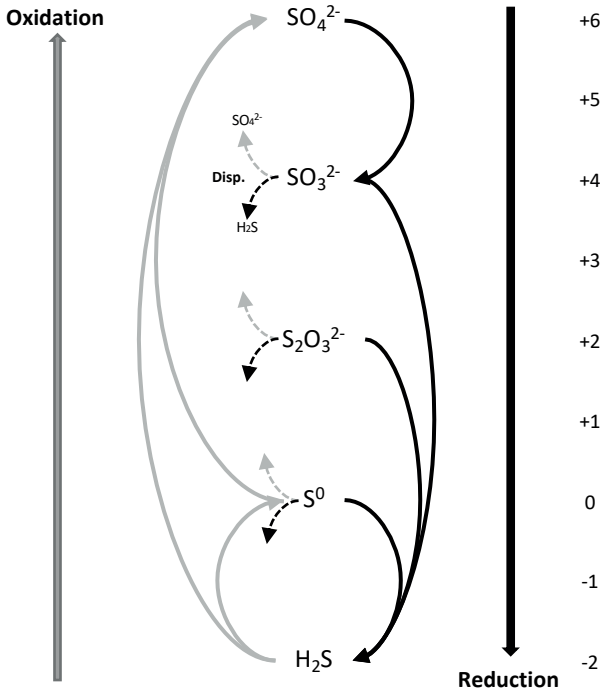

Figure 2: Schematic representation of main reactions occurring in dissimilatory sulfur metabolism using inorganic sulfur compounds as electron donor (oxidation, grey arrows), electron acceptor (reduction, black arrows), or (disproportionation (disp., dashed arrows, grey to SO_4^{2-}, black to H_2S). Oxidation state of sulfur atoms in specific sulfur compounds is indicated on the scale on the right.

Pyrite and the sulfur cycle

The S cycle is tightly linked to the cycling of other major elements, such as iron (Fe), carbon (C), and oxygen (O). This is illustrated by the processes involved in the formation of pyrite (FeS_2), the most abundant sulfide mineral in the Earth crust (Berner, 1984; Rickard and Luther, 2007), and as its elemental composition indicates, a main connection between the S and Fe cycle. Because microbial SO_4^{2-} reduction is the main source of H_2S for pyrite formation in marine sediments (Berner, 1984) and is tightly coupled to the oxidation of organic carbon compounds (Jørgensen, 1982; Jørgensen et al., 2019), pyrite formation also connects the S and Fe cycles to the C cycle. Because the organic carbon used as energy source for sulfate reduction is in large part produced by oxygenic photosynthesis, pyrite formation (indirectly) connects the S, C, and Fe cycles to the O cycle (Canfield and Farquhar, 2012). From a (bio)geochemical perspective, pyrite deposits serve as a record of the Earth's past oxidation states, and the isotopic fractionation of S in FeS_2 is used to assess the relative contribution of different microbial sulfur metabolisms to pyrite formation (Fike et al., 2015).

Pyrite formation furthermore plays a key role in the chemoautotrophic iron-sulfur world theory of the origin of life (Wächtershäuser, 1988). As discussed in more detail in **chapter 2**, pyrite formation can occur through two pathways, the polysulfide pathway (or Bunsen reaction), and the sulfide pathway (or Berzelius reaction) (Rickard and Luther, 2007). Both involve the formation of an (aqueous) Fe monosulfide intermediate (equation 3), which in the polysulfide pathway reacts with a polysulfide, formed from S_8^0 and HS^- (equation 4), forming FeS_2 and a shorter chain polysulfide (equation 5). In the sulfide pathway, the S in FeS is oxidized by H_2S, resulting in FeS_2 and H_2 (equation 6).

$$Fe^{2+} + H_2S \rightarrow FeS + 2H^+ \quad (3)$$

$$\frac{n-1}{8} S_8^0\,(s) + HS^- \rightarrow S_n^{2-} + H^+ \quad (4)$$

$$FeS + S_5^{2-} \rightarrow FeS_2 + S_4^{2-} \quad (5)$$

$$FeS + H_2S \rightarrow FeS_2 + H_2 \quad (6)$$

In the iron-sulfur world theory, the sulfide pathway plays a key role, as the H_2 produced is hypothesized to provide the reducing power required for inorganic carbon (e.g. CO_2) fixation. The sulfide pathway is therefore also sometimes referred to as the Wächtershäuser reaction (Thiel, 2020).

The sulfur cycle in acidic environments

Sulfur compounds play an important role in natural and anthropogenic acidic (pH 3 – 6) to extremely acidic (pH < 3) environments such as acidic volcanic hot pools and acidic waters that form in regions with concentrated metal sulfide deposits (Nordstrom et al., 2009, 2015; Johnson and Aguilera, 2015). In both types of environments, the extreme acidity is in large part the result of the formation of sulfuric acid, either chemically (equation 1) or through microbial oxidation of reduced sulfur compounds such as H_2S and S_8^0 (Figure 2). Acidic volcanic waters, which can form acidic volcanic hot pools when they collect at the surface, are generated in volcanic areas such as Yellowstone National Park (WY, USA) or the Pisciarelli volcanic area (Italy) where hydrothermal fluids rising to the surface separate into a liquid and a vapor phase. The vapor phase consists

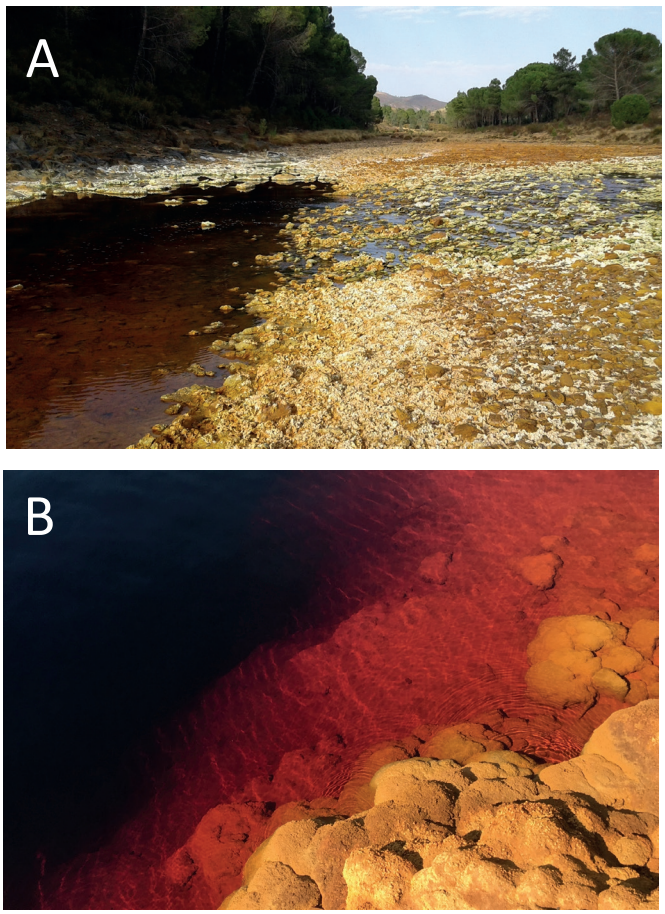

Figure 3: (A) acid mine drainage in Rio Tintillo (Huelva, Spain), (B) close-up of acid mine drainage in the acidic pit lake Filón Centro (Huelva, Spain). Pictures by author and Irene Sanchez-Andrea.

of gases such as hydrogen (H_2), methane (CH_4), and H_2S (Nordstrom et al., 2005, 2009), and upon mixing with surface waters part of the H_2S is oxidized to sulfuric acid by O_2, generating acidity. Although this can occur chemically, it is accelerated by the activity of (aerobic) thermoacidophilic sulfur-oxidizing microorganisms (Colman et al., 2019).

While acidic volcanic hot pools are characterized by high temperatures, acidic environments with more moderate temperatures can be found in regions containing concentrated metal sulfide deposits such as the Iberian Pyrite Belt (IPB) (Huelva, Spain). There, extremely acidic, metal-laden waters form as a result of oxidation of the metal sulfides, which is triggered by their exposure to water and oxidants such as O_2 or ferric iron (Fe^{3+}). This can occur naturally, in which case the resulting waters are referred to as acid rock drainage (ARD). The Tinto River in the IPB is one of the best-known examples

of ARD, with its acidic (mean pH 2.3), metal-rich (e.g., Fe 2.26 g·L^{-1}, Cu 0.11 g·L^{-1}, Zn 0.24 g·L^{-1}) (López-Archilla et al., 2001) waters originating from chemolithotrophic microbial activity in the subsurface (Amils et al., 2011). Alternatively, exposure and oxidation of metal sulfides can be due to mining activities, in which case the resulting waters are referred to as acid mine drainage (AMD) (Figure 3A, B). Depending on the metal sulfide, oxidation occurs through the thiosulfate or polysulfide pathway (Schippers and Sand, 1999), named after the sulfur intermediate forming in the first step. The three metal sulfides FeS_2, MoS_2 and WS_2 are oxidized via the thiosulfate mechanism, in which thiosulfate as intermediate is chemically oxidized to sulfate by Fe^{3+} (equation 7-8). The other metal sulfides are oxidized via the formation of polysulfides (equation 9), which decompose into H_2S and S_8^0 at acidic pH, with H_2S subsequently oxidized to S_8^0 by Fe^{3+} (equation 10). Contrary to thiosulfate however, S_8^0 is chemically stable in the presence of Fe^{3+}, and complete oxidation to SO_4^{2-} via the polysulfide oxidation mechanism therefore requires the activity of sulfur-oxidizing microorganisms (Sand et al., 2001) (equation 11).

Thiosulfate mechanism:

$$FeS_2(s) + 6\,Fe^{3+}(aq) + 3\,H_2O(l) \rightarrow S_2O_3^{2-}(aq) + 7\,Fe^{2+}(aq) + 6\,H^+(aq) \quad (7)$$

$$S_2O_3^{2-}(aq) + 8\,Fe^{3+}(aq) + 5\,H_2O(l) \rightarrow 2\,SO_4^{2-}(aq) + 8\,Fe^{2+}(aq) + 10\,H^+(aq) \quad (8)$$

Polysulfide mechanism

$$MS\,(s) + Fe^{3+}(aq) + H^+(aq) \rightarrow M^{2+}(aq) + Fe^{2+}(aq) + \tfrac{1}{2}\,H_2S_n(aq) \quad (n\geq 2) \quad (9)$$

$$\tfrac{1}{2}\,H_2S_n(aq) + Fe^{3+}(aq) \rightarrow \tfrac{1}{8}\,S_8^0(s) + Fe^{2+}(aq) + H^+(aq) \quad (10)$$

$$\tfrac{1}{8}S_8^0\,(s) + 1.5\,O_2\,(g) + H_2O \rightarrow SO_4^{2-}(aq) + 2H^+(aq) \quad (11)$$

Although microbial metabolism is only directly involved in complete oxidation of metal sulfides in the polysulfide pathway, both mechanisms are strongly influenced by microbial activity. Even though at low pH metal sulfide oxidation with Fe^{3+} as an oxidant proceeds much faster than with O_2 (Sand et al., 2001), the subsequent reoxidation of the produced ferrous iron (Fe^{2+}) to Fe^{3+}, required for oxidation to continue, is extremely slow abiotically (Johnson and Hallberg, 2008). Microbial reoxidation of Fe^{2+}, coupled

to the reduction of O_2, for example by *Leptospirillum* species, can be sustained at much higher rates, greatly accelerating AMD formation (Johnson and Hallberg, 2008).

Dissimilatory reduction of oxidized sulfur compounds at low pH

The abovementioned examples, acidic volcanic hot pools and AMD/ARD, illustrate the importance of oxidative microbial sulfur metabolism in the generation of acidity, through oxidation of reduced sulfur compounds to sulfuric acid. However, reductive dissimilatory sulfur metabolism also plays an important role in these environments (Kletzin, 2006; Rabus et al., 2006b; Sánchez-Andrea et al., 2014a; Florentino et al., 2016b; Johnson and Sánchez-Andrea, 2019). In the regions of the water column and sediments where electron acceptors with more positive redox potentials, predominantly O_2, have been depleted, anaerobic acidophiles can use oxidized sulfur compounds such as SO_4^{2-}, S_8^0, and $S_2O_3^{2-}$ as electron acceptors (Figure 2), producing H_2S, or disproportionate $S_2O_3^{2-}$, SO_3^{2-}, or S_8^0, resulting in SO_4^{2-} and H_2S (Finster, 2008). The final product of reductive dissimilatory sulfur metabolism, H_2S, can strongly affect the local physicochemical conditions, as discussed in more detail below.

(Moderately) acidophilic SO_4^{2-}- and S_8^0-reducing microorganisms

Although microbial S_8^0 and SO_4^{2-} reduction has been reported both in acidic volcanic hot pools and in AMD/ARD environments, the physiological characteristics of the S_8^0- and SO_4^{2-}-reducing species isolated so far suggest that S_8^0 is a preferred electron acceptor among acidophiles (pH_{opt} < 3.0). To date, 8 acidophilic S_8^0-reducing species have been officially published, of which 7 are (hyper)thermophiles (T_{opt} > 60°C) from the archaeal genera *Acidianus, Thermoplasma, Stygiolobus,* and *Acidilobus* (see Table 1A for references), and one is the mesophilic bacterial species *Acidithiobacillus ferrooxidans* (Table 1A). In contrast, no extreme acidophilic sulfate reducers are known, and dissimilatory sulfate reduction at low pH has so far only been described in moderate acidophiles (pH_{opt} 3 – 6) (Table 1B). Of these, 4 are (hyper)thermophilic archaeal species from the genera *Thermoproteus, Vulcanisaeta, Caldivirga,* and *Archaeoglobus* (see Table 1B for references), although the capacity for dissimilatory sulfate reduction in *C. maquilingensis* and *V. distributa* was disputed, and they were recently shown to lack essential genes for sulfate reduction (Chernyh et al., 2020). In mesophilic to moderately thermophilic moderate acidophiles, dissimilatory sulfate reduction has been described in 7 species, from the bacterial genera *Desulfosporosinus, Thermodesulfobium,* and *Desulfothermobacter*, and the recently published novel genus *Acididesulfobacillus* (Sánchez-Andrea et al., 2022), described in **chapter 5** of this thesis.

Table 1: overview of (A) published acidophilic S_8^0-reducing bacterial and archaeal species, and (B) moderately acidophilic or acidotolerant SO_4^{2-}-reducing bacterial and archaeal species.

(A) Acidophilic S_8^0 reducers	T range (opt)	pH range	reference
Bacteria			
Acidithiobacillus ferrooxidans	10-37 (30-35)	1.3-4.5 (2.5)	(Kelly and Wood, 2000)
Acidianus ambivalens	ND-87 (80)	1-3.5 (ND)	(Zillig et al., 1986)
Thermoplasma volcanicum	33-67 (60)	1-4 (2)	(Segerer et al., 1988)
Thermoplasma acidophilum	45-63 (59)	1-4 (1-2)	(Segerer et al., 1988)
Stygiolobus azoricus	57-89 (80)	1-5.5 (2.5 - 3.0)	(Segerer et al., 1991)
Acidianus brierleyi	45-75 (opt 70)	1-6 (1.5-2)	(Segerer et al., 1986)
Acidianus infernus	60-95 (90)	1.0-5.5 (2.0)	(Segerer et al., 1986)
Acidilobus sulfurireducens	62-89 (81)	2.0-5.5 (3.0)	(Boyd et al., 2007)
(B) Acidotolerant or moderately acidophilic sulfate reducers			
Bacteria			
Desulfosporosinus acidiphilus	25-40 (30)	3.6 - 5.5 (5.2)	(Alazard et al., 2010)
Desulfosporosinus acididurans	15-40 (30)	3.8 - 7.0 (5.5)	(Sánchez-Andrea et al., 2015)
Desulfosporosinus metallidurans	4-37 (28)	4.0 - 7.0 (5.5)	(Panova et al., 2021)
Thermodesulfobium narugense	37-65 (50-55)	4.0 - 6.5 (ND)	(Mori et al., 2003)
Thermodesulfobium acidiphilum	37-65 (55)	3.7 - 6.5 (4.8 - 5.0)	(Frolov et al., 2017)
Desulfothermobacter acidiphilus	42-70 (55)	3.5* - 6.5 (opt 4.5)	(Frolov et al., 2018)
Acididesulfobacillus acetoxydans	25-42 (25-35)	3.8 - 6.5 (5.0)	(Sanchez-Andrea et al. 2022)
Archaea			
Thermoproteus thermophilus	75-90 (opt 85)	4.0 - 6.0 (opt 5)	(Yim et al., 2015)
*(Vulcanisaeta distributa)***	70-92	3.5-5.6 (ND)	(Itoh, 2002)
*(Caldivirga maquilingensis)***	60-92	2.3***-6.4 (3.7-4.2)	(Itoh et al., 1999
Archaeoglobus profundus	65-90	4.5-7.5 (ND)	(Burggraf et al., 1990)

*this strain was reported to be active at pH 2.9, but growth only started after the pH had increased to 3.5; ** Sulfate reduction in these species was disputed, and they were recently shown to lack genes essential for sulfate reduction; ***the pH range for growth was determined with S_8^0 as electron acceptor, while the use of SO_4^{2-} was only tested at pH 4.0.

A bottleneck in the isolation truly acidophilic SRB could be related to methodological choices such as the use of organic acids as electron donor and/or carbon source, as proposed by (Johnson and Sánchez-Andrea, 2019). At pH values below their pK_a organic acids exist predominantly in protonated form, enabling their passive diffusion over the cell membrane. At the more neutral intracellular pH values, the acids deprotonate, acidifying the cell and requiring active H^+ export to maintain pH homeostasis (Baker-Austin and Dopson, 2007). This results in a futile cycle that is detrimental to growth. Using organic acids as electron donors and/or carbon source at low pH therefore results in toxicity and growth inhibition already at relatively low concentrations, as shown for example by lactate concentrations of 5 mM inhibiting growth in *Desulfosporosinus acididurans* (Sánchez-Andrea et al., 2013). Furthermore, even when using non-ionic compounds such as glycerol, organic acid toxicity can become an important inhibiting factor. The majority of the acidophilic SRB described so far do not oxidize organic compounds completely to CO_2, but instead produce both CO_2 and partly oxidized intermediates such as acetic acid, resulting in its accumulation to inhibiting concentrations. Complete oxidation of organic carbon compounds by moderately acidophilic SRB had until recently only been reported to occur in low amounts in the moderately acidophilic SRB *Desulfosporosinus metallidurans* (Panova et al., 2021). Therefore, the ability of *Acididesulfobacillus acetoxydans* to completely oxidize glycerol to CO_2 (Sánchez-Andrea et al., 2022), described in **chapter 5**, is of great interest.

In addition to cultivation conditions hindering isolation efforts, the source of inoculum could play a role. The moderately acidophilic or acidotolerant SRB described so far originate from AMD sediments or microbial mats. These could provide microenvironments or microniches with less harsh conditions, resulting in growth of microorganisms that are less extremophilic than the physicochemical parameters of their bulk environment would suggest, although this is still a matter of debate (Koschorreck, 2008). The conditions encountered in AMD/ARD environments can be considered poly-extreme, as they are often a combination of extreme acidity, high metal concentrations, and high salinity (Nordstrom et al., 2015). Of great interest, therefore, is the detection of sulfate-reducing microorganisms in the water column of AMD-impacted lakes, without a clear possibility for the formation of microniches (Wendt-Potthoff et al., 2012; Diez-Ercilla et al., 2014; Falagán et al., 2014). In the water column the protection from the extreme conditions is minimal, and these APL therefore have great potential as sources for isolation of poly-extremophilic SRB.

Likewise, the water column of AMD-impacted lakes can be expected to harbor more polyextremophilic S_8^0-reducing and disproportionating microorganisms. As indicated

above, oxidative dissolution of most metal sulfides results in the formation of S_8^0 as intermediate (equation 10) (Schippers and Sand, 1999), which is an electron acceptor for anaerobic respiration, or can be disproportionated. As with SRB, enrichment and isolation studies focusing on S_8^0 reduction at acidic conditions in AMD/ARD environments such as Tinto River have so far used sediments as inoculum (Sánchez-Andrea et al., 2013; Florentino et al., 2015). S_8^0-reducing activity was observed in these enrichments between pH 3 and pH 5, not at pH 2 (Florentino et al., 2015), and the S_8^0-reducing species that was isolated, *Desulfurella amilsii* (Florentino et al., 2016a) was only moderately acidophilic (pH 3 – 7, pH_{opt} 6-6.5). The water column of AMD-impacted lakes could therefore be a valuable source of more acidophilic S_8^0-reducing microorganisms. In **chapter 4** the presence of acidophilic SO_4^{2-}- and S_8^0-reducing species in the water column of several AMD-impacted lakes is investigated in more detail.

Challenges associated with using S_8^0 as electron acceptor at acidic pH

In contrast to SO_4^{2-}, the use of S_8^0 as electron acceptor imposes specific challenges on microorganisms due to its low solubility in aqueous solutions, between 6.1 nM at 4 °C and 478 nM at 80°C in pure water (Kamyshny, 2009). At more neutral pH, S_8^0-reducing bacteria such as *Wolinella succinogenes* overcome this by using soluble polysulfides (S_n^{2-}), which form through nucleophilic attack of S_8^0 rings by H_2S (and polysulfides) (equation 12), instead of S_8^0 as the actual electron acceptor (Klimmek et al., 1991; Hedderich et al., 1998).

$$\frac{n-1}{8} S_8^0\,(s) + HS^- \rightarrow S_n^{2-} + H^+ \qquad (12)$$

At low pH, however, polysulfide is highly unstable, and the reverse of the reaction shown in (equation 12) is favored. Equilibrium calculations at conditions relevant for thermoacidophilic S_8^0 reducers indicate polysulfide concentrations on the order of 10^{-11} M (pH 3, 80°C, 1 mM H_2S) (Schauder and Müller, 1993; Boyd and Druschel, 2013). Therefore, although the use of polysulfide at acidic pH cannot be ruled out, acidophilic S_8^0-reducing microorganiss are hypothesized to use other mechanisms for interaction with and reduction of solid S_8^0 (Boyd and Druschel, 2013; Florentino et al., 2016b). These either involve direct contact between cells and S_8^0 (nano)particles, or the use of intermediate sulfur compounds, such as thiols.

Previous studies investigated the requirement for direct contact of cells with solid S_8^0 at low pH using dialysis membranes to physically separate bulk S_8^0 from cells at the start of incubations. These experiments were performed with several (moderately)

thermoacidophilic microorganisms: *Acidilobus sulfurireducens*, grown at pH 3.0, 81 °C (Boyd and Druschel, 2013); *Acidianus* DS80, grown at pH 3.0 and 81 °C (Amenabar and Boyd, 2018); *Thermovibrio ammonificans*, grown at pH 5.5, 75 °C (Jelen et al., 2018); and *D. amilsii*, grown at pH 3.5 and 6.5 (Florentino et al., 2019), 50 °C. Results showed that trapping S_8^0 in dialysis membranes affected rates of sulfide production, which served as a proxy for S_8^0 reduction. For *A. sulfurireducens* and *D. amilsii* (Boyd and Druschel, 2013; Florentino et al., 2019), trapping S_8^0 resulted in up to 50% reduction of rates compared to rates observed with free S_8^0. With *T. ammonificans* trapping S_8^0 in dialysis membranes inhibited sulfide production entirely (Jelen et al., 2018), compared to positive controls, although closer inspection of the biological incubations with S_8^0 sequestered in dialysis tubing did indicate low levels of S_8^0 reduction. Together, these results suggested that direct contact with bulk S_8^0 was (highly) beneficial but not strictly necessary.

Interestingly, in the thermoacidophilic incubations polysulfides were detected at concentrations higher than those predicted by equilibrium calculations, suggesting that unknown processes were contributing to polysulfide dynamics (Boyd and Druschel, 2013), and possibly indicating that the use of polysulfide as electron acceptor is less unfavorable than generally hypothesized. However, these experiments also showed that the decrease in H_2S production rates was related to the membrane pore size, with a larger pore size enabling higher rates (Boyd and Druschel, 2013). It was therefore hypothesized that nanoparticulate sulfur particles, formed upon the rapid dissociation of the acid-unstable polysulfides, played an important role as electron acceptor. Their size-distribution could be expected to restrict diffusion over the dialysis membranes, explaining the effect of membrane pore size on H_2S production rates. The importance of nanoparticulate S_8^0 particles through polysulfide formation and rapid subsequent disproportionation (equation 8) for S_8^0 reduction at low pH could further be supported by the observation that when *Acidianus* DS80 was grown through S_8^0 oxidation, with Fe^{3+} as electron acceptor, sequestration of S_8^0 in dialysis membranes inhibited S_8^0 oxidation entirely (Amenabar and Boyd, 2018). This could be explained by the absence of H_2S, formed in S_8^0 reduction, preventing the formation of polysulfides and thereby of nanoparticulate S_8^0.

Although the formation of nanoparticulate S_8^0 likely plays an important role in S_8^0 reduction at acidic pH, the exact mechanism for interaction with nanoparticulate S_8^0 has not been elucidated, and it is not yet clear whether this nanoparticulate S_8^0 functions as a soluble acceptor, or merely as a solid with increased bioavailability due to its smaller particle size. It has been proposed for *T. ammonificans* that nanoparticulate S_8^0 is able to diffuse directly over the cell membrane, and serves as electron acceptor for

an intracellular sulfur-reducing enzyme resembling the NAD(P)H dependent elemental sulfur oxidoreductase (NSR) (Jelen et al., 2018). In the thermoacidophilic archaeon *Acidianus ambivalens*, S_8^0 reduction by the membrane-bound sulfur reductase (SR) did not require the presence of H_2S (Laska et al., 2003), suggesting the absence of polysulfides, and indicating that solid S_8^0 was directly reduced. Comparative proteomics in the moderately acidophilic S_8^0 reducer *D. amilsii* indicated an important role for rhodanese-like sulfurtransferases, in addition to sulfur reductase, during S_8^0 reduction (Florentino et al., 2019). Rhodanese-like sulfurtransferases have previously been shown to play an important role in transferring sulfur substrates to S_8^0-reducing and S_8^0-oxidizing enzymes in the cytoplasm of *Aquifex aeolicus* (Aussignargues et al., 2012), although this does not answer the question how S_8^0 enters the cell. It has furthermore been hypothesized that sulfur atoms are transported into the cell by reaction with thiol groups on specialized outer membrane proteins, as is the case in acidophilic S_8^0-oxidizing species (Rohwerder and Sand, 2003).

Application of biosulfidogenesis for bioremediation and metal recovery

The enrichment and isolation of novel acidophilic S_8^0- and SO_4^{2-}-reducing species and the elucidation of mechanisms enabling S_8^0 reduction at acidic pH is scientifically important, but also relevant for application in bioremediation and metal recovery technologies. The final product of S_8^0 and SO_4^{2-} reduction, H_2S, reacts with dissolved metals, forming insoluble metal sulfides that precipitate out of solution (equation 13).

$$Me^{2+}(aq) + HS^-(aq) \rightarrow MeS + H^+ \quad (13)$$

Furthermore, when H_2S originates from SO_4^{2-} as electron acceptor (equation 14), but not with S_8^0 (equation 15), its production is proton (H^+)-consuming at acidic pH, resulting in the natural remediation of extreme acidity.

$$SO_4^{2-}(aq) + 4\,H_2\,(g) + 2\,H^+(aq) \rightarrow H_2S\,(g) + 4\,H_2O\,(l) \quad (14)$$

$$S^0(s) + H_2\,(g) \rightarrow H_2S\,(g) \quad (15)$$

Biosulfidogenesis at acidic conditions is therefore of great interest for the *in-situ* bioremediation of acidic metal-contaminated waters such as AMD, and the selective recovery of metals as metal sulfides from metalliferous waste streams generated during metal extraction processes.

Biosulfidogenesis for *in situ* bioremediation of acid mine drainage

Biosulfidogenesis can be used for *in situ* bioremediation of the artificial lakes that form in abandoned open pit polymetallic sulfide mines, or coal mines with high sulfur contents (Geller et al., 2013). Upon closure, these open pits are commonly abandoned and left to fill up with water, enabling oxidative dissolution of the reduced sulfur moieties in the pit walls to sulfuric acid, and dissolved metals in the case of metalsulfide deposits (equation 3-7). The resulting artificial lakes are referred to as acidic pit lakes (APL), and are a pervasive global feature of regions with metalsulfide deposits, such as the IPB (Sánchez-España et al., 2008; Sánchez-España et al., 2013) (Figure 4A, B), and in coal-mining regions such as the Lusatian mining district in Germany (Geller et al., 2013). Another iconic example is the Berkeley Pit lake in Montana (USA) due to its size and extreme chemistry, and its proximity to the nearby town of Butte (Tucci and Gammons, 2015; Gammons and Icopini, 2020).

The physicochemical properties of APL vary widely, but in many cases they develop meromixis (permanent stratification) due to the relatively large volume to surface ratio (Castro and Moore, 2000; Schultze et al., 2017). This results in an upper, oxygenated layer (mixolimnion) often characterized by a deep red color due to high Fe^{3+} concentrations, a transitional redoxcline, and a lower, anoxic layer (monimolimnion) that is a clear blue due to high Fe^{2+} concentrations (inset Figure 4B). APL have historically rarely been properly remediated due to a combination of economic and technical factors (Blanchette and Lund, 2016), although there are exceptions, such as the APL in the Lusatian mining district (Benthaus et al., 2020).

In AMD environments, biosulfidogenesis, and the associated increase in pH and removal of metals, has been observed to establish naturally, both in AMD sediments (Sánchez-Andrea et al., 2012a; Falagán et al., 2015) and in the water column of APL (Falagán et al., 2014; Sánchez-España et al., 2020). It can furthermore be strongly enhanced by supplementation with organic carbon, which has been explored as a passive remediation strategy at (abandoned) AMD sites (Tuttle et al., 1969; Christensen et al., 1996; Hiibel et al., 2011; Valkanas et al., 2021). Triggering biosulfidogenesis in APL is a straightforward solution for their passive treatment, as it requires minimal monitoring and can be achieved with biomass waste streams such as composted manure, domestic wastewater, sewage, and green (kitchen) waste as sources of

Figure 4: Acidic Pit Lakes (A) Filón Centro, and (B) La Zarza in the Iberian Pyrite Belt (Huelva, Spain), described in more detail in chapter 3. Inset in (B) shows water samples from the mixolimnion (0 m) (top) and monimolimnion (30 and 70 m) (middle and bottom).

organic carbon, depending on local availability (Kumar et al., 2011; McCullough and Lund, 2011).

Biosulfidogenesis for metal recovery

In addition to bioremediation, biosulfidogenesis can be applied for the recovery of metals from metalliferous waters produced during metal extraction (equation 13). The solubility of different metal sulfides is pH-dependent (Lewis, 2010), and sulfide precipitation therefore allows the selective precipitation of different metals from metalliferous waters at sufficient purity for recovery and recycling. This principle has been applied to develop industrial metal recovery processes, such as the SULFATEQ

and THIOTEQ Metal processes developed by Paques Global B.V. (Huisman et al., 2006), and the BioSulphide technology developed by BioteQ (now BQE water) (Adams et al., 2008), using biosulfidogenesis from SO_4^{2-} (SULFATEQ) or S_8^0 (THIOTEQ, BioSulphide) as electron acceptor. Biosulfidogenesis has several important advantages over chemical H_2S production. It can be carried out on-site, avoiding the need for transport of hazardous H_2S. In addition, H_2S production rates can be modified rapidly to meet process demands, avoiding the need for storage of large quantities of sulfide on-site, which would require additional permits and storage capacity. Furthermore, the use of biogenic H_2S instead of chemical sulfide salts such as Na_2S and NaHS avoids the need for addition of acid, as sodium sulfide salts are very basic, and prevents the accumulation of Na^+ ions in the process (Huisman et al., 2006; Adams et al., 2008).

In most cases, SO_4^{2-} is already present in the metalliferous streams mentioned above, and its use as electron acceptor would therefore both remove the need for external supplementation, as well as contribute to lowering sulfate concentrations to meet environmental requirements. Microbial SO_4^{2-} reduction for metal recovery has therefore been investigated extensively (Weijma et al., 2002; Muyzer and Stams, 2008; Sánchez-Andrea et al., 2014a; Johnson and Sánchez-Andrea, 2019). However, process economics can be improved by using S_8^0 instead of SO_4^{2-}, as reduction of S_8^0 only requires 2 electrons for reduction to H_2S, compared to 8 electrons required for SO_4^{2-} (Figure 2), thereby lowering the costs associated with electron donor supply four-fold. Even though additional costs are associated with external supply of S_8^0, still an overall reduction in operating costs can be achieved (Florentino et al., 2016b).

Biosulfidogenesis from S_8^0 for metal recovery has been applied for example for the recovery of dissolved copper (Cu^{2+}) from leach streams generated during gold extraction. Gold ores often contain large amounts of other sulfide minerals, predominantly copper sulfides such as chalcocite (Cu_2S), covellite (CuS) and chalcopyrite ($CuFeS_2$) (Adams et al., 2008), and by application of cyanide leaching of gold from crushed ore, cyanide waste streams with elevated Cu concentrations are produced. In a case study of the BioSulphide process (BQE Water), Cu^{2+} was removed from a cyanide leach stream through sulfide precipitation at > 99 % recovery, and the resulting CuS precipitate was sold to a local smelter (Adams et al., 2008). In another example, the THIOTEQ Metal process (Paques Global B.V.) used offline biosulfidogenesis from S_8^0 for Cu^{2+} recovery from hydrometallurgical process streams generated at the Pueblo Viejo gold mine in the Dominican Republic (Sánchez-Andrea et al., 2016) (Figure 5).

So far, the commercial processes mentioned above are based on offline biosulfidogenesis, in a separate bioreactor that is not in direct contact with the metal-contaminated stream (Figure 6A). As a result, the microbial species carrying out

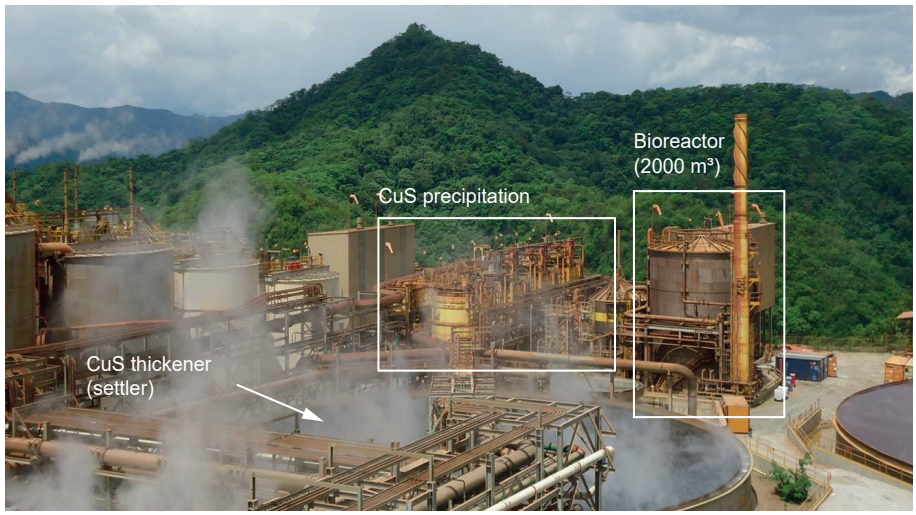

Figure 5: copper recovery section at the Pueblo Viejo mine in the Dominican Republic. Biosulfidogenesis from S80 occurs in the bioreactor, copper sulfide (CuS) precipitation occurs in separate precipitation reactors, and CuS is dewatered in a thickener. Image courtesy of Paques Global B.V.

biosulfidogenesis are not required to withstand the extreme conditions of these streams. Further improvements in process economics could be achieved by developing a process for biosulfidogenesis from S_8^0 directly in the waste streams. This would avoid the need for separate bioreactors, thereby reducing capital costs (Figure 6B). Taking AMD and metallurgy waste streams as target examples, this would require acidophilic S_8^0-reducing communities thriving at ambient (AMD, < 30 °C), or high temperature (metallurgy wastestreams, T > 70 °C) conditions, as metallurgy waste streams are generally both hot and acidic. As detailed above, multiple species of (extremely) acidophilic S_8^0-reducing species are known, both mesophilic and (hyper)thermophilic (Table 1), and the extreme pH and temperature are therefore not expected to hinder the microbiological feasibility. However, for the process to be economically feasible, rates of biosulfidogenesis that can compete with S_8^0 reduction at neutral pH need to be achieved (Zhang et al., 2021). A main challenge in this regard is the difficulty associated with the use of S_8^0 as electron acceptor at low pH, as explained above. In this thesis, biosulfidogenesis from S_8^0 at elevated temperatures and acidic pH is investigated in **chapter 2**, and at ambient temperatures and neutral to acidic pH in **chapter 3**.

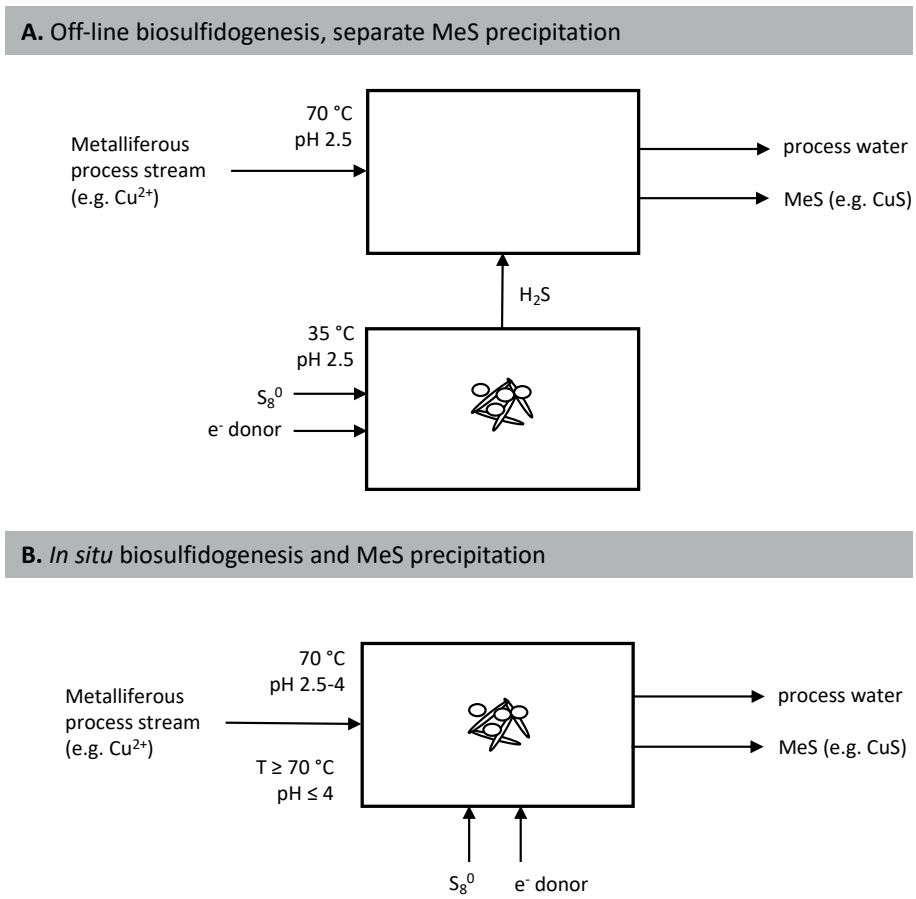

Figure 6: Schematic representation of (proposed) metal recovery processes based on metal sulfide precipitation, with biosulfidogenesis as source of H_2S. The example streams are hot, acidic metalliferous waste streams enriched in dissolved copper (Cu2+). (A) Process scheme showing biosulfidogenesis in a separate bioreactor operated at mesophilic (35 °C) and neutro-philic (pH 7.5) conditions; (B) proposed process scheme with biosulfidogenesis occurring in the process stream, at acidophilic (pH 2.5 – 4.0), thermophilic (70°C) conditions. For treatment of AMD, the temperature of the process stream would be close to ambient conditions (< 35 °C).

Thesis Outline

In this thesis sulfidogenesis from S_8^0 and SO_4^{2-} at acidic pH and low (30 °C) to high (80 °C) temperatures was investigated, with as main aims to (i) expand the operating conditions at which biosulfidogenesis can be achieved, to lower pH and higher T for application in metal recovery processes (**chapter 2** and **3**), and (ii) investigate biosulfidogenesis and the associated remediation of acidity and metal concentrations in AMD environments at more poly-extreme conditions (**chapter 4** and **5**).

In **chapter 2** we aimed to develop a laboratory-scale process for biosulfidogenesis at high temperature (> 70 °C) and low pH (< pH 4). Enrichment screenings for thermoacidophilic S_8^0-reducing microbial communities were set up, using samples from acidic volcanic hot pools as inoculum. Although sulfidogenic enrichments were obtained at 80 °C, pH 4, with H_2 as electron donor, and extensive efforts were made to characterize the microbial community, follow-up investigations revealed that sulfidogenesis did not result from microbial S_8^0 reduction, but instead from an unexpected, abiotic process enabling chemical reduction of S_8^0 with H_2. Intriguingly, pyrite formed in these incubations, and was later shown to play a key role as catalyst. This surprising finding, pyrite-mediated chemical reduction of S_8^0 by H_2, has not been described previously and therefore became the focus of this part of the thesis. Both pyrite formation and subsequent reduction of S_8^0 by H_2 mediated by pyrite are investigated in detail.

In **chapter 3**, we focused on biosulfidogenesis from S_8^0 in a continuous bioreactor at ambient temperature and neutral to acidic pH, with H_2/CO_2 as electron donor and carbon source, respectively, using anaerobic digester sludge as inoculum. We investigated the effect of pH change on sulfide production rates, and on the microbial community composition.

In **chapter 4** we investigated biosulfidogenesis in the water column of AMD-impacted waters, where microorganisms are more exposed to poly-extreme conditions. As described in the introduction, microbial SO_4^{2-} reduction has so far been shown to occur only at moderately acidic pH, and the SRB isolated to date can only be classified as moderate acidophiles (pH_{opt} > 3.0). However, the water column of AMD-impacted waters are likely to harbor more polyextremophilic microorganisms due to the lack of protective microenvironments, and this could include more acidophilic SRB. Therefore, in **chapter 4** the occurrence of biosulfidogenesis and the presence of (novel) sulfidogenic taxa in the water column of two previously microbiologically unexplored APL is investigated using a combination of 16S rRNA gene amplicon sequencing, membrane lipid analysis, physicochemical profiling of the water column, and electron microscopy.

In **chapter 5**, a novel species of a novel genus of moderately acidophilic SRB, *Acididesulfobacillus acetoxydans*, is described and investigated in detail. This species has the capacity for complete oxidation of organic acids, which is uncommon among the moderately acidophilic SRB described so far, and likely provides an important mechanism to cope with acid stress. The main acid stress resistance mechanisms enabling this novel species to grow at lower pH are investigated through a combination of bioreactor studies, proteomics and membrane lipid analysis.

Finally, in **chapter 6** the results from the different chapters are discussed within the overarching aim of this thesis.

1

Pyrite formation at acidothermal conditions and its catalytic role in sulfidogenesis from elemental sulfur and hydrogen

C.M. van der Graaf [1], J. Sánchez-España [2], A. Ilin [3], I. Yusta [3], A.J.M. Stams [1,4], I. Sánchez-Andrea [1]

[1]Laboratory of Microbiology, Wageningen University & Research, Stippeneng 4, 6708 WE Wageningen, The Netherlands;
[2] Mine Waste and Environmental Research Group, Department of Geological Resources, CN IGME-CSIC, Calera 1, Tres Cantos, 28760 Madrid, Spain;
[3] Dept of Geology, University of the Basque Country (UPV/EHU), Apdo. 644, 48080 Bilbao, Spain;
[4] Centre of Biological Engineering, University of Minho, Campus de Gualtar, 4710-057 Braga, Portugal

Abstract

Sulfide production (sulfidogenesis) in surface environments at moderate temperature is generally assumed to be of microbial origin (biosulfidogenesis), while chemical sulfide production appears restricted to higher temperatures (> 100 °C). This boundary might not be as clear as previously thought, since recent research showed that abiotic sulfidogenesis might be important at lower temperatures. Here, we report a previously undescribed abiotic process for sulfidogenesis catalyzed by pyrite at conditions resembling those in hot, acidic, elemental sulfur (S_8^0)-containing environments such as volcanic hot springs and acidic hydrothermal vents. The process was first observed during enrichment screenings for (hyper)thermoacidophilic (pH 4.0, 80 °C), S_8^0-reducing microbial communities. Unexpected near-complete chemical reduction of S_8^0 (25 mM) by H_2 to H_2S occurred, catalyzed by pyrite particles that either formed *in situ* from H_2S, S_8^0 and Fe^{2+} present in the medium, or were supplemented from an external source. The pyrite particles are shown to act as catalysts for chemical sulfur reduction, enabling the transfer of electrons from H_2 to S_8^0.

The process was influenced by the presence of yeast extract (YE). YE increased the lag phase, possibly by decreasing the initial rate of pyrite formation, but not the rate of sulfidogenesis. Scanning Electron Microscopy coupled to Energy Dispersive X-Ray analysis (SEM-EDX) showed that the pyrite particles were spherical, but not framboidal, regardless of whether YE was present during formation. (Scanning) Transmission Electron Microscopy analysis ((S)TEM) provided evidence for the formation of intermediate Fe monosulfides, possibly pyrrhotite, as potential precursors in pyrite formation. The surface structure of the pyrite spheroids consisted of aggregated lenticular nanocrystals (16 – 35 nm wide x 70 – 640 nm long) with an increasing degree of organization observed in samples without YE. The process was investigated in detail at 80 °C and pH 4 but was observed to occur at temperatures as low as 40 °C (tested at pH 4), and at pH 6 (tested at 80 °C). The absence of H_2 production in control incubations, combined with geochemical modelling, suggest that pyrite formation in these incubations occurred through the polysulfide pathway, which is unexpected at acidic conditions.

Introduction

Sulfur is an abundant element in the Earth's mantle (McDonough and Sun, 1995) and exists in a range of oxidation states, from +6 (SO_4^{2-}) to -2 (H_2S) (Steudel, 2020a). Its cycling between these different redox states is strongly determined by both geological and biological processes (Canfield and Raiswell, 1999; Canfield and Farquhar, 2012). In its most reduced form, sulfide (H_2S), sulfur serves as an energy source for H_2S-oxidizing microorganisms, underpinning extensive chemolithotrophic ecosystems (Dubilier et al., 2008; Dick, 2019). H_2S also is an important connective molecule linking the sulfur cycle with chalcophilic metal cycles through metal sulfide formation, for example pyrite (FeS_2) (Rickard and Luther, 2007). From a more applied perspective, H_2S is well known as a severe operational hazard due to its toxicity and extremely corroding effects. In oil and gas production, extensive efforts are made to remove H_2S from natural gas (sour gas) and convert it to unharmful forms such as elemental sulfur (S_8^0) (Eow, 2002). It can also have beneficial applications, however, as it can be used to selectively precipitate metals as metal sulfides, making it of great interest for the remediation of, or metal recovery from, metalliferous waste streams typical for mining and metallurgy processes (Lewis, 2010; Johnson and Sánchez-Andrea, 2019). This is especially relevant in the transition to a 'fossil-free' economy given the projected surge in metal demands associated with the use of renewable energy technologies (Herrington, 2021; Pell et al., 2021).

Production of H_2S in the environment occurs both through chemical (abiotic) and biological processes (biotic). Chemical sources of H_2S in the global sulfur cycle include the disproportionation of sulfur dioxide (SO_2) to H_2S and SO_4^{2-} during volcanic outgassing (Canfield, 2004), and the thermochemical (abiotic) reduction of SO_4^{2-} to H_2S at high temperatures (>100 °C) (Machel, 2001). H_2S production in surface environments with more moderate temperatures is generally attributed to reductive dissimilatory sulfur metabolism performed by microorganisms, predominantly by sulfate-reducing bacteria (SRB). Dissimilatory sulfur metabolism is a form of anaerobic respiration, or in some cases disproportionation, where in the absence of oxygen (O_2) oxidized sulfur compounds such as sulfate (SO_4^{2-}), thiosulfate ($S_2O_3^{2-}$) and elemental sulfur (S_8^0) are used as terminal electron acceptors and reduced to H_2S (biosulfidogenesis) (Rabus et al., 2006a).

Biosulfidogenesis through reductive dissimilatory sulfur metabolism has been especially studied in environments characterized by elevated concentrations of sulfur compounds such as marine settings (Jørgensen et al., 2019; Jørgensen, 2021), acid mine drainage (AMD) (Sánchez-Andrea et al., 2014a; Florentino et al., 2015, 2016b; Johnson and Sánchez-Andrea, 2019), and acidothermal volcanic waters (Kletzin et al.,

2004). In marine environments, the abundance of SO_4^{2-} (28 mM on average in seawater) supports the activity of sulfate-reducing bacteria (SRB) in anoxic parts of the water and sediment columns where electron acceptors with higher reduction potentials such as nitrate have been depleted. In AMD environments, also characterized by high sulfate concentrations, as well as extreme acidity and metal concentrations, biosulfidogenesis from SO_4^{2-} and other oxidized sulfur compounds in anoxic parts of the water and sediment columns impacts the cycling of (chalcophilic) metals by enabling their (re)precipitation as metal sulfides (Diez-Ercilla et al., 2014; Sánchez-Andrea et al., 2014a; van der Graaf et al., 2020). In contrast to marine and AMD environments, biosulfidogenesis in acidothermal volcanic waters results mostly from the use of S_8^0 instead of SO_4^{2-} as terminal electron acceptor, judging from the low number of hyperthermophilic bacterial and archaeal species capable of dissimilatory sulfate reduction known to date. So far, hyperthermophilic sulfate reduction has been reported in one hyperthermophilic bacterial genus, *Thermodesulfobacterium* (Zeikus et al., 1983; Hamilton-Brehm et al., 2013), and in four hyperthermophilic archaeal genera: *Archaeoglobus* (Zellner et al., 1989): *Caldivirga* (Itoh et al., 1999), *Thermoproteus* (Yim et al., 2015), and *Vulcanisaeta* (Itoh, 2002; Chernyh et al., 2020), although the ability for sulfate reduction in the *Caldivirga* and *Thermoproteus* species was recently disputed (Chernyh et al., 2020). In contrast, a large number of hyperthermo(acido)philic S_8^0 reducers have been described (Florentino et al., 2016b).

Biosulfidogenesis from S_8^0 at acidothermal conditions is of both fundamental and applied interest. Due to its extremely low solubility in water (from 6.1 nM at 4 °C to 478 nM at 80 °C in pure water (Kamyshny, 2009)), S_8^0 is essentially a solid electron acceptor. At more neutral pH, S_8^0-reducers are known to use the soluble polysulfides as the actual electron acceptor (Klimmek et al., 1991; Hedderich et al., 1998), but due to the instability of polysulfides at low pH, acidophilic S_8^0-reducers are expected to use other mechanisms for interaction with solid S_8^0 (Boyd and Druschel, 2013; Florentino et al., 2016b) which remains to be definitively shown. From an applied perspective, acidothermal S_8^0 reduction can contribute to the development of more economical, biosulfidogenesis processes for metal recovery and recycling. Because only two electrons are needed to reduce S_8^0 to H_2S, compared to eight for SO_4^{2-}, using S_8^0 reduces electron donor requirements fourfold, lowering operational costs. Furthermore, biosulfidogenesis at acidothermal conditions enables *in situ* sulfidogenesis in the hot, acidic process waters typical for metallurgy processes, contribution to lower capital expenditures as no separate bioreactor is needed. Thermoacidophilic S_8^0-based biosulfidogenesis for application in metal recovery has only recently been explored (Hidalgo-Ulloa et al., 2020)

We aimed to enrich thermoacidophilic S_8^0-reducing microbial communities, using H_2 as electron donor, S_8^0 as electron acceptor, and Fe^{2+} as reducing agent. However, during the enrichment screenings we observed an unexpected, abiotic sulfide-producing process. We discovered that this was pyrite-mediated abiotic reduction of S_8^0 by H_2, which we describe here in more detail. We performed chemical batch incubations under varying conditions to assess the potential role of different chemical compounds, as well as the influence of pH and temperature. Mineral precipitates forming in the incubations were characterized by X-ray diffraction (XRD), scanning electron microscopy (SEM) coupled to energy dispersive X-ray spectroscopy (EDX), transmission and scanning transmission ((S)TEM) electron microscopy both coupled to EDX, and selected area electron diffraction (SAED) to identify their composition, morphology, particle size, mineralogical nature and crystallinity degree. Abiotic sulfidogenesis from S_8^0 and H_2 mediated by catalytic pyrite under these mild conditions not been described previously, and can expand our understanding of the geological and biological sulfur cycle in acidothermal environments.

Materials & Methods

Anaerobic batch incubations

Incubations were performed in 117 mL glass serum bottles filled with 50 mL of liquid. Original enrichment screenings were performed with minimal medium with 0.1 $g \cdot L^{-1}$ yeast extract (YE) (Becton Dickinson, Cockeysville, MA). Subsequent chemical incubations were performed with either basal medium or acidified demiwater, with or without YE. The basal medium consisted of 2 mM KH_2PO_4, 2.81 mM $(NH_4)_2SO_4$, 1.71 mM NaCl, 0.50 mM $MgSO_4.7H_2O$, 0.75 mM $CaCl_2.2H_2O$, and a modified trace element solution based on (Stams et al., 1993) and the water chemistry of acidothermal volcanic waters as reported in (McCleskey et al., 2005). The final trace element composition (in μM) consisted of 49.4 HCl, 1.0 H_3BO_3 , 0.5 $MnCl_2$, 7.4 $FeCl_2$, 0.5 $CoCl_2$, 0.1 $NiCl_2$, 0.5 $ZnCl_2$, 0.1 $CuCl_2$, 10 NaOH, 0.1 Na_2SeO_3, 0.1 Na_2WO_4, 0.1 Na_2MoO_4, 0.1 $AlCl_3$, 0.5 RbCl, 0.1 $BaCl_2$, 0.1 $SrCl_2$, 0.02 VCl_2, 0.006 $PbCl_2$, 0.004 $CdCl_2$. Basal medium was prepared without vitamins, $CaCl_2$, YE, and $FeCl_2 \cdot 4H_2O$, and boiled to remove oxygen. After boiling, medium was cooled in ice water to room temperature under continuous N_2 sparging. The gas flow was switched to N_2/CO_2 to let the pH equilibrate, after which the pH was adjusted to 3.8, 2.9, or 1.9 with 2 M HCl, depending on the desired starting pH for the original enrichments, and with 1 M – 5 M H_2SO_4 solutions for the later sterile incubations. Cooled medium (47 mL) was then transferred with a liquid dispenser under

N_2/CO_2 flow to 117 mL serum bottles containing 0.040 g of colloidal or orthorhombic chemical elemental sulfur (S_8^0) (Sigma Aldrich, St. Louis, MI) equivalent to 25 mM.

Serum bottles were capped with butyl rubber stoppers (Ochs Larborbedarf, Bovenden, Germany). The headspace was exchanged with N_2/CO_2 or H_2/CO_2 by 5 cycles of vacuum-purging to a final pressure of 1.7 atm (room temperature). Bottles were autoclaved at 105 °C for 30 minutes to prevent melting of S_8^0, which has a melting temperature of 115 °C (Steudel and Eckert, 2003). YE, $FeCl_2$, vitamins and $CaCl_2$ (if applicable) were added after autoclaving from sterile stock solutions to give a final liquid volume of 50 mL. A 1000X vitamin stock solution was diluted 10-fold by addition to a separately autoclaved 75 mM $CaCl_2$ stock solution through a 0.22 μm filter (MDI membrane technologies, Camp Hill, PA, USA) to give a 100x concentrated stock solution (Stams et al., 1993). Ferrous iron was added from a sterile anoxic 1 M $FeCl_2.4H_2O$ solution to a final concentration of 2 mM. For one set of chemical incubations a sterile 1 M $FeCl_3.6H_2O$ stock was used. The pH in these incubations was adjusted after addition of the ferric iron. In one set of chemical incubations without Fe^{2+}, L-cysteine was added as reducing agent to a final concentration of 1 mM. The pH in these incubations was adjusted after addition of the L-cysteine stock. The effect of increased salinity was investigated in acidified demineralized water with 3.0 $g \cdot L^{-1}$ Na_2SO_4 and 21.0 $g \cdot L^{-1}$ NaCl. One chemical incubation was started in medium without YE with amendment of filtered precipitate instead of H_2S and Fe^{2+}, to investigate whether the precipitate alone enabled sulfidogenesis. The amount of precipitate was not quantified, but was obtained from one incubation at the end of sulfidogenesis with material lost during filtration.

For sulfide supplementation, an anoxic 1 M Na_2S stock solution was prepared. Na_2S crystals were rinsed with anoxic water, padded dry and dissolved in anoxic water by weight to a final concentration of 1 M. This solution was diluted (using a 0.22 μm filter) to a ~50 mM sulfide stock solution in sterile anoxic water. This stock was acidified to the desired pH with sterile, anoxic 1 M H_2SO_4. Due to gas-liquid partitioning the final aqueous concentration in the acidified stock was approximately 30 mM, as determined by the methylene blue method (see below). In these acidic sulfide stock solutions, formation of elemental sulfur (judging from the milky appearance within seconds and settled precipitates after several hours) was not prevented. The acidified stock solutions were made fresh on the day of use.

For the original enrichment screenings either H_2 or organic electron donors were tested. For the latter, acetic acid, ethanol, or glycerol were added to a final concentration of 5 mM from 1 M sterile stock solutions with adjusted pH. Enrichment screenings were performed at different combinations of pH (2, 3, 4) and temperature

(70, 80 °C). Samples from the Pisciarelli volcanic area (PSC) (Italy) were used as inocula. For inoculation of the original enrichments, 1-1.5 mL of slurry sample was added with a 1.6 mm needle (Becton Dickinson and Co ltd, Ireland) to minimize size selection of particles. For the enrichments, controls were included for each pH and temperature combination with inoculum and H_2 but no S_8^0, and with inoculum and S_8^0 but no H_2. Chemical controls without inoculum were included with S_8^0 with and without H_2 and with H_2 but no S_8^0.

The subsequent chemical incubations to investigate pyrite formation and chemical sulfidogenesis from S_8^0 and H_2 were performed with either minimal medium with or without YE or with acidified demineralized water with or without YE. Bottles were incubated statically in the dark at 40, 60, or 80 °C, at starting pH of 2, 3, 4 or 6.

Microorganisms

For control purposes, *Acidianus ambivalens* strain LEI 10 (DSM3772) (Zillig et al., 1986) was ordered from DSMZ (Braunschweig, Germany) and maintained according to cultivation conditions prescribed by DSMZ. Control incubations were inoculated from active cultures.

Elemental sulfur type and commercially sourced pyrite

Two different types of elemental sulfur (S_8^0) were used in this study. For the initial enrichments colloidal chemical sulfur was used (Sigma Aldrich, St. Louis, MI). This had a smaller particle size than chemical sulfur and was characterized by a brown color, even though no other compounds than sulfur were reported in the product specifications. After autoclaving medium with colloidal sulfur, the sulfur turned off-white, whereas the liquid was still transparent but had a brown color. In the sterile incubations carried out to investigate the chemical process, orthorhombic elemental sulfur (α-S_8^0) (Steudel, 2020b) was used (Sigma Aldrich, St Louis, MI), which was coarser and had a yellow color.

In addition, control incubations were performed using commercially sourced pyrite (Sigma Aldrich, St. Louis, MI). This pyrite was milled in 2-mL Eppendorf tubes using a laboratory mixer mill (Retsch MM200, Retsch GmbH, Haan Germany) with a 3 mm tungsten carbide bead per Eppendorf (Qiagen GmbH, Hilden, Germany), and sieved to obtain a final particle size of <50 μm. The powder was checked for purity by XRD before incubation (data not shown).

Monitoring incubations

Incubations were monitored by measuring pH and total sulfide concentration in the liquid at the time of sampling. Aliquots were frozen and kept for ion chromatography and determination of dissolved iron concentrations. During sampling, bottles were kept in a water bath to maintain the corresponding incubation temperature. The pH was measured with a pH probe designed for high temperature and low pH (QP150X/12x50/6x150, Prosense, Oosterhout, The Netherlands). The probe was recalibrated at room temperature in fresh buffer solutions at pH 4.0, 7.0 and 10.0 (Acros Organics, Geel, Belgium, or Hamilton, Bonaduz, Switzerland) at each sampling time and preheated to the incubation temperature. Heated buffer standard solutions were used to monitor the performance of the probe at high temperature. The probe was stored in a pH 4 buffer solution or 3 M KCl between sampling points.

At each timepoint, 1.5 mL of liquid was sampled from the bottle with a sterile 3 mL syringe and a 25 mm length, 0.5 mm diameter needle (Becton Dickinson and Co ltd, VV, Ireland). Part of the sample was dispensed in an Eppendorf tube, and the desired sampling volume for the methylene blue assay (100, 50, or 20 µl, depending on the expected sulfide concentration) was withdrawn immediately with a pipet to minimize loss of sulfide (see below). From the remaining sample volume, 950 µl was pipetted into a prepared Eppendorf tube containing 50 µl 99% methanol and stored at -20° C for determination of total dissolved iron and ion chromatography. The remaining sample volume was used to measure pH in a heating block kept at the desired temperature.

Total dissolved sulfide (H_2S_{aq}) was measured using the methylene blue assay (Cline, 1969). Briefly, an assay solution was prepared by adding 50 µL of a 5% Zn acetate solution to 9 mL demineralized water. This solution was then brought to pH > 9 with 2 M NaOH to minimize loss of sulfide. The chosen sampling volume for the methylene blue assay was pipetted into the glass reagent tube with assay solution to fix sulfide as ZnS. After sampling, 1000 µL of reagent A (2 g L^{-1} Dimethyl-p-phenylenediamine and 200 ml L^{-1} H_2SO_4) and 500 µL of reagent B (1 g L^{-1} $Fe((NH_4)(SO_4))^{2}\cdot 12H_2O$ and 0.2 mL·L^{-1} H_2SO_4) were added simultaneously to the sampling tubes and mixed immediately. Absorbance was measured after 10-20 minutes using a Spectroquant Multy colorimeter (Merck Millipore, Darmstadt, Germany) following a pre-programmed sulfide protocol (660 nm), giving a total sulfide concentration in mg·L^{-1}. In subsequent data handling and plotting, values below detection limit were converted to 0.

Sulfate concentrations were determined through ion chromatography on a Dionex ICS2100, using an AS17 column (Thermo Fisher Scientific, Waltham, MA, USA). Samples were run for 20 minutes at 30 °C, at 0.3 mL·min^{-1}. Standard curves were prepared in the range of 2.5 – 20 mM sulfate. 30 µl of samples and standards were diluted in

970 µl 0.25 mM internal standard (KOH), of which 10 µl was injected. Gas samples were analyzed for H_2 content with a Gas Chromatograph (Compact GC 4.0, Global Analyser Solutions, The Netherlands) equipped with a Carboxen 1010 pre-column and a Molsieve 5A column followed by a pulsed discharge detector (PDD). The injection oven was operated at 80 °C, the column oven at 90 °C, and the PDD at 110 °C. Helium was used as carrier gas. A H_2 standard curve was prepared with 1 % (10 000 ppm), 0.1 % (1 000 ppm), 0.001 % (100 ppm), 0.0001 % (10 ppm) and 0.0001 % (1 ppm) H_2 gas mixtures in air. HPLC and GC chromatograms were analyzed with Chromeleon software (Thermo Fisher Scientific, Waltham, MA, USA).

Ferrous iron and total dissolved iron were measured using the ferrozine assay (Stookey, 1970). A 1N HCl extraction step was added at the start (compare with e.g. (Janssen et al., 1996), which was later found to induce Fe^{2+} oxidation in the samples, resulting in differences between ferrous iron and total dissolved iron that were not representative of actual concentrations. This difference was not observed in the standards prepared from a 1 M $FeCl_2{\cdot}4H_2O$ stock solution. When the extraction step was omitted, ferrous iron and total dissolved iron in the samples were equal, and therefore total dissolved iron concentrations are taken to represent ferrous iron concentrations. This is a reasonable assumption, given the low ORP and sulfidic conditions in the incubations.

Data processing and analysis

Data was processed in R (Core Team, 2021) using ggplot2 (Wickham, 2008), ggpubr (Kassambara, 2020) and dplyr packages in the tidyverse (Wickham et al., 2019). Calculations and constants used can be found on https://github.com/mibwurrepo/van-der-Graaf-et-al-2022. For data handling and plotting purposes, values below detection were converted to 0. The Henry gas-liquid partitioning coefficient was corrected for incubation temperature according to the relation

$$k_H(T) = k^{\circ}_H e^{\frac{d(\ln(k_H))}{d(\frac{1}{T})} * (\frac{1}{T} - \frac{1}{298.15K})}$$

using k°_H = 0.1 and $d(\ln(k_H))/d(1/T)$ = 2100 for H_2S, and 0.00078 and 500 for H_2, respectively as tabulated by (Sander, 2021). This was converted to a dimensionless gas-liquid partitioning coefficient (M/M) of 1.0179 for H_2S and 56.7 for H_2 at 353 K.

Geochemical Modeling

The geochemical software package PHREEQCI (Version 3.0.5-7748) (Parkhurst and Appelo, 1999) was used to calculate the theoretical molar equilibrium concentrations

of different sulfide species in solution at varying pH, and the saturation indices (SI) of selected iron sulfide minerals (including pyrite, pyrrhotite, mackinawite and amorphous FeS). All the calculations were conducted using the MINTEQA2 thermodynamic database (Allison et al., 1991). We selected this database because it is the only one, among those provided with the PHREEQCI modelling package, that includes equilibrium constants for different polysulfide species (e.g. S_4^{2-}, S_5^{2-}, S_6^{2-}, …). Based on the concentrations of aqueous Fe^{2+} and H_2S used in the experiments, the ionic activities of all dissolved constituents were calculated. The saturation indices of selected iron sulfides were calculated by using the corresponding solubility products (log Ksp values) included the MINTQA2.V4 database, except for pyrrhotite, which is not included in this database but was taken from (Davison, 1991) and manually introduced in the program. The assumptions for the computations (chosen to resemble the experimental conditions) are indicated in every plot.

Electron microscopy: SEM and (S)TEM

The mineral precipitates formed in the incubations were studied by scanning electron microscopy (SEM) coupled to energy dispersive X-ray analysis (EDX), and transmission and scanning/transmission ((S)TEM) electron microscopy at the SGIker Advanced Research Facilities (UPV/EHU). Precipitates were sampled from incubations by withdrawing 10 – 15 mL of liquid volume with sterile needles and syringes in a Coy anaerobic chamber (Coy Laboratory Products, Grass Lake, MI). Liquid was filtered over a 0.1 μm track-etch 13 mm diameter membrane filter (Whatman Nucleopore, Merck, Darmstadt DE) in a 13 mm Swinnex filter holder (Swinnex, Merck Millipore, Germany). Filter plus precipitates were carefully transferred to a glass Petri dish with forceps and left to dry in the anaerobic chamber. Dried samples plus filters were transferred to 10 mL glass serum vials, which were sealed in the anaerobic chamber before removing. Samples were sent in anoxic vials at room temperature to the SGIker facilities of the University of the Basque Country (UPV/EHU) (Bilbao, Spain).

Solid phase were either transferred onto double-sided adhesive carbon tape and adhered onto a SEM carbon specimen mount (Ted Pella, CA, USA), or the sample was resuspended in ethanol and 3 μL was pipetted onto carbon tape. Prior to SEM analysis the mount went through a plasma cleaning process of 3 min and subsequent carbon-coating. Samples were characterized using the JSM-7000F field emission scanning electron (FEG) microscope (JEOL, Japan) working in both secondary electron (SE) and backscattered electron (BSE) modes at 20 kV beam voltage, 1 nA beam current, 10 mm working distance, vacuum $<8.35 \times 10^{-4}$ Pa and 60 s acquisition time at every

point of chemical analysis of EDX. Raw X-ray intensity values were ZAF corrected using the INCA software (Oxford Instruments, Abingdon, UK) with a set of standards for quantification.

TEM was used to further investigate the elemental composition and identify the mineral phase. For this, the solid fraction was resuspended in either ethanol or MilliQ water in an Eppendorf tube and sonicated. Afterwards, a small volume of 3-5 µL was pipetted on holey carbon-coated TEM support Cu grids (300 Mesh). Imaging, compositional point analysis and SAED analyses of neoformed sulfides were performed on Philips CM200 TEM microscope with LaB6 filament operating at 200 KeV and equipped with DX-4 microanalysis system (EDAX, Pleasanton, CA, USA). Further imaging in high-angle annular dark field (HAADF) mode, elemental mapping and SAED was carried out on FEI Talos F200i Scanning/Transmission Electron microscope ((S) TEM) (ThermoFisher Scientific, Oregon, USA) operated at 200 KeV and incorporating Bruker X-Flash EDX system and FEI Titan Cubed G2 60-300 KV (ThermoFisher Scientific, Oregon, USA) with a gun monochromator, a Cs-objective aberration corrector and Bruker Super-X EDX detector operated at 300 KeV (Bruker, Massachusetts, USA).

X-Ray Diffraction (XRD)

For XRD analysis, samples were transferred onto a sample holder with an optional airtight seal to maintain anaerobic conditions. Analysis was tried both with and without the anaerobic seal, showing no significant influence of exposure to oxygen. Analysis of the bulk mineralogy was performed by powder X-Ray Diffraction (XRD). The XRD analysis was performed with a Bruker D8 Advance diffractometer (Bruker AXS) with Cu-Kα radiation (λ = 0.154 nm) generated at 40 kV - 40 mA in the angular range 10 — 70 ° / 10 — 90 ° (2Θ) with a step size of 0.02 ° and acquisition time of 1.2 s / 3 s per step, and a Lynxeye_XE_T detector. The sample was rotated during the measurement (15 rpm). The X-ray diffractogram was evaluated by the software DIFFRAC.EVA V5.2 (Bruker AXS).

Results

Batch enrichment screening for thermoacidophilic S_8^0 reduction

Because the initial aim of this study was to obtain thermoacidophilic S_8^0-reducing microbial communities, enrichment screenings were performed at different combinations of pH (2, 3, 4) and temperature (70, 80 °C), with organic (ethanol, acetic acid, glycerol) or inorganic (H_2) electron donors. Samples from acidic volcanic hot pools were used as inocula. H_2 as electron donor resulted in the highest H_2S production, but only at a starting pH 4 and 80 °C. These enrichments (with H_2, at pH 4, 80°C) were selected for follow-up investigation, and sulfidogenic activity was maintained during repeated transfers over a period of more than two years. Uninoculated control incubations did not show H_2S production during the same period.

Sulfidogenesis was initially attributed to microbial growth, but the inability to obtain DNA from the incubations through multiple extraction methods, which were validated using both *Acidianus ambivalens* cell pellets and original inoculum samples as positive controls, combined with a lack of conclusive images from both light and electron microscopy led to the hypothesis that a chemical instead of a microbiological process could take place. This self-catalyzing process should then enable sulfidogenesis from H_2 and S_8^0 in these incubations, likely involving the Fe^{2+} supplied as reducing agent. We hypothesized that the sulfidogenic activity maintained upon transfer of active 'culture' was not due to the presence of microorganisms in the active cultures, but of H_2S, enabling a more rapid onset of the chemical process resulting in S_8^0 reduction. The appropriate control for this possibility, addition of H_2S from a sterile chemical stock at time 0, was not considered in the initial experimental design of the enrichment screenings.

Chemical sulfidogenesis from S_8^0 and H_2 involving Fe^{2+}

To test the hypothesis that sulfidogenesis in these incubations was the result of a self-catalyzing chemical process, anaerobic sterile batch incubations were performed at 80 °C, starting pH 4, with H_2, S_8^0, and Fe^{2+}, but with supplementation of H_2S (to H_2S_{aq} of approximately 0.3 - 0.5 mM) from a sterile, acidified stock instead of 'active culture' at time 0. In a first round of experiments this hypothesis was tested in minimal salts medium with YE (Figure 1A), without YE (Figure 1B), or with only acidified demineralized water (Figure 1C) to assess the effect of different medium components. As controls, incubations were performed omitting H_2, H_2S or Fe^{2+} (Figure 1D-F, respectively). In addition, the role of several parameters was investigated: supplementation of Fe^{3+} instead of Fe^{2+} to assess the impact of (partial) oxidation of the $FeCl_2$ stock (Figure 1G),

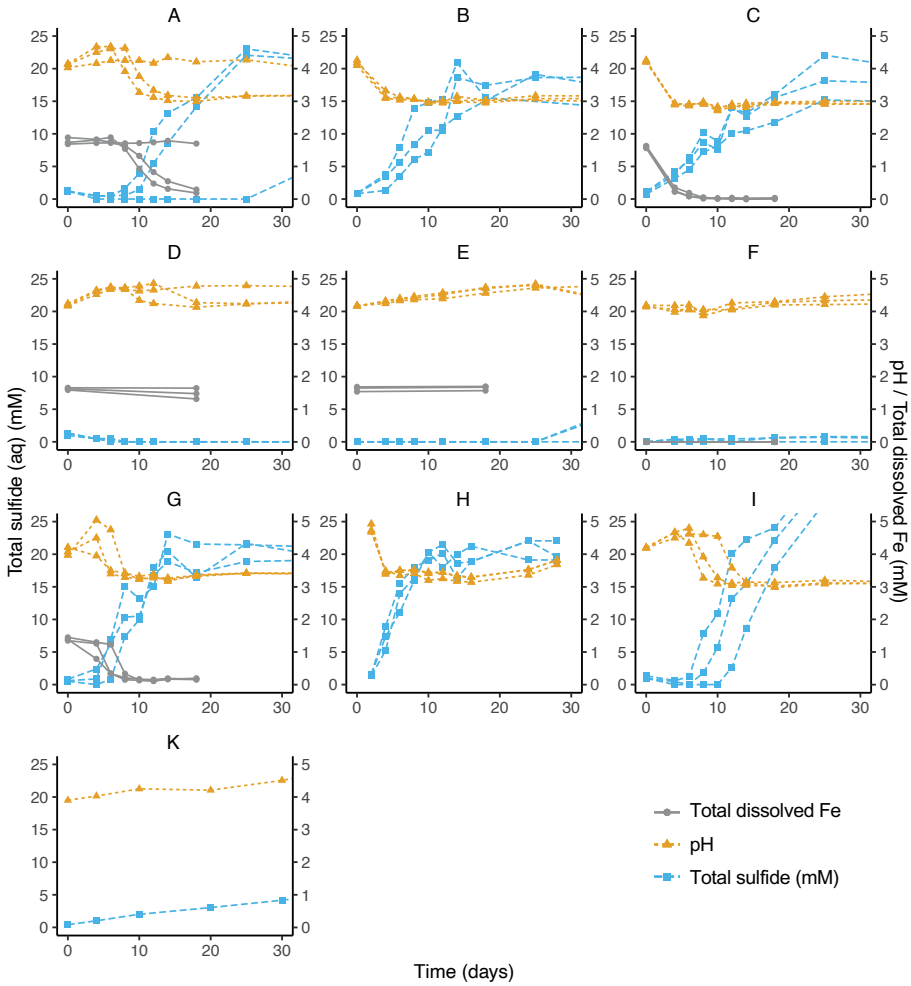

Figure 1: Physicochemical parameters monitored in the chemical incubations: pH (triangles, yellow), total sulfide (squares, blue)) expressed in mM over remaining liquid, and total dissolved iron (circles, grey) with different starting conditions: (A) medium with YE, H_2, Fe^{2+} and H_2S, (B) medium w/o YE, with H_2, Fe^{2+}, H_2S, (C) demineralized water with H_2, Fe^{2+}, H_2S, (D-F) controls: as in (A) but without H_2 (D), without H_2S supplementation (E), or without Fe^{2+} and without H_2S supplementation (L-cysteine as alternative reducing agent) (F), and (G) incubations with Fe^{3+} instead of Fe^{2+}, (H) higher [H_2S] at time 0, (I) 50 mM instead of 25 mM S_8^0, (K) amendment with harvested precipitate instead of Fe^{2+} and H_2S. Total dissolved iron concentrations (mM) and pH are plotted on the secondary y-axis. Incubations were performed in triplicate and individual replicates are shown.

supplementation to higher H_2S starting concentrations to assess the impact on the duration of the lag phase (Figure 1H), or doubling the starting concentration of S_8^0 to 50 mM (Figure 1I). One incubation was started in medium without YE with amendment of filtered precipitate (obtained from one incubation at the end of sulfidogenesis) instead of H_2S and Fe^{2+}, to investigate whether the precipitate alone enabled sulfidogenesis (Figure 1K).

In minimal medium with and without YE and in demineralized water, (near-)complete abiotic reduction of the 25 mM S_8^0 occurred when incubations were supplemented with Fe^{2+}, H_2 and H_2S (Figure 1A-C). When H_2 or Fe^{2+} were omitted, sulfidogenesis did not occur (Figure 1D, F), while without H_2S supplementation at time 0 sulfidogenesis was observed after a longer lag phase (more than 30 days) (not shown). The presence of YE in the medium increased the lag phase and increased the variability between replicates: the lag phase lasted 9 ± 1 days in two of the three triplicates, and more than 25 days in the third replicate (Figure 1A). A similar variability was observed when this incubation was repeated: in two of the three replicates sulfidogenesis started after 8 ± 2.9 days, while in the third replicate the lag phase lasted more than 28 days (not shown). When YE was omitted, the lag phase lasted less than 4 days in all replicates, in both medium and demineralized water (Figure 1B, C). H_2S concentrations in incubations with YE dropped to below detection limit in the lag phase before the onset of sulfidogenesis (Figure 1A). Dissolved total Fe concentrations remained approximately constant during the lag phase (Figure 1A) and started decreasing simultaneously with the onset of H_2S production. When YE was present, dissolved total Fe concentrations dropped to a final concentration of 0.24 ± 0.07 mM (after 18 days in the 2 replicates showing H_2S production) (Figure 1A), whereas dissolved Fe dropped to below detection in the absence of YE (Figure 1C).

In addition to YE, other factors affected the duration of the lag phase. Supplementation with Fe^{3+} instead of Fe^{2+} (only tested in medium with YE) shortened the lag phase considerably, to 5.3 ± 1.2 days, compared to 9.0 ± 1.0 days with Fe^{2+} (Figure 1G). A higher starting concentration of H_2S_{aq} (in medium with YE), of 0.62 ± 0.05 mM instead of 0.51 ± 0.03 mM, shortened the lag phase to less than 2 days (Figure 1H). Doubling the starting amount of S_8^0 to 50 mM had little effect on the duration of the lag phase, to 8.7 ± 3.1 days, but lowered the variability between the triplicates, as sulfidogenesis started in all 3 replicates within a similar timeframe (Figure 1I). In the incubation supplemented with filtered precipitate instead of Fe^{2+} and H_2S, the onset of sulfidogenesis was nearly immediate, showing a linear profile during the entire measurement period, albeit at a much lower rate (Figure 1K). One set of incubations was performed with acidified demineralized water and increased salinity. Rates were

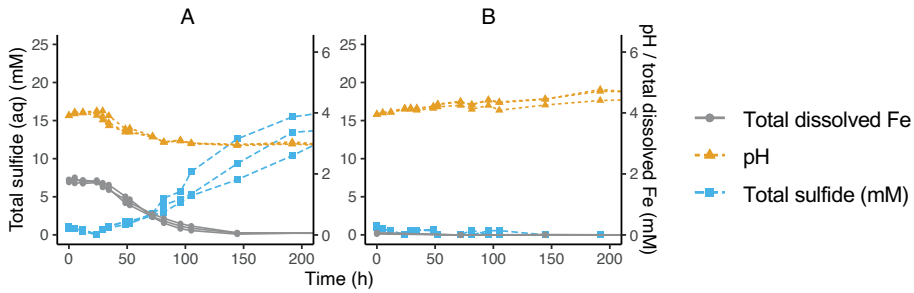

Figure 2: Physicochemical parameters monitored in chemical incubations: pH (triangles, yellow), total sulfide (squares, blue) expressed in mM over remaining liquid (primary y-axis), and total dissolved iron concentrations (mM) (circles, grey) (both on secondary y-axis) in minimal salts medium without YE, with S_8^0, H_2/CO_2, supplementation of H_2S at time 0, and with (A) or without (B) supplementation of 2 mM $FeCl_2$. Incubations were performed in triplicate, and individual replicates are plotted.

not determined, but total [H_2S] expressed over the liquid reached 10.16 ± 2.64 mM after 21 days (supplementary Figure 12B).

Apart from the duration of the lag phase, the pH profiles in incubations with YE also showed differences depending on the incubation parameters. In the presence of YE, the pH increased during the lag phase, from 4.1 ± 0.1 at day 0 to 4.5 ± 0.2 at day 8, before decreasing with the onset of increasing H_2S concentrations to a final pH of 3.2 ± 0.0 (Figure 1A, calculated for the 2 bottles showing sulfidogenesis). A similar pH increase was observed in the absence of H_2 (Figure 1D), from 4.2 ± 0.0 to 4.7 ± 0.0 by day 6, or without initial H_2S supplementation (1E), from 4.2 ± 0.0 to 4.8 ± 0.1 by day 25. At the onset of H_2S production, the pH started dropping, to 3.1 ± 0.1 and 3.0 ± 0.1 in medium with and without YE, respectively (Figure 1A - B) or 3.0 ± 0.1 in acidified demineralized water (Figure 1C). Minimum pH values were reached before sulfidogenesis ceased.

Because incubations without YE were not sampled sufficiently at the start of the incubations to be able to conclude whether a pH increase or H_2S decrease occurred during the lag phase, incubations without YE were repeated and sampled every 4 - 12 hours (Figure 2). In these incubations the lag phase lasted 29 ± 0 h, during which the pH increased slightly, from 3.9 ± 0.0 to 4.0 ± 0.0 in the first 22 hours. The pH then started to drop simultaneously with dissolved Fe concentrations and the onset of H_2S production. In the control incubations without Fe^{2+} the pH increased from 4.0 ± 0.0 to 4.6 ± 0.2 over a period of 8.7 days (Figure 2B). As in the incubations with YE (Figure 1A), H_2S concentrations dropped to below detection before increasing, and the onset of the increase in H_2S concentration coincided with the start of decreasing pH and dissolved iron concentrations.

Investigation of the influence of T and pH

The experiments reported above were conducted at 80 °C, with a starting pH around 4. To investigate the range of temperatures and initial pH at which this process could occur, incubations were performed with both minimal salts medium with YE and demineralized water at starting pH 2 - 6 and 40 - 80 °C (Figure 3). At 80 °C, pH 2, no H_2S production was observed after 45 days, in either medium with YE or demineralized water (Figure 3 A-B). At 60 °C, pH 4, sulfidogenesis was observed in incubations without YE after 12 days, with a similar initial increase in pH in the lag phase and subsequent drop with the onset of increasing H_2S concentrations as observed at pH 4, 80 °C (Figure 1A-C). No sulfidogenesis was detected in the incubations with medium with YE after 56 days (Figure 3C-D). A final measurement after 285 days showed, however, that in the incubations with medium with YE at 60 °C, pH 4, all S_8^0 had been reduced to H_2S (indicated with diamond in Figure 3C). At 80 °C, pH 6, H_2S production started in the first 2 days, both with and without YE (Figure 3E-F). At pH 6, 80 °C the pH did not show a pronounced variation in medium with YE, from 6.2 ± 0.0 on day 0 to 6.1 ± 0.0 on day 24. In demineralized water the pH dropped from 6.1 ± 0.1 on day 0 to 5.7 ± 0.3 on day 24. Incubations at 40 °C were only performed in demineralized water at starting pH 4, and no H_2S production was observed after 24 days. However, a final measurement after 253 days showed a final total H_2S concentration of 24.8 ± 4.5 mM over the liquid, indicating that the process occurs at temperatures as low as 40 °C (not shown).

Comparison of rates of sulfidogenesis

To compare the rates of sulfidogenesis between different incubation conditions, the average rates were calculated from the slope of the linear part of the H_2S curves (Table 1). Total H_2S in liquid and gas phase was expressed in mM over the liquid phase. As indicated above, the incubations with medium with YE showed a high variability between triplicates, which was again observed when this incubation was repeated. Therefore, the average rates were calculated over the two replicates showing sulfidogenesis after approximately 9 days.

The resulting rates were 1.25 ± 0.15 $mM \cdot day^{-1}$ and 1.74 ± 0.70 $mM \cdot day^{-1}$, further underscoring the higher variability in these incubations. In incubations with medium without YE, the rates of sulfidogenesis were similar compared to incubations with YE: 1.30 ± 0.26 $mM \cdot day^{-1}$ (Figure 1B), whereas in acidified demineralized water (without YE) the rates were lower: 0.72 ± 0.13 $mM \cdot day^{-1}$ (Figure 1C). It should be noted that when incubations with medium without YE were repeated and sampled at shorter time intervals, rates of sulfidogenesis were higher: 1.94 ± 0.46 $mM \cdot day^{-1}$. In the incubations supplemented with Fe^{3+} instead of Fe^{2+} (Figure 1G), increased H_2S supplementation

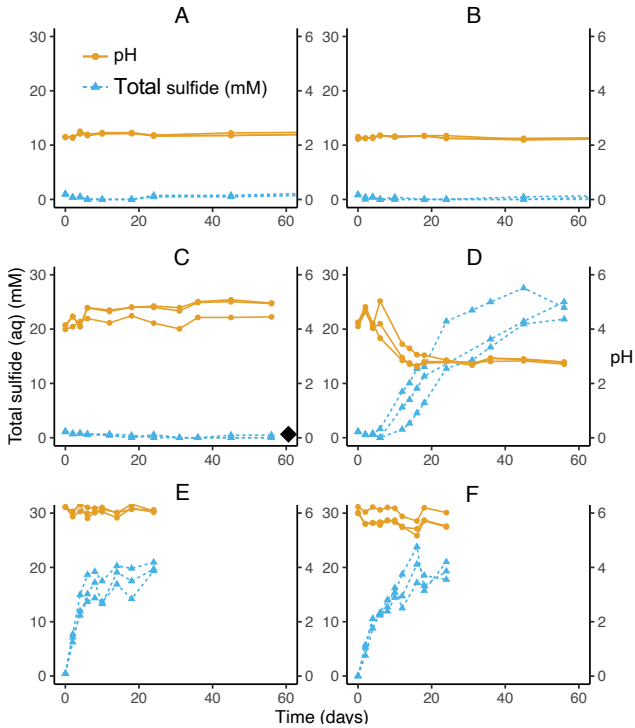

Figure 3: Physicochemical parameters monitored in incubations performed at a wider range of temperature and pH. pH (circles, yellow) and total sulfide (triangles, blue) expressed over the liquid volume in incubations at starting pH 2, 80 °C with medium with YE (A) or dH_2O (B), at starting pH 4, 60°C with medium with YE (C) or dH_2O (D), and at starting pH 6, 80 °C with medium with YE (E) or dH_2O (F). The diamond in (C) indicates that visual inspection indicated that by day 285 all S_8^0 had been reduced to H_2S. The Incubations were performed in triplicate, and individual replicates are plotted.

at time 0 (Figure 1H), or double S_8^0 (Figure 1I), the rates of sulfidogenesis were slightly higher than in medium with YE: 2.02 ± 0.44 mM·day^{-1}, 1.76 ± 0.14 mM·day^{-1}, and 1.93 ± 0.10 mM·day^{-1}, compared to between 1.25 ± 0.15 mM·day^{-1}, and 1.74 ± 0.70 mM·day^{-1}. Interestingly, in incubations performed at 80 °C, pH 6, the rate was higher in medium with YE than in demineralized water, 2.54 ± 0.41 mM·day^{-1} versus 1.09 ± 0.19 mM·day^{-1}, respectively. At 60 °C pH 4, in the first 56 days sulfidogenesis was only observed in demineralized water, at 0.44 ± 0.06 mM·day^{-1}. When incubations with medium and YE were sampled after 285 days, all S_8^0 had been reduced in these incubations, but rates were not determined.

Table 1: Average rates of total H_2S production in mM·day^{-1}. Standard deviations are calculated over triplicates, except for main (1A), this was calculated over 2 of the three bottles, and precipitate (1K) was only performed in one bottle. The corresponding plots in figures 1 and 3 are indicated in brackets behind the descriptions.

Description	H_2 or N_2	S_8^0	Medium (M) or dH_2O	YE	Fe^{2+}	H_2S	Rate (mM·day^{-1})
Medium with YE (1A)	H_2	+	*M*	+	+	+	*1.25 ± 0.15*
Medium with YE-repeat	H_2	+	*M*	+	+	+	*1.74 ± 0.70*
Medium no YE (1B)	H_2	+	*M*	-	+	+	*1.30 ± 0.26*
Medium no YE-repeat	H_2	+	*M*	-	+	+	*1.94 ± 0.48*
dH_2O, no YE (1C)	H_2	+	*dH_2O*	-	+	+	*0.72 ± 0.13*
Medium with YE ,No H_2 (1D)	N_2	+	*M*	+	+	+	-
Medium with YE, No H_2S (1E)	H_2	+	*M*	+	+	-	-
Medium with YE, No Fe^{2+} (1F)	H_2	+	*M*	+	-	+	-
Medium with YE, Fe^{3+} (1G)	H_2	+	*M*	+	*Fe^{3+}*	+	*2.02 ± 0.44*
Medium with YE, Higher H_2S (1H)	H_2	+	*M*	+	+	+	*1.93 ± 0.10*
Medium with YE, 50 mM S_8^0 (1I)	H_2	+	*M*	+	+	+	*1.76 ± 0.14*
Medium no YE, Precipitate (1K)	H_2	+	*M*	-	+	-	*0.24*
60°C, dH_2O no YE (3D)	H_2	+	*dH_2O*	-	+	+	*0.44 ± 0.06*
pH6, Medium with YE (3E)	H_2	+	*M*	+	+	+	2.54 ± 0.41
pH6, dH_2O no YE (3F)	H_2	+	*dH_2O*	-	+	+	*1.1 ± 0.19*

Characterization of precipitates through XRD and SEM-EDX

In all incubations producing H_2S, neoformation of a fine black precipitate was observed, which did not disappear after all S_8^0 had been reduced. The requirement of Fe^{2+} or Fe^{3+} (Figure 1F) suggested that these precipitates were iron sulfides. In order to characterize the precipitates, mineralogical analysis was performed through XRD on samples harvested at different time points along the incubation. In incubations without H_2 harvested after 28 days, representing late lag phase, when H_2S was below the detection limit and S_8^0 appeared 'greyish', S_8^0 was the only crystalline phase identified in the peaks of the diffractogram (Figure 4A). In the sample from early sulfidogenesis (H_2S_{aq} = 1.14 mM) both pyrite (FeS_2) and S_8^0 were identified (Figure 4B-C). Although the higher abundance of S_8^0 compared to FeS_2 in the sample resulted in overlapping peaks at positions characteristic for FeS_2, a clear difference was observed at 2.71 Å, 2.22 Å and 1.92 Å. In the sample from the end of sulfidogenesis (H_2S_{aq} = 6.52 ± 0.51

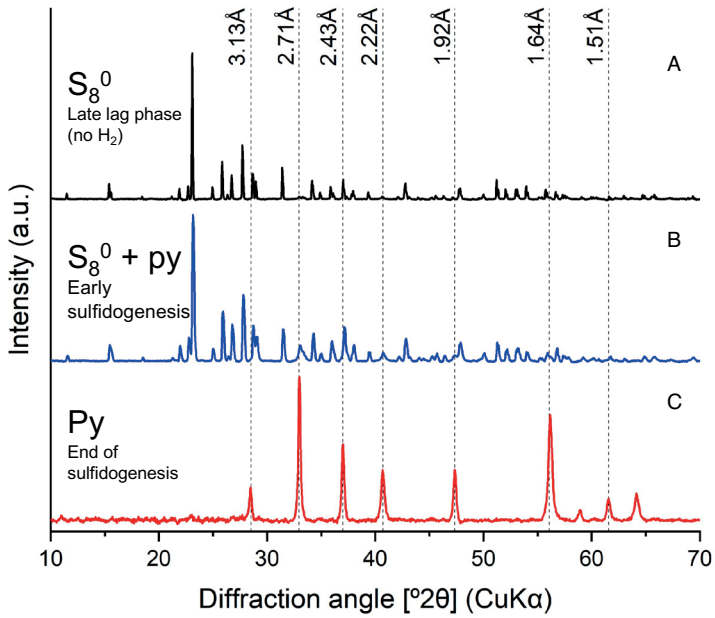

Figure 4: X-Ray Diffraction spectra obtained for precipitates harvested from incubations with medium with YE at (A) after 28 day incubation without H_2 (representing the late lag phase); (B) early sulfidogenesis (H_2S_{aq} 1.12 mM), measured under oxic conditions; and (C) the end of sulfidogenesis (H_2S_{aq} 6.52 ± 0.51 mM) measured under anoxic conditions. No difference was observed between the sampe from B measured under oxic and anoxic conditions. Py: pyrite, S_8^0: orthorhombic elemental sulfur. The dotted lines indicate peak positions characteristic for pyrite as identified in the mineralogical database (ICSD: 01-071-2219). Peaks for sulfur (ACSD: 01-083-2284) are not indicated with lines.

mM), consisting of fine black powder without visible traces of S_8^0, FeS_2 was the only crystalline compound identified through XRD (Figure 4D).

The morphology of the precipitates and the presence of other low-crystalline iron sulfides was investigated with SEM. Samples were harvested from incubations with medium with and without YE at the end of the lag phase and the early stage of sulfidogenesis (H_2S_{aq} < 2 mM). While not detected by XRD, SEM analysis on samples without YE from the late lag phase (H_2S_{aq} below detection, pH 4.1) did show abundant neoformed pyrite growing on larger S_8^0 particles, which were already present before the onset of sulfidogenesis (Figure 5A). This was further supported by the detection of pyrite particles in samples harvested after 8 days (the approximate duration of the lag phase in sulfidogenic incubations) from a control incubation with medium with YE, H_2S and Fe^{2+} but without H_2, (Figure 5B).

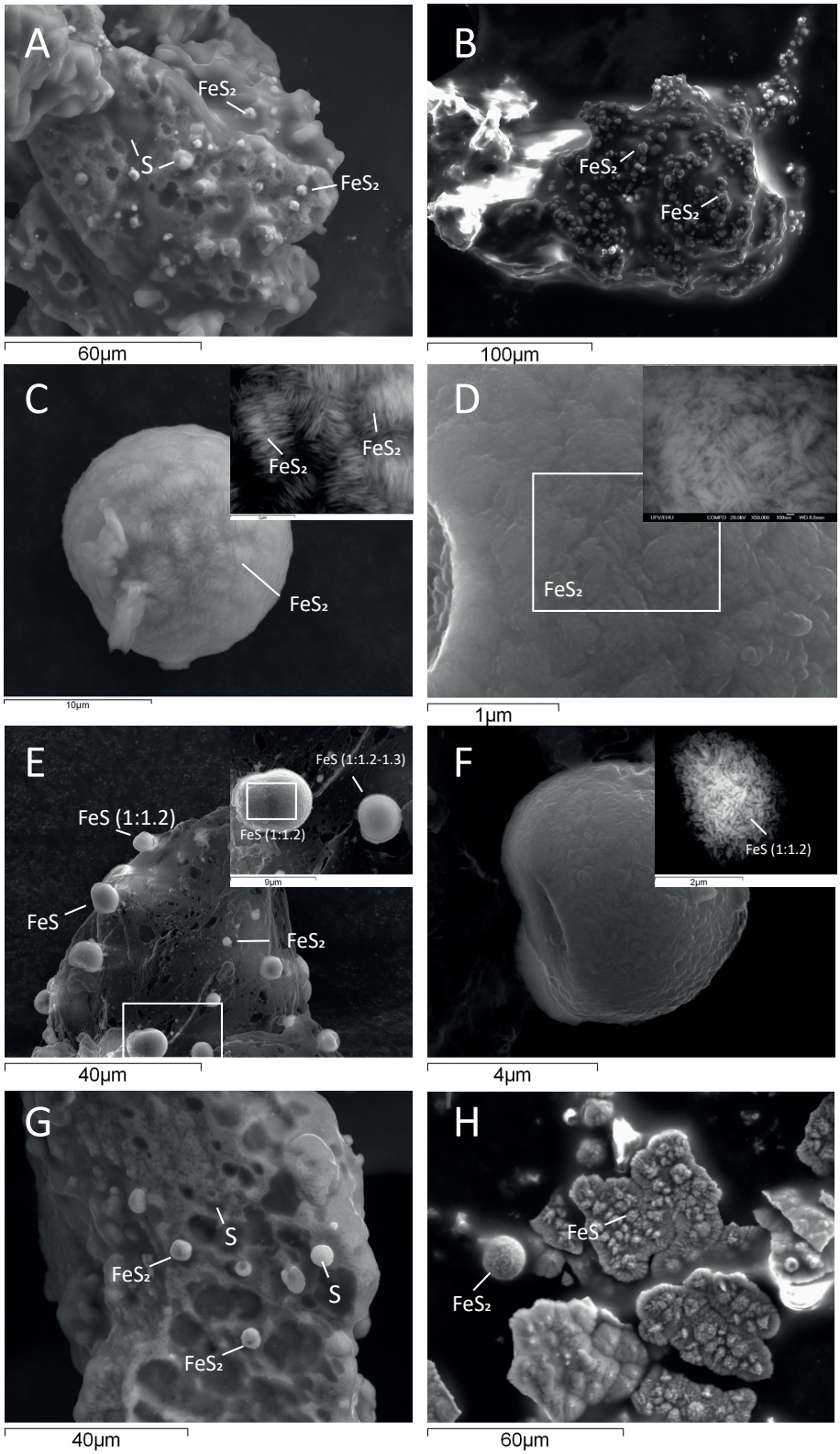
A
FeS₂
S
FeS₂
60µm
B
FeS₂
FeS₂
100µm
C
FeS₂
FeS₂
FeS₂
10µm
D
FeS₂
1µm
E
FeS (1:1.2-1.3)
FeS (1:1.2)
FeS (1:1.2)
FeS
FeS₂
40µm
F
FeS (1:1.2)
4µm
G
S
FeS₂
S
FeS₂
40µm
H
FeS
FeS₂
60µm

Figure 5: SEM images showing pyrite and iron monosulfide (FeS) particles as identified by SEM-EDX. (A, B): pyrite detected before the onset of sulfidogenesis in incubations at [H_2S] still below detection limits with medium without YE, with H_2, (A), and with medium with YE without H_2 (B). (C, D): different surface structure of pyrite particles observed in medium without YE (C) and with YE harvested at early sulfidogensis). The insets are high resolution backscatter electron (BSE) images highlighting individual nanocrystals; (E, F) Iron monosulfides (ratio Fe:S 1:1.1 – 1:1.3) detected in incubations with medium with YE; inset in E is an enlarged secondary electron image of the area indicated by the dotted line; inset in F is a BSE image of F; (G) sulfur particle showing rounded indents as well as FeS_2 and S_8^0 spheres on the surface, harvested from an incubation with medium without YE, at H_2S_{aq} 0.25 mM, pH 3.48; (H) aggregated pyrite particles observed in sample from medium without YE, harvested at 0.51 mM H_2S_{aq}, pH 3.59.

The pyrite particles observed in the different samples were predominantly micrometric spheroids, although in two samples from incubations without YE (0.25 mM H_2S_{aq}, pH 3.5 and 0.51 mM H_2S_{aq}, pH 3.6) pyrite particles were also observed resembling aggregated clumps, possibly a precursor stage to the more spherical particles (Figure 5H) or a type of growth induced by the walls of the glass bottles used. Pyrite precipitates also appeared in larger aggregates of 120 x 60 μm or even larger, likely formed by coalescence of smaller (1-10 μm) spheroids. The spherical pyrite aggregates appeared to be composed of lenticular or acicular nanocrystals displaying varying degrees of organization, with the most ordered particles showing patches of crystals oriented lengthwise in the same direction. This higher degree of organization was already observed in the incubations without YE at a very early stage of sulfidogenesis (H_2S_{aq} 0.25 mM, pH 3.5) (Figure 5C), whereas in incubations with YE this was only observed at a later stage (with higher H_2S_{aq} 1.2 mM, pH 3.8) (Figure 5D). The size of the FeS_2 nanocrystals differed between samples, with nanocrystals of 16-20 nm wide and 160 – 640 nm long in the incubations without YE (Figure 5C), compared to 21-35 nm wide and 70-450 nm long in samples with YE (Figure 5D).

In incubations with and without YE, EDX analysis on several iron sulfide particles showed an Fe:S atomic ratio of 1:1.1 – 1:1.3, suggestive of iron monosulfides (FeS; Figure 5E). However, these FeS particles were far more difficult to detect than pyrite particles, and could not be found in all samples, suggesting low abundance, high reactivity, or both. Upon closer inspection, lenticular or rod-like nanocrystals were observed on the surface of some FeS particles, resembling the nanocrystals seen on the pyrite spheroids, but without a discernable organization (Figure 5F). These crystals were between 140 and 450 nm long and 24 – 94 nm wide. SEM images further indicated a role of the S_8^0 particles in the formation of pyrite. In multiple instances FeS_2 particles were observed on the surface of S_8^0 grains, next to what appeared to be rounded indentations in the S_8^0 surface (Figure 5A, G). This could indicate that the S_8^0 surface served as nucleation site where pyrite formation was favored over the solution. Several spherical particles were identified consisting of only sulfur, indicating that S_8^0 was also present as small globular particles (Figure 5G).

Given the low crystallinity of the precipitates at the start of the incubations, combined with the abundance of S_8^0 masking other less crystalline phases in XRD, (S)TEM analysis was used to investigate the mineralogical evolution of the system in more detail. The combination of high-resolution imaging with punctual EDX analysis and SAED of the same spot allowed determination of mineral phases other than pyrite during the initial stages of pyrite formation and sulfidogenesis. The images showed a morphological evolution from the early non-crystalline precipitates towards acicular nanocrystals in

highly porous aggregates (Figure 6A), and their subsequent agglomeration (Figure 6B). Similar to SEM-EDX, (S)TEM-EDX analysis showed a bimodal distribution of Fe:S atomic ratios of 1-1.2:1 and 0.44-0.5:1, which was coherent with the presence of Fe monosulfide and Fe disulfides. SAED analysis of spots with both Fe and S (confirmed by EDX) showed either no diffraction (not shown), indicating a non-crystalline Fe sulfide precipitate; or a ring pattern (top left inserts of Figure 6A-B), indicating polycrystalline aggregates with randomly oriented discrete nanocrystals, each producing diffraction spots distributed at a certain distance from the transmitted beam (Kohl and Reimer, 2008).

The diffraction pattern of the lower insets were obtained using circular averages of the image intensity as a function of the distance from the ring center (g=1/d in 1/nm). These show wide humps for highly disordered precipitates and evolve to narrower peaks as the order increases. Combining direct ring measurements with the intensity profiles, the diameter of these rings was converted to d-spacings and introduced in American Mineralogist Crystal Structure Database (Robert T Downs and Hall-Wallace, 2003). The elements and Fe:S atomic ratios detected by EDX along with the lowest possible degree of tolerance were used as constraints to determine the most probable mineral phases. The combined results of (S)TEM analysis suggested the presence of pyrite (FeS_2) coexisting with Fe monosulfide pyrrhotite ($Fe_{1-x}S$), which is coherent with the SEM-EDX observations (Figure 5).

Investigation of the role of pyrite in chemical sulfidogenesis and the mechanism of pyrite formation

The identification of pyrite combined with the requirement for Fe^{2+} suggested a crucial role for this iron disulfide in the chemical sulfidogenesis observed in the incubations. To test whether this property was related to specific physicochemical conditions during crystallization, incubations were performed with 2 mM of commercially sourced pyrite (Sigma Aldrich, St. Louis MI, USA), that was milled and sieved to obtain a final particle size of < 50 μm, instead of supplementation with Fe^{2+} and H_2S. Although rates were not determined, Total H_2S concentrations reached 4.93 ± 0.33 mM after 18 days (Figure 7A). No H_2S production was observed after 18 days when milled pyrite and H_2 were incubated without the presence of S_8^0 (Figure 7B), further indicating that H_2S production does not result from direct reductive dissolution of FeS_2 by H_2.

Two main mechanisms of pyrite formation have been described and thoroughly studied to date: the polysulfide pathway and the sulfide pathway (Rickard, 1975, 1997; Schoonen and Barnes, 1991; Graham and Ohmoto, 1994; Rickard and Luther, 1997, 2007), see discussion for more details.

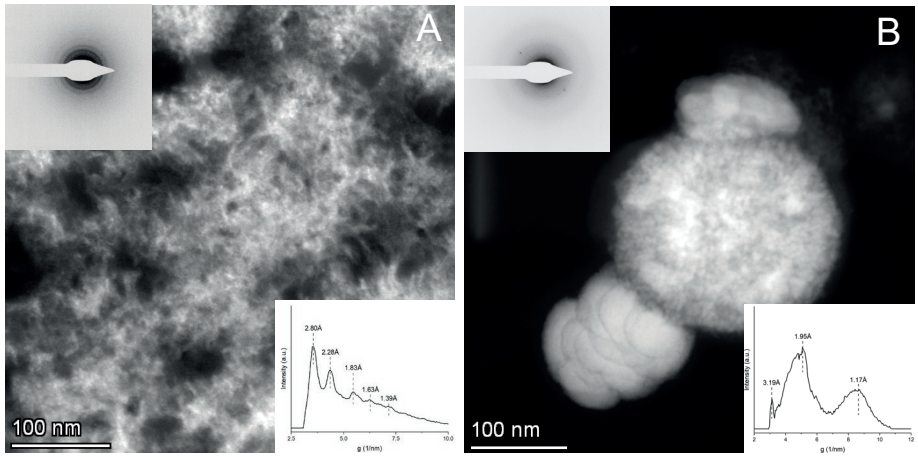

Figure 6: HAADF STEM micrographs of iron sulfide precipitates from different stages of incubation, along with SAED patterns (top left insert) and intensity versus distance (g; 1/nm) profiles (bottom right insert). (A) Acicular nano-crystalline aggregate of pyrrhotite and (B) spherical pyrite aggregate with radial porous structure in sample from medium with YE harvested at pH 3.83, H_2S_{aq} 1.2 mM..

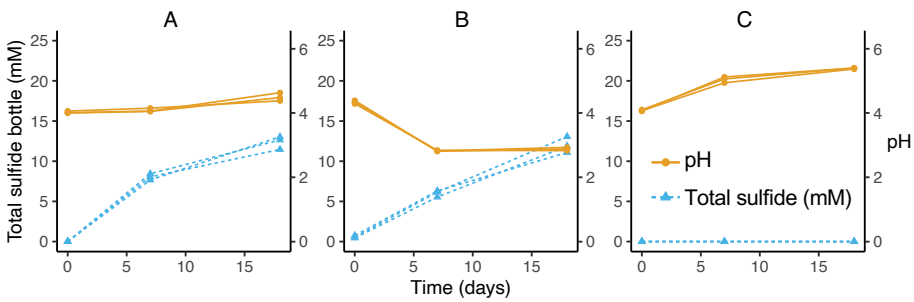

Figure 7: Physicochemical parameters monitored in incubations: pH (circles, yellow) and total sulfide (triangles, blue) expressed in mM over the liquid in incubations with acidified demineralized water and H_2/CO_2 in the headspace, and (A) 2 mM of milled commercially sourced pyrite (particle size <50 μm) with 25 mM S_8^0, (B) a positive control with 2 mM Fe^{2+}, 25 mM S_8^0, and 0.5 mM H_2S amendment at time 0, and (C) milled pyrite but without S_8^0.

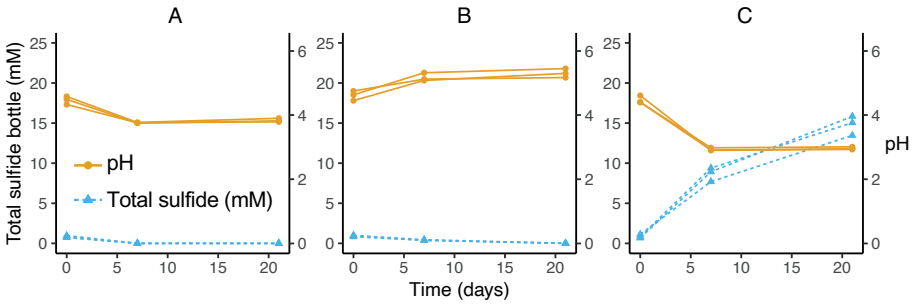

Figure 8: Physicochemical parameters monitored in incubations testing for the production of H_2. pH (circles, yellow) and total sulfide (triangles, blue) expressed in mM over the liquid in incubations with acidified demineralized water, S_8^0, H_2S and (A) N_2/CO_2 and Fe^{2+}; (B) N_2/CO_2 but no Fe^{2+}; or (C) H_2/CO_2 and Fe^{2+}.

Because the sulfide pathway results in the production of H_2, it was inferred that detection of H_2 formation in our incubations would provide strong support for pyrite formation through the sulfide mechanism. Therefore, incubations were repeated with S_8^0, H_2S, Fe^{2+} and N_2/CO_2 instead of H_2/CO_2 in the headspace were repeated (Figure 8A), and composition of the gas phase was monitored using a high sensitivity CompactGC (detection limit of 10 ppm). Incubations with S_8^0, H_2S and N_2/CO_2 but no Fe^{2+} (Figure 8B), and incubations with S_8^0, H_2S, Fe^{2+} and H_2/CO_2 (Figure 8C) were started simultaneously as negative and positive controls.

After 21 days, no H_2 accumulation was observed in the incubations with N_2/CO_2 compared to the controls. In the incubations with N_2/CO_2 and added Fe^{2+}, the pH had dropped from 4.5 ± 0.1 to 3.8 ± 0.1 by day 21 (Figure 8A). H_2 measured in these incubations was 21 ± 7 ppm (Supplementary File 1). In the incubations without amended Fe^{2+} the pH had increased from 4.6 ± 0.2 to 5.3 ± 1.4 (Figure 8B), and H_2 measured in these incubations was 36 ± 19 ppm (Supplementary File 1). In both sets of incubations, H_2S concentrations in the liquid had dropped to below detection on day 21, from 0.82 ± 0.13 mM and 0.92 ± 0.09 mM on day 0, respectively). In the (positive control) incubations with H_2/CO_2, H_2S_{aq} had increased to 14.78 ± 1.21 mM total sulfide expressed over the liquid volume (Figure 8C). In these incubations the pH had dropped from 4.5 ± 0.1 on day 0 to 3.0 ± 0.0 on day 21.

Discussion

The inability to enrich thermoacidophilic sulfur-reducing microorganisms from samples obtained from acidic, volcanic hot pools was unexpected, as these environments are well-known for harboring thermoacidophilic S_8^0 reducers such as *Acidianus* spp. (Amend and Shock, 2001; Kletzin et al., 2004). The absence of microbial activity was likely related to the use of chemical colloidal sulfur, which in a later control experiment was found to inhibit growth of the thermoacidophilic sulfur reducing Archaeon *Acidianus ambivalens* (Supplementary Figure 13). Although no additional compounds were listed by the manufacturer, autoclavation of the colloidal sulfur powder in aqueous medium resulted in a brownish (transparent) color, which might suggest the presence of (an) unidentified compound(s), or the formation of sulfur intermediates. At lower temperatures, use of this same colloidal sulfur did not prevent enrichment of acidophilic S_8^0-reducing communities (pH 2-5, 30 °C) (Florentino et al., 2015), suggesting its potential inhibitory (biocidal) effects could be aggravated at higher temperatures.

The chemical origin of sulfidogenesis in the incubations with H_2 initially went unnoticed because the role of H_2S in the acceleration of the chemical process was not recognized. When H_2S-producing enrichments from the initial screenings were transferred to fresh medium, H_2S profiles resembled microbial growth curves, with a lag phase, followed by an exponential "growth" phase and a subsequent stationary phase. Combined with the absence of H_2S production in the uninoculated incubations, this seemed to demonstrate microbial activity. However, as will be explained below, it was later recognized that sulfidogenesis was not catalyzed by microorganisms, but by the H_2S present in the transferred 'inoculum' from active bottles. This enabled the formation of small amounts of catalytic pyrite, and thereby accelerated the onset of chemical sulfidogenesis from S_8^0 and H_2.

In subsequent chemical (sterile) incubations at acidothermal conditions (pH 4, 80 °C) this phenomenon was investigated in detail, and complete abiotic reduction of S_8^0 (25 mM) by H_2 involving μm-sized spherical pyrite particles was observed (Figure 1). Although chemical sulfide production from S_8^0 in (sterile) high temperature (88 – 110 °C) incubations was shown previously (Belkin et al., 1985), this was ascribed to sulfur disproportionation as it did not require an electron donor such as H_2, and H_2S concentrations only reached on the order of 10 μM after 24 h. In the incubations reported in the current study, however, H_2S concentrations reached 7-8 mM in the liquid, H_2 was required, and no stoichiometric increase in sulfate (SO_4^{2-}) concentrations typical for disproportionation was observed (Supplementary Figure 14). Together with

the thermodynamically unfavorable Gibbs free energy for sulfur disproportionation at already low H_2S concentrations (Finster, 2008), this ruled out chemical disproportionation as the cause of sulfidogenesis in these incubations. Instead, the requirement for pyrite, either through in situ formation from supplemented Fe^{2+} or added from an external source (Figure 1 and Figure 7A), as well as for H_2, indicated that sulfidogenesis resulted from the reduction of S_8^0 by H_2 and was mediated by pyrite, a process that has not been previously described. Both aspects, pyrite formation at acidothermal conditions and pyrite-mediated sulfidogenesis from S_8^0 and H_2, will be discussed in more detail below.

Pyrite formation at acidic, mildly hydrothermal conditions

Pyrite formation has been studied extensively for more than a century, and two main mechanisms for formation are proposed, the polysulfide pathway, or Bunsen reaction, and the sulfide pathway, or Berzelius reaction (Rickard and Luther, 2007), both involving the formation of an (aqueous) Fe monosulfide intermediate (equation 1). In the polysulfide pathway the S in FeS is replaced by a polysulfide, formed from S_8^0 and HS^- (equation 2) through nucleophilic attack (equation 3). In the sulfide pathway, FeS is oxidized to FeS_2 and H_2 (equation 4).

$$Fe^{2+} + H_2S \rightarrow FeS + 2H^+ \quad (1)$$

Polysulfide mechanism:

$$\frac{n-1}{8}S_8^0 + HS^- \rightarrow S_n^{2-} + H^+ \quad (2)$$

$$FeS + S_n^{2-} \rightarrow FeS_2 + S_{n-1}^{2-} \quad (3)$$

Sulfide mechanism

$$FeS + H_2S \rightarrow FeS_2 + H_2 \quad (4)$$

Both the polysulfide and sulfide pathway are thermodynamically favorable at 85 °C (358 K, the tabulated temperature for Gibbs energy of formation at higher temperature according to Amend & Shock 2001) and reactant concentrations present at the start of the incubations ($2 \cdot 10^{-3}$ M Fe^{2+}, $0.5 \cdot 10^{-3}$ M H_2S_{aq}, 10^{-4} M H^+ (pH 4), $1.2 \cdot 10^{-3}$ M H_2 (g), activity of pyrite and S_8^0 of 1): -55.6 and -24.9 kJ·mol^{-1}, respectively (Supplementary Table 1). However, Gibbs energy values just indicate that both mechanisms are thermodynamically feasible at the encountered conditions, and not whether the

kinetics of the two different mechanisms are feasible, as also emphasized in (Rickard and Luther, 2007).

Kinetic studies of pyrite formation through the sulfide and polysulfide pathways (Rickard, 1975, 1997; Rickard and Luther, 1997) resulted in an overall rate equation combining both pathways (Rickard and Morse, 2005; Rickard and Luther, 2007) (equation 5).

$$\frac{dFeS_2}{dt} = k_{H_2S}[FeS][H_2S] + k_{S_n^{2-}}[A_{FeS}]^2[S_8^0][S^{2-}]_{tot}[H^+] \quad (5)$$

In this equation the first and second term represent the sulfide and polysulfide pathways, respectively, with k_{H_2S} and $k_{S_n^{2-}}$ as their respective rate constants. [H_2S], [S_8^0], [$S^{2-}]_{tot}$, and [H^+] reflect the concentration of H_2S, elemental sulfur, total sulfide, and protons, respectively. Although [FeS] appears in both the first and second term, it reflects the total concentration of FeS in the first term, but the total surface area of FeS in the second term (Butler et al., 2004; Rickard and Luther, 2007). This indicated that as long as there was no excess elemental sulfur available, rates of pyrite formation through the polysulfide pathway were orders of magnitude smaller than through the sulfide pathway (Butler et al., 2004; Rickard and Morse, 2005; Rickard and Luther, 2007)

Equation 5 has been used to estimate rates of pyrite formation in environments with neutral pH. Its application at acidic pH to propose the most likely mechanism for pyrite formation in the current study, is not straightforward. Firstly, the rate constants for both mechanisms were determined at more neutral pH values (pH 6 and higher) (Rickard, 1975, 1997) and were not experimentally verified at acidic pH. Furthermore, the rate equations formulated for those conditions might not accurately represent the mechanism of pyrite formation at acidic pH. For example, the surface area of FeS required in the second term is likely not appropriate at acidic pH. At low pH, iron monosulfides will not form larger FeS precipitates, but instead be present as aqueous FeS clusters consisting of between 2 and 250 molecules (Rickard and Luther, 2007), consequently resulting in a very large 'surface area'. Comparing the theoretical rates of pyrite formation through either pathway at the conditions applied in this study to assess through which mechanism pyrite forms, is therefore a rough approximation at best.

It is generally assumed that at more acidic pH values, the sulfide pathway is the dominant mechanism for pyrite formation (Rickard and Luther, 2007; Gartman and Luther, 2013). This is in large part due to the instability and low concentrations of polysulfide at acidic pH (Kamyshny et al., 2004, 2007). However, if pyrite formation in the current study indeed occurred through the sulfide pathway, this would imply the

formation of H_2 (equation 4). Control incubations without H_2 in the headspace showed no accumulation of H_2 after 21 days (Figure 8), while theoretically an H_2 concentration of approximately 0.37 mM could have been reached in the headspace if all H_2S added on day 0 was converted to FeS_2 according to (equation 4), using the dimensionless gas-liquid Henry partitioning coefficient calculated for 80 °C (see supplementary File 2). This would be in the order of 5000 ppm (assuming 1.7 atm total pressure at room temperature), well above the detection limit of 10 ppm determined for the instrument. This could indicate that pyrite formation in our incubations occurs through the polysulfide mechanism, although this is still speculative at this stage, and previous investigations reported difficulties with recovering H_2 from systems where pyrite formed through the polysulfide pathway (Rickard, 1997).

It could be hypothesized that the presence of S_8^0 enabled accumulation of polysulfides at the surface of the S_8^0 grains to concentrations higher than those in the bulk liquid, providing locally favorable conditions for pyrite formation through the polysulfide pathway. The occurrence of FeS and FeS_2 spheroids on the surface of S_8^0 particles, combined with what appeared to be 'dissolution pits' (Figure 5G) could support that the surface of S_8^0 played an important role in pyrite nucleation and crystal growth, as also hypothesized in previous studies on the synthesis of hydrothermal pyrite (Berner, 1969; Graham and Ohmoto, 1994; Ohfuji and Rickard, 2005). In these studies, elemental sulfur particles and liquid sulfur droplets were proposed to provide sites for higher local polysulfide concentrations (Graham and Ohmoto, 1994), making pyrite nucleation on the sulfur surface more favorable. Although these studies considered higher temperatures (150 – 350 °C) and the formation of liquid sulfur droplets from S_8^0, which is unlikely at the conditions tested in the current study, the spherical pyrite crystals synthesized in the presence of excess S_8^0 showed similarities with the pyrite crystals observed here. As in our study, the pyrite spheres in some cases appeared to be embedded in the S_8^0 surface, as if they were 'growing out of' the larger sulfur particles. A similar finding was reported in (Berner, 1969), where pyrite microspheres appeared to be embedded in the surface of sulfur particles.

The spherical shape of the pyrite particles observed in this study is in agreement with previous work indicating that this occurs at high supersaturation of pyrite (Wang and Morse, 1996) and acidic conditions (Morse and Wang, 1997). Equilibrium solubility and speciation calculations of the saturation index for pyrite in our system indicated a high degree of supersaturation (Figure 9). The size of the pyrite spheroids indicates that nucleation was favored over crystallization, which is also typical for supersaturation conditions (Sánchez-España, 2017). Although the pyrite spheres resembled the shape and dimension of framboidal pyrite, no clear framboidal inner structure could be

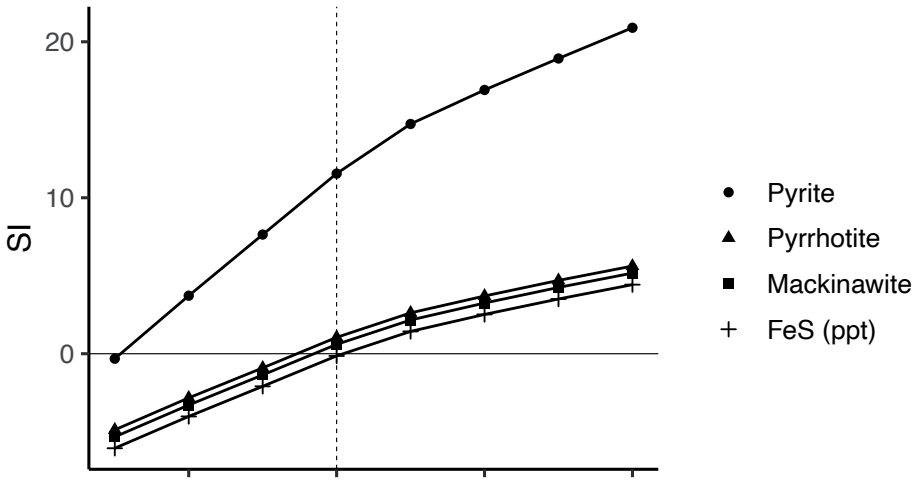

Figure 9: Saturation Index (SI) calculated for selected iron sulfides at 80 °C and pH 1 to 8, using initial total sulfide and ferrous iron concentrations of 1 and 1.5 mM, respectively.

determined, as this would require the spheroids to be composed of densely packed discrete microcrystals of similar dimensions and morphology (such as cubes, octahedra or cuboctahedrons) (Ohfuji and Rickard, 2005). Rather, the pyrite particles appeared to be formed through aggregation of lenticular nanocrystals displaying varying degrees of organization, with the most ordered particles showing interlocking patches of crystals oriented lengthwise in the same direction. This higher degree of organization was observed at a very early stage in the incubations without YE (Figure 5C), whereas in incubations with YE this was only observed at higher H_2S_{aq} (Figure 5D). This suggests an important, partly inhibitory role of the organic compounds from YE in the process of crystal growth and aggregation, which is in line with the inhibitory effects of organic compounds on pyrite formation observed by previous authors (Morse and Wang, 1997). Furthermore, it has been proposed that spherical pyrite could be an indicator for (past) biological activity, and recent work in support of this hypothesis suggested that formation of spherical pyrite particles required the presence of organic matter (Duverger et al., 2021). However, the results presented in the current study counter this hypothesis, as they clearly show that organic matter is not required for the formation of spherical pyrite particles.

The detection of spherical particles with an Fe:S ratio between 1:1.1 and 1:1.3 (Figure 5E), albeit in low abundance compared to FeS_2, suggested the presence of solid iron monosulfides. This was further confirmed by EDX and SAED with the identification of pyrrhotite (Figure 6B), which was also the most likely iron monosulfide to precipitate according to speciation calculations (Figure 9). The surface of these spherical FeS particles appeared to be composed of rodlike nanocrystals, similar to the lenticular nanocrystals observed on the surface of the pyrite spheres (Figure 5D, F). This could indicate that pyrite formation occurred via a solid FeS intermediate, possibly amorphous FeS or pyrrhotite. Alternatively, the recently described 'novel' solid nanocrystalline FeS, referred to as FeS_{nano} (Matamoros-Veloza et al., 2018), should also be considered. Of particular relevance was the observation in that study that the FeS_{nano} phase was stable at acidic pH (< 4.5) and reduced conditions, closely resembling the conditions applied in our study. It could be hypothesized that in our incubations pyrrhotite or FeS_{nano} forms as a solid precursor phase from Fe^{2+} and H_2S in the incubations, and subsequently reacts with polysulfide (or H_2S) to form pyrite. The occurrence of spherical aggregates of acicular FeS particles could suggest that, at least in some cases, this occurred after aggregation of crystals into spheroids. It cannot be excluded, however, that FeS_2 formation also occurred prior to aggregation. It could be speculated that the degree of organization of nanocrystals observed on the spheroid surfaces is related to the order of FeS_2 formation and aggregation. Increased organization could result when aggregation occurs after FeS_2 formation, and a lower degree of organization when formation of FeS_2 from FeS occurs after aggregation. This is highly speculative, however, and requires further investigation. A schematic representation of the proposed steps is given in (Figure 10).

Possible mechanisms for pyrite-mediated sulfidogenesis from S_8^0 and H_2

Pyrite was found to be essential for chemical sulfidogenesis from S_8^0 and H_2 in our incubations, and two scenarios were considered as possible mechanisms for this process: reductive dissolution of pyrite by H_2 to H_2S and to pyrrhotite (equation 6) (Truche et al., 2010; Hassannayebi et al., 2019), or to Fe^{2+} (equation 7); or electron transfer from H_2 to S_8^0 enabled by conductive properties of the pyrite nano-crystals (equation 8) (Faber and Jin, 2014; Faber et al., 2014).

$$FeS_2 + (1\text{-}x)H_2 \rightarrow FeS_{1+x} + (1\text{-}x)H_2S \quad (6)$$

$$FeS_2 + H_2 + 2H^+ \rightarrow Fe^{2+} + H_2S \quad (7)$$

$$H_2 + \frac{1}{8}S_8^0 \xrightarrow{FeS_2} H_2S \quad (8)$$

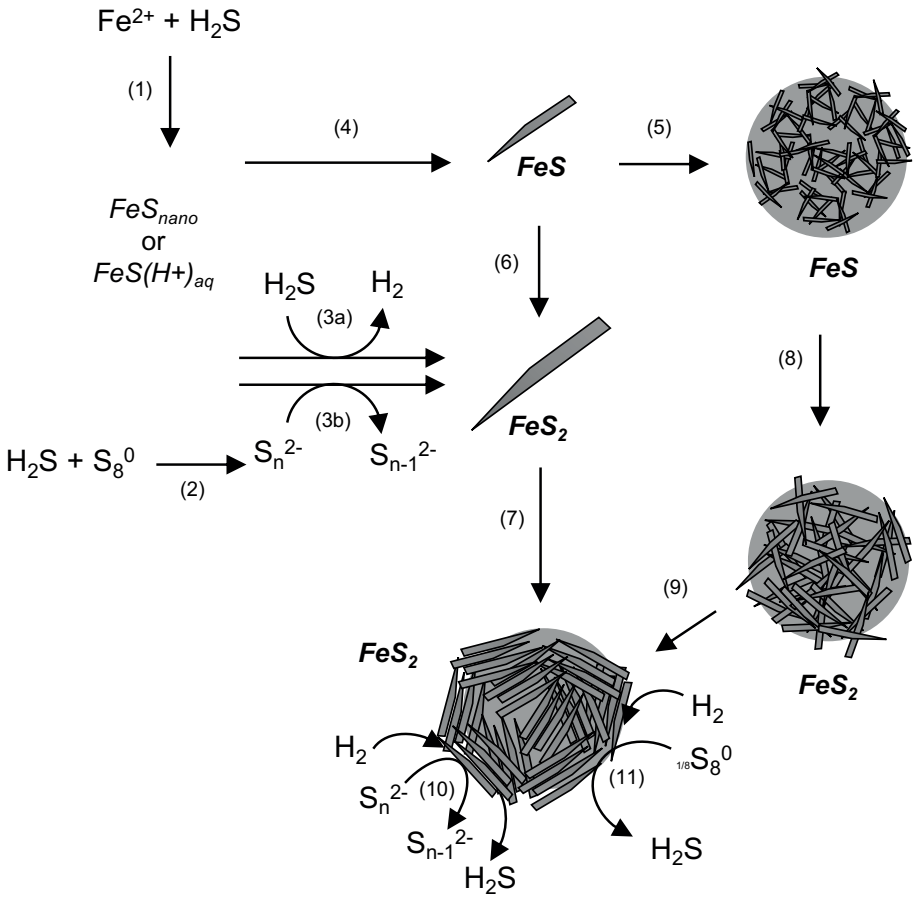

Figure 10: Schematic representation of possible pyrite crystallization and aggregation pathways, and catalytic role of FeS_2 in sulfidogenesis. (1) formation of FeS clusters or aqueous $FeS(H^+)_{aq}$ complexes; (2) formation of polysulfides (S_x^{2-}) from H_2S and S_8^0; (3a) pyrite formation from FeS through the sulfide pathway, (3b) pyrite formation through the polysulfide pathway; (4) formation of FeS lenticular nanocrystals; (5) aggregation of FeS lenticular nanocrystals to form FeS spheroids; (6) formation of FeS_2 from FeS via either the sulfide or polysulfide pathway (see 3a and 3b); (7) organized aggregation of FeS_2 lenticular crystals into FeS_2 spheroids; (8) formation of FeS_2 aggregates from FeS via the sulfide or polysulfide pathway (see 3a and 3b) after FeS aggregation; (9) unknown mechanism for increased organization of FeS_2 aggregates; sulfidogenesis from H_2 and (10) (S_n^{2-}) or (11) S_8^0 catalyzed by pyrite.

In the first hypothesis, reductive dissolution of pyrite by H_2 would regenerate FeS (equation 6) or Fe^{2+} (equation 7) and H_2S, enabling reformation of FeS_2 through reaction with S_8^0 and H_2S (polysulfide mechanism) (equation 1-3). This would then constitute a 'cycle' until all S_8^0 was consumed. Reductive dissolution of pyrite by H_2 was predicted to be possible at elevated H_2 pressures (>8 bar) in the context of nuclear waste disposal (Truche et al., 2010, 2013) and underground H_2 storage (Hassannayebi et al., 2019).

Geochemical modeling of possible interactions between the pressurized H_2 and the minerals in the cave walls indicated that reductive dissolution of certain iron sulfides, especially pyrite to Fe^{2+} and HS^-, was more favorable than generally considered. However, in addition to high H_2 pressures, those studies considered more alkaline pH values, and pyrite dissolution occurred over a longer timescale (months) than observed in our experiments, making it less likely for this process to be occurring in our incubations. Even though pyrrhotite was detected at trace amounts in our incubations (Figure 6), the absence of H_2S production in incubations with only pyrite and H_2 (no S_8^0) (Figure 6B) further indicates that reductive dissolution of pyrite is not occurring. Interestingly, reductive dissolution of pyrite at milder conditions was recently reported in cultures of methanogenic *Archaea* (Payne et al., 2021). These microorganisms, grown at 38 °C, were able to mediate the reductive dissolution of pyrite for use as their sole Fe and S-source, although the exact mechanism enabling reduction is still unknown (Payne et al., 2021) and was not observed to occur in the absence of microorganisms.

The second hypothesis, proposing conductive properties of the pyrite crystals formed in the incubations, is in line with observations that nano- to micrometer-sized pyrite crystals display conductive properties (Faber and Jin, 2014; Faber et al., 2014), predominantly related to the different physical dimensions of the crystals (Hochella et al., 2008). For example, nano- to micrometer-sized pyrite spherules were proposed to confer electrical conductivity in hydrothermal vent chimneys (Nakamura et al., 2010; Yamamoto et al., 2017, 2018). They are furthermore implicated as conductors in microbial extracellular electron transfer (EET) (Nielsen et al., 2010), and are actively investigated for application as more sustainable electrocatalysts in e.g. photovoltaic cells and water electrolyzers (Faber and Jin, 2014). According to this second hypothesis, the pyrite spheroids formed in the incubations here would catalyze the oxidation of H_2 to $2H^+$ and $2e^-$, known as the Hydrogen Oxidation Reaction (HOR), and facilitate the subsequent transfer of the electrons and protons to oxidized sulfur species, resulting in H_2S formation. This hypothesis is strongly supported by the observation that externally sourced pyrite also enabled sulfidogenesis in the presence of S_8^0, while no H_2S increase was observed when S_8^0 was absent, indicating that H_2 does not directly react with FeS_2 (equation 6, 7).

Possible rate limiting factors for pyrite formation and sulfidogenesis

The H_2S production curves (Figure 1) showed that after an initial increase, rates of sulfidogenesis remained constant while Fe^{2+} concentrations continued to decrease. Taking Fe^{2+} as a proxy for FeS_2 formation, this indicated that increasing pyrite concentrations did not result in higher rates of sulfidogenesis, suggesting that something other than

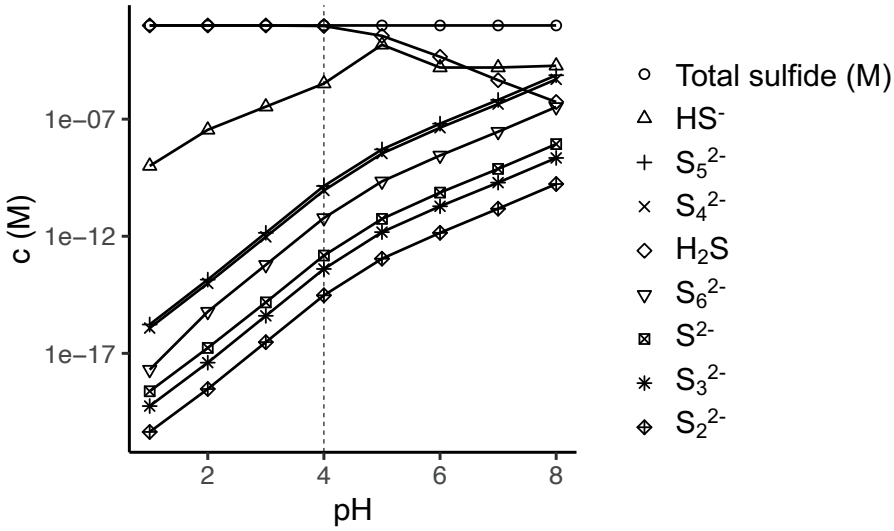

Figure 11: theoretical equilibrium concentrations of sulfide and different polysulfide species (maximum chain length 6) at 80 °C and pH 1 to 8, with total sulfide concentration of 1 mM. Legend is ordered according to order of lines from top to bottom plotted at pH 8.

pyrite availability was rate-limiting. Based on the demonstrated electrocatalytic activity of pyrite towards polysulfide reduction (Faber et al., 2014) it could be hypothesized that the electrons resulting from H_2 oxidation are not transferred to S_8^0 directly, but to polysulfides, which are highly unstable at acidic pH (Kamyshny et al., 2004, 2007; Rickard and Luther, 2007). Calculated equilibrium concentrations of polysulfides at pH 4.0 and 80 °C were in the order of 10^{-10} mol.L^{-1} (Figure 11), which is in agreement with previously reported values (Boyd and Druschel, 2013). Assuming that the rate of polysulfide formation is lower than their rate of reduction at the pyrite surface, the availability of the electron acceptor would be a rate-limiting factor. It could be speculated that the increased rates and the shorter lag phase observed when Fe^{3+} was supplemented instead of Fe^{2+} are related to this. Under reducing conditions in the presence of H_2S, Fe^{3+} is reduced to Fe^{2+} and elemental sulfur (Roberts et al., 1969) with a smaller particle size than the chemical sulfur added to the incubations initially. Because the rate of polysulfide formation is proposed to depend on the surface area of elemental sulfur instead of its concentration (Kleinjan et al., 2005), an increased particle size would enable an increase in the rate of polysulfide formation and thereby of sulfidogenesis.

The pH profiles observed in the different incubations suggest the consumption of protons in the lag phase. This was clearly visible in incubations with medium and yeast extract (Figure 1 A) but was also observed when incubations without YE were repeated and sampled at shorter time intervals (Figure 2A). The cause for the pH increase has not been determined. Control incubations without addition of H_2S (Figure 1E) initially appeared to suggest that the pH increase was related to interaction between Fe^{2+} and S_8^0, as no clear pH increase was observed in the incubations with L-cysteine instead of Fe^{2+} as reducing agent (and no H_2S supplementation at time 0) (Figure 1F). However, in subsequent incubations, a pH increase was observed in control incubations with medium without YE, supplemented with H_2S but no Fe^{2+} (Figure 2B), similar to (Figure 8B), suggesting the pH increase is related to interaction between H_2S and S_8^0, possibly for polysulfide formation. However, it is not clear how polysulfide formation from sulfide and S_8^0 would be net consuming of protons (equation 2), and the cause for the pH increase remains to be elucidated.

The presence of YE clearly delayed the initial formation of pyrite, as indicated by the longer lag phase, but did not appear to be a rate-limiting factor for sulfidogenesis, since in medium with and without YE rates were similar (Table 1). It should be noted, however, that when incubations using medium with and without YE were repeated in a second batch of experiments, higher rates were measured: 1.25 ± 0.15 and 1.30 ± 0.26 $mM \cdot day^{-1}$ compared to 1.74 ± 0.70 and 1.94 ± 0.48 $mM \cdot day^{-1}$, indicating that a possible batch effect should be considered when interpreting these values. In contrast to YE, the use of demineralized water versus minimal salts medium did appear to lower the rates of sulfidogenesis: 0.72 ± 0.13 $mM \cdot day^{-1}$ in demineralized water compared to 1.30 ± 0.26 for medium without YE. This could suggest that the ionic strength of the medium played a role in the process, or alternatively that the presence of certain medium components affected the conductive characteristics of the pyrite crystals, for example through the incorporation of trace metals in the pyrite crystals, or by influencing the size of the pyrite particles. Although the effect of crystallization conditions on the rates of sulfidogenesis could not be determined from this study, the observation that finely milled pyrite also catalyzed sulfidogenesis from S_8^0 and H_2 suggests that the size of the pyrite particles might be a more important factor than their (surface) morphological characteristics.

If pyrite formation in our study indeed occurred through the polysulfide pathway, as argued above, the key role of polysulfides could (partly) explain the lag phase observed before the onset of sulfidogenesis. Polysulfides are highly unstable at acidic pH (Kamyshny et al., 2004, 2007), resulting in very low maximal concentrations, and affecting reaction rates. In addition, kinetic studies of polysulfide formation from sulfide

and S_8^0 showed that their formation through nucleophilic attack of S_8^0 by HS^- (equation 2) displayed autocatalytic behavior (Kleinjan et al., 2005). Their initial formation was slow, but accelerated once polysulfides were formed, since they themselves acted as nucleophiles (equation 9-10).

$$S_n^{2-} + S_8^0 \rightarrow S_{n+8}^{2-} \quad (9)$$

$$S_{n+8}^{2-} + HS^- \rightarrow S_n^{2-} + S_9^{2-} + H^+ \quad (10)$$

This resulted in a characteristic 'S-curve', with a lag phase at the start (Kleinjan et al., 2005). In that study, performed at pH 8.0 and 50 °C, the lag phase was on the order of minutes and was shortened by higher initial sulfide and S_8^0 concentrations. This was still much shorter than the lag phase observed in the current study, 9 ± 1 days in medium with YE, or 29 h without YE. However, even though according to the Arrhenius equation increasing temperature (80 °C versus 50 °C) could be expected to increase reaction rates, the HS^- concentration at acidic pH is extremely low (< 0.1 % of H_2S_{aq} at pH 4.0). Because concentrations impact reaction rates, this likely was a rate-limiting factor for the initial formation of polysulfide, which would contribute to a longer lag phase if pyrite formed through the polysulfide pathway. Furthermore, it is important to note that, similar to studies of pyrite formation, the pH applied in the current study (<4.0) is outside the pH range commonly considered in studies of polysulfide formation and kinetics (> 5.5), and that kinetic parameters have not been experimentally validated for more acidic conditions (Kleinjan et al., 2005; Kamyshny et al., 2007, 2009; Avetisyan et al., 2019; Kafantaris and Druschel, 2020).

Conclusions

We described a previously unconsidered chemical process for pyrite-mediated sulfidogenesis from S_8^0 and H_2. The experiments focused predominantly on conditions found in hot, acidic environments (pH 4, 80 °C), but the process was also observed to occur at lower temperatures (40 °C) and higher pH (pH 6). Pyrite was hypothesized to have a catalytic role, predominantly related to its size, since both in situ formed pyrite and externally sourced, milled pyrite mediated sulfidogenesis from H_2 and S_8^0. Organic matter in the form of yeast extract increased the duration of the lag phase preceding sulfidogenesis, and resulted in less organized FeS_2 nanocrystals on the surface of the pyrite spheroids. Spherical pyrite particles formed both in the presence and absence

of YE, countering the hypothesis that spherical pyrite is an indicator for the presence of organic matter. The role of polysulfides in both pyrite formation and sulfidogenesis was not experimentally determined, but it is proposed that polysulfides might play a more important role at acidic pH than generally assumed. Although polysulfide determinations at acidic pH are notoriously difficult, detailed determination of their chemistry and associated kinetics at low pH are greatly needed, both in the context of chemical reactions as described here, and in the context of the fundamental questions surrounding microbial S_8^0 reduction at acidic pH.

Acknowledgements

This study was funded by the research program TTW under project number 14797, which is financed by the Dutch Research Council (NWO) to IS-A, by a Gravitation grant (SIAM 024.002.002) of the Netherlands Ministry of Education, Culture and Science to AS, and by the Spanish Ministry of Economy, Industry and Competitiveness through the National Research Agency (FEDER funds, grant CGL2016-74984-R) to JSE and IY. The authors gratefully acknowledge personnel support provided by SGIker facilities of the University of the Basque Country (UPV/EHU), especially for the SEM, S/TEM, and XRD work (Ana Martínez-Amesti, Sergio Fernández, and Javier Sangüesa). We thank Jan Weijma, Henk Dijkman, and Jan Klok for helpful discussions. We thank Ilse Gerrits from the WUR XRD facility for expert technical assistance, and Hennie Halm from WUR for help with pyrite milling.

Supplementary Information

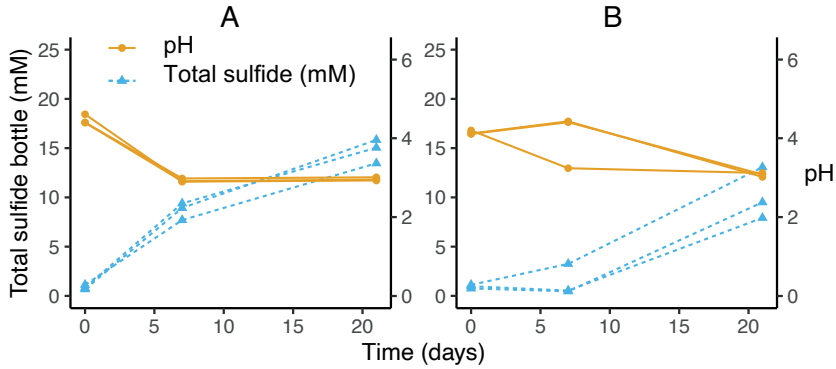

Figure 12: pH (black) and total sulfide (red) expressed in mM over the liquid in incubations with S_8^0, H_2/CO_2, Fe^{2+}, H_2S and (A) acidified demineralized water, or (B) acidified demineralized water with 3 g/L Na_2SO_4 and 21 g/L NaCl.

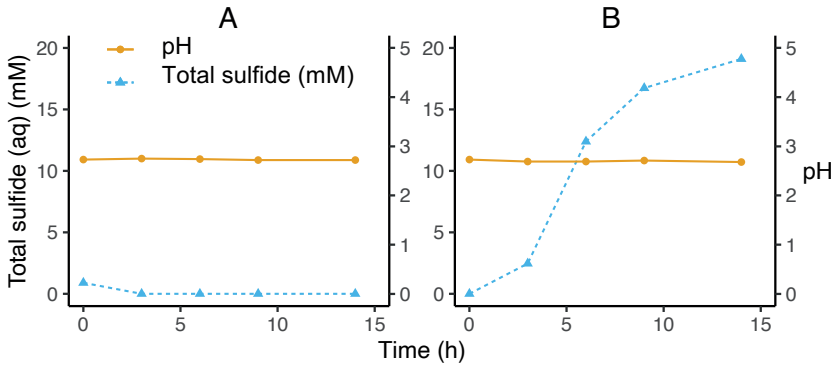

Figure 13: pH (black) and total sulfide (red) of Acidianus ambivalens (DSM3772) grown with H_2 and colloidal sulfur (circles) and chemical sulfur powder (triangles) in DSM medium 358.

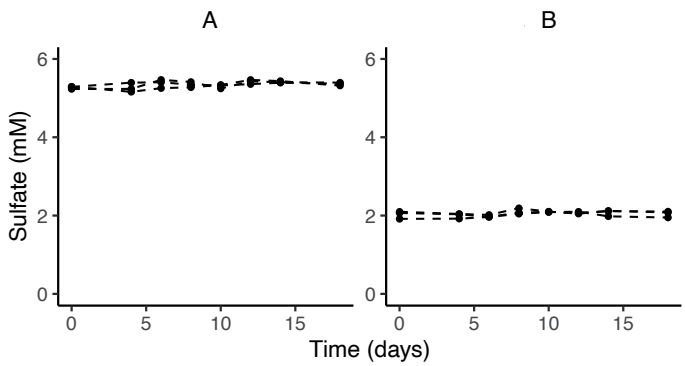

Figure 14: sulfate concentrations (mM) (black circles) in incubations with (A) medium plus YE (compare figure 1A) and (B) acidified demiwater (compare figure 1C) during the first 18 days of incubation.

Supplementary Data 1: Gibbs Free energy calculations for pyrite formation through the polysulfide and sulfide pathways at the conditions used in the current study.

Estimating the Gibbs free energy change of pyrite formation through the polysulfide and sulfide pathway

Overall reactions

polyulfide pathway $Fe^{2+}(aq) + H_2S(aq) + 1/8\ S^0 \Rightarrow FeS_2(s) + 2\ H^+(aq)$

sulfide pathway $Fe^{2+}(aq) + 2\ H_2S(aq) \Rightarrow FeS_2(s) + 2\ H^+(aq) + H2(aq)$

T, pH, chemical composition				activity coefficients (Amend et al. 2019)	
Temperature	358	K	Use 85'C to match tabulated values		
	concentration		**activity**	2+ at 0.001 m	0.86
H+	0.0001	M	0.000096	1+ at 0.001 m	0.96
H2S	0.0005	M	0.0005	0 at 0.001 m	1.00
Fe2+	0.002	M	0.00172		
S0	0.025	M	1		
FeS2	?		1		
H2 (see below)	0.0012	M	0.0012		

calc dGo from dGf0; calculate Q and then overall dGr

NB: T-corrected dGf0 is taken from Amend and Shock 2001, they corrected dGf0 for T and p with integral, using revised-HKF)

dGr0 = SUM dGf0

dGr = dGr0 + RTlnQ

dGf0 from Shock & Amend 2001				Polysulfide pathway dGr0 (kJ/mol)				Sulfide pathway dGr0 (kJ/mol)			
	dGf0	dGf0	dGf0	$Fe^{2+}(aq) + H_2S(aq) + S^0 \Rightarrow FeS_2(s) + 2\ H^+(aq)$				$Fe^{2+}(aq) + 2\ H_2S(aq) \Rightarrow FeS_2(s) + 2\ H^+(aq) + H2(g)$			
compound	**298 K (25'C)**	**343 K (70'C)**	**358 K (85'C)**	**reaction 1**	**298 K (25'C**	**343 K (70'C**	**358 K (85'C**	**reaction 1**	**298 K (25'C**	**343 K (70'C**	**358 K (85'C)**
$Fe^{2+}(aq)$	-91.5	-86.66	-85.02	-1	91.5	86.66	85.02	-1	91.5	86.66	85.02
H2S (aq)	-27.92	-34.12	-36.39	-1	27.92	34.12	36.39	-2	55.84	68.24	72.78
S0 (s)	0	-1.51	-2.04	-0.125	0	0.18875	0.255	0	0	0	0
FeS2 (s)	-160.22	-162.81	-163.76	1	-160.22	-162.81	-163.76	1	-160.22	-162.81	-163.76
2 H+ (aq)	0	0	0	2	0	0	0	2	0	0	0
H2 (g)	0	-5.97	-8.00	0	0	0	0	1	0	-5.97	-8
H2 (aq)	17.72	14.62	13.39	0	0	0	0	0	0	0	0
				dGr0 (kJ/m	**-40.8**	**-41.8**	**-42.1**	**dGr0 (kJ/m**	**-12.9**	**-13.9**	**-14.0**

Polysulfide pathway				Sulfide pathway			
R	8.314 J/(K*mol)			R	8.314 J/(K*mol)		
Q = (FeS2 * [H+]^2)/(Fe2+ * H2S * S0)				Q = (FeS2 * [H+]^2 * H2)/(Fe2+ * H2S^2)			
Q corrected for activity				Q corrected for activity			
Q	**lnQ**	**RTlnQ**	**dGr**	**Q**	**lnQ**	**RTlnQ**	**dGr**
0.0107	-4.536	-13.50	-55.6	0.0257	-3.661	-10.90	-24.9

Supplementary Data 2: GC measurements and calculation of theoretical maximum H_2 concentration attainable via sulfide pathway.

H2 GC - standards & samples

Standards	Area (raw measurements)			ppm		
	0	standards day 7	standards day 21			
3000 ppm H2, CH4, CO, 35		0.1848	0.1981	3000	3000	
air		0.0004	0.0005			
0.0001% H2 0.2 mL		0.0005	0.0006	1	1	
0.001% H2 0.2 mL		0.0022	0.0011	10	10	
0.01% H2 0.2 mL		0.008	0.0063	100	100	
0.1% H2 0.2 mL		0.0922	0.089	1000	1000	
1% H2 0.2 mL		0.7175	0.7135	10000	10000	
air		0.0003	0.001			
	a (slope)	0.00007	0.00007			

	Area (raw measurements)			ppm (=AREA/slope)			mM (using molar V of 100% gas at 1.7 atm) see below			uM	
Sample	0	7	21	0	7	21	0	7	21	ave d21 (uM)	stdev
46A-1		0.0011	0.0020		15.7	28.6		0.0011	0.0020		
46A-2		0.0016	0.0021		22.9	30.0		0.0016	0.0021		
46B-1		0.0023	0.0010		32.9	14.3		0.0023	0.0010		
46B-2		0.0020	0.0011		28.6	15.7		0.0020	0.0011		
46C-1		0.0050	0.0009		71.4	12.9	Ave	0.0050	0.0009		
46C-2		0.0049	0.0016		70.0	22.9	21 +- 7 ppm	0.0049	0.0016	0.0015	0.0005
47A-1		0.0019	0.0039		27.1	55.7		0.0019	0.0039	1.4597	0.5279
47A-2		0.0025	0.0045		35.7	64.3		0.0025	0.0045		
47B-1		0.0012	0.0017		17.1	24.3		0.0012	0.0017		
47B-2		0.0012	0.0017		17.1	24.3		0.0012	0.0017		
47C-1		0.0010	0.0018		14.3	25.7	Ave	0.0010	0.0018		
47C-2		0.0014	0.0015		20.0	21.4	36 +- 19 ppm	0.0014	0.0015	0.0025	0.0013
air		0.0004	0.0004		5.7	5.7		0.0004	0.0004	2.5336	1.3301

Theoretical max [H2]

From % to ppm to mM at specific pressure

		mM ideal gas	
%	**ppm**	**1 atm**	**1.7 atm**
100	1000000	41.45331	70.470635
10	100000	4.145331	7.047063
1	10000	0.414533	0.704706
0.1	1000	0.041453	0.070471
0.01	100	0.004145	0.007047
0.001	10	0.000415	0.000705
0.0001	1	4.15E-05	0.000070

Molar volume gas n/V = p/(RT)

p (atm)	1	1.7
p (Pa)	101325	172252.5
R	8.314	8.314
T	294	294
n/V (mol/	0.041	0.070
V/n (L/m	24.1	14.2

Heating to 353 results in pressure:

p (Pa) (353K)=nRT/V	206820
p (atm)	2.04

Henry's constant > conversion to mol/L /

298K	**353K**	
0	-0.00052	
0.0008	0.0006	(mol/kg*bar)
1282.1	1663.7	bar/(mol/kg)
43683.8	56687.6	(mol/m3)/(mol/kg)
43.68	**56.69**	**(mol/l)/(mol/l)**

Theoretical maximum H2 concentration

H2S (aq) at time 0 is approximately 1 mM (total in bottle expressed over 50 mL liquid)
so total mmol added is 1 mM * 0.05L = 0.050 mmol

total mmol H	0.050	mmol
Assuming:	Fe2++ 2H2S -> FeS2 + H2 + 2H+	
Then	0.025	max mmol H2 formed

What is speciation of this H2 over liquid and gas phase?

Henry C (353	56.69	mM(gas phase)/mM(liqui
V liq (L)	0.050	
V gas (L)	0.067	
c liq (mM)	0.0065	
c gas (mM)	0.3683	
check	0.025	mmol

How much ppm would this be, assuming 1.7 atm at RT to calculate molar volume of gas

n/V ideal gas	70.5	mM	=100 % = 1.000.000 ppm
theoretical r	**5226.1**	ppm	

Biological sulfur reduction in a H_2/CO_2-fed bioreactor operated at neutral (pH 6.9) and acidic (pH 3.8) conditions using neutrophilic industrial sludge as inoculum

Hidalgo-Ulloa, A.[1*]; van der Graaf, C.M.[2*]; Buisman, C.J.N.[1]; Sánchez-Andrea,I[2**]; Weijma, J.[1]

[1]Department of Environmental Technology, Wageningen University & Research, Wageningen 6708 WG, the Netherlands;
[2]Laboratory of Microbiology,
Wageningen University & Research, Wageningen 6708 WE, the Netherlands;
[*]These authors contributed equally
[**]corresponding author

Abstract

Biosulfidogenesis is a promising technology for the selective recovery of chalcophile bulk metals (e.g. Cu, Zn, and Co) from metal-contaminated waters such as acid mine drainage (AMD) and metallurgy waste streams. The use of elemental sulfur (S_8^0) instead of sulfate (SO_4^{2-}) as electron acceptor reduces electron donor requirements four-fold, lowering process costs, and can expand the range of operating conditions to more acidic pH. We previously investigated autotrophic S_8^0 reduction using an industrial mesophilic granular sludge as inoculum under thermoacidophilic conditions. Here, we examined the effect of pH on the S_8^0 reduction performance of the same inoculum, in a continuously fed gas-lift reactor run at 30 °C under neutral (pH 6.9) and acidic (pH 3.8) conditions. Steady-state volumetric sulfide production rates (VSPR) dropped 2.3-fold upon transition to acidic pH, from 1.79 ± 0.18 g $S^{2-}\cdot L^{-1}\cdot d^{-1}$ to 0.71 ± 0.07 g $S^{2-}\cdot L^{-1}\cdot d^{-1}$. Microbial community analysis via 16S rRNA gene amplicon sequencing showed that at pH 6.9, *Sulfurospirillum, Sulfurovum* and *Desulfurella* were the most abundant S_8^0-reducers, while at pH 3.9 *Desulfurella* dominated the sequenced reads. The detection of acetic acid and the abundance of *Acetobacterium* at pH 6.9 pointed towards acetogenesis, explaining the dominance of the heterotrophic genus *Sulfurospirillum* in this H_2 and CO_2–fed bioreactor.

Introduction

Metal removal from hydrometallurgical streams through metal sulfide precipitation is advantageous compared to more commonly used chemical neutralization methods, as it enables pH-dependent selective metal recovery at sufficient purity for recycling (Lewis, 2010). Microbial sulfide production (biosulfidogenesis) is a preferred source of hydrogen sulfide (H_2S), as it can be carried out on-site and modified to meet process demands (Johnson and Sánchez-Andrea, 2019). Although biosulfidogenic processes have been commissioned on an industrial scale (Huisman et al., 2006; Adams et al., 2008), predominantly based on sulfate (SO_4^{2-}) as the electron acceptor, the technology is not widely used in the hydrometallurgical industry, partly due to the operational expenditure (OPEX) related to substrate requirements (Sun et al., 2020a). Substrate utilization can be lowered by using elemental sulfur (S_8^0) instead of SO_4^{2-} as electron acceptor, as this enables a theoretical fourfold decrease in the electron donor consumption for the same amount of sulfide generated (Florentino et al., 2016b).

Further process optimization and reduction of the OPEX and CAPEX (capital expenditure) can be achieved by integrating biosulfidogenesis and metal recovery in one reactor unit, where hydrogen sulfide production occurs in the hydrometallurgical process waters (Kumar et al., 2021). These waters are often characterized by high acidity (pH < 4) and, depending on the upstream mineral leaching process, high temperature (40 – 80 °C). This requires sulfidogenic microbial communities that can thrive under these conditions. Previously we investigated a S_8^0-reducing continuous gas-lift bioreactor operating at thermoacidophilic conditions (pH 3.6, 60°C), using a neutrophilic industrial granular sludge as inoculum, and H_2 and CO_2 as electron donor and carbon source, respectively (Hidalgo-Ulloa, personal communication). Under these operating conditions, we observed a volumetric sulfide production rate (VSPR) up to 270 mg $H_2S \cdot L^{-1} \cdot d^{-1}$, which is up to fivefold lower than those obtained in other studies at mesophilic temperatures, both at acidic (pH 6.5-2.1) (Sun et al., 2020b) and neutral pH (Sun et al., 2018; Zhang et al., 2018). Although differences in system configuration do not allow direct comparison, this could suggest that lower VSPR are reached at higher temperatures. In addition, thermophilic conditions can have disadvantages such as bioreactor corrosion, or formation of secondary minerals, causing valuable leached elements to uncontrollably re-precipitate, decreasing the metal recovery yield intended with this technology (Batty and Rorke, 2006; Hedrich et al., 2018).

We hypothesized that higher VSPR could be achieved in our system at lower temperatures. Therefore, we followed up on our previous study by investigating reactor performance at mesophilic temperature (30 °C), and both neutral (6.9 ± 0.1),

and acidic pH (3.8 ± 0.1), using the same neutrophilic granular sludge as inoculum. By comparing the steady-state VSPR achieved in this study with those achieved under thermoacidophilic conditions, we identified possible limitations of our system. Furthermore, we investigated the adaptability of the original inoculum by determining the microbial community composition in the two pH regimes through 16S rRNA gene amplicon sequencing.

Materials and methods

Reactor configuration and inoculum preparation

We operated a glass gas-lift reactor with a working volume of 4 L, using wet granular sludge originated from a sulfate-reducing bioreactor with low methane production at the industrial chemical plant Getec park (formerly Emmtec), located in Emmen, the Netherlands (Hulshoff Pol et al., 2001)as inoculum. The inoculum was prepared with 400 g (25 g dry weight) of the industrial wet granular sludge (henceforth Emmen sludge), which prior to inoculation was suspended in 500 mL of demineralized water. The pH of the suspension was corrected to 6.9 using a 1 M H_2SO_4 solution. The sludge suspension was sparged with N_2 gas at 25 mL·s^{-1} for 60 minutes and successively inoculated in the gas-lift reactor.

At the start of reactor operation, mineral media (3 L) was added, and was sparged with N_2 gas at a rate of 25 mL·s^{-1} (1 h). Subsequently, N_2 gas was substituted with a mixture of H_2 gas (>99.999%, Linde Gas Benelux B.V) and CO_2 (>99.99%, Linde Gas Benelux B.V) with a gas rate equal to the initial operating conditions (1 h). Concurrently, 10 g S_8^0·L^{-1} of biological elemental sulfur (henceforth S_8^0) was added to the reactor. The mineral media was composed of (in mM): $CaCl_2$·$2H_20$, 0.75; KH_2PO_4, 0.6; $(NH_4)_2SO_4$, 0.55; NaCl, 5.13; $MgSO_4$·$7H_2O$, 0.49. A trace element solution (1 mL per liter of culture medium) was added, containing (in mM): $ZnSO_4$·$7H_2O$, 3.48; $CuSO_4$·$5H_2O$, 8.01; $MnSO_4$·H_2O, 5.92; $NaMoO_4$·$2H_2O$, 2.28; $CoCl_2$·$6H_2O$, 2.47; Na_2SeO_2, 2.78; $Fe_2(SO_4)_3$ · H_2O, 3.75; H_3BO_4, 1; $NiCl_2$·$6H_2O$, 4.21. Only during the batch operation, 0.1 g·L^{-1} BBL yeast extract was added as an initial carbon source. After 38 days of operation, we determined ammonium deficiency in the reactor; thus, we increased the concentration of $(NH_4)_2SO_4$ from 0.55 mM to 2.53 mM to satisfy the microbial demand of the nutrient. The preparation of the sulfur used in this study and origin is described in detail by Hidalgo-Ulloa et al. (2020).

The reactor was initially operated in batch mode for six days. Subsequently, mineral media was continuously fed to the reactor through a feed port using a peristaltic pump (Watson Marlow 120U, UK), maintaining a constant hydraulic retention time (HRT) at 2.5

days and temperature at 30 °C, respectively. H_2 and CO_2 were supplied as sole electron and carbon donors, and the influent gas flow was controlled using two mass flow controllers (Bronkhorst EL-FLOW F-201CV, the Netherlands). Enhanced gas transfer and mixing were achieved by recirculating the gas at a rate between 50-80 $L \cdot h^{-1}$ using a vacuum pump (KNF Neuberger type N820.3FT.18, Germany). Influent media was continuously sparged with N_2 (O_2<0.5 ppmv, Linde Gas Benelux B.V., the Netherlands), to maintain the anaerobic conditions. Settleable solids and suspended biomass were retained using a 1.1 L external glass settler and recirculated to the reactor using a peristaltic pump (Watson Marlow Qdos 30 equipped with a ReNu 30 Santoprene pump head), at the same rate of the influent flow. The reactor, settler, and gas condenser temperature were maintained using two heat exchanger units (Julabo F25-HL, Germany). All connectors and tubing were made of PTFE (Serto A.G, Germany), Tygon A-60-G (Saint-Gobain, France) and Marprene (Watson Marlow, UK). During the continuous operation, S_8^0 was added to the reactor in batch through a feed port. The amount of S_8^0 supplied was based on a mass balance over the sulfide produced. Sulfide productivity was assessed from the effluent gas, where sulfide was scrubbed from the effluent gas using a 5M NaOH scrubbing solution.

The volumetric sulfide producing rates (VSPR) were estimated from the sulfide concentration in the gas effluent scrubber over the period of time elapsed between two measurements

$$VSPR = \frac{C_{S^{2-}SCBt_{n+1}} - C_{S^{2-}SCBt_n}}{t_{n+1} - t_n} \cdot \frac{V_{SCB}}{V_R} \qquad (1)$$

Where the *VSPR* is expressed in g $S^{2-} \cdot L^{-1} \cdot d^{-1}$, $C_{S^{2-}_{SCB}}$ is the sulfide concentration in the scrubber (g $S^{2-} \cdot L^{-1}$) at time $t_{(n, n+1)}$, V_{SCB} is the scrubber volume (L), V_R is the effective working reactor volume (4 L), and t_n and t_{n+1} are the sampling time (days) at time *n* and *n+1*, respectively.

This research intended to examine the sulfidogenic capacity of the granular sludge at neutral (6.9 ± 0.1) and acidic (3.8 ± 0.1) pH. The operation was started at neutral pH. A 0.1 M NaOH solution was used to maintain a constant pH, for the pH tended to decrease during operation at neutral pH. Steady-state was considered reached when the standard deviation of the average VSPR measured during ten consecutive operational days remained within 10%. Once steady-state conditions were reached, the reactor pH was decreased to 3.8. The pH was decreased and maintained using a 0.1 M H_2SO_4 solution during the initial 14 days of the acidic pH regime. However, to limit the contribution of sulfate reduction to the VSPR, the pH control solution was replaced with a 0.1 M HCl solution. Additionally, different influent H_2 and CO_2 flow rates were tested. The

reactor was initially fed with 2.8 $L \cdot h^{-1}$ of H_2 and 0.7 $L \cdot h^{-1}$ of CO_2. The H_2 influent was increased to 5.6, 11.2, and 28 $L \cdot h^{-1}$ along the process and subsequently decreased to 8 $L \cdot h^{-1}$ until reaching steady-state. Likewise, The CO_2 influent was increased to 2 $L \cdot h^{-1}$ and afterward decreased to 0.7 $L \cdot h^{-1}$ until reaching steady-state.

Microbial community analysis

The microbial community was investigated through 16S rRNA gene sequencing. Triplicate samples from Emmen anaerobic sludge used as inoculum and from washed S_8^0 were harvested by centrifugation and stored at -20°C until further processing. The anaerobic sludge was initially collected from the Emmen plant in January 2018 and kept in a 10 L container at 4 °C at our laboratory. Samples for DNA extraction were obtained from this batch in March 2020, and in June 2021, six months after the start of the reactor. Samples for microbial community analysis along reactor operation were obtained on days 24, 59, 73, 101, 118 and 130, using a 60 mL syringe connected to a line reaching the center of the reactor vessel. Lines were pre-flushed before sampling. Triplicate samples of 20 mL each were drawn at each time point, and immediately centrifuged in 50 mL Falcon tubes for 20 min at 4700 rpm (4120 x g). The supernatant was discarded, and pellets were stored at -20°C until further processing. DNA extractions were performed on the triplicate samples using the FastDNA Spin Kit for Soil (M.P. Biomedicals, OH, USA), according to the manufacturer's instructions. DNA concentrations were measured using a Qubit 2.0 fluorometer (Life Technologies, Darmstadt, Germany), with the Qubit dsDNA B.R. assay kit. The V4-V5 region from the 16S rRNA gene was amplified using PCR with barcoded revised Earth Microbiome Project (EMP) primers (Thompson et al., 2017): 515F (GTGTGYCAGCMGCCGCGGTAA) and 806R (CCGGACTACNVGGGTWTCTAAT). PCR amplification was performed in a total reaction volume of 50 µL, containing 10 µL 5X H.F. buffer, 200 µM of dNTP, 10 µM of barcoded forward and reverse primers, 2 $U \cdot \mu L^{-1}$ Phusion Hot Start II DNA polymerase (ThermoFisher Scientific), and 0.4 $ng \cdot \mu L^{-1}$ DNA template. As negative control, nuclease-free water was used. The cycling protocol consisted of an initial 30 s denaturation step at 98 °, followed by 28 cycles of 10 s denaturation at 98 °C, 10 s annealing at 56 °C, and 10 s elongation at 72 °C. A final elongation step was done for 7 min at 72 °C. Duplicate PCR reactions were performed for each sample, checked on gel, and pooled before cleanup with magnetic beads using the CleanNA PCR kit (G.C. Biotech B.V., The Netherlands). Cleaned samples were pooled at equimolar amounts into a final library, which was also cleaned with magnetic beads and eluted in 50 µL. PCR amplicons were sequenced in 150 bp paired-end reads on an Illumina HiSeq at Novogene (Novogene Bioinformatics Technology Co. Ltd, Beijing, China).

Paired-end amplicon sequences were processed using NG-Tax 2.0 on the Galaxy platform https://ngtax.systemsbiology.nl (Poncheewin et al., 2020). Sequences were clustered into Amplicon Sequence Variants (ASVs) using a *de novo* clustering approach, and the following default settings: forward and reverse read length 70 nt, ratio ESV abundance 2, classify ratio 0.8, minimum percentage threshold 0.01, identity level 100%, error correction of 1 mismatch. The filtered reads were demultiplexed per sample, keeping only the reads with perfectly matching barcodes. Taxonomy was assigned to the ASV's using the SILVA SSU rRNA reference database v138 (Quast et al., 2013b; Yilmaz et al., 2014). Results were exported as a .biom1 file for further analysis with R (Core Team, 2021) in RStudio, using the phyloseq (McMurdie and Holmes, 2013), microbiome (Lahti and Shetty, 2017), ggplot2 (Wickham, 2008), ggpubr (Kassambara, 2020) and dplyr packages in the tidyverse (Wickham et al., 2019). Alpha diversity was calculated on rarefied data (sample size 22050). Beta diversity was calculated on non-rarefied relative abundance data. R scripts and input files can be accessed at **https://github.com/mibwurrepo/Hidalgo-Ulloa-et-al-2022**. Sequences are available at the European Nucleotide Archive (ENA) at EMBL-EBI under project number PRJEB50572, and submission number ERA8814161.

Chemical Analysis

Detailed description of the procedures and equipment used for these analyses can be found in Hidalgo-Ulloa et al. (2020). In brief, sulfate, phosphate, and thiosulfate were measured by ion chromatography on a Dionex ICS 6000 equipped with an IonPac AS17-C analytical column (4x2550 mm), and a AS17-C guard column (Dionex, USA) eluted at 30 °C with potassium hydroxide (5 mM, 0.25 $mL \cdot min^{-1}$). Volatile fatty acids (VFA) were measured with a GC system Agilent 7890B equipped with a flame ionization detector and an HP-FFAP column (25m × 0.32mm). Total organic carbon (TOC) was determined during steady-state of both pH regimes. TOC was determined using a TIC-TOC analyzer (TOC-L CPH/CPN series, Shimadzu, Japan), equipped with a non-dispersive infrared detector (NDIR). Inorganic carbon was removed by the acidification of the sample with 1 M H_2SO_4, and the produced CO_2 flushed with CO_2-free synthetic gas (C_xH_y<1 ppm, Linde Gas Benelux B.V) and the sample injected at 720 °C. Free dissolved sulfide and ammonium were analyzed using Hach Lange kits LCK-653 and LCK-303, respectively (Hach, Germany). Free sulfide samples were diluted in anaerobic water and preserved using a solution with 12 mM sodium hydroxide and zinc acetate. Headspace gas composition was analyzed through gas chromatography.

Results

Sulfidogenic productivity

During the initial six days of operation, the reactor was operated in batch, after which the continuous feed of mineral media to the reactor was started. During the next 40 days of operation, several interruptions to the continuous operation arose due to the high concentration of granular sludge in the reactor which obstructed the influent and recirculation lines. These interruptions delayed reaching steady-state conditions. A summary of these events is provided in the supplementary material (S.I.1).

The reactor was operated in a neutral and acidic pH regime. In the neutral pH regime, the pH was maintained at 6.9 ± 0.1. The steady-state during this regime was reached on day 92 of operation, with an average VSPR of 1.787 ± 0.177 g $S^{2-}\cdot L^{-1}\cdot d^{-1}$ (Figure 1). Sulfate reduction occurred along during the entire operation, however, its contribution to the VSPR was limited. Under this regime, S_8^0 reduction accounted for 98.5% of total VSPR, whereas sulfate reduction, supplied to the reactor as macronutrient salts, accounted for the remaining 1.5 ± 0.5% of the VSPR at steady-state conditions (98 % reduction of sulfate loaded). During the neutral pH regime, we observed the formation of thiosulfate in the reactor liquor (S.I.2).

After the steady-state criteria in the neutrophilic regime were satisfied, on day 103, we decreased the pH of the reactor (Figure 1). The pH during this regime was controlled and maintained at 3.8 ± 0.1. Steady-state conditions were reached 17 days after the transition to acidic pH, and were maintained during 10 more days (day 120-130). The pH decrease had an immediate decreasing effect on the VSPR. During steady-state, an average VSPR of 0.705 ± 0.068 g $S^{2-}\cdot L^{-1}\cdot d^{-1}$ was observed, a 2.5-fold decrease of the VSPR was observed during the neutral pH regime. During the initial operation at acidic conditions, the pH was controlled using a 0.1 M H_2SO_4 solution. However, after 15 days (day 118) the pH control solution was replaced with a 0.1 M HCl solution to limit the contribution of sulfate reduction to the VSPR (Figure 1). Sulfate reduction accounted for 5.1 ± 0.2% of the total VSPR during this regime. Despite the relative increase of sulfate reduction during the acidic regime, the absolute sulfate reduction remained equivalent to that at neutral pH. In steady-state conditions during the acidic regime, the VSPR from sulfate reduction was 0.334 g $S^{2-}\cdot L^{-1}\cdot d^{-1}$, while at neutral pH this was 0.329 g $S^{2-}\cdot L^{-1}\cdot d^{-1}$. No thiosulfate was detected during operation at acidic pH (S.I.2).

During the initial 48 days of operation, we observed an increase in concentrations of VFAs, reaching a maximum of 1474 mg $VFA\cdot L^{-1}$ on day 48. Subsequently, VFA concentrations decreased to below the limit of detection (LOD) (< 2.5 $mg\cdot L^{-1}$) on day 64 (Figure 2). Acetate accounted for the majority of VFA production during this period

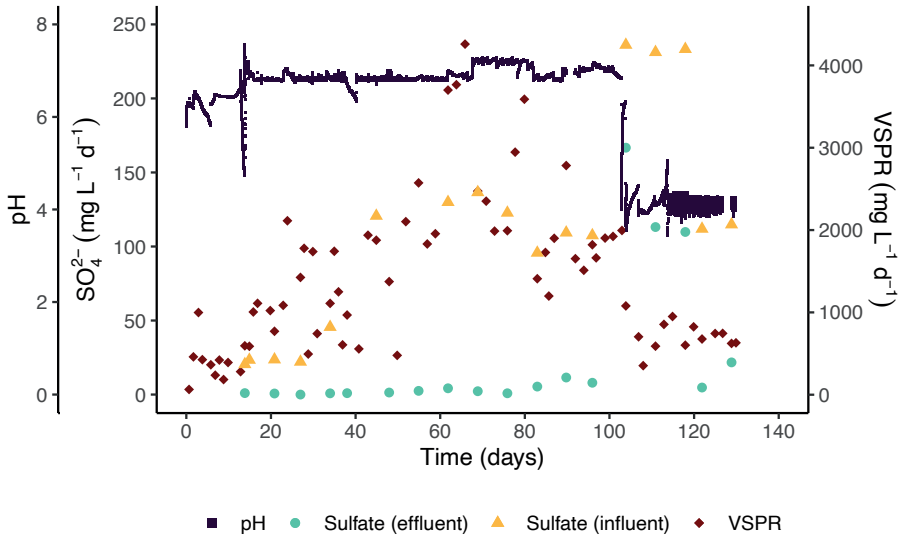

Figure 1: Volumetric sulfide production rates (VSPR) of the Emmen sludge in the 4L gas lift reactor (secondary axis, blue circles) contrasted with the pH changes (primary axis, orange circles) and sulfate loading rate in the influent (primary axis, golden squares) and effluent (primary axis, yellow triangles).

(93 ± 5% total molar VFA) (S.I.3). Additionally, on day 27 of operation, the ammonium concentration in the effluent was below detection (LOD < 0.1 mg $NH_4^+ \cdot L^{-1}$) (Figure 2). The ammonium deprivation lasted until day 38 of operation when we increased the ammonium concentration in the influent to meet the microbial demand of this nutrient. During this period, the VSPR fluctuated, reaching a maximum of 4.260 g $S^{2-} \cdot L^{-1} \cdot d^{-1}$ (day 66).

Because VFA concentrations were below detection during the steady-state in both pH regimes, total organic carbon (TOC) measurements were used to approximate the biomass concentration during this period. During the steady-state at pH 6.9 (day 92 - 103), the TOC concentration was 26.5 ± 1.7 mg·L^{-1}, while during the steady-state at pH 3.8 this was 18.6 ± 1.0 mg·L^{-1}. The concentration of TOC was converted into biomass concentrations using Abbott and Clamen's general empirical biomass formula for bacteria ($CH_{1.666}O_{0.270}N_{0.200}$) (Abbott and Clamen, 1973). This resulted in estimated biomass concentrations of 46.0 ± 3.0 mg·L^{-1} and 32.2 ± 1.7 mg·L^{-1} in the neutral and acidic pH regimes, respectively.

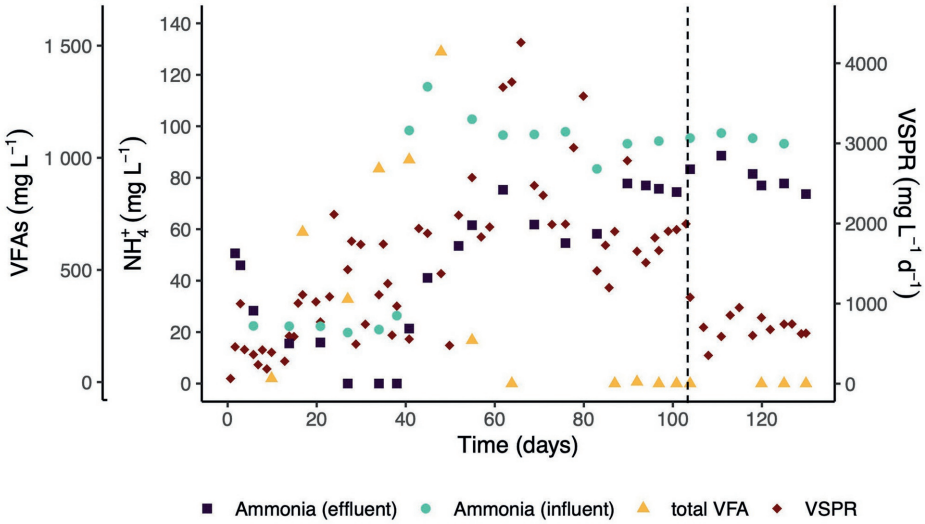

Figure 2. Total volatile fatty acid (VFA) concentration in the reactor (primary axis, red markers) and ammonium concentrations in the influent (primary axis, dark green squares) and effluent (primary axis, light green triangles) and the VSPR (secondary axis). Dotted line indicates the switch from neutral to acidic pH.

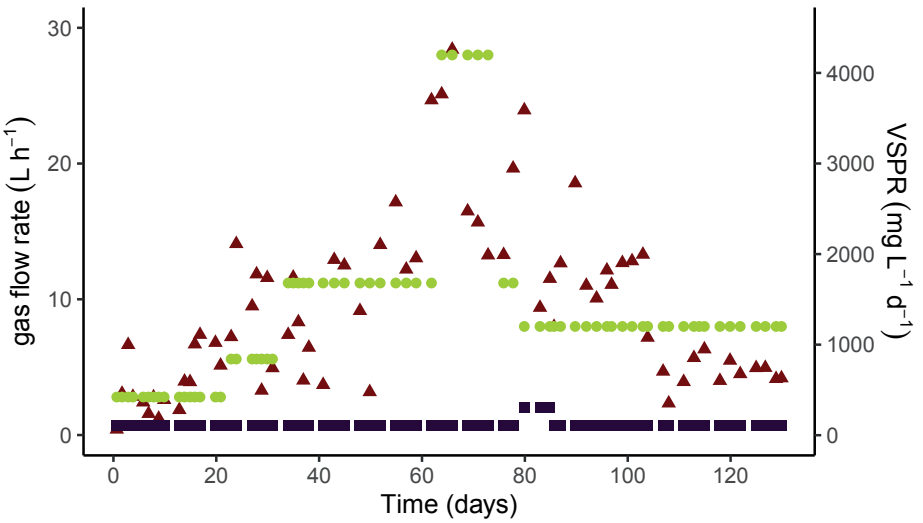

Figure 3. Changes in the influent gas rate (primary axis) and VSPR (secondary axis). Hydrogen (primary axis, green markers) and carbon dioxide (primary axis, orange markers).

We also intended to determine possible limitations in the electron (H_2) and carbon (CO_2) source transfer to the reactor liquor through cause-and-effect experimentations. Therefore, we examined the VSPR changes at increased H_2 and CO_2 influent flow rate regimes. Four different H_2 flow rate regimes were tested: 5.6 (day 23 - 34), 11.2 (day 34 – 64, and day 75 - 79), 28.0 (day 64 - 80), and 8.0 (day 80 - end) $L{\cdot}h^{-1}$. Similarly, two CO_2 gas flow regimes were evaluated 0.7 (day 1 – 80, day 86 - end) $L{\cdot}h^{-1}$ and 2.0 (day 80 - 86) $L{\cdot}h^{-1}$. During the steady-state operation of both pH regimes, the H_2 and CO_2 remained at 8 and 0.7 $L{\cdot}h^{-1,}$ respectively. Although we observed changes in the VSPR upon increasing the H_2 flow rate on day 64, these changes were not consistent and did not lead to an increased steady-state VSPR. Likewise, increments in the CO_2 flow rate did not lead to an immediate effect on the VSPR.

Microbial community composition

To assess the effect of the pH decrease on the microbial community composition, and determine the dominant (sulfidogenic) microbial taxa in the bioreactor, reactor samples for 16S rRNA gene amplicon sequencing were obtained on day 24, 59, 73, and 101 (neutral pH, 6.9) and day 118 and 130 (acidic pH, 3.8). After filtering and quality control, between 22058 and 696963 reads remained per sample (S.I.4). The alpha diversity decreased upon lowering the pH. At pH 3.8, the dominance was 0.69 ± 0.05, compared to 0.42 ± 0.07 at pH 6.9 (Figure 4A). The inoculum and the biosulfur used as S_8^0 source had a dominance of 0.23 ± 0.03 and 0.28 ± 0.03, respectively. Comparison of the diversity between samples (beta diversity) indicated a clear separation between reactor samples from both pH regimes, the inoculum, and S_8^0 (Figure 4B). Even though steady-state was reached only on day 92, the microbial community diversity on day 24 and day 101 was already highly similar (Figure 4B).

Different taxa were detected at pH 6.9 differed compared to pH 3.8, and the dominant taxa in samples from both regimes differed from the original inoculum and the added S_8^0 (Figure 5, S.I.5). Of the ten most abundant taxa detected at both pH regimes (Figure 5), *Sulfurospirillum, Sulfurovum, Desulfovibrio, Acetobacterium*, and an unknown genus from the order OPB41 within the *Coriobacteria* class (*Actinobacteria* phylum) were abundant at pH 6.9, but decreased to below abundance at pH 3.8. Conversely, *Thiomonas* and *Thermodesulfobium* were abundant taxa at pH 3.8, but were not detectable (*Thermodesulfobium*) or only present at 1.0 ± 0.2 % relative abundance during operation at pH 6.9. The remaining three taxa from the top ten ASVs, classified as *Desulfurella*, *Methanobacterium*, and *Microbacter*, were present throughout both pH regimes with *Desulfurella* becoming highly dominant at pH 3.8.

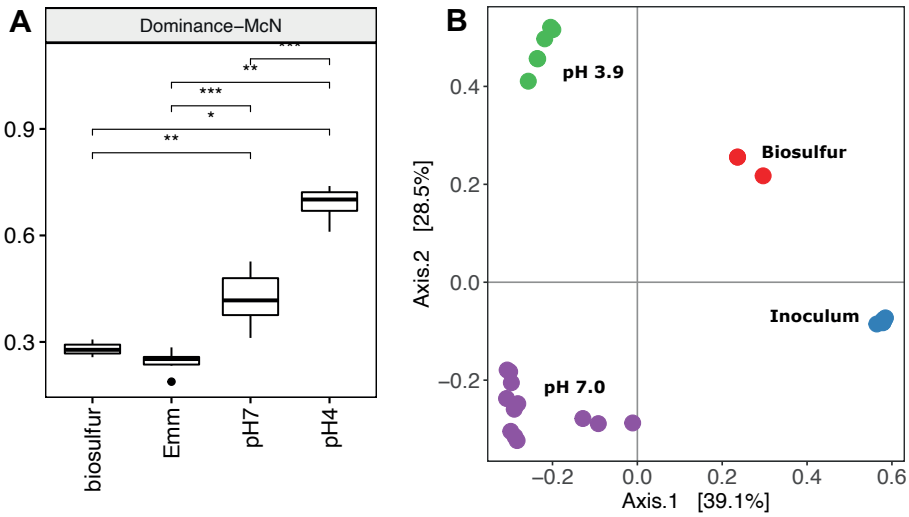

Figure 4: (A) Alpha diversity of samples from S_8^0, inoculum (Emm), and the S_8^0-reducing reactor at pH 6.9 and pH 3.8 expressed as McNaughtons Dominance. Statistical significance of the difference between means of the four groups was determined using the Wilcoxon rank-sum test. Significance is indicated by "*" where "****", "***", "**", and "*", correspond to a p-value less than 0.0001, 0.001, 0.01, 0.05, and and "n.s" indicates the difference is not significant. (B) Principal Coordinates Analysis (PCoA) plot comparing the beta diversities (Bray-Curtis dissimilarity index) between samples from S_8^0 (red), inoculum (Emm, blue), and the S_8^0-reducing reactor at pH 6.9 (purple) and pH 3.8 (green).

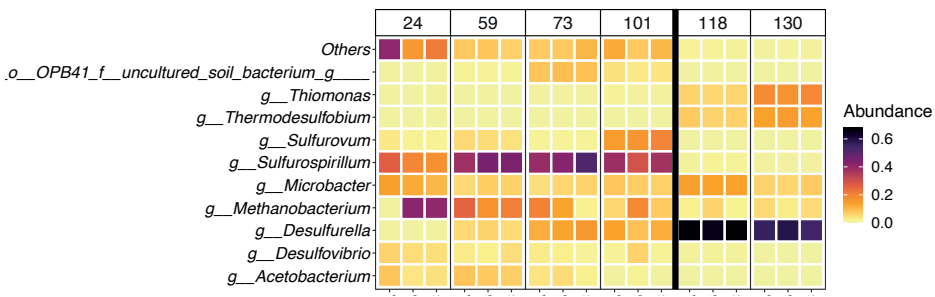

Figure 5: Top 10 most abundant taxa in samples from the neutrophilic (pH 6.9) and acidophilic (pH 3.8) operating regimes, with remainder grouped under 'others'. Colors represent the relative abundance of sequenced reads assigned to the taxa indicated on the y-axis. Individual replicates from triplicate samples are shown, grouped per day of sampling. The black line indicates the separation of the neutrophilic (days 24 – 101) and acidophilic (day 118 & 130) regimes. o__: order; f__: family; g__: genus.

During operation at pH 6.9, reads assigned to the genus *Sulfurospirillum* were most abundant, increasing from 21.2 ± 5.0 % on day 24 to 44.4 ± 6.7 % on day 73, and dropping slightly to 35.0 ± 4.7 % on day 101, before dropping to 0.25 ± 0.1 % upon the transition to pH 3.8. Similarly, albeit at lower relative abundance, reads assigned to the genus *Sulfurovum* increased in abundance during operation at pH 6.9, from 2.3 ± 1.1 % on day 24 to 17.1 ± 2.5 % on day 101, but dropped to below detection upon the transition to acidic pH. The relative abundance of *Desulfovibrio* and *Acetobacterium* decreased throughout the neutrophilic regime, from 5.1 ± 0.8 % and 5.5 ± 2.5 % on day 24 to 2.9 ± 2.8 % and 0.8 ± 0.7 % on day 101, respectively, and dropped to below detection limit at acidic pH. Sequences affiliated to *Thermodesulfobium* were absent or below detection limit at pH 6.9, and sequences related to *Thiomonas* were present at low abundance, between 0.04 ± 0.08 % on day 24 to 1.0 ± 0.2 % on day 101. However, upon the transition to pH 3.8, reads assigned to *Thermodesulfobium* increased to 14.2 ± 0.7 % on day 130, and reads assigned to *Thiomonas* increased to 18.2 ± 1.2 % on day 130.

Of the three top ten taxa present in both pH regimes, *Methanobacterium and Microbacter* were already detected on day 24. The abundance of *Methanobacterium* decreased during operation at pH 6.9, from 27.5 ± 23.7 % on day 24 to 10.5 ± 6.9 % on day 101, while the abundance of *Microbacter* remained approximately constant, between 12.2 ± 2.0 % on day 24 and 7.2 ± 0.8 % on day 101. The third taxon detected at both pH values, *Desulfurella*, accounted for < 0.1 % of reads on day 24, and then increased to 11.5 ± 2.4 % on day 101. Upon the switch to acidic pH, *Desulfurella* became the most abundant taxon in the sequenced reads, accounting for 66.4 ± 1.8 % of total sequenced reads on day 118 and 56.3 ± 2.3 % on day 130.

Discussion

Reactor performance

One of our aims was to compare the VSPR achieved at mesophilic temperatures with those observed at thermoacidophilic conditions (Hidalgo-Ulloa personal communication), using the same reactor set-up and anaerobic sludge as inoculum. This would enable us to identify the most critical limiting factors for achieving high VSPR at acidic pH and high temperatures and assess the suitability of the Emmen granular sludge as inoculum source for expanding process conditions to lower pH. We found that at the mesophile conditions here tested, the VSPR during the neutral (1.78 ± 0.17 g $S^{2-} \cdot L^{-1} \cdot d^{-1}$) and acidic pH regime (0.71 ± 0.07 g $S^{2-} \cdot L^{-1} \cdot d^{-1}$) were higher than the

VSPR under thermoacidophilic conditions (0.27 g $S^{2-}\cdot L^{-1}\cdot d^{-1}$) reported using the same reactor configuration and inoculum. It has been hypothesized that microbial sulfur conversion rates are limited due to the low S_8^0 solubility in water (Florentino et al., 2015). Under acidic conditions, the higher temperature (60°C) tested by (Hidalgo-Ulloa personal communication) increases S_8^0 solubility by one order of magnitude compared to the lower temperature used here (Kamyshny, 2009). However, the VSPR reported here under the acidic regime had a 3.1-fold increase compared to that reported under thermoacidophilic conditions (Hidalgo-Ulloa personal communication). This indicates that S_8^0 conversion limitations, using this sludge as inoculum under thermoacidophilic conditions, were likely not inherent to S_8^0 or system limitations but rather the result of the extreme conditions the microorganisms were exposed to. At circumneutral pH conditions, sulfur has an increased solubility compared to acidophilic conditions due to the formation of polysulfides (Kamyshny, 2009). Therefore, the increased VSPR at pH 6.9 likely is the product of increased sulfur availability, and the more neutral pH and lower temperature conditions during that regime.

Using the VSPR that we obtained at mesophilic-neutrophilic conditions, we evaluated the effect on the VSPR of a switch to acidic conditions (pH 3.8). Upon the transition from pH 6.9 to pH 3.8, a 2.3-fold decrease in the steady-state VSPR was observed, from 1.78 ± 0.17 g $S^{2-}\cdot L^{-1}\cdot d^{-1}$ to 0.71 ± 0.07 g $S^{2-}\cdot L^{-1}\cdot d^{-1}$. Given the absence of VFAs in the steady-state, TOC measurements were used to estimate the biomass concentration in the reactor. Biomass concentrations decreased upon the change to the acidic regime, from 46.0 ± 3.0 $mg\cdot L^{-1}$ during the steady-state at pH 6.9 to 32.2 ± 1.7 $mg\cdot L^{-1}$ during the steady-state at pH 3.8, which could partly account for the decrease in VSPR. The total relative abundance of reads assigned to the (inferred) S_8^0-reducing genera *Sulfurospirillum, Desulfurella, Sulfurovum, Desulfovibrio,* and *Methanobacterium* decreased from 77.9 % on day 101, representing the steady-state at pH 6.9, to 60.1 % on day 130, representing the steady-state at acidic pH (3.8). This could partly explain the lower VSPR, although the VSPR changes are likely the result of a multifactorial effect.

We hypothesize that the decrease in VSPR at acidic pH is in large part due to the increased difficulties associated with using S_8^0 as electron acceptor at acidic pH. S_8^0 has extremely low solubility, meaning it is predominantly solid in water (Kamyshny, 2009). The bonding energy of polymeric sulfur chains is 2.4 $kJ\cdot mol^{-1}$ lower than that of cyclooctasulfur bonds (Franz et al., 2007), and it has therefore been suggested that polysulfides (S_n^{2-}) are the primary terminal electron acceptor in S_8^0-reducing processes (Schauder and Müller, 1993; Hedderich et al., 1998). However, S_n^{2-} chain length and concentration is limited under acidic conditions: the average S_n^{2-} chain length at neutral

pH conditions is four to six sulfur atoms (S_4^{2-}-S_6^{2-}), whereas at acidic conditions, the average polysulfide chain is limited to two sulfur atoms (S-S^{2-}) (Kamyshny et al., 2007). Furthermore, H_2S_n might be the dominant polysulfide form under acidic conditions, which has been reported to be almost insoluble in water (Steudel, 2020b). Hence, it is still debated whether polysulfides or the solid elemental sulfur are the terminal electron donor used by acidophilic S_8^0-reducers (Boyd and Druschel, 2013; Florentino et al., 2016b). Similar VSPR were reported in a heterotrophic S_8^0-reducing process in a packed-bed reactor under relevant conditions (pH 3.5, room temperature, not specified) (0.844 ± 0.115 g $S^{2-}\cdot L^{-1}\cdot d^{-1}$) (Sun et al., 2020b). Despite differences in inoculum used and the operational parameters and reactor configurations, the VSPR similarities between the two systems could indicate that at acidic conditions (pH <4), the VSPR are capped at <1 g $S^{2-}\cdot L^{-1}\cdot d^{-1}$ due to sulfur bioavailability rather than other system limitations.

The VSPR showed a sinusoidal pattern in the period before steady-state during the neutral pH regime. Changes in the VFA concentration and ammonium consumption rates suggest this is driven by VFA oxidation, predominantly acetate oxidation. On day 27, the effluent ammonium concentration was below detection (LOD<0.1 mg$\cdot L^{-1}$), meaning that all ammonium had been consumed and could be limiting microbial growth. After increasing the ammonium concentration in the influent (day 38), the ammonium consumption rate increased (from 11 to 31 mg $NH_4^+\cdot L^{-1}\cdot d^{-1}$, days 41-45), suggesting a significant increase of microbial biomass. A mass balance over the metabolite production, presuming H_2 as the sole electron donor consumed, predicts that the increase in microbial growth to be predominantly attributable to acetogenic biomass, for up to 59 % of the electron donor consumption was used for acetate formation (day 41). After day 48, a drop in the acetate concentration coincided with a peak in the VSPR (4.260 g $S^{2-}\cdot L^{-1}\cdot d^{-1}$, day 66). During this period, the ammonium consumption rates decreased from 31 mg $NH_4^+\cdot L^{-1}\cdot d^{-1}$ (day 45) to 9 mg $NH_4^+\cdot L^{-1}\cdot d^{-1}$ (day 62). The decrease of acetate concentration and ammonium consumption rate in the reactor during this period suggests a decreasing growth of acetogenic microorganisms. The decrease in measured total VFA concentrations is most likely due to increased acetate oxidation associated with heterotrophic S_8^0 reduction, resulting in the higher VSPR trend observed during the same period. We observed a repeating pattern on days 73-80, where decreasing ammonium consumption rates followed a temporal increase in the VSPR. However, in steady-state during both pH regimes, we observed similar rates of ammonia consumption (6.95 ± 0.65 mg $NH_4^+\cdot L^{-1}\cdot d^{-1}$, days 92-103; 6.97±.78 mg $NH_4^+\cdot L^{-1}\cdot d^{-1}$, days 120-130), and the total VFA concentration was below detection. Therefore, these results suggest that before steady-state was

reached, heterotrophic S_8^0 reduction was an important contributor to VSPR, but S_8^0 reduction was predominantly autotrophic once the steady-state was reached.

The influent gas flow rates were varied to examine a cause-and-effect correlation with the VSPR. The variations in the VSPR during this period did not appear to be a direct result of the changes in the influent gas supply. Instead, they were likely correlated with VFA production and oxidation, as previously discussed. During days 41-52, VSPR were similar to those observed on days 24-40 (Figure 3). On days 55-64, the VSPR increased up to 3.8 g $S^{2-} \cdot L^{-1} \cdot d^{-1}$, without the gas-influent rate being increased in that period. Therefore the increase in the VSPR on day 66 appears to be a consequence of the already increasing trend observed in the days prior rather than the gas flow rate increase on days 64-73. After day 66, upon increasing the H_2 flow rates on days 64-73, the VSPR decreased. Although the decrease in VSPR could be interpreted as a CO_2 limitation, for the increased H_2 flow rates were not accompanied by a similar increase in CO_2 flow rates, diluting the CO_2 influent concentration and thus affecting its transfer rate, this is likely not the case. During this period, we observed increased ammonium consumption rates, from 8 mg $NH_4^+ \cdot L^{-1} \cdot d^{-1}$ (day 62) to 15 mg $NH_4^+ \cdot L^{-1} \cdot d^{-1}$ (day 69), suggesting an increase in microbial growth for which CO_2 fixation is needed to generate new biomass, therefore not limiting in this period. The decreased VSPR values observed during the increased H_2 flow rates (days 64 – 73) were not lower than those at lower H_2 flow rates (days 24 – 40), suggesting CO_2 was not limiting further. The subsequent changes in influent gas flow rate did not yield predictable changes in the VSPR, and in consequence, the gas flow rates were considered not limiting to the process.

Microbial community composition

A clear change in microbial community composition was observed in the reactor samples upon the switch from neutral (pH 6.9, days 0-101) to acidic conditions (pH 3.8, days 101-130) (Figure 3), as well as a reduction of diversity as reflected by both the alpha (Figure 2A) and beta diversity indexes (Figure 2B). In the neutrophilic regime (pH 6.9), S_8^0-reducing genera already dominated the sequenced reads on day 24 (Figure 3), even though steady-state conditions were not yet reached. According to sequenced reads, the dominant S_8^0-reducing taxon at pH 6.9 was *Sulfurospirillum*, followed by *Sulfurovum*, *Desulfurella*, and *Desulfovibrio*. The physiological characteristics of isolated representatives of these genera support the observed transition from heterotrophic to autotrophic S_8^0 reduction, as derived from the VFA measurements discussed above. Several *Sulfurospirillum* species, such as *S. arcachonense* (Finster et al., 1997; Stolz et al., 1999) and *S. deleyianum* (Wolfe and Pfennig, 1977; Schumacher

et al., 1992), are capable of S_8^0 reduction with H_2 as electron donor, but cannot use CO_2 as carbon source. Previous amplicon sequencing studies of neutrophilic S_8^0-reducing bioreactors fed with glucose and acetate also detected *Sulfurospirillum* as one of the dominant taxa performing S_8^0 reduction (Qiu et al., 2017). Their reported neutrophilic nature corresponds to the disappearance of *Sulfurospirillum* upon the switch to acidic pH.

Similarly, the high relative abundance of reads assigned to *Sulfurovum* during neutrophilic operation and its subsequent disappearance at pH 3.8, agreed with the pH range of growth of the three neutrophilic isolates described so far, *S. lithotrophicum* (Inagaki et al., 2004), *S. aggregans* (Mino et al., 2014) and *Sulfurovum* sp. NBC37-1 (Nakagawa et al., 2005; Yamamoto et al., 2010). and S_8^0 reduction with H_2 and CO_2 as sole energy and carbon source was confirmed in *S. aggregans* and *Sulfurovum* sp. NBC37-1. Although reads classified as *Desulfovibrio* decreased in relative abundance during operation at pH 6.9, they still represented 2.9 ± 2.8 % of total sequenced reads on day 101, suggesting this genus still partly accounted for S_8^0 reduction at the end of the neutrophilic regime. Multiple *Desulfovibrio* species are capable of S_8^0 reduction, spanning a pH region between 5, the minimum pH determined for *D. legallis* (Thabet et al., 2011)and 9.8, the maximum pH determined for *D. gigas* (Biebl and Pfennig, 1977). Generally, *Desulfovibrio* species are not able to grow on hydrogen with CO_2 as the sole C source, requiring acetate, but it was recently shown that *D. desulfuricans* is able to grow autotrophically (Sánchez-Andrea et al., 2020).

The increasing abundance of reads classified as *Desulfurella* during operation at pH 6.9, and their subsequent dominance at pH 3.8 suggested an important role for this genus throughout reactor operation. Closer inspection of the individual ASVs classified as *Desulfurella* showed that 31 different ASVs were detected throughout reactor operation, of which 13 occurred in samples from both pH 6.9 and pH 3.8, 2 were unique to samples from pH 6.9, and 16 were unique to pH 3.8. Although 1 ASV consistently accounted for 77 to 100 % of reads classified as *Desulfurella* in all samples, the variation among the other ASVs could indicate that another, more acidophilic *Desulfurella* species became dominant at pH 3.8. All *Desulfurella* species, both neutrophilic and acidophilic, are capable of S_8^0-reduction, with *D. acetivorans* (Bonch-Osmolovskaya et al., 1990), *D. kamchatkensis* and *D. propionica* (Miroshnichenko et al., 1998), and *D. multipotens* (Miroshnichenko et al., 1994) growing between pH 6.7 and 7.2, and *D. amilsii* at pH 3.8 – 6.9 (Florentino et al., 2016a). *Desulfurella* species can utilize both organic and inorganic substrates as carbon and energy sources. This versatility is reflected by the dominance of *Desulfurella* in many different studies, such as acidophilic S_8^0-reducing enrichments using either acetic acid, methanol, or H_2/CO_2

as energy and carbon source (Florentino et al., 2015) and in heterotrophic (Guo et al., 2019, 2021) and autotrophic reactors (current study) at neutral and acidic pH.

Next to *Desulfurella*, reads assigned to *Thiomonas* and *Thermodesulfobium* increased in relative abundance at pH 3.8. *Thiomonas* was already observed at low abundance on the final day of sampling at neutral pH, but *Thermodesulfobium* remained below detection before the switch to acidic pH. *Thiomonas* species have been isolated predominantly from acid mine drainage sediments and hot spring environments (Akob et al., 2020), and grow at acidic pH, with minimum pH 3.0 for *T. metallidurans* (Akob et al., 2020), to neutral pH (8.5, maximum pH for *T. bhubaneswarensis*) (Panda et al., 2009). Furthermore, *T. islandica* is capable of autotrophic growth on H_2, and utilization of organic and inorganic energy and carbon sources (Vésteinsdóttir et al., 2011). However, chemolithotrophic growth with H_2 was not confirmed with S_8^0, raising the question of which energy metabolism is utilized by the *Thiomonas* species detected in the reactor. Like *Thiomonas*, *Thermodesulfobium* species were reported to grow chemolithoautotrophically with H_2/CO_2, using oxidized sulfur compounds such as sulfate or thiosulfate as electron acceptors, but were not able to use S_8^0 (Mori et al., 2003; Frolov et al., 2017). Its potential role as sulfate reducer could be further supported by the observation that sulfate concentrations again started decreasing 19 days after the pH decrease (Figure 1).

The high relative abundance of reads assigned to *Methanobacterium* at both neutral and acidic conditions could indicate the occurrence of methanogenesis from H_2 and CO_2. During operation at pH 6.9, methane was not monitored, and its formation in the first 103 days can therefore not be excluded. During operation at pH 3.8, the gas composition was measured on day 104 and day 129, but no CH_4 was detected. We propose that rather than methanogenesis, *Methanobacterium* performed S_8^0 reduction with H_2 as electron donor, as demonstrated previously (Stetter and Gaag, 1983). More recently, *Methanobacterium* was implicated as the S_8^0-reducing species responsible for unwanted H_2S formation from S_8^0 formed in an H_2S removal process (Zhou et al., 2011).

Even though the bioreactor was operated under chemolithoautrophic conditions, there were several indications that organic carbon compounds played an important role. For example, sequences affiliated with *Microbacter* were detected during operation at both pH 6.9 and pH 3.8. The only *Microbacter* species isolated to date, *M. margulisiae*, relies on a fermentative lifestyle, excreting acetic acid, lactic acid or propionic acid as fermentation products (Sánchez-Andrea et al., 2014b). The substrate for fermentation in the current study is unclear, however, with the most likely candidates being dead biomass and disintegrating granules from the original inoculum, although this was not quantified.

Accumulation of acetic acid in the reactor in the first 40 days of operation indicated acetogenesis. This corresponded well with the detection of *Acetobacterium* in the sequenced reads from this period, as *Acetobacterium* species, with the type strain *A. woodii* as well-studied example (Balch et al., 1977), are capable of acetogenesis from H_2 and CO_2. The presence of acetic acid could explain the dominance of *Sulfurospirillum* in the sequenced reads during operation at pH 6.9. Even though the enzymes required for the reverse operation of the citric acid cycle (rTCA) for carbon fixation were detected in the genome of several *Sulfurospirillum* species (Ross et al., 2016), this genus has so far not been demonstrated to be capable of autotrophic growth, and instead grows mixotrophically, using H2 and acetate as energy and carbon source as shown for *S. arcachonense* (Finster et al., 1997; Stolz et al., 1999) and *S. deleyianum* (Wolfe and Pfennig, 1977; Schumacher et al., 1992). Although it cannot be excluded that the *Sulfurospirillum* species enriched during operation at pH 6.9 were able to fix CO_2, it is more likely that they utilized organic carbon compounds produced by other community members, such as the acetic acid produced by *Acetobacterium*.

Although *Sulfurospirillum* was the dominant genus detected in the sequenced reads between day 24 and day 73, a steady-state was only reached on day 92, at lower VSPR than observed between day 55 and day 76. In the sample taken from the steady-state on day 101, *Sulfurospirillum* was still a dominant community member, but reads assigned to *Sulfurovum*, capable of autotrophic S_8^0 reduction, had increased in abundance, which together with *Desulfurella* likely accounted for increased autotrophic S_8^0 reduction. The decrease in ammonium consumption and the sharp decrease in reads assigned to the acetate producer *Acetobacterium* during steady-state could indicate that the unavailability of organic carbon limited growth of *Sulfurospirillum* in the steady-state. Possibly *Acetobacterium* was inhibited by increasing H_2S concentrations, as shown for homoacetogenic mixed cultures where acetogenesis was inhibited at concentrations above 3.3 mM (Ntagia et al., 2020). While heterotrophic S_8^0 reduction was dominant in the first 80 days, the VSPR in the steady-state appeared to be in larger part due to autotrophic S_8^0 reduction. For a schematic overview of the different metabolic processes hypothesized to occur in the bioreactor in the different pH regimes see (Figure 3-6).

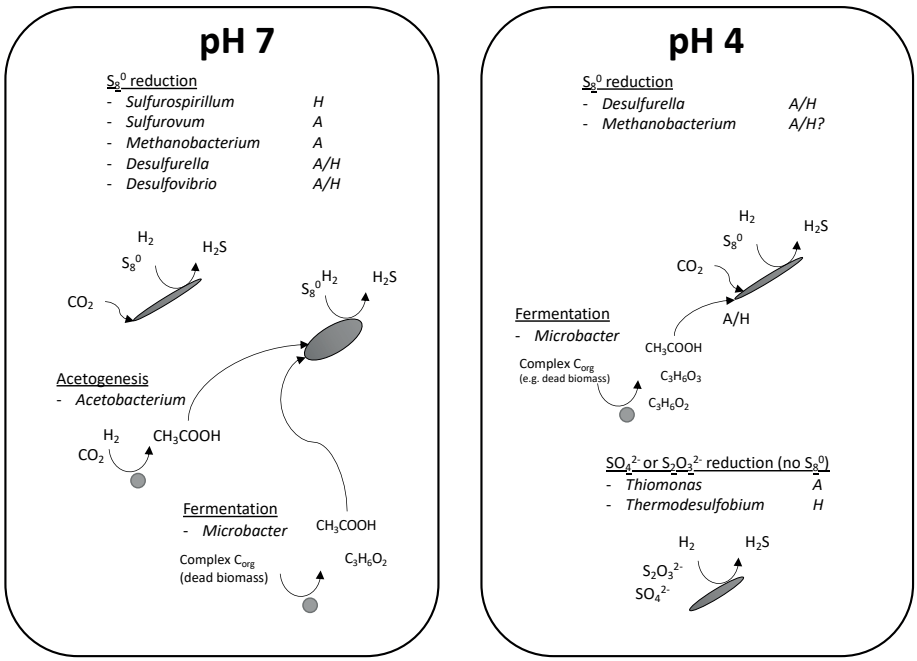

Figure 6: Schematic representation of proposed dominant energy metabolisms and associated microbial taxa detected in the 16S rRNA gene amplicon sequencing reads obtained from the pH 6.9 and pH 3.8 regime. A: autotrophic, H: heterotrophic.

Conclusions

The results from this study, combined with previous experiments at high temperature and acidic pH, indicate that when using the Emmen granular sludge as inoculum for S_8^0-reducing continuous bioreactors, temperatures of 60 °C or higher seem to have a stronger inhibitory effect on the VSPR than pH. Although at mesophilic temperatures the VSPR dropped 2.5-fold when the pH was decreased from 6.9 to 3.8, this was still around 3.1-fold higher than the VSPR achieved at thermoacidophilic conditions (pH 3.5, 60 °C). This increase in the VSPR is most likely related to the mesophilic, neutrophilic conditions at which the Emmen inoculum was harvested, and it can be expected that higher rates can be obtained with sludge more adapted to thermoacidophilic condition.

The microbial community composition indicates that S_8^0 reduction at pH 6.9 was initially predominantly carried out by *Sulfurospirillum* species, supported by acetate production by *Acetobacterium*. This likely became limiting at higher VSPR due to increasing H_2S concentrations in the reactor, enabling the autotrophic S_8^0-reducing genera *Sulfurovum* and *Desulfurella* to become abundant. Upon the switch to acidic pH, the microbial community was dominated by *Desulfurella*. Based on analysis of individual ASVs assigned to this taxon, this likely was a different species than at pH 6.9.

Acknowledgements

This study was funded by the research program TTW under project number 14797, which is financed by the Dutch Research Council (NWO) to JW and IS-A. We thank Ineke Heikamp-de Jonge and Laura Vandionant for technical assistance with library preparation for amplicon sequencing.

Supplementary Information

S.I.1 Reactor event log

Table S.I. 1 Log summary of the events occurred during the operation of the gas-lift reactor and corrective actions taken.

Day	Event	Corrective action
1	Online pH drifted in 0.5 units of that of the offline measurements.	Probe was recalibrated, but the difference between online and offline measurements persisted. The pH control limits were modified to match the offline measurements.
8	Cloggage in the influent line due to granules accumulation in the influent entrance.	The lines were backflushed and contents returned to the reactor. Reactor was sealed and all influent and recirculation lines were replaced. Replaced lines were filled with anaerobic water to reduce/avoid oxygen introduction to the reactor.
9	Power failure during four hours.	All gas and liquid influent and recirculation systems were off during this period of time. The system was operated in batch during 3 hours after power restorage.
10	Flow calibration of the influent pump lost. HRT increased to 3.6 days.	All liquid pumps were re-calibrated.
13	Online pH measurements started to drift to that of the offline measurements. Actual reactor pH 4.8.	The pH electrode was replaced with a new electrode. New electrode was calibrated and verified.
23	Power cut during 24 hours.	Planned maintenance of power lines. Heat exchanger units, gas recirculation and media influent pumps were off. pH control and influent gas mass flow controllers remained on with an alternate power supply. The reactor was operated in batch mode during this time.
35	Cloggage in the liquid recirculation line. Sulfur accumulation in the line.	Line flow backflushed. To contain backflush liquid leaving the reactor, the effluent line was closed. After successful liberation of the line, the influent wa turned off during 30 minutes to allow the solids to settle in the external settler.
57	Cloggage and rupture of the liquid recirculation line. Sulfur accumulation in the line. ~200 mL recirculation fluid lost.	Liquid recirculation line replaced. The line was filled with liquid from the settler to prevent oxygen entering to the reactor through the line. Recirculation rate was increased to 3.6 $mL.min^{-1}$ to increase the solid flow in the line and avoid solid settlement in the line.
59	Decrease efficiency of suspended solids recovery.	Liquid recirculation rate decreased to 2.0 $mL.min^{-1}$
64	Gas effluent line clogged.	Carbonate accumulation in the effluent gas line. Line replaced and new sparger installed.
66	Cloggage and rupture of the liquid recirculation line. Sulfur accumulation in the line. No fluid lost.	Liquid recirculation line replaced. The line was filled with liquid from the settler to prevent oxygen entering to the reactor through the line.
69	Decrease efficiency of suspended solids recovery.	As part of the corrective procedure on day 66, the liquid recirculation pump was left at 8.0 $mL.min^{-1}$ by error. The flow was corrected to 2.0 $mL.min^{-1}$.
83	Gas effluent line partially clogged. Gas partially leaving the through liquid effluent.	Carbonate accumulation in the effluent gas line. Line replaced and new sparger installed.
113	Damage of the pump head of the liquid recirculation line.	No flow of liquid through the pump. The pump head was replaced. The line was filled with liquid from the settler to prevent oxygen entering to the reactor through the line.

S.I.2 Thiosulfate formation

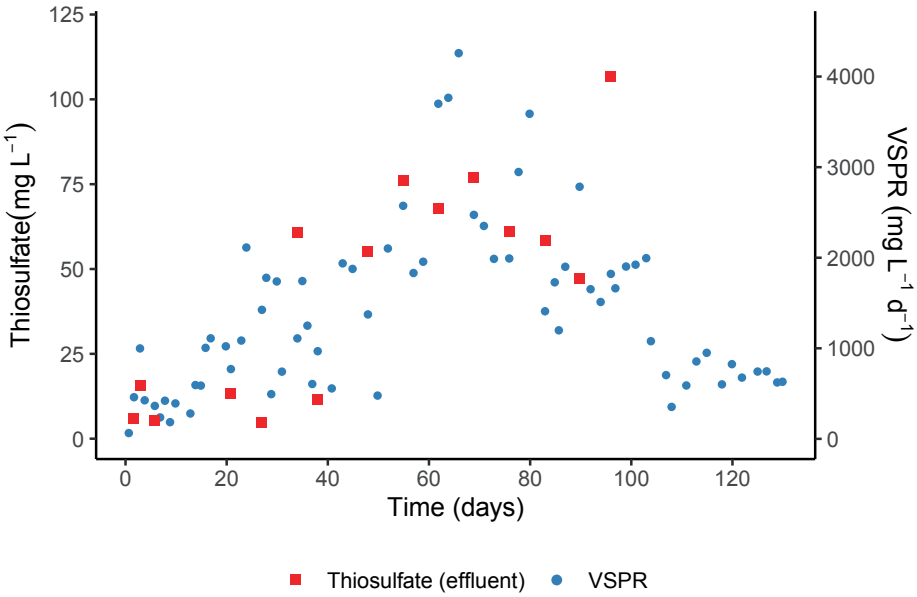

Figure S.I. 1 Concentration of dissolved thiosulfate (red triangles) contrasted with the volumetric sulfide producing rates (VSPR) in the 4 L gas lift rector.

S.I.3 Volatile fatty acid (VFA) composition

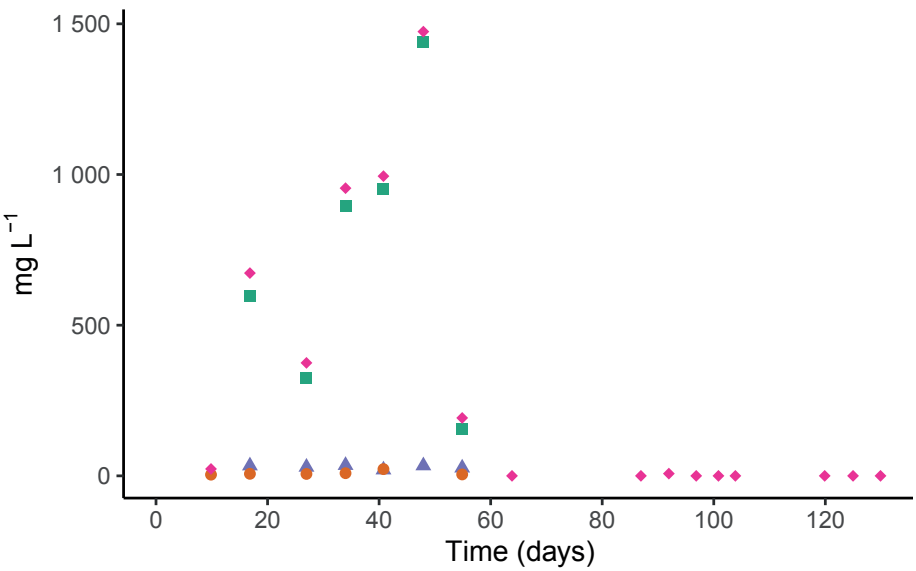

Figure S.I. 2 Fraction of the volatile fatty acid (VFA) found in the gas-lift samples. In the plot are shown only the VFA fraction found in the samples. VFA fractions measured under the limit of quantification are not shown.

S.I.4 16S rRNA gene amplicon sequence reads

Table S.I. 2 sequencing depth per sample after quality control and filtering

Sample	Reads
biosulfur_A	599508
biosulfur_B	100273
biosulfur_C	233324
Emm_20200306_A	561669
Emm_20200306_B	480109
Emm_20200306_C	143427
Emm_20210604_A	637884
Emm_20210604_B	360171
Emm_20210604_C	22058
Negcontrol_A	581
R2_d24_A	350499
R2_d24_B	471115
R2_d24_C	449994
R2_d59_A	305673
R2_d59_B	614855
R2_d59_C	529843
R2_d73_A	398199
R2_d73_B	522318
R2_d73_C	524306
R2_d101_A	696963
R2_d101_B	462725
R2_d101_C	421098
R2_d118_A	595869
R2_d118_B	560330
R2_d118_C	393985
R2_d130_A	152177
R2_d130_B	84542
R2_d130_C	254896

S.I.5 Relative read abundance of top 50 most abundant taxa

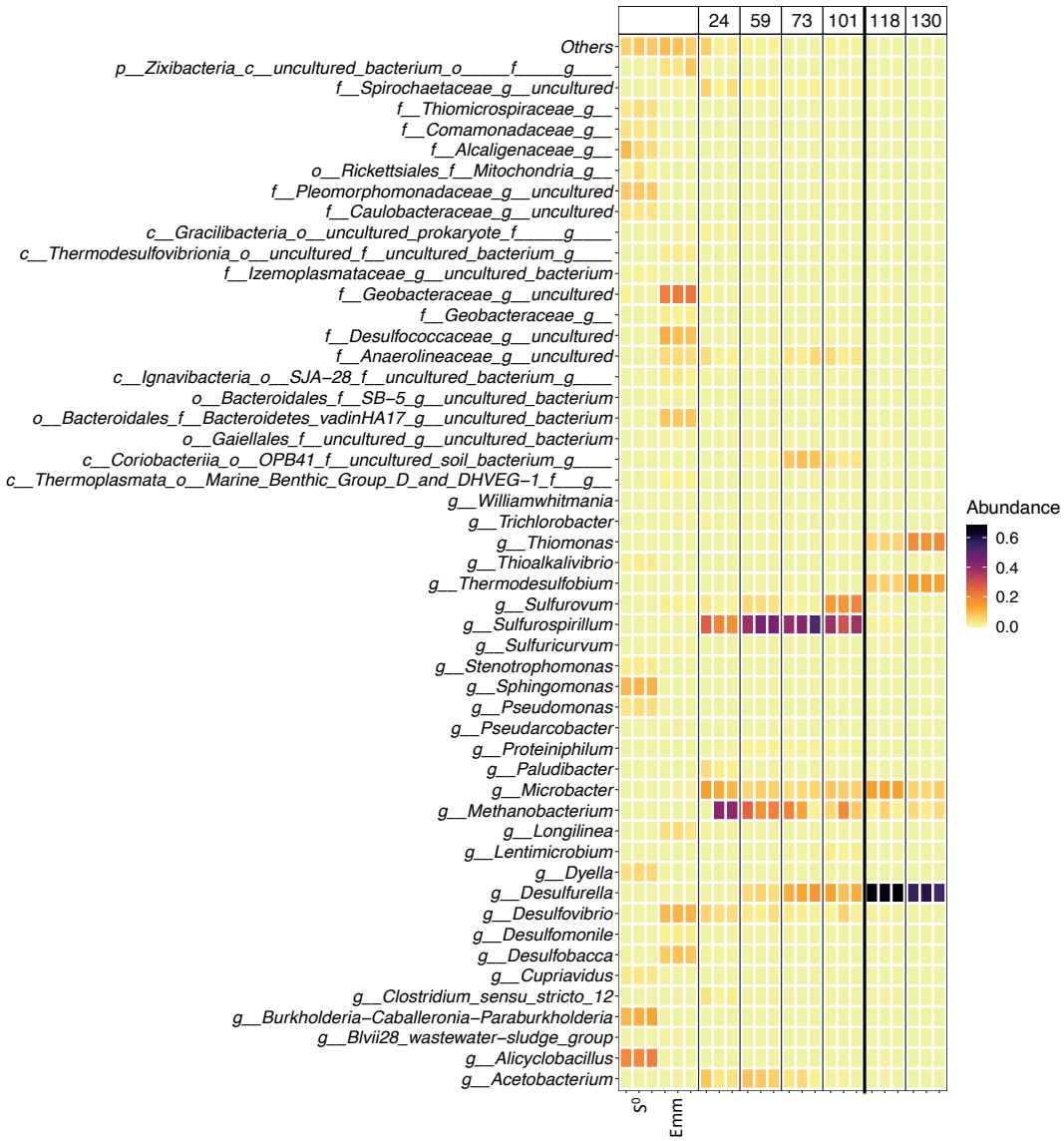

Figure S.I. 3 Top 50 most abundant taxa detected in samples from the original anaerobic sludge used as inoculum (Emm), the biosulfur (S0), and the reactor operated at pH 6.9 (days 24 – 101) and pH 3.9 (day 118 and 130), separated by the

S.I.6 Microscopy images

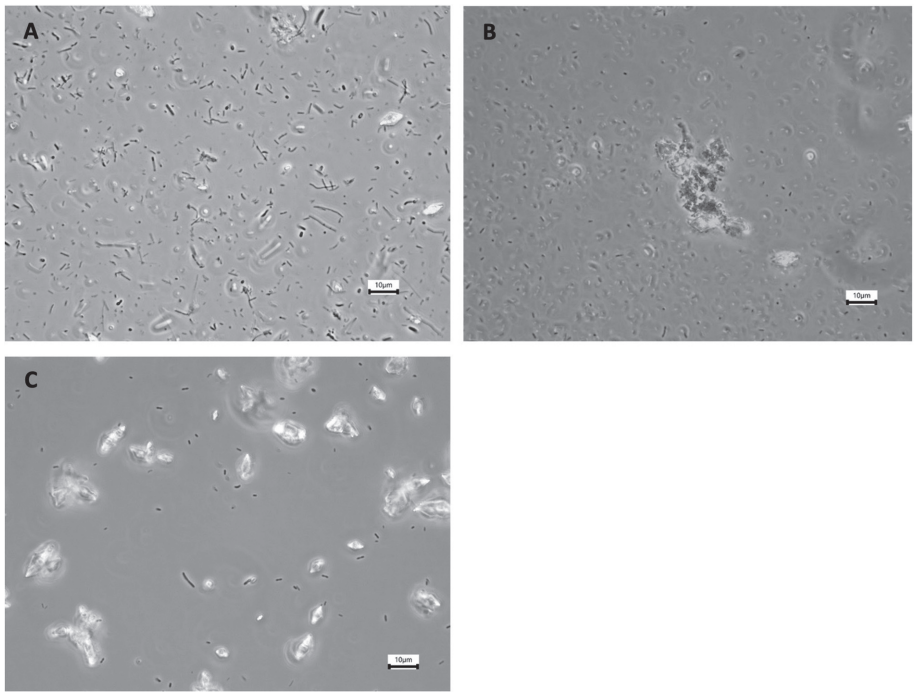

Figure S.I. 4 Phase contrast microscopy images of the gas lift reactor samples on operational days (A) 20, (B) 92 (steady-state pH 6.9), and (C) 120 (steady-state pH 3.9).

Biosulfidogenesis mediates natural attenuation in acidic mine pit lakes

Charlotte M. van der Graaf[1*], Javier Sánchez-España[2], Iñaki Yusta[3], Andrey Ilin[3] Sudarshan A. Shetty[1], Nicole J. Bale[4], Laura Villanueva[4], Alfons J.M. Stams[1,5], Irene Sánchez-Andrea[1*]

This chapter was published as: van der Graaf, C. M., Sánchez-España, J., Yusta, I., Ilin, A., Shetty, S. A., Bale, N. J., et al. (2020). Biosulfidogenesis mediates natural attenuation in acidic mine pit lakes. *Microorganisms* 8, 1–26. doi:10.3390/microorganisms8091275.

[1] Laboratory of Microbiology, Wageningen University, Stippeneng 4, 6708 WE Wageningen, The Netherlands;
[2]Mine Waste and Environmental Research Group, Department of Geological Resources, CN IGME-CSIC, Calera 1, Tres Cantos, 28760 Madrid, Spain;
[3]Dept of Geology, University of the Basque Country (UPV/EHU), Apdo. 644, 48080 Bilbao, Spain;
[4] NIOZ Royal Netherlands Institute for Sea Research, Department of Marine Microbiology and Biogeochemistry, and Utrecht University, Landsdiep 4, 1797 SZ 't Horntje, The Netherlands;
[5] Centre of Biological Engineering, University of Minho, Campus de Gualtar, 4710-057 Braga, Portugal
*corresponding authors

Abstract

Acidic pit lakes are abandoned open pit mines filled with acid mine drainage (AMD)—highly acidic, metalliferous waters that pose a severe threat to the environment and are rarely properly remediated. Here, we investigated two meromictic, oligotrophic acidic mine pit lakes in the Iberian Pyrite Belt (IPB), Filón Centro (Tharsis) (FC) and La Zarza (LZ). We observed a natural attenuation of acidity and toxic metal concentrations towards the lake bottom, which was more pronounced in FC. The detection of Cu and Zn sulfides in the monimolimnion of FC suggests precipitation of dissolved metals as metal sulfides, pointing to biogenic sulfide formation. This was supported by microbial diversity analysis via 16S rRNA gene amplicon sequencing of samples from the water column, which showed the presence of sulfidogenic microbial taxa in FC and LZ. In the monimolimnion of FC, sequences affiliated with the putative sulfate-reducing genus *Desulfomonile* were dominant (58 %), whereas in the more acidic and metal-enriched LZ, elemental sulfur reducing *Acidianus* and *Thermoplasma spp*., and disproportionating *Desulfocapsa spp*. were more abundant. Furthermore, the detection of reads classified as methanogens and *Desulfosporosinus* spp., although at low relative abundance, represents one of the lowest pH values (2.9 in LZ) at which these taxa have been reported to our knowledge. Analysis of potential biomarker lipids provided evidence that high levels of phosphocholine lipids with mixed acyl/ether glycerol core structures were associated with *Desulfomonile*, while ceramide lipids were characteristic of *Microbacter* in these environments. We propose that FC and LZ function as natural bioremediation reactors where metal sulfide precipitation is mediated by biosulfidogenesis starting from elemental sulfur reduction and disproportionation at an early stage (LZ), followed by sulfate reduction at a later stage (FC).

Introduction

Acidic pit lakes form when abandoned open pit mines are allowed to flood, and exposure of the polymetallic sulfide ores to water and oxidants such as oxygen (O_2) and ferric iron (Fe^{3+}) catalyzes their oxidative dissolution. This results in the generation of acid mine drainage (AMD)—highly acidic, metalliferous waters that pose a severe threat to the environment. Due to economic and technical factors, proper remediation of acidic pit lakes rarely occurs, and these lakes persist for decades. Assessment of the long-term hazards posed by these lakes requires a better understanding of the different factors influencing their development, which include the microbial activity in these waters. In the past decade, several studies of acidic pit lakes in the Iberian Pyrite Belt (IPB), one of the largest massive sulfide districts on Earth and harboring many such lakes due to a long history of mining (Leistel et al., 1997; Sánchez-España et al., 2008; Tornos, 2008), demonstrated the tight connection between microbiology and physicochemical dynamics in IPB pit lakes (Wendt-Potthoff et al., 2012; Santofimia et al., 2013; Diez-Ercilla et al., 2014; Falagán et al., 2014), similar to what is known for AMD streams (Church et al., 2007; Rowe et al., 2007; González-Toril et al., 2011) and the naturally acidic, metalliferous Tinto River (Gonzalez-Toril et al., 2003; Sánchez-Andrea et al., 2011; García-Moyano et al., 2012; Amils et al., 2014).

A common characteristic of acidic pit lakes in the IPB is their conical shape, and relatively small surface area and large depth (Sánchez-España et al., 2008; Sánchez-España et al., 2013). In most cases, density differences between layers and a low surface to volume ratio result in the establishment of *meromixis*, a permanent stratification of the water column into an upper oxygenated layer (mixolimnion), and a lower anoxic layer (monimolimnion). Due to the abundance of pyrite (FeS_2) in the IPB ores, AMD waters in the IPB are characterized by extremely high concentrations of dissolved iron and sulfate (SO_4^{2-}). The generally low organic carbon content and low phosphate availability (due to adsorption to ferric iron precipitates), makes most acidic pit lakes oligotrophic (Spiteri et al., 2008; Falagán et al., 2014). As a result of these extreme conditions, AMD is generally characterized by low microbial diversity, and often dominated by microorganisms involved in the oxidation and reduction of iron (Johnson and Hallberg, 2003; Johnson and Aguilera, 2015). For example, a cultivation-independent study of the water column of Tinto River, in the IPB, showed that 80 % of 16S rRNA gene sequences were assigned to only three genera, *Leptospirillum*, *Acidiphilium* and *Acidithiobacillus* (González-Toril et al., 2003), which predominantly mediate the cycling of iron and sulfur. Similarly, cultivation-independent studies of four acidic pit lakes in the IPB, Cueva de la Mora, Herrerías-Guadiana, Concepcion and Nuestra Senora del Carmen, also showed a low

diversity, with most detected taxa involved in the cycling of iron (Wendt-Potthoff et al., 2012; Santofimia et al., 2013; Falagán et al., 2014).

In addition to the importance of microorganisms for the cycling of iron, microorganisms involved in the sulfur cycle also have a profound effect on the physicochemical dynamics in AMD waters. Sulfur-oxidizing bacteria, predominantly *Acidithiobacillus* spp., play an important role in AMD formation by mediating the oxidation of the intermediate sulfur compounds formed by indirect leaching of metal sulfides, such as elemental sulfur (S_8^0), to SO_4^{2-}. This generates further acidity and contributes to AMD formation (Sand et al., 2001). In contrast, however, reductive microbial sulfur metabolism—the reduction of oxidized sulfur compounds to sulfide (H_2S) (biosulfidogenesis)—has the opposite effect. The H_2S produced by these microorganisms mediates the removal of dissolved metals by their precipitation with H_2S as metal sulfides, effectively reversing AMD formation. Furthermore, at low pH sulfidogenesis from SO_4^{2-} has an attenuating effect on the acidity through the consumption of protons (H^+). For example, the complete oxidation of acetic acid to CO_2 with SO_4^{2-} as electron acceptor at a pH below the pK_a of acetic acid (4.75), H_2S (7.02) and CO_2 (6.37), requires H^+ (equation 1). This is not the case for sulfidogenesis from S_8^0, as this reaction is H^+-neutral at low pH (equation 2) (Johnson and Sánchez-Andrea, 2019).

$$C_2H_4O_2 + SO_4^{2-} + 2H^+ \rightarrow 2\ CO_2 + H_2S + 2\ H_2O \qquad (1)$$

$$C_2H_4O_2 + 4\ S_8^0 + 2\ H_2O \rightarrow 2\ CO_2 + 4\ H_2S \qquad (2)$$

The role of acidotolerant or acidophilic sulfidogenic microorganisms, predominantly sulfate-reducing bacteria (SRB), for the bioremediation of AMD through metal sulfide precipitation is well-recognized (Sánchez-Andrea et al., 2014a; Ňancucheo et al., 2017; Johnson and Sánchez-Andrea, 2019). Most SRB isolated from acidic environments such as AMD streams and the Tinto River are merely acidotolerant or moderately acidophilic, for example *Thermodesulfobium narugense* (pH 4 - 6.5) (Mori et al., 2003), *Thermodesulfobium acidiphilium* (pH 3.7 - 6.5) (Frolov et al., 2017), *Desulfosporosinus acididurans* (pH 3.8 – 7) (Sánchez-Andrea et al., 2015) and *Desulfosporosinus acidiphilus* (pH 3.6 -5.5) (Alazard et al., 2010). This is likely related to the fact that in acidic environments SRB were detected mostly in sediments (Sánchez-Andrea et al., 2013), where they are potentially protected from the 'poly-extreme' conditions (low pH, high salinity, high metal concentrations), through the creation of micro-niches, although this is still a matter of debate (Koschorreck, 2008). Very few reports exist of SRB and biosulfidogenesis in the water column of highly acidic water bodies. In the IPB, this was

until recently only reported in the acidic pit lake Cueva de la Mora (Wendt-Potthoff et al., 2012; Diez-Ercilla et al., 2014; Falagán et al., 2014). The detection of SRB in the water column of highly acidic and metal-rich pit lakes is interesting, as the potential for formation of microenvironments there is minimal (Koschorreck, 2008). These SRB likely are more resistant to extreme conditions, making them valuable for biotechnological applications.

We recently reported a high abundance of SRB in the water column of the extremely acidic and saline pit lake formed in the Brunita open pit mine (south-eastern Spain), as well as their attenuating effect on the extreme physicochemical characteristics of this lake (Sánchez-España et al., 2020). Most notable was the amelioration of acidity (pH ~2.0 in the mixolimnion *vs.* pH 5.0 in the lower monimolimnion) with the partial or complete removal of certain major (Cu, Zn) and trace (Cd, Cr, Pb, Th, Ni, Co) metals from the water column. The observation of abundant Cu and Zn sulfide particles in the SEM-EDS analysis of suspended particulate matter (SPM) indicated the removal of these metals as sulfide precipitates. This abundance of Cu and Zn sulfides, together with the dominance of 16S rRNA gene sequences from the SRB genus *Desulfomonile* (58.8 % of total filtered reads) (DeWeerd et al., 1990; Tiedje et al., 2015), supported the functioning of this pit lake as a large-scale natural bioremediation reactor, where biosulfidogenesis by acidophilic SRB mediated metal sulfide precipitation and neutralization of acidity.

Here, we study two previously microbiologically unexplored acidic mine pit lakes in the IPB, Filón Centro (FC) and La Zarza (LZ), that flooded in the 1960's and 1990's, respectively. Although metal concentrations and salinity in FC and LZ are not as extreme as in the Brunita pit lake, where they are among the highest reported for acidic pit lakes to date (Sánchez España et al., 2008), the nutrient conditions in Brunita are more favorable than in FC and LZ due to input of nitrogen and phosphorus from its surroundings, and the resulting availability of organic carbon due to phototrophic production. This is not the case in FC and LZ, and the detection of SRB in the water column of these two pit lakes, would not only widen the physicochemical limits at which biological sulfate reduction is detected, but would also have great potential for application in AMD bioremediation technologies. We hypothesized that if biosulfidogenesis has triggered the attenuation of extreme conditions in these lakes, as per Brunita pit lake, then this attenuation process will have progressed further in the older pit lake (FC). We investigated this hypothesis through combined physicochemical and microbiological characterization. For the microbiological characterization of the water column, we combined 16S rRNA gene amplicon sequencing with intact polar lipid (IPL) analysis, as certain IPL profiles could serve as biomarkers for specific taxonomic groups relevant to natural bioremediation processes in AMD environments.

Materials and Methods

Study Sites

FC (37°35'27.4"N, 7°07'27.5"W) was mined for copper and pyrite (Tornos et al., 1997). This mine was first exploited in the 19th century until 1880, and then re-opened in 1956 until its closure in 1968 (Pinedo Vara, 1963; Tornos et al., 1997). The open pit is 600 m long and 230 m wide. The pit lake that formed after the mine flooded has a surface area of 3.57 ha, with a maximum length of 430 m, a maximum width of 140 m (Figure 1a,c), and a maximum depth of 50 m. LZ (37°42'35.5"N, 6°51'01.4"W) was mined for the extraction of pyrite (for sulfuric acid production), copper (chalcopyrite), and zinc (sphalerite) by both underground and open pit methods. The open pit operations started in 1886 and lasted for almost a century. In 1980 the mine was only exploited by underground mining, and the mine complex was finally closed in 1991 (Checa Espinosa et al., 2000). Some maintenance and dewatering works were conducted until the pumps were stopped in 1995, and the pit had been flooding continuously until 2015. The resulting pit lake currently has a surface area of 8 ha, with a maximum length of 700 m, a variable width of between 42 m (western side) and 200 m (eastern side), and a maximum depth of 80 m (Figure 1b,d). The total depth of the open pit is 140 m.

Field site exploration and sample collection

FC was sampled during seven different field campaigns in October and December 2017, October 2018, March, May and December 2019, and July 2020. LZ was only sampled in two field campaigns in October and December 2017 due to extremely difficult access for rubber boats and scientific equipment. Physicochemical profiles of the water column in both lakes were obtained using a Hydrolab MS5 multi-parametric probe (Hach, Loveland, CO, USA) calibrated according to the manufacturer's instructions. Depth profiles were determined for pH, oxidation-reduction potential (ORP), temperature (T), dissolved oxygen concentration (DO), and specific conductivity (SpC). For FC, the turbidity was measured in May 2019, December 2019 and July 2020 using a HI 93414 portable turbidity meter (Hanna Instruments, S.L., Eibar, Spain) calibrated on-site with fresh standards. The nutrient content of surface water in FC and LZ was analyzed in July 2020. Nitrogen as ammonium, nitrogen as nitrate, and phosphorus as phosphate were measured using Hach Lange cuvette tests LCK 304, LCK 339 and LCK 349 (Hach, Loveland, CO, USA), respectively, and a UV-VIS DR2800 spectrophotometer (Hach, Loveland, CO, USA).

Chemical composition of the water column at different depths was determined in FC (0, 10, 15, 25, 30, 45 m) and in LZ (0, 30, and 70 m) in October 2017. Samples were collected using a 5 L Van Dorn sampling bottle (KC Denmark). Water samples (125

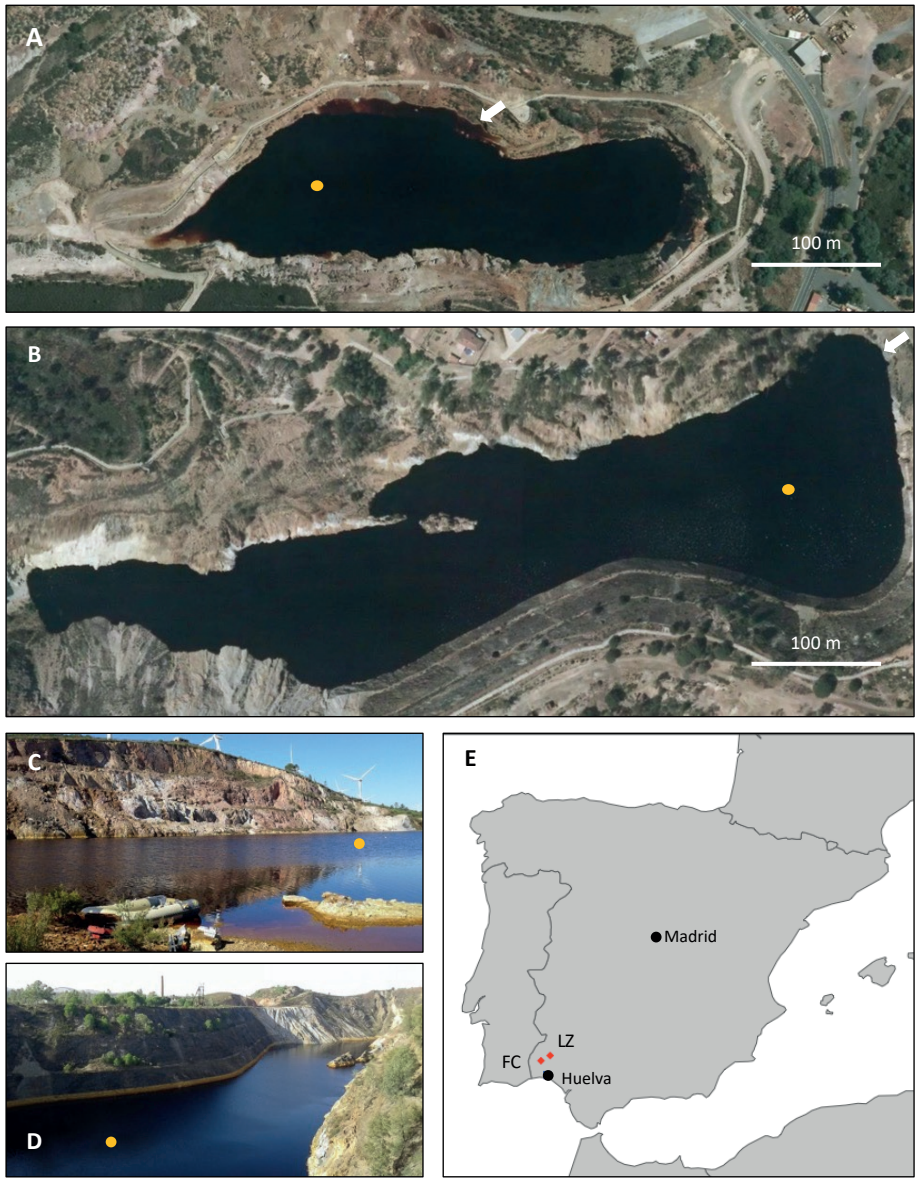

Figure 1: The acidic pit lakes Filón Centro (FC, Tharsis) (a, c) and La Zarza (LZ) at the La Zarza Perrunal mine (b, d); (e) the two pit lakes are located in Huelva province, southwest Spain. The orange dot indicates the sampling location. The white scalebar indicates 100 m. The orange arrows in (a, b) indicate the location and direction from which picture (c, d) were taken, respectively.

mL) were filtered on-site using a Merck-Millipore manual filtration unit and 0.45 µm nitrocellulose membrane filters (Merck Millipore, Burlington, MA USA). Filtered water was stored in 125 mL polyethylene bottles, acidified with 1 M HCl and kept at 4 °C until chemical analysis in the laboratory. Suspended particulate matter (SPM) was sampled by additional filtering of 125 mL over the first 0.45 µm nitrocellulose membrane filter (Merck Millipore, Burlington, MA USA). The filter was washed by further filtration of 100 mL milliQ-water, and stored in separate plastic boxes after air-drying until chemical-mineralogical analysis by electron microscopy.

Samples for microbial community analysis and analysis of intact polar lipids (IPL) were obtained by filtration of biomass from the water samples over ~0.3 µm glass fiber filters (Advantec Grade G75 glass fiber filters, 47 mm, CA, USA). Prior to sampling, filters were heated at 350 °C for 30 min to remove residual organics. Water was filtered on-site using a Merck-Millipore manual suction filtration system (Merck, Burlington MA, USA). The amount of water filtered per sample depended on the SPM content, which determined the volume after which filters became clogged. Filters were preserved on ice while sampling and stored at -20 °C until laboratory analysis. In FC, biomass samples were taken in October 2017 at 0, 15, 30, and 45 m depth, representative of the chemical zonation observed in the physicochemical profile at that time point and detected in previous sampling campaigns (Sánchez-España et al., 2008; López-Pamo et al., 2009). In LZ, samples for microbial community analysis were taken from 0, 30, and 70 m depth, representing the mixolimnion and the upper and lower part of the monimolimnion.

Chemical analyses and electron microscopy

Concentrations of element species in the water samples were measured by atomic absorption spectrometry (AAS) (Na, K, Ca, and Mg) using the Varian SpectrAA 220 FS, inductively coupled plasma-atomic emission spectrometry (ICP-AES) (Al, Cu, Fe, Mn, SO_4, SiO_2, and Zn) using an Agilent 7500ce, or inductively coupled plasma-mass spectrometry (ICP-MS) (As, Cd, Co, Cr, Ni, Pb, Se, Th, U) using a Varian Vista MPX instruments. The detection limit was 1 $mg \cdot L^{-1}$ for major elements, and 1 $\mu g \cdot L^{-1}$ for trace elements.

SPM samples were examined with a JEOL JSM-7000F field emission scanning electron microscope (SEM) coupled with an Oxford INCA 350 energy-dispersive X-ray spectrometry (EDS) detector at the SGIker Facilities (UPV/EHU). The working conditions included an acceleration voltage of 20 kV, a beam current of 1 nA and 10 mm working distance. Samples were prepared by passing a small piece of carbon tape over the filter and adhered to the carbon holder. After a plasma cleaning process

of 4 min it was coated with a 15 nm thick carbon layer in a Quorum Q150T ES turbo-pumped sputter coater.

Transmission electron microscopy (TEM) was completed at SGIker using a Philips CM200 microscope equipped with an EDS detector (EDAX Inc.) and LaB_6 filament. An acceleration voltage of 200 kV was used. Selected area electron diffraction (SAED) imposes substantial limitations on the particle thickness. Therefore, all samples were embedded in epoxy resin and cut at room temperature to 80 nm using a Leica EM UC6 ultramicrotome with a diamond knife, and mounted on 200 mesh Ni grids. Interplanar d-spacings were measured on SAED patterns with CrysTBox software (Klinger, 2017) and identified using the American Mineralogist Crystal Structure Database (Robert T Downs and Hall-Wallace, 2003).

Microbial community analysis

For DNA extractions one filter per depth was cut into 6 pieces. Three were used for triplicate DNA extractions, with the exception of FC at 30 m, for which only 2 parts were successfully extracted. DNA extractions were performed using the FastDNA Spin Kit for Soil (MP Biomedicals, OH, USA) according to the manufacturer's instructions. DNA concentrations were measured using a Qubit 2.0 fluorometer (Life Technologies, Darmstadt, Germany), with the Qubit dsDNA BR assay kit. PCR amplification of the V4-V5 region of the 16S rRNA gene was performed in triplicate per sample using the updated EMP primers (Thompson et al., 2017): 516F (5'-GTGYCAGCMGCCGCGGTAA-3') and 806R (5'-GGACTACNVGGGTWTCTAAT-3'). The total reaction volume was 50 µL, consisting of 10 µL 5X HF buffer, 200 µM of dNTP, 10 µM of barcoded forward and reverse primers, 2 $U \cdot \mu L^{-1}$ Phusion Hot Start II DNA polymerase (ThermoFisher Scientific), and 0.4 $ng \cdot \mu L^{-1}$ DNA template. A negative control was included using nuclease-free water instead of template. After an initial denaturation step at 98 °C for 30 s, 28 cycles were run of 10 s denaturation at 98 °C, 10 s annealing at 56 °C, and 10 s elongation at 72 °C. A final elongation step was done for 7 min at 72 °C. Triplicate PCR reactions were pooled before clean-up and further processing. The pooled PCR products were cleaned with magnetic beads using the CleanNA PCR kit (GC Biotech BV, The Netherlands), and the final concentrations were determined using a Qubit 2.0 fluorometer (Life Technologies, Darmstadt, Germany). PCR amplicons were sequenced with the Illumina HiSeq 150 bp paired-end read sequencing (GATC Biotech, Konstanz, Germany). The sequences have been deposited in European Nucleotide Archive (ENA) at EMBL-EBI under accession number PRJEB38636 (secondary accession number ERP122073). Paired-end reads were processed using NG-Tax version 2.0 (Poncheewin et al., 2020) on the Galaxy platform at https://www.systemsbiology.nl/ngtax/.

The obtained 16S rRNA gene amplicon sequences were clustered into Exact Sequence Variants (ESV's) using an open reference approach. The following default settings were used: forward and reverse read length 70 nt, ratio ESV abundance 2, classify ratio 0.8, minimum percentage threshold 0.01, identity level 100%, error correction of 1 mismatch. In the paired-end libraries only paired sequences were kept with perfectly matching barcodes. These barcodes were also used to demultiplex the reads by sample. ESV's were classified according to the SILVA SSU rRNA database (v128) (Quast et al., 2013a; Yilmaz et al., 2014). ESV's were exported in the biom format and further analyzed with R (v 3.6.3) in RStudio (v 1.2.5042). Alpha diversity was calculated on rarefied data (sample size 14600), and beta diversity was calculated on non-rarefied relative abundance data using the microbiome (v1.8.0) (Lahti and Shetty, 2017) and phyloseq (1.30.0) (McMurdie and Holmes, 2013) packages in R. Graphs were plotted using ggpubr (v 0.2.5) (Kassambara, 2020). The scripts used for data analysis can be found at mibwurrepo/van-der-Graaf-et-al-2020-Acidic-mine-pit-lakes.

Membrane lipid analysis

IPL extraction and analysis was carried out as described previously (Bale et al., 2016). Briefly, freeze dried glass fiber filters or freeze dried biomass were extracted using a modified Bligh & Dyer procedure: ultrasonic extraction three times in methanol:dichl oromethane:phosphate buffer (2:1:0.8, v/v/v) before the organic phase was separated by adjusting the solvent ratio to 1:1:0.9 and removed and dried under N_2. Before analysis, the extract was redissolved in a mixture of hexane:2-propanol:water (72:27:1, v/v/v) and aliquots were filtered through 0.45 µm regenerated cellulose syringe filters. Analysis was carried out by high performance liquid chromatography/ ion trap mass spectrometry (HPLC-ITMS) on an Agilent 1200 series LC coupled to an LTQ XL linear ion trap with Ion Max source with electrospray ionization (ESI) probe. All equipment and conditions were as described in (Bale et al., 2016). The IPL groups were identified through comparison of their masses and fragmentation patterns with authentic standards or with those described in the literature (Sturt et al., 2004; Brandsma et al., 2012; Moore et al., 2016). IPLs were examined in terms of their peak area response and, due to ionization differences between the IPLs, may not reflect their actual relative abundance. However, this method allows for comparison between the samples analyzed in this study. For comparison purposes, IPL analysis was also performed on *Microbacter margulisiae* (Sánchez-Andrea et al., 2014b), which was taken from the culture collection at the laboratory of Microbiology at Wageningen University.

Results

Physicochemical characteristics and water chemistry

Filón Centro

The physicochemical profiles of the water column of FC obtained in our study and reported previously (Sánchez España et al., 2008; López-Pamo et al., 2009) showed that FC is a meromictic lake (Figure 2). An approximately 15 m-thick mixolimnion is separated seasonally into an epilimnion, the upper layer that is regularly mixed due to heating by solar radiation (0 - 7 m), and a hypolimnion, where mixing is absent (7 - 13 m). A transitional redoxcline separates the mixolimnion from the lower, anoxic monimolimnion which extends to the lake bottom (50 m). The absence of mixing is partly illustrated by the temperature profiles of the water column (Figure 2a), which vary markedly in the epilimnion depending on the season: from 12 °C in December 2017 to 24 °C in October 2018. In the hypolimnion the temperature variation is less pronounced, fluctuating between 10 and 12 °C, and below 15 m the temperature profiles overlapped regardless of the season. The small shift in temperature at 15 m and the gradual increase from 12 °C at 15 m to 16 °C at the lake bottom is likely the result of heat released by the exothermic oxidative dissolution of metal sulfides, mainly pyrite (Nordstrom and Alpers, 1999).

The depth and sharpness of the oxycline varies with the season (Figure 2b), with dissolved oxygen completely removed at 6 m (May 2007), 14 m (Oct 2017, Oct 2018) or 16 m (March 2008, December 2017, March 2019). This could reflect a variation in oxygen consumption by aerobic respiration between early summer, fall, and winter, as well as the temperature dependence of oxygen solubility. The redox potential (ORP) dropped from around +700 mV to +450-500 mV when oxygen was depleted (Figure 2c), and then dropped further between 25 and 30 m, from approximately +450 mV to between +300 mV and -100 mV, depending on the time of sampling. The pH profile showed a pronounced increase along the water column (Figure 2d). At the lake surface the pH was highly acidic, between 1.9 and 2.4, and remained relatively constant down to a depth of 24 m. The pH increased sharply, from 2.5 to 3.9, between 24 and 29 m and then more gradually to around 4.8 between 40 m and the lake bottom. The specific conductivity (SpC) increased slightly between 15 and 16 m, from 5000 to 6000 $\mu S \cdot cm^{-1}$, and remained approximately constant until 27 m, after which it increased sharply to 13000 $\mu S \cdot cm^{-1}$ at the lake bottom (Figure 2e).

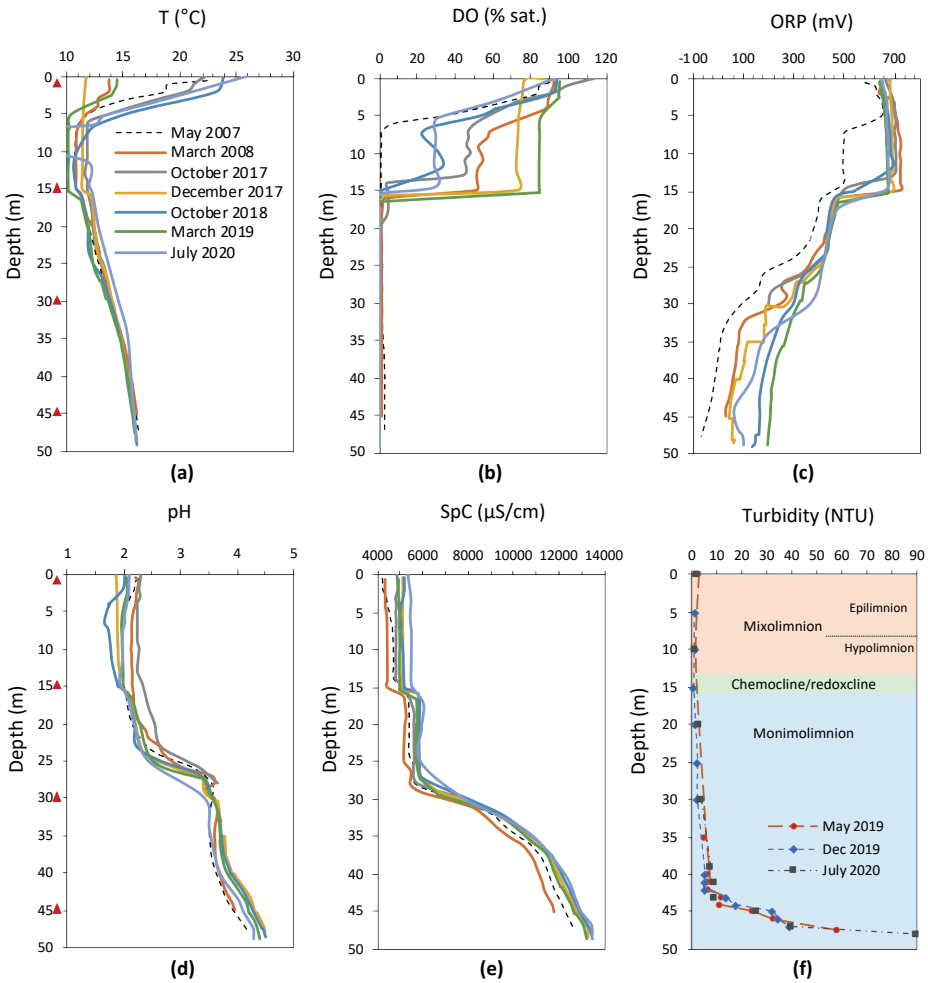

Figure 2: Physicochemical profiles of the water column in Filón Centro (FC). (a) temperature (T), (b) dissolved oxygen (DO), (c) oxidation-reduction potential (ORP), (d) acidity (pH), (e) specific conductivity (SpC), (f) turbidity (in nephelometric turbidity units, NTU) profile combined with the chemical zonation of the water column inferred from the combined physicochemical profiles. Triangles indicate the sampling depths for biomass filtration in October 2017. Data from May 2007 and March 2008 were taken from previous studies for comparison purposes (Sánchez-España et al., 2008; López-Pamo et al., 2009).

Analysis of the chemical composition of the water column of FC showed that the concentrations of several major (Na, SiO_2, Cu, Al, Zn) and trace (As, Be, Cd, Cr, Pb, Se, Th, Tl, U, V) elements decrease in the monimolimnion (Figure 3c and d, Supplementary Table S1), indicating that they participate in (bio)geochemical reactions. This is referred to as reactive behavior. Most striking in these profiles is the increase in concentrations between the lake surface and the chemocline (28 m), followed by a sharp decrease towards the lake bottom, in the case of Cu, Al, Cr, Tl, Pb, Cd, Sb to close to 0 $mg{\cdot}L^{-1}$ (Figure 3c and Supplementary Table S1). In the case of Zn, its reactive behavior was not as clear when considering only one time point, but it could be inferred from a decrease in concentration over time from 190 $mg{\cdot}L^{-1}$ at 40 m in March 2008, to 151 $mg{\cdot}L^{-1}$ at 45 m in October 2017 (Figure 3d). In contrast, the concentrations of several major (K, Mg, Ca, Mn, Fe, SO_4^{2-}), as well as trace elements (As, Co, Ni, Ag, Ba, Mo), remained constant or increased with depth (Figure 3a and b, Supplementary Table S1), indicating that they were not affected by (bio)geochemical reactions. This is referred to as conservative behavior. The total iron content increased from 824 $mg{\cdot}L^{-1}$ at the lake surface, which was predominantly Fe^{3+} as reflected by the rusty red color of the water, to 7564 $mg{\cdot}L^{-1}$ at 45 m (Figure 3a). The ORP profile indicated that below 18 m (ORP < +400 mV) (Figure 2c) iron was mostly present as Fe^{2+}, which was supported by previous measurements of iron speciation along the water column (Sánchez-España et al., 2008). The phosphate phosphorus ($P\text{-}PO_4^{3-}$) concentration in the mixolimnion (0 m) was 0.146 $mg{\cdot}L^{-1}$ (Supplementary Table S2). Nitrogen as nitrate ($N\text{-}NO_3$) and nitrogen as ammonium ($N\text{-}NH_4^+$) were measured at 2.99 $mg{\cdot}L^{-1}$ and 0.013 $mg{\cdot}L^{-1}$, respectively.

The turbidity in FC increased gradually from 2.7 to 7.0 Nephelometric Turbidity Units (NTU) between 0 and 42 m depth, and then more sharply from 7.0 to 58-86 NTU (depending on the season) between 42 and 47.5 m, indicating a high concentration of SPM in this layer (Figure 2f). SEM-EDS analysis of SPM in the water column in the mixolimnion showed the presence of detrital phase and minor ferric oxides and (oxy)-hydroxysulfates (schwertmannite and jarosite). In contrast, SEM-EDS analysis of SPM from the deep monimolimnion of FC showed an increase in Cu content, from less than 0.5 weight percent (wt %) at 40 m, to 1.5 wt % at 43 m, coinciding with the first turbidity peak maximum (Figure 2f). At 43 m rosette-like aggregates (0.33 µm) of lenticular Cu-S crystals were detected (Figure 4a), with a Cu to S molar ratio ($[Cu/S]_m$) slightly above 2.0. This suggests the presence of reduced Cu minerals ranging from digenite ($Cu_{1.8}S$) to chalcocite (Cu_2S) or djurleite ($Cu_{1.96}S$). At 45 m Cu accounted for 3.5 wt % in the SPM, showing up as globular Cu sulfides with $[Cu/S]_m$ of 1.05-1.79, generally of 0.25-0.38 microns in size and with trace amounts of As. At 47m, Cu sulfides ($[Cu/S]_m$ =1.3-2.2), and mineralized rods (Figure 4b) and spherical shapes resembling mineralized

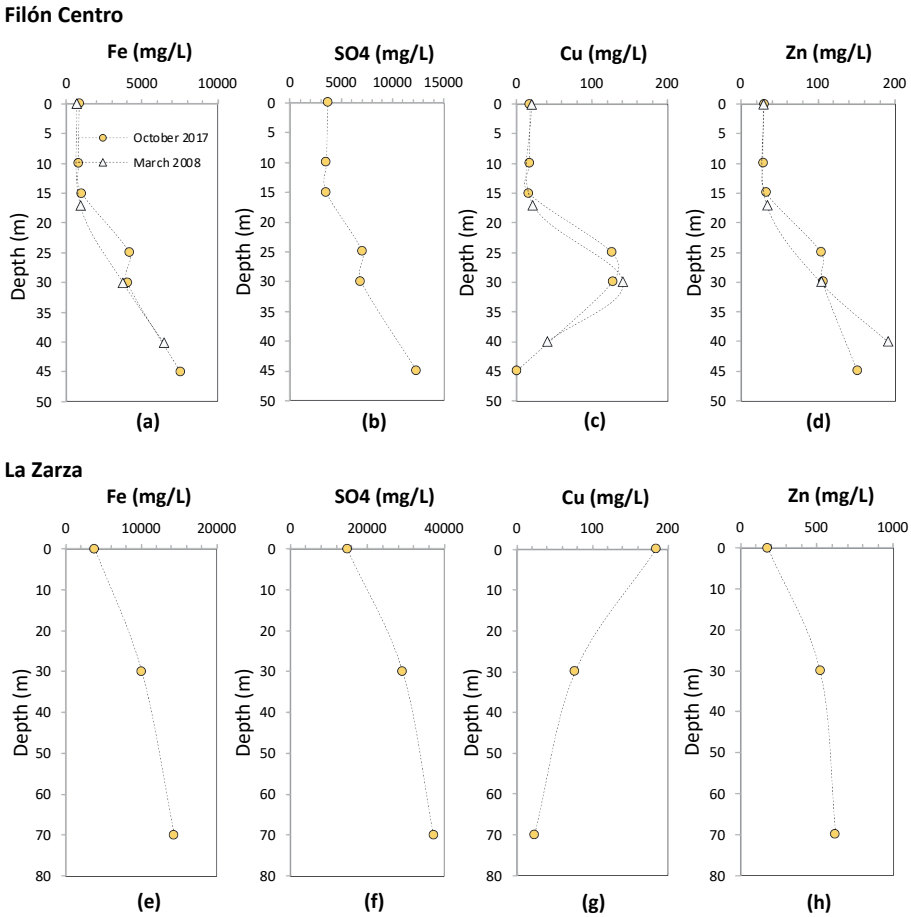

Figure 3: Depth profiles of total dissolved iron (Fe), sulfate (SO_4^{2-}), copper (Cu^{2+}), and zinc (Zn^{2+}) in $mg{\cdot}L^{-1}$ in Filón Centro (a-d) and La Zarza (e-h) as measured in October 2017 (yellow circles). Data from FC is compared with chemical data from March 2008 (Sánchez-España et al., 2008; López-Pamo et al., 2009).

microbial cells became abundant, along with scarcer Zn-S spherical particles (Figure 4c). The Zn to S molar ratio in the ZnS particles was close to 1.0, which is coherent with the presence of wurtzite (ZnS). ZnS particles were generally larger in size than the Cu-S particles (0.66 μm against 0.25-0.5 μm for Cu), and both minerals, in some cases, showed incorporation of trace amounts of As and Cd. TEM-SAED analyses suggested the presence of digenite, djurleite and chalcocite (Figure 4d-f). Furthermore, TEM images and ring SAED patterns (typical of nanocrystalline samples) revealed that the apparently individual globular particles seen under SEM were actually aggregates of smaller discrete (nanometric) spherical crystals.

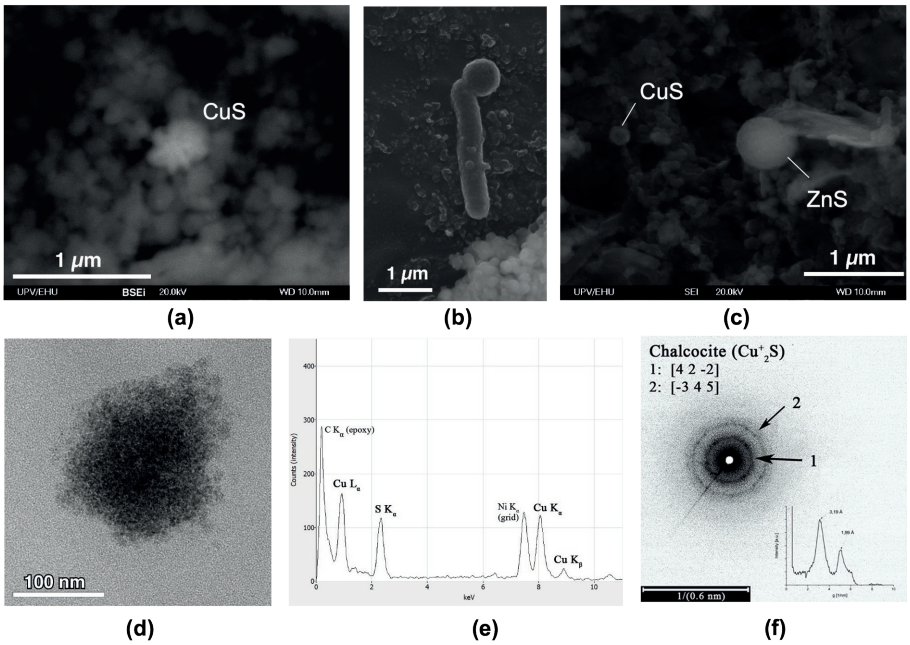

Figure 4: SEM (a-c) and TEM (d-f) images obtained on suspended particulate matter sampled at 43 m (a) and 47 m (b-f) depth in the acidic pit lake of Filón Centro in October 2018; (a) backscattered electron image of lenticular aggregate of chalcocite-like Cu sulfide; (b) mineralized bacterial rod associated with a spherical particle; (c) secondary electron image of globular ZnS with trace Cd and small darker particles which are globular Cu sulfides; (d) Globular chalcocite (Cu_2S) particle from SPM at 47m; (e) EDS pattern of the particle shown in (d) confirming composition dominated by Cu and S; (f) TEM selected area electron diffraction of globular sulfide shown in (d) with arrows indicating diffraction rings and calculated profile inset, characteristic of chalcocite (Cu_2S) with 0.01 degree of confidence.

La Zarza

Even though no time series data are available, the T and DO profiles (Figure 5a and b) indicate that the LZ pit lake is meromictic, with a very thin upper, oxic mixolimnion (0 - 4 m), and a lower, anoxic and reducing monimolimnion around 76 m thick. The physicochemical profiles obtained in October and December 2017 show a sharp drop in redox potential from +700 mV to + 450 mV in the upper 4 meters, followed by a slight increase to +480-500 mV, after which the ORP decreases more gradually to +260 mV in the lowest 8 m of the lake (Figure 5c). The pH remained constant in the upper 8 meters, around 2.0 (Figure 5d), and then increased to 2.5 between 8 and 16

m, followed by a slight decrease to 2.4 before increasing to 2.6 between 15 and 26 m. The pH remained constant until 70 m, and increased further from 2.6 to 3.0 towards the lake bottom at 80 m.

Analysis of the chemical composition of the water column in LZ indicated that several major (Ca, SiO_2, Cu) and trace (Pb, Th) elements displayed clear reactive behavior, indicating their involvement in (bio)geochemical processes (Figure 3c and Supplementary Table S1). The specific conductivity in the water column increased sharply in the upper 10 m, from 12000 $\mu S \cdot cm^{-1}$ to 23000 $\mu S \cdot cm^{-1}$, and remained constant until 45 m (Figure 5e). Between 45 m and the lake bottom (78 m) the SpC increased slowly to 26000 $\mu S \cdot cm^{-1}$, suggesting there was little precipitation of metals as insoluble compounds. SEM analysis of the SPM on the filter from 0 m showed the scarce presence of Fe(III) oxy-hydroxysulfates typical of oxidized AMD environments (schwertmannite and lesser jarosite) mixed up with detrital minerals, such as ore minerals (mainly pyrite and minor galena), phyllosilicates, quartz or rutile. Despite filtering the same volume of water as in the mixolimnion, very little SPM could be recovered from 30 m and 70 m, and no SEM images could be obtained of sulfide minerals at these depths.

The concentrations of other dissolved major and trace element increased with depth (Na, K, Mg, Mn, Fe, SO_4, Al, Ni, As, Se, Be, Tl) (Figure 3e and f, Supplementary Table S1), indicating conservative behavior. This is in line with the initial increase and subsequent constant values determined for SpC, an indication of dissolved elements (Figure 5e). However, this parameter will mainly reflect the concentrations of Fe^{2+} and SO_4^{2-} as they are an order of magnitude higher than the rest of the solutes (Figure 3e and f). The speciation of iron into ferrous and ferric iron was not determined in this lake, but from the clear, colorless water sample obtained at 30 m and using the ORP profile as a proxy for the Fe^{2+}/Fe^{3+} ratio in these mine waters (Nordstrom, 2000; Sánchez-España et al., 2005) it could be inferred that dissolved iron at that depth was mostly present as Fe^{2+}. Due to practical difficulties, no depth profiles could be obtained for nitrogen and phosphate, and only the mixolimnion (0 m) was sampled in July 2020. The extremely high concentration of dissolved iron interfered with the colorimetric determination of nitrate, so that $N\text{-}NO_3$ could not be analyzed. The $N\text{-}NH_4^+$ and $P\text{-}PO_4^{3-}$ concentrations in the mixolimnion were 27 and 57 $\mu g \cdot L^{-1}$, respectively (Supplementary Table S2).

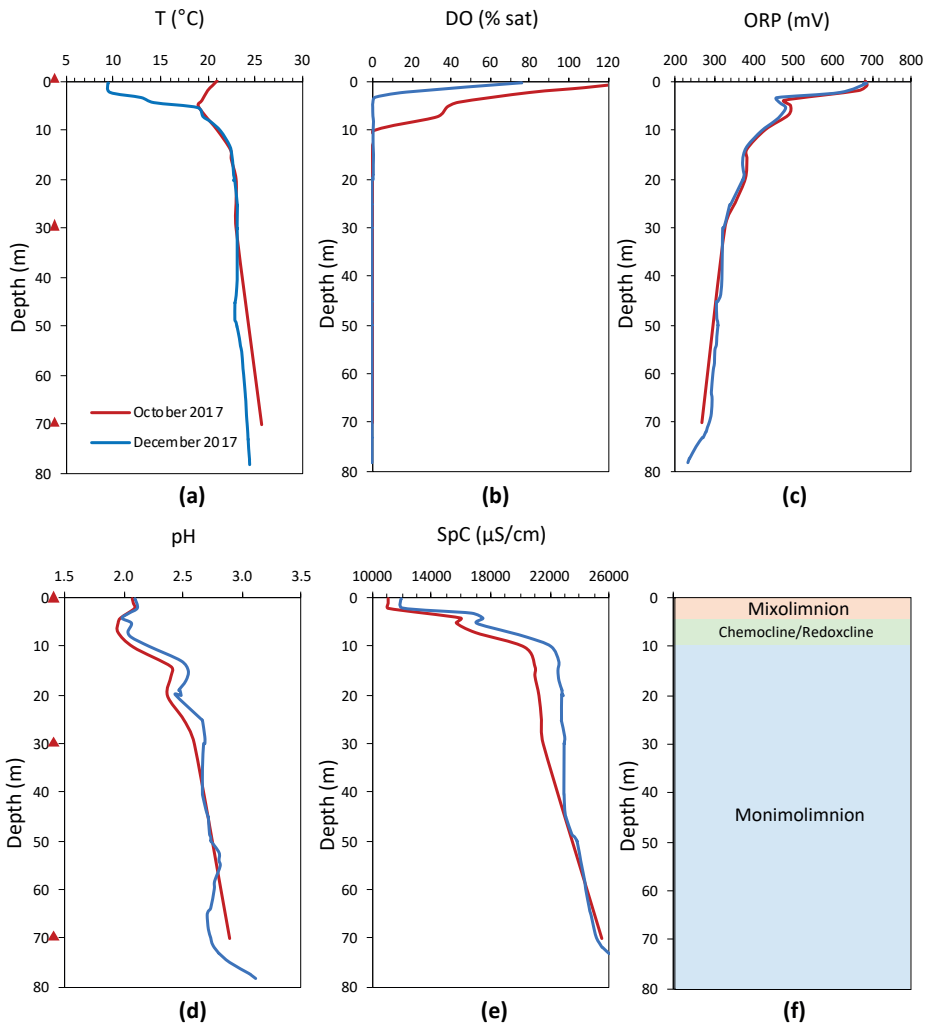

Figure 5: Physicochemical profiles of the water column in La Zarza. (a) temperature (T), (b) dissolved oxygen (DO), (c) oxidation-reduction potential (ORP), (d) acidity (pH), (e) specific conductivity (SpC), (f) inferred chemical zonation of the water column. Triangles indicate the sampling depths for biomass filtration in October 2017.

Microbial Diversity

The microbial community composition in the water column of FC and LZ was investigated by 16S rRNA gene amplicon sequencing of filtered biomass from different depths. After the filtering and quality control steps, between 14791 and 241230 reads remained per replicate (Supplementary Table S3). A clear differentiation between the microbial communities was observed with depth, as reflected in the ordination plot (Figure 6). Most apparent was that in the mixolimnion of FC and LZ the communities were very similar, and that they differed strongly in the monimolimnion. Species richness (Chao1) increased towards the bottom of both lakes (Supplementary Table S3). It should be noted that the replicates for FC at 45 m and for LZ at 30 m and at 70 m showed a large variation, suggesting spatial effects of subsampling the filters. This is also reflected in the phylum and family level diversity observed in the individual replicates (Figure 7a). The overall diversity in FC increases with depth, as expressed by the Inverse Simpson index, which calculates a diversity index based on the total number of species and the relative abundance of each species. The McNaughton's dominance (DMN), which measures the relative abundance of the two dominant taxa (McNaughton and Wolf, 1970), was high in the mixolimnion of both FC (between 0.627 and 0.686), and LZ (between 0.612 and 0.647) (Supplementary Table S3). While in FC the DMN first decreased to 0.144 at 30 m, and then increased to 0.533 - 0.611 at 45 m, in LZ the DMN decreased progressively towards the lake bottom.

Filón Centro

In the mixolimnion of FC (1 m), 79.0 % of filtered reads were assigned to two genera, the autotrophic, aerobic, iron-oxidizing genus *Leptospirillum* (40.2 % ± 7.5 %) and the heterotrophic genus *Acidiphilium* (38.8 ± 9.1 %), from the *Nitrospira* and *Alphaproteobacteria* class, respectively (Figure 7a and 8b). The family *Legionellaceae* accounted for 6.0 ± 0.4 % of filtered reads, followed by sequences affiliated with three genera: *Metallibacterium* (1.9 ± 0.2 %), *Acidibacter* (1.9 ± 0.3 %) and *Acidocella* (1.4 ± 0.1 %). The next sampling point was at 15 m, just below the oxycline, which at the time of sampling (October 2017) was situated at 13-14 m. A similar number of total ESV's (72) were detected at this depth compared to the mixolimnion (69) (Supplementary Table S3). Three genera accounted for an average of 68.4 % of filtered reads: *Metallibacterium* (36.8 ± 1.9 %), *Leptospirillum* (16.6 ± 0.8 %) and *Acidithiobacillus* (15.0 ± 0.4 %) (Figure 7b). In contrast to the upper layer, the euryarchaeal order *Thermoplasmatales* was detected (8.3 ± 0.8 %): the genus *Thermoplasma* accounted for 2.4 ± 0.6 % of total reads, and the family BSLdp125 for 4.7 ± 0.4 %. One ESV, assigned to the *Chloroflexi* class JG37-AG-4, accounted for 5.8 ± 1.8 % of filtered reads. The bacterial family

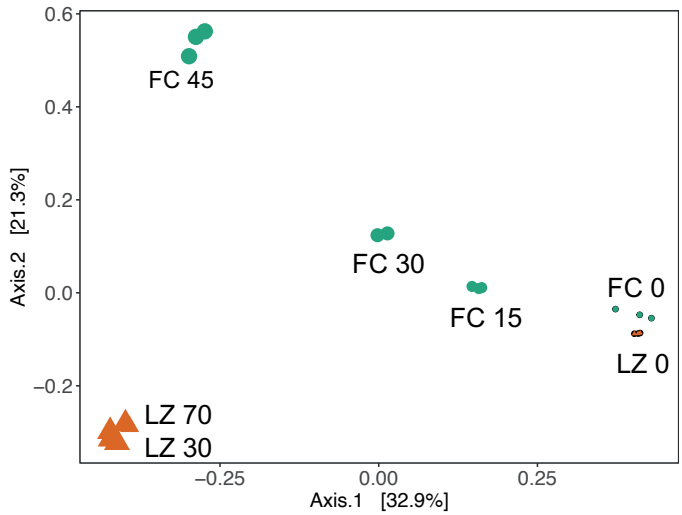

Figure 6: Ordination plot based on Bray-Curtis dissimilarity index showing spatial separation between microbial community composition at different depths in Filón Centro (green) and La Zarza (orange);

Acidobacteriaceae (Subgroup I) accounted for 3.6 ± 0.7 % of reads in this layer, with one ESV classified as an uncultured genus within *Acidobacteriaceae* (Subgroup I) accounting for 3.5 ± 0.7 % of filtered reads (Figure 7b).

At 30 m the taxonomic diversity increased compared to the mixolimnion (1 m) and oxycline (15 m) (Supplementary Table S3, Figure 7a). Sequences classified as *Thermoplasmatales* accounted for 23.4 ± 1.9 % of filtered reads, with the family BSLdp125 being the most abundant (8.1 ± 0.8 %). Similar to 15 m, reads classified as an uncultured genus from the family *Acidobacteriaceae* accounted for 8.5 ± 2.2 %. *Acetobacteraceae* accounted for 17.8 ± 1.1 % of reads, of which an ESV representing an uncultured genus (8.5 ± 1.5 %) and an ESV classified as *Acidiphilium* (7.6 ± 0.5 %) were the most dominant ESV's in this 'transition layer'. In addition, several taxa were detected at 30 m that are known to be involved in the microbial sulfur cycle: *Desulfurellaceae* (uncultured genus H16) (2.2 ± 0.3 %), *Sulfuriferula* (1.4 ± 0.2 %), *Desulfitobacterium* (0.9 ± 0.1 %), *Desulfosporosinus* (0.4 ± 0.3 %) and *Desulfomonile* (0.3 ± 0.1 %). An ESV classified as unknown genus from the family *Peptococcaceae*, which also harbors the genus *Desulfosporosinus*, accounted for 7.9 ± 1.0 % of filtered reads at 30 m.

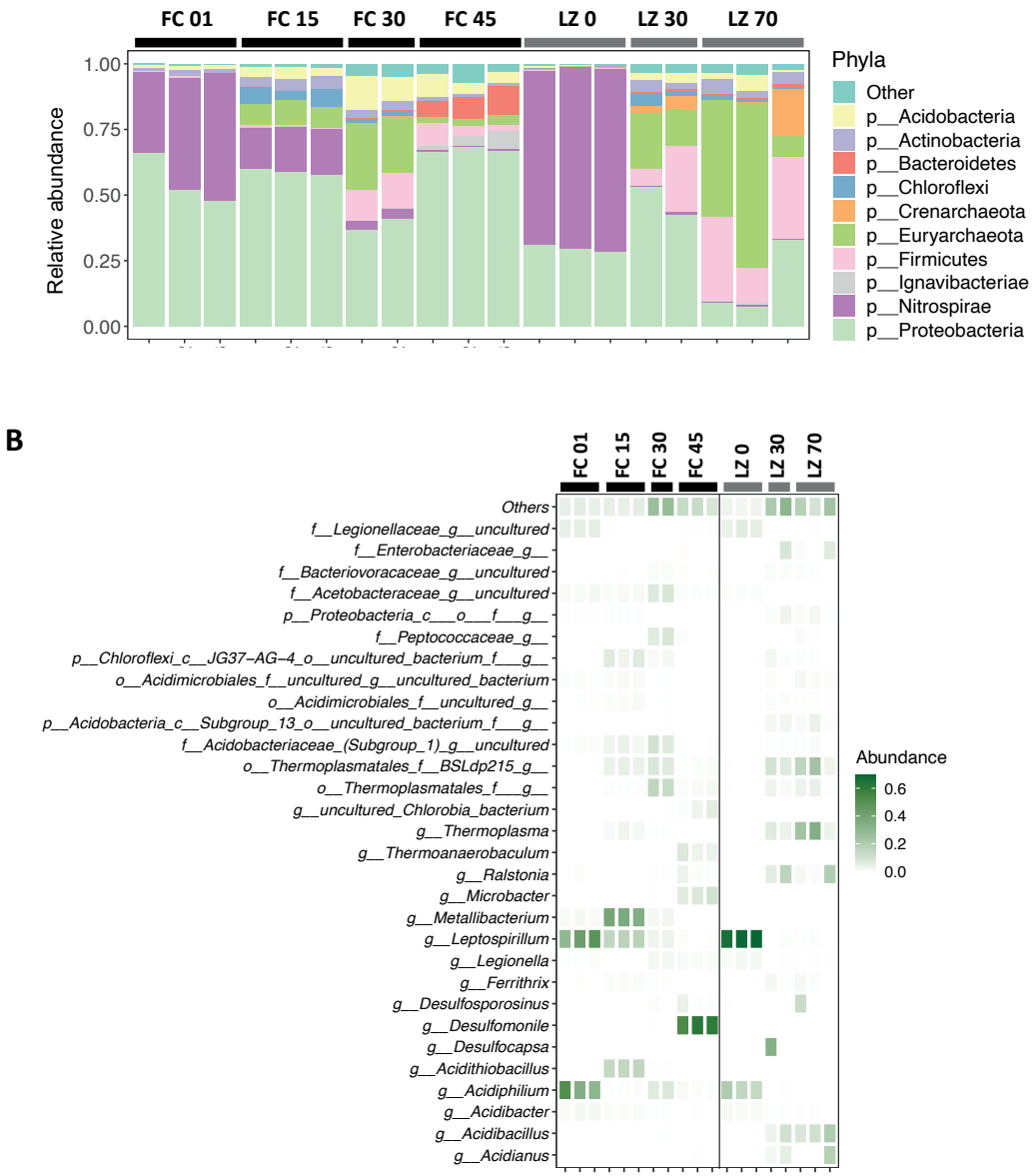

Figure 7: (a) Phylum level composition in replicate samples of Filón Centro (FC, grey bars) and La Zarza (LZ, black bars) expressed as relative read abundance; (b) relative read abundance heatmap of the top 30 genera in individual replicates obtained per site, p_, c_, o_, f_, and g_ denote phylum-, class-, order-, family- and genus-level assignment of ESVs, respectively.

In the lower, reducing monimolimnion (45 m), the microbial community showed a high number of ESV's, but 75.1 ± 5.0 % of reads were represented by just four taxa (Figure 7a). Most striking is the dominance of *Desulfomonile*, accounting for 58.5 ± 3.5 % of the total reads. An ESV classified as the sulfate-reducing genus *Desulfosporosinus* accounted for 2.0 ± 1.7 % of total reads, and *Microbacter* and *Thermoanaerobaculum* for 8.3 ± 1.8 % and 5.1 ± 2.1 % of total reads. Sequences assigned to *Thermoplasmatales* were less abundant at 45 m than at 30 m, but still accounted for 2.7 ± 0.7 % of reads. The detection of reads classified as methanogens, although in very low amounts and therefore not reflected in Figure 7, was of interest, as these are not commonly observed at such low pH. The euryarchaeal classes *Methanobacteria* (erroneously named bacteria), with *Methanobrevibacter* (0.018 ± 0.03 %), and *Methanomicrobia*, with *Methanospirillum* (0.005 ± 0.007 %), were detected.

Similar to FC, the two dominant ESV's in the mixolimnion (0 m) of LZ were classified as *Leptospirillum* (67.6 ± 1.6 %) and *Acidiphilium* (16.5 ± 2.5 %) (Figure 7b). Reads classified as *Acidibacter* accounted for 2.0 ± 0.3 %. As in FC, *Legionellaceae* was present in significant abundance: 7.4 ± 1.5 % of filtered reads were assigned to two ESV's within this family. Because the lake surface and oxycline in LZ almost coincided or overlapped (Figure 5c), the oxycline was not sampled for DNA sequencing. Instead, the microbial community was sampled at 30 and 70 m, representing the upper and lower regions of the monimolimnion. At 30 m, reads assigned to the genus *Desulfocapsa* were the most abundant (16.4 ± 16.3 %) (Figure 7a). The family *Desulfobulbaceae* (*Deltaproteobacteria*) accounted for 19.0 ± 18.9 % of reads in this layer. The large standard deviation indicated a large spatial variation on the filter. The next most abundant genus was *Ralstonia* (11.1 ± 5.3 %), followed by the euryarchaeal order *Thermoplasmatales* (17.0 ± 3.8 %), with the family BSLdp125 (8.9 ± 1.5 %) and genus *Thermoplasma* (5.6 ± 1.4 %). The crenarchaeal genus *Acidianus* from the *Sulfolobaceae* accounted for 4.2 ± 1.4 % of reads.

At 70 m, the lower region of the reducing monimolimnion, archaeal sequences represented 46.9 ± 16.6 % of reads, compared to 22.2 ± 2.8 % at 30 m and 0.5 ± 0.2 % at 0 m (Figure 7a). Reads classified as *Thermoplasmatales* were most abundant, at 38.3 ± 22.8 % of reads. Within *Thermoplasmatales,* the genus *Thermoplasma* accounted for 20.8 ± 12.5 % of the total reads, and the family BSLdp125 for 14.4 ± 8.5 %. *Acidianus* accounted for 6.1 ± 8.4 % of reads. The large standard deviation in this layer again underscores the spatial variation on the filter. *Thaumarchaeota* accounted for 0.26 ± 0.12 % of reads, with 0.21 ± 0.13 % assigned to the class '*South African Gold Mine GP1'*. Bacterial sequences were dominated by *Acidibacillus* (13.4 ± 4.9 %), *Ralstonia* (7.5 ± 8.2 %), and *Desulfosporosinus* (4.4 ± 6.0 %). Noteworthy is that, similar to the monimolimnion of FC (45 m) low amounts of sequences were classified as the

euryarchaeal classes *Methanobacteria*, with *Methanobrevibacter* (0.012 ± 0.018 %) and *Methanothermobacter* (0.006 ± 0.009 %), and *Methanomicrobia*, with *Methanospirillum* (0.013 ± 0.018 %).

Microbial membrane lipids

To assess the presence of unique microbial membrane lipid signatures in extreme AMD environments and their potential as biomarkers, the intact polar lipid (IPL) composition was determined in the filtered biomass from the water columns of FC and LZ. In the mixolimnion of LZ (0 m), IPLs were below the limit of detection. In the remaining filtered biomass samples extracts a wide range of IPLs were detected (Table 1) including the isoprenoidal archaeal lipids glycerol dialkyl glycerol tetraethers (GDGTs) and archaeols (AR). The proportion of archaeal IPLs correlated positively with the relative abundance of archaeal 16S rRNA gene sequences in the different samples (Linear regression, r = 0.98, n = 6; Figure 7a, Table 1). The non-archaeal IPLs included two types of aminolipids [ornithine lipids (OLs) and betaine lipids (BLs)], a wide range of phospholipids [phosphocholines (PC), phosphoethanolamine (PE), monomethyl PE (MMPE) and dimethyl PE (DMPE), phosphoglycerol (PG)] and glycolipids [sulfoquinovosyldiacylglycerol (SQDG), mono- and digalactosyldiacylglycerol (MGDG and DGDG)]. The core components of the phospholipids were either diacyl glycerol (DAG), diether glycerol (DEG), mixed acyl/ether glycerol (AEG) or ceramides (CR). Certain IPLs were detected uniquely or in high relative percent in FC 45 m. In particular, PC-AEG lipids accounted for 45 % of the total in FC at 45 m, whereas they accounted for 14 – 23 % at other depths in FC and in LZ 30 and 70 m. A series of ceramides with PE and MMPE headgroups were unique to FC 45 m (Table 1). The ceramide cores ranged in size between 32 and 36 carbons. For comparison purposes we analyzed the IPL profile of *Microbacter margulisiae* (Supplementary Table S4), a *Bacteroidetes* species isolated from the nearby Tinto River and often found in co-occurrence with SRB in these environments (Sánchez-Andrea et al., 2014b).

Table 1: Relative proportions of the intact polar lipid (IPL) groups, as determined by HPLC-ITMS. DAG: diacylglycerol, DEG: diether glycerol, AEG: mixed acyl/ether glycerol, CR: ceramides, PC: phosphocholine, PG: phosphoglycerol, PE: phosphoethanolamine, MMPE: monomethyl phosphoethanolamine, DMPE: dimethyl phosphoethanolamine, MGDG: monogalactosyldiacylglycerol, DGDG: monogalactosyldiacylglycerol, SQDG: sulfoquinovosyldiacylglycerol, BL: betaine lipid, OL: ornithine lipid, GDGT: glycerol dialkyl glycerol tetraethers, AR: archaeol. The numbers in parentheses denote the number of different lipids within each group, differing by carbon number. Location is abbreviated as FC: Filón Centro, or LZ: La Zarza, with a number indicating depth; nd denotes not detected.

Polar headgroup	PC			PG		PE				MMPE		DMPE							
Core structure	DAG (6)	AEG (42)	DEG (23)	DAG/AEG (3)	DEG (1)	DAG (10)	AEG (8)	DEG (6)	CR (5)	DAG/AEG (6)	CR (1)	DAG/AEG (5)	MGDG (6)	DGDG (4)	SQDG (3)	BL (18)	OL (8)	GDGT (14)	AR (4)
Location																			
FC 1	1.1	19.6	7.9	5	0.2	6.5	1.8	nd	nd	nd	nd	7	0.1	1.7	4.7	36.1	0.6	nd	7.5
FC 15	1.3	14.4	3	1.7	0.4	16.4	5.8	nd	nd	11.7	nd	11.1	0.2	0.8	1.6	14	6.2	7.3	4.1
FC 30	2.4	21.5	2.4	1.4	1	10	5	nd	nd	6.3	nd	10.4	0.3	0.8	1.5	12.1	3	19.3	2.6
FC 45	0.9	44.6	1.4	0.7	1.2	3.9	1.9	3	4.3	3	0.7	4.6	0.4	0.9	2.5	12.9	1.9	9.3	1.8
LZ 30	16.7	23.2	0.2	0.3	0.6	5.9	6.8	2.7	nd	nd	nd	2.9	1.9	9.1	0	6.8	1	15.2	6.8
LZ 70	5.1	17.1	nd	nd	0.3	6.9	5.8	4.2	nd	nd	nd	3.7	2	12.8	0	9	nd	26.3	6.6

Discussion

Depth profiles of pH and several metals in the water column of FC and LZ show an attenuation of the extreme acidity and toxic metal concentrations characteristic for AMD towards the lake bottom, which was most pronounced in FC. The upper, oxic layers (mixolimnion) of FC and LZ were similar and typical for acidic pit lakes (Sánchez-España et al., 2008), with a pH around 2.0 (Figure 2d and Figure 5d) and ORP values around +700 mV (Figure 2c and Figure 5c), dictated by the high concentrations of Fe^{3+}. The dissolved metal concentrations in LZ were more extreme than in FC, however, with abnormally high concentrations of Fe (14,334 mg·L^{-1} at 70 m depth), Al (up to 2,178 mg·L^{-1}), Mn^{2+} (up to 647 mg·L^{-1}) and Zn^{2+} (up to 624 mg·L^{-1}), and the trace elements As (up to 16,529 µg·L^{-1}), Ni (up to 10,394 µg·L^{-1}) and Co (up to 11,081 µg·L^{-1}), to name only the most conspicuous ones (Figure 3 and Supplementary Table S1). This pattern of increasing pH and decreasing concentrations of certain metals is not always observed in (meromictic) acidic pit lakes in the IPB. For example, pit lakes like San Telmo or Confesionarios show a stable monimolimnion with nearly constant pH and ORP values (Sánchez España et al., 2008; López-Pamo et al., 2009; Sánchez-España et al., 2013). The physicochemical profiles for FC and LZ are similar to those of Cueva de la Mora pit lake (IPB) and Brunita pit lake outside of the IPB (Sánchez-España et al., 2009; Wendt-Potthoff et al., 2012; Sánchez-España et al., 2020).

In both lakes, several dissolved metals, most notably Cu, were removed from the water column towards the lake bottom, indicating their involvement in (bio) geochemical processes affecting their solubility. In FC, Cu was removed completely at 45 m (Figure 3c). In LZ the Cu concentration dropped from 184 mg·L^{-1} at the lake surface to 23.2 at 70 m (Figure 3g). Although metal removal may be partly affected by other indirect mechanisms, such as adsorption to Al oxyhydroxysulfates (Sánchez-España et al., 2006, 2011, 2016), the detection of copper and zinc sulfides in the SPM from the monimolimnion of FC (Figure 4) strongly suggests the active coprecipitation of metals as metal sulfides in the monimolimnion of FC. A similar metal removal mechanism was reported for the acidic IPB pit lake Cueva de la Mora (Wendt-Potthoff et al., 2012; Diez-Ercilla et al., 2014) and more recently for the saline, acidic pit lake of the Brunita open pit mine in SE Spain (Sánchez-España et al., 2020). In both cases SRB were identified as the source of sulfide in the monimolimnion, which we hypothesized is also the case in FC and LZ. Microbial diversity analysis of the water column in FC and LZ supported this hypothesis, as it confirmed the presence of sulfidogenic taxa such as *Desulfomonile*, *Desulfosporosinus*, and *Desulfocapsa* in the monimolimnion.

In the mixolimnion of FC (1 m) and LZ (0 m) (Figure 5) the microbial community composition and physicochemical conditions were similar, and the community was dominated by *Leptospirillum* and *Acidiphilium* (Figure 7b). These two genera are typical for AMD environments and are mainly involved in the iron and carbon cycles, respectively (Johnson and Aguilera, 2015). *Leptospirillum* oxidizes Fe^{2+} to Fe^{3+}, with O_2 as electron acceptor, which is a key factor for the continuation of oxidative dissolution of metal sulfides by Fe^{3+} (Sand et al., 1995). The high ORP associated with the Fe^{2+}/Fe^{3+} couple (+710 - +720 mV in sulfate rich acidic solutions) means that O_2 is the only available electron acceptor for ferrous iron oxidation, restricting *Leptospirillum* to aerobic environments (Johnson and Aguilera, 2015). The strong oxycline in both lakes also supports high rates of O_2 consumption. The *Leptospirillum* species described to date are obligate chemolithoautotrophic ferrous iron oxidizers, partly accounting for primary production in the lake (Hippe, 2000; Christel et al., 2017). Similar to our observations in Brunita pit lake, but contrary to what is generally seen in AMD waters, *Leptospirillum* outcompetes *Acidithiobacillus* as the dominant Fe^{2+} oxidizing genus (González-Toril et al., 2010; Sánchez-España et al., 2020). This could reflect a lower tolerance of *Acidithiobacillus* to the extreme pH (around 2.0) and metal concentrations found in both lakes, favoring growth of *Leptospirillum* over *Acidithiobacillus* as reported previously (Bond et al., 2000b, 2000a).

The dominance of *Acidiphilium* in the mixolimnion of FC (1 m) and LZ (0 m) further underscores the importance of the iron and carbon cycles in this layer. *Acidiphilium* is capable of Fe^{2+} reduction, and some *Acidiphilium* spp. also carry out sulfur oxidation (Hiraishi et al., 1998; Okamura et al., 2015). Except for *A. acidophilum*, which is capable of autotrophic growth (Hiraishi et al., 1998), *Acidiphilium* species are obligate heterotrophs and play an important role in the removal of organic compounds such as organic acids that are toxic to autotrophic microorganisms like *Leptospirillum* (Sánchez-Andrea et al., 2014a). Three genera found at lower abundance in the reads, *Metallibacterium* (1.9 ± 0.2 %), *Acidibacter* (1.9 ± 0.3 %) and *Acidocella* (1.3 ± 0.3 %) are also known for heterotrophic growth and likely play a similar role (Jones et al., 2013; Ziegler et al., 2013; Falagán and Johnson, 2014). Interestingly, in both FC and LZ, 2 ESV's were assigned to the family *Legionellaceae,* one classified as the genus *Legionella* and the other as an uncultured genus. These were found at all depths investigated, with the highest relative read abundance in the upper layers, 6.0 ± 0.5 % in FC (1 m) and 7.4 ± 1.8 % in LZ (0 m). Although uncommon in AMD environments, the detection of reads classified as the family *Legionellaceae* was previously reported in acidic pit lakes (Auld et al., 2013; Santofimia et al., 2013; Grettenberger et al., 2020), and could indicate a so far unexplored role for this taxa in AMD waters.

In the monimolimnion, the physicochemical profiles and microbial community composition of the two pit lakes diverged. The greatest difference was the more pronounced pH increase and metal removal, and the dominance of the SRB genus *Desulfomonile* in FC at 45 m (Figure 7b). In FC the pH increased to 4.3 in the lower region of the monimolimnion (45 m) (Figure 2d), whereas in LZ the pH remained around 2.8 (Figure 5d). Concentration profiles of several dissolved elements, such as K, Fe, SO_4^{2-} and Co, showed an increase in concentration towards the lake bottom. This is related to the conical shape of the pit lakes, which modifies the water/rock ratio and increases the amount of reactive rock surface per liter of acidic water. In the absence of (bio)geochemical processes removing dissolved elements from the water column, this decreased water/rock ratio will result in increasing concentrations with depth, referred to as conservative behavior. In contrast, reactive elements are removed from the water column towards the lake bottom, likely as insoluble mineral phases. Concentration profiles of dissolved elements in FC and LZ indicated a higher number of reactive elements disappearing from the water column in FC (Na, SiO_2, Cu, Al, Zn, As, Be, Cd, Cr, Pb, Se, Th, Tl, U, V), than in LZ (Ca, Cu, Pb, Th, SiO_2) (Figure 3, Supplementary Table S1). Since the oxidative dissolution rates of pyrite to Fe^{3+} and SO_4^{2-} are orders of magnitude higher than for most other elements, removal of reactive elements from the water column is not clearly reflected in the specific conductivity (SpC) profiles. Furthermore, the inflow of water from underground mine tunnels with higher concentrations of dissolved elements cannot be excluded and would contribute to an increased SpC. The near-complete removal of Cu from the water column in FC, and the partial removal of Cu in LZ (Figure 3c and g) strongly indicates the formation of copper precipitates, most likely Cu_2S and CuS as these are one of the first metal sulfides to precipitate according to their solubility products under these conditions (Diez-Ercilla et al., 2014). The detection of zinc sulfides (ZnS) in the SPM in the lower layers of FC (Figure 4), and the turbidity peak observed at this depth (Figure 2f) indicate intense microbial activity and associated biosulfidogenesis. These observations strongly suggest metal removal through reaction with biogenic H_2S, followed by precipitation as metal sulfides in the water column.

Biosulfidogenesis in the monimolimnion of FC and LZ is supported by the detection of sulfidogenic taxa. This is most apparent in FC, where the monimolimnion is characterized by a transition from a diverse microbial community at 30 m, to a community at 45 m that is dominated by just one ESV (58.2 ± 3.5 % of filtered reads) classified as the putative sulfate-reducing *Desulfomonile spp*. The two described *Desulfomonile* species, *D. tiedjei* (DeWeerd et al., 1990) and *D. limimaris* (Tiedje et al., 2015), were isolated from neutrophilic 3-chlorobenzoate reducing consortia originating

from sewage sludge and marine sediments, respectively, and both strains are capable of autotrophic and heterotrophic sulfate reduction. Although no acidophilic *Desulfomonile* species have been described to date, this is not the first report of sequences classified as *Desulfomonile* in AMD environments. *Desulfomonile* was detected in the anoxic, reducing layer of the meromictic pit lake Cueva de la Mora (Falagán et al., 2013), and more recently in the acidic Brunita pit lake (Sánchez-España et al., 2020), where it is also proposed to play a major role in the natural attenuation of extreme conditions in the monimolimnion. Its dominance in the water column, compared to more commonly found SRB species in AMD sediments such as *Desulfosporosinus* and *Candidatus* Desulfobacillus (Alazard et al., 2010; Sánchez-Andrea et al., 2015), suggests that this species is highly adapted to extreme acidity and metal toxicity, and provides an interesting candidate for application in bioremediation processes.

In LZ the attenuation of extreme acidity and metal concentrations was not as pronounced as in FC, but still a clear removal of Cu and Pb was observed (Figure 3c and g, Supplementary Table S1), usually the less soluble metals in AMD-affected zones (Rowe et al., 2007; Diez-Ercilla et al., 2014). Together with the detection of taxa known to perform sulfidogenesis from S_8^0, this supports biosulfidogenesis in the water column and the associated metal sulfide precipitation in the monimolimnion of LZ. Formation of S_8^0 in AMD environments occurs through the oxidative dissolution of certain metal sulfides (MS) through the polysulfide mechanism (equation 3) (Sand et al., 1995). S_8^0 can then be oxidized aerobically or anaerobically to SO_4^{2-} by sulfur-oxidizing microorganisms such as *Acidithiobacillus* spp., or (partly) reduced to H_2S by sulfur-reducing ordisproportionating microorganisms (Florentino et al., 2015). In contrast to SO_4^{2-} reduction, S_8^0 reduction is not H+ consuming, which fits the less pronounced pH increase in LZ.

$$8\,MS + 16Fe^{3+} \rightarrow 8M^{2+} + S_8^0 + 16Fe^{2+} \qquad (3)$$

In the upper part of the monimolimnion (30 m) in LZ, one of the dominant ESV's was classified within the genus *Desulfocapsa*, of which two species are described: *Desulfocapsa thiozyomogenes* (Janssen et al., 1996), isolated from a freshwater lake, and *Desulfocapsa sulfoexigens* (Finster et al., 1998), isolated from marine sediments. Both species are capable of the disproportionation of sulfur compounds such as S_8^0 or thiosulfate ($S_2O_3^{2-}$) to H_2S and SO_4^{2-}. As *D. thiozyomogenes* and *D. sulfoexigens* are neutrophilic, and LZ is an extremely acidic environment with very high metal concentrations, the *Desulfocapsa* sequences detected in LZ likely represent novel (poly-) extremophilic species of this genus. Although *Desulfocapsa* was only detected

in one of the two replicates, indicating the impact of spatial variation of the biomass on the filter, the absence of *Desulfocapsa* sequences in other samples supports the conclusion that this is not due to contamination and that this taxon plays a role at this depth.

In addition to the S_8^0 disproportionating genus *Desulfocapsa*, several S_8^0 reducing sulfidogenic taxa were detected at 30 m. *Acidianus* accounted for 4.2 ± 2.0 % of filtered reads, and *Thermoplasma* for 5.6 ± 2.0 %. The detection of *Acidianus* was surprising, since this genus is generally found in thermoacidophilic environments (Zillig et al., 1986; Plumb et al., 2007; Ding et al., 2011). Isolated *Acidianus* spp. predominantly obtain energy through aerobic or anaerobic dissimilatory sulfur metabolism (Kletzin et al., 2004; Kletzin, 2007). *Acidianus ambivalens*, for example, is capable of chemolithoautotrophic oxidation and reduction of S_8^0, and *Acidianus* strain DS80, is reportedly capable of both S_8^0 reduction and disproportionation (Amenabar and Boyd, 2018). Because the dissolved oxygen concentration in LZ at 30 m was below the detection limit, sequences classified as *Acidianus* likely indicate anaerobic respiration with oxidized sulfur compounds by this species, resulting in H_2S production. Similarly, the detection of sequences classified as *Thermoplasma* (5.6 ± 2.0 %), for which *Thermoplasma volcanium* and *Thermoplasma acidophilum* are the isolated representatives, suggests active H_2S production. Both strains are capable of (heterotrophic) S_8^0 reduction, and were first isolated from coal refuse piles (Segerer et al., 1988). *Thermoplasma* belongs to the euryarchaeal order *Thermoplasmatales*, which is commonly detected in AMD environments under both aerobic and anaerobic conditions (Druschel et al., 2004; Sánchez-Andrea et al., 2012b).

In the lower region of the monimolimnion in LZ (70 m) the removal of reactive elements was most pronounced, suggesting more active sulfidogenesis in this layer. Although not nearly as dominant as in FC, SRB were detected in this layer: sequences assigned to *Desulfosporosinus* accounted for 4.4 % of filtered reads. At a pH of 2.9, this is one of the most acidic environments where this genus has been detected so far (Alazard et al., 2010; Sánchez-Andrea et al., 2015). Although not uncommon in AMD environments, *Desulfosporosinus* is generally reported in AMD sediments where the potential for protection in less acidic micro-niches is higher, as mentioned above. The proportion of *Thermoplasma* increased (20.8 %) compared to 30 m, as did *Acidianus* sequences (6.1 %), further supporting active sulfidogenesis at 70 m.

The detection of a low number of reads classified as methanogens in the water column of LZ and FC is noteworthy. Methanogenesis was previously observed in AMD environments (Sanz et al., 2011), but so far only one acidophilic methanogen, *Methanoregula boonei* 6A8, has been reported, with an optimum pH of 5 and no activity

below pH 4 (Bräuer et al., 2011). An acidotolerant methanogen, *Methanobacterium espanolae GP9*, was isolated from sludge from a waste treatment facility of a pulp mill in Espanola (Canada), with an optimal pH range of 5.6 – 6.2 (Patel et al., 1990). Lastly, the acidotolerant, hydrogenotrophic *Methanobrevibacter acididurans* ATM (OCM 804), isolated from an acidogenic digester, grows in a pH range of 5.0 – 7.5, with an optimum at pH 6.0 (Savant et al., 2002). Acidophilic methanogens could be highly relevant for application in the treatment of organic waste, where acidification of the process conditions can pose a significant challenge (Tabatabaei et al., 2010).

We observed low concentrations of $N\text{-}NH_4^+$ and $P\text{-}PO_4^{3-}$, 13 and 146 $\mu g \cdot L^{-1}$ in FC and 27 and 57 $\mu g \cdot L^{-1}$ in LZ, respectively, and both lakes can be classified as oligotrophic (Wetzel, 2001). For comparison purposes, in the eutrophic Brunita pit lake $N\text{-}NH_4^+$ and $P\text{-}PO_4^{3-}$ concentrations were 700 and 200 $\mu g \cdot L^{-1}$, respectively. The establishment of SRB in the water column of FC therefore shows that the potential for natural metal attenuation through biosulfidogenesis extends to even more extreme conditions than previously proposed from findings in the acidic pit lakes Cueva de la Mora and Brunita (Wendt-Potthoff et al., 2012; Sánchez-España et al., 2020). In the case of Brunita, an increase in pH and a removal of metals was observed in the lower monimolimnion, and together with the high abundance of SRB (*Desulfomonile*, *Desulfurispora*, *Desulfobacca*, and *Desulfosporosinus*), this pointed towards biosulfidogenesis in the water column. However, although the Brunita pit lake represents a worst case scenario in terms of salinity and metal concentrations, the presence of carbonate minerals in the open pit, not prevalent in the IPB (Leistel et al., 1997; Tornos et al., 1997), contributed to the reduction of acidity (driving pH to values of 5.0 in the pit lake bottom) and potentially aided in the establishment of SRB. Furthermore, the abundance of inorganic nitrogen (nitrate and ammonium) and phosphate in the water column provided ample opportunity for phototrophic primary producers to establish, which is also reflected in the observation of abundant green microalgae in surface waters and the high abundance of sequences classified as chloroplasts in the mixolimnion (Sánchez-España et al., 2020). Growth of phototrophic microorganisms provided organic carbon to organotrophic microorganisms in the water column, which could aid the establishment of SRB. In Cueva de la Mora, the high availability of phosphorus enabled extensive phototrophic activity, thereby supplying organic carbon (Wendt-Potthoff et al., 2012). In contrast, the very low abundance of chloroplast sequences in FC and LZ and the absence of visual cues of algal growth in the mixolimnion, indicated very limited growth of phototrophic primary producers, and consequently a low availability of organic carbon in the two lakes. This further supports their oligotrophic nature.

In addition to 16S rRNA amplicon sequencing, we characterized the IPL profiles for microbiological characterization of FC and LZ. The IPLs detected in the SPM from FC and LZ contained a range of amino-, phospho- and glyco-lipids of bacterial/eukaryotic origin as well as GDGTs and archaeols of archaeal origin. Overall, the distribution of IPLs was quite similar to that reported for a highly polluted meromictic lake in eastern Massachusetts (Ertefai et al., 2008). In particular there was, as per FC, a predominance of betaine lipids in the epilimnion. Also comparable between that lake, and FC and LZ was the increase with depth in diether PEs (PE-DEGs), which the authors of (Ertefai et al., 2008) attributed to SRB. Of particular relevance to our study were the ceramide lipids with PE and MMPE polar groups that were only detected in the FC 45 samples. PE ceramides are known to be dominant sphingolipids in several *Bacteroidetes* species (Panevska et al., 2019), which corresponds well with the relative abundance of *Bacteroidetes* at this depth in FC. Among them was the *Bacteroidetes* genus *Microbacter*, accounting for 8.3 ± 1.8 % of filtered reads. The only described species so far, *Microbacter margulisiae,* was isolated from acid rock drainage sediments in the nearby Tinto River (Sánchez-Andrea et al., 2014b). *M. margulisiae* is a fermentative bacterium often found in co-occurrence with SRB in sulfidogenic enrichment cultures (Sánchez-Andrea et al., 2011, 2014b) and in natural and engineered acidic environments (Church et al., 2007; Dann et al., 2009; Gaidos et al., 2009; Lindsay et al., 2011; Sánchez-Andrea et al., 2013). For comparison purposes we determined the IPL profile of *M. margulisiae*, showing that in this species PE-ceramides account for around 15 % of the total lipid sum (Supplementary Table S4). As the *Bacteroidetes* species so far reported to contain PE ceramides (for example *Flectobacillus major, Bacteroides fragilis*, *Porphyromonas gingivalis*) are not typical for AMD environments (Olsen and Jantzen, 2001; Panevska et al., 2019), we propose that the detection of PE ceramides in these environments could serve as a biomarker for the presence of *Microbacter* species in future studies in similar systems.

Another interesting feature of the IPLs detected in the FC 45 m samples was the high proportion (45 %) of phosphocholine lipids (PC) with mixed acyl/ether glycerol (AEG) core structures (Table 1). AEG lipids, which include plasmalogen lipids, are generally associated with anaerobic bacteria and are thought to contribute to membrane homeostasis in extreme environments (Grossi et al., 2015). PC-AEGs have been found as characteristic lipids of *Desulforhabdus amnigena,* which, like *Desulfomonile*, belongs to the order *Syntrophobacterales* (Rütters et al., 2001), and we therefore postulate that the dominance of PC-AEGs at FC 45 m relates to the high proportion of the SRB genus *Desulfomonile* at this depth.

Based on the results presented here, we propose that compared to Brunita and Cueva de la Mora, the FC and LZ pit lakes provide more extreme examples of natural (metal) attenuation mediated by biosulfidogenesis, with LZ on the far end of the spectrum, as its acidity and metal concentrations are among the highest found in the IPB and elsewhere (Sánchez-España et al., 2008; López-Pamo et al., 2009). We further propose that LZ is an example of this process in an earlier stage than FC, which is likely related to its age: LZ flooded in the 1990's, whereas FC flooded in the late 1960's. We suggest a scenario where initial attenuation in the form of metal removal is mostly mediated by biosulfidogenesis through reduction or disproportionation of S_8^0, triggering metal attenuation and enabling the establishment of SRB. SRB subsequently contribute to the amelioration of acidity, as sulfate reduction at low pH is H^+ consuming. Contrary to what is often proposed (Koschorreck, 2008), the availability of organic carbon does not seem to be the limiting factor, given that in both FC and LZ, phototrophic primary production is apparently very low.

A better understanding of the biogeochemical processes that influence the development of these pit lakes, specifically the establishment of sulfidogenic micro-organisms, could promote their function as low-cost natural remediation solutions for AMD waters. Acidic pit lakes furthermore pose extremely interesting targets for biomining of secondary resources, provided that the precipitated metal sulfides can be recovered efficiently. As an illustration of the economic potential of such lakes: a rough estimation of total copper removed from LZ pit lake through metal sulfide precipitation in the past 25 years indicates a removal of 400 tons, or roughly 16 tons of copper annually. In FC this amounts to 8 tons Cu in total (over the past 50 years) or 160 $kg \cdot year^{-1}$, underscoring the extreme nature of LZ even by AMD standards. At the current market price of copper (~5800 $US\$ \cdot Ton^{-1}$), these rough estimates indicate a potential for biomining of mine water in acidic pit lakes via sulfidogenesis. In a global context of resource scarcity and the need for waste recycling, this option should be further explored.

Conclusions

This study shows that natural attenuation of extreme metal concentrations in acidic pit lakes through precipitation as metal sulfides is more widespread than previously recognized, and that biosulfidogenesis by sulfate-reducing and elemental sulfur-reducing and disproportionating microorganisms plays a key role in this process. The detection of SRB in the water column of the FC and LZ pit lakes is of great interest,

as it expands the physicochemical limits under which SRB are observed to be active. FC and LZ are examples of natural bioremediation reactors at different stages of the process and at different degrees of extremophilic conditions, where S_8^0 precedes SO_4^{2-} as the dominant inorganic sulfur compound for H_2S production. Our results suggest that organic carbon availability is not necessarily the limiting factor for establishment of SRB, since both lakes could be classified as oligotrophic. The extreme acidity and metal concentrations suggest a high tolerance of the detected SRB species to these conditions, making them species of great interest for the development of AMD bioremediation and biomining technologies.

Author Contributions: Conceptualization and methodology, I.S-A., J.S-E., C.G.; R software & sequencing data analysis, S.S., C.G.; SEM: I.Y., A.I., lipid analysis: N.B., L.V., writing—original draft preparation, C.G.; writing—review and editing, I.S-A., J.S-E., C.G., A.J.M.S., I.Y., A.I., N.B., L.V., S.S.,; visualization, J.S-E., C.G., S.S.; supervision, J.S-E., I.S-A. A.J.M.S.; funding acquisition: I.S-A., J.S-E, A.J.M.S. All authors have read and agreed to the published version of the manuscript.

Funding: This work is part of the research program STW with project number 14797, which is financed by the Dutch Research Council (NWO). I.S-A. was funded by the Netherlands Ministry of Education, Culture and Science through SIAM Gravitation grant 024.002.002. Field work and sampling was partly funded by the Spanish Ministry of Science through grant number CGL2016-74984-R. N.B. is funded by the European Research Council (ERC) under the European Union's Horizon 2020 research and innovation program (grant agreement no.694569).

Acknowledgments: We gratefully acknowledge Dr. I. Alves Guedes for technical support with DNA extractions. We thank personnel at the SGIker facilities of the UPV/EHU (Ana Martínez-Amesti and Sergio Fernández), and Michel Koenen for lipid extraction and analysis.

Conflicts of Interest: The authors declare no conflict of interest. The funders had no role in the design of the study; in the collection, analyses, or interpretation of data; in the writing of the manuscript, or in the decision to publish the results.

Supplementary information

Table S1 Dissolved element concentrations measured in Filón Centro in October 2017 (top) and March 2008 (middle) as described in previous studies (Sánchez España et al., 2008; López-Pamo et al., 2009); and in La Zarza in October 2017 (bottom); n.a. not analysed.

Filon Centro																											
Oct-17																											
Depth	Na	K	Mg	Ca	Fe	SO_4^{2-}	SiO_2	Mn	Cu	Zn	Al	As	Be	Cd	Cr	Co	Ni	Pb	Se	Th	Tl	U	Ag	Ba	Hg	Mo	Sb	V
m	mg/l	mg/l	mg/l	mg/l	mg/l	mg/l	mg/l	mg/l	mg/l	mg/l	mg/l	µg/l	µg/l	µg/l	µg/l	µg/l	µg/l	µg/l	µg/l	µg/l	µg/l	µg/l	µg/l	µg/l	µg/l	µg/l	µg/l	µg/l
0	31.6	0.76	220	166	824	3704	137	37.7	17.6	30	166	286	8.66	71.7	40.3	1367	766	121	23	4.09	1.2	6.79	1	1.72	n.a.	< 0,8	3.59	n.a.
10	29	0.48	214	162	765	3573	130.0	36.1	16.9	28.5	157	223	8.56	70.2	40.1	1301	721	88.8	20.4	3.3	0.96	6.31	1.97	1.98	n.a.	< 0,8	2.65	n.a.
15	28.4	0.34	219	164	994	3543	133	38.6	16.1	33	191	145	8.43	89.2	43.2	1422	747	107	19.2	2.79	2.16	6.02	< 0,2	1.86	n.a.	< 0,8	3.72	n.a.
25	19.7	5.78	294	153	4159	7054	92.6	85.7	126	104	163	512	10.1	746	32	3252	1641	180	13.1	0.23	19.4	5.44	0.36	19.8	n.a.	< 0,8	6.67	n.a.
30	19.2	5.81	295	150	4023	6943	88.8	82.2	127	106	157	394	11.3	843	34	3583	1824	194	13.7	< 0,5	20.7	5.75	< 0,5	16.2	n.a.	< 2	3.57	n.a.
45	19.6	17.5	435	202	7564	12339	30.8	126	0.165	151	28.3	623	3.96	5.87	3.09	5428	1859	48.7	7.82	< 0,5	3.89	2.8	< 0,5	24.3	n.a.	< 2	0.3	n.a.
Mar-08																											
Depth	Na	K	Mg	Ca	Fe	SO_4^{2-}	SiO_2	Mn	Cu	Zn	Al	As	Be	Cd	Cr	Co	Ni	Pb	Se	Th	Tl	U	Ag	Ba	Hg	Mo	Sb	V
m	mg/l	mg/l	mg/l	mg/l	mg/l	mg/l	mg/l	mg/l	mg/l	mg/l	mg/l	µg/l	µg/l	µg/l	µg/l	µg/l	µg/l	µg/l	µg/l	µg/l	µg/l	µg/l	µg/l	µg/l	µg/l	µg/l	µg/l	µg/l
0	28.1	0.73	194	154	681	n.a.	n.a.	35.0	19.3	29.1	164	365	9	63.8	30.3	1552	764	152	<200	3.04	2.13	5.57	<0,8	<2	<4	<2	2.8	4.52
17	29.9	0.53	202	144	917	n.a.	n.a.	39.5	21.5	33.6	187	156	9	78.2	34.3	1752	820	163	<200	2.73	0.7	5.54	<0,8	<2	<4	<2	3.47	16.7
30	20.6	6.26	274	148	3736	n.a.	n.a.	71.5	141	103	164	806	11	660	42.9	2850	1745	537	<200	<2	13.0	5.43	<2	14.1	<10	<5	26.5	131
40	18.8	6.51	396	184	6405	n.a.	n.a.	108	40.9	190	104	1104	10	679	26.1	3200	1972	345	<200	<2	14.8	6.30	<2	6.26	<10	<5	23.8	65.5
La Zarza																											
Oct-17																											
Depth	Na	K	Mg	Ca	Fe	SO_4^{2-}	SiO_2	Mn	Cu	Zn	Al	As	Be	Cd	Cr	Co	Ni	Pb	Se	Th	Tl	U	Ag	Ba	Hg	Mo	Sb	V
m	mg/l	mg/l	mg/l	mg/l	mg/l	mg/l	mg/l	mg/l	mg/l	mg/l	mg/l	µg/l	µg/l	µg/l	µg/l	µg/l	µg/l	µg/l	µg/l	µg/l	µg/l	µg/l	µg/l	µg/l	µg/l	µg/l	µg/l	µg/l
0	37.0	0.6	756	552	3,901	14,712	150	317	184	182	876	5,688	37	355	156	4,126	3,994	408	167	40	12	118	< 0,5	9	n.a.	3	18	177
30	38.9	8.5	1190	453	10,072	29,108	136	489	76.8	523	1870	9,878	59	1,086	329	7,295	6,877	465	187	5	136	195	< 1	14	n.a.	< 4	70	1,556
70	50.1	16.0	1536	510	14,334	37,044	122	647	23.2	624	2178	16,529	83	1,268	290	11,081	10,394	389	254	5	253	204	< 1	20	n.a.	< 4	74	1,432

Table S2: Phosphorus as phosphate ($P\text{-}PO_4^{3-}$), nitrogen as nitrate ($N\text{-}NO_3^-$), and nitrogen as ammonium ($N\text{-}NH_4^+$) in the mixolimnion of Filón Centro (FC) and La Zarza (LZ) in July 2020. ND: not determined (due to interference of dissolved ferric iron concentrations).

	$P\text{-}PO_4^{3-}$ $mg{\cdot}L^{-1}$	$N\text{-}NO_3^-$ $mg{\cdot}L^{-1}$	$N\text{-}NH_4^+$ $mg{\cdot}L^{-1}$
FC (0 m)	146	2990	13
LZ (0 m)	57	ND	27

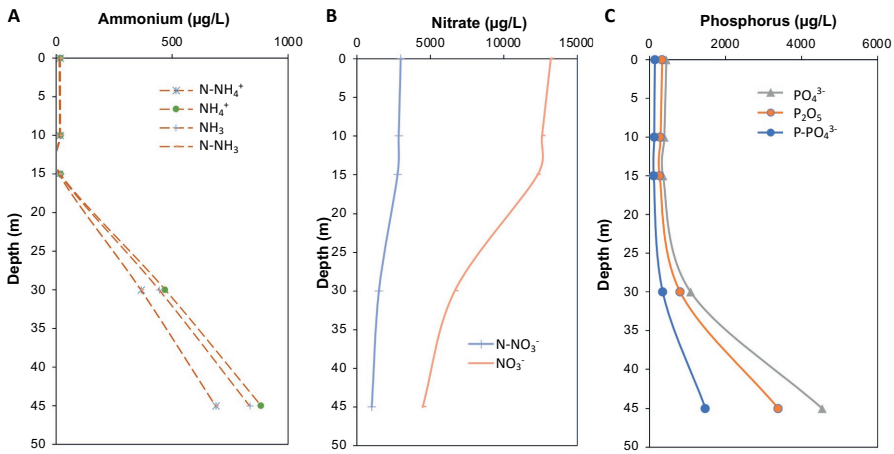

Figure S1: Nutrient profiles determined in Filón Centro in July 2020; (a) nitrogen as ammonium; (b) nitrogen as nitrate; (c) phosphorus as phosphate.

Table S3. Summary of 16S rRNA amplicon sequencing data. Total number of reads remaining after quality filtering. Rarefied data (sample size 14600) was used to determine the observed ESV's per replicate, species richness (Chao1), diversity and evenness (Inverse Simpson and Simpson Index), and relative abundance of two most abundant ESV's (Dominance). Sample name is represented as SITE-depth-replicate

Sample Name	Filtered reads	Observed ESV's	Richness: Chao1	Diversity: Inverse-Simpson	Evenness: Simpson	Dominance: DMN
FC01r1	187063	352	363.5	4.8	0.014	0.63
FC01r2	211695	260	280.9	4.6	0.018	0.64
FC01r3	135447	254	274.3	3.9	0.015	0.69
FC15r1	181849	362	373.7	6.0	0.016	0.48
FC15r2	61905	373	400.5	6.3	0.017	0.48
FC15r3	103664	395	416.0	6.7	0.017	0.47
FC30r1	171659	483	500.4	32.8	0.068	0.15
FC30r2	121181	599	634.6	36.4	0.061	0.14
FC45r1	25576	477	503.1	4.5	0.010	0.53
FC45r2	145176	423	455.6	3.3	0.008	0.61
FC45r3	79092	377	391.2	3.6	0.010	0.6
LZ00r1	152023	216	222.7	3.2	0.015	0.65
LZ00r2	149480	232	243.7	3.2	0.014	0.62
LZ00r3	241230	259	274.1	3.3	0.013	0.61
LZ30r1	14791	786	838.4	11.8	0.015	0.34
LZ30r3	83649	693	726.1	20.0	0.029	0.24
LZ70r1	202160	538	578.1	14.7	0.027	0.31
LZ70r2	98208	320	342.5	6.7	0.021	0.51
LZ70r3	112621	772	803.0	12.0	0.016	0.33

Table S4. Distribution of PE ceramides in FC 45 and in the *M. margulisiae* isolate

	PE ceramides					
	$C_{32:0}$	$C_{33:0}$	$C_{35:0}$	$C_{35:1}$	$C_{36:0}$	$C_{37:0}$
FC 45 m	10	10	45	13	23	
M. margulisiae			43		6	51

Acetate degradation at low pH by the moderately acidophilic sulfate reducer *Acididesulfobacillus acetoxydans* gen. nov. sp. nov.

Irene Sánchez-Andrea[1,^,*], Charlotte M. van der Graaf[1,^], Bastian Hornung[2], Nicole J. Bale[3], Monika Jarzembowska[1], Diana Z. Sousa[1], W. Irene C. Rijpstra[3], Jaap S. Sinninghe Damsté[3,4], Alfons J.M. Stams[1,5]

This chapter has been published as: Sánchez-Andrea, I., van der Graaf, C. M., Hornung, B., Bale, N. J., Jarzembowska, M., Sousa, D. Z., et al. (2022). Acetate Degradation at Low pH by the Moderately Acidophilic Sulfate Reducer *Acididesulfobacillus acetoxydans* gen. nov. sp. nov. *Front. Microbiol.* 13. doi:10.3389/fmicb.2022.816605.

[1]Laboratory of Microbiology, Wageningen University & Research, Stippeneng 4, 6708 WE Wageningen, The Netherlands;
[2]Laboratory of Systems and Synthetic Biology, Wageningen University & Research, Stippeneng 4, 6708 WE Wageningen, The Netherlands;
[3]Department of Marine Microbiology and Biogeochemistry, NIOZ Royal Netherlands Institute for Sea Research, PO Box 59, 1790 AB Den Burg, The Netherlands;
[4]Department of Earth Sciences, Faculty of Geosciences, Utrecht University, Princetonlaan 8a, 3584 CD Utrecht, The Netherlands;
[5]Centre of Biological Engineering, University of Minho, Campus de Gualtar, 4710-057 Braga, Portugal.

^ These authors contributed equally
*Corresponding author

Abstract

In acid drainage environments, biosulfidogenesis by sulfate-reducing bacteria (SRB) attenuates the extreme conditions by enabling the precipitation of metals as their sulfides, and the neutralization of acidity through proton consumption. So far, only a handful of moderately acidophilic SRB species have been described, most of which are merely acidotolerant. Here, a novel species within a novel genus of moderately acidophilic SRB is described, *Acididesulfobacillus acetoxydans* gen. nov. sp. nov. strain INE, able to grow at pH 3.8. Bioreactor studies with strain INE at optimum (5.0) and low (3.9) pH for growth showed that strain INE alkalinized its environment, and that this was more pronounced at lower pH. These studies also showed the capacity of strain INE to completely oxidize organic acids to CO_2, which is uncommon among acidophilic SRB. Since organic acids are mainly in their protonated form at low pH, which increases their toxicity, their complete oxidation may be an acid stress resistance mechanism. Comparative proteogenomic and membrane lipid analysis further indicated that the presence of saturated ether-bound lipids in the membrane, and their relative increase at lower pH, was a protection mechanism against acid stress. Interestingly, other canonical acid stress resistance mechanisms, such as a Donnan potential and increased active charge transport, did not appear to be active.

Introduction

Acid rock and acid mine drainage (ARD, AMD) environments are among the most extreme habitats on Earth due to their high acidity and high metal concentrations. Acid drainage is generated by the oxidative dissolution of metal sulfides to sulfuric acid and dissolved metals upon exposure to water and oxidants such as oxygen (O_2) or ferric iron (Fe^{3+}) (Sand et al., 2001; Johnson and Hallberg, 2005). This can be triggered naturally (ARD), or by mining operations (AMD) (Lottermoser, 2010). The Tinto River, which flows through the massive sulfide deposits of the Iberian Pyrite Belt (IPB; Huelva, Southwestern Spain), is one of the best-known examples of ARD. Although mining activity reportedly occurred in the IPB already > 5000 years ago, the acid drainage does not exclusively originate on the surface by mining activities but also in the subsurface, as a result of chemolithotrophic microbial activity (Amils et al., 2011).

Microorganisms thriving in acid drainage environments are polyextremophiles, as they need to withstand high acidity (the mean pH of the water column of the Tinto River is 2.3), extremely high metal concentrations (e.g., Fe 2.26 $g{\cdot}L^{-1}$, Cu 0.11 $g{\cdot}L^{-1}$, Zn 0.24 $g{\cdot}L^{-1}$ (López-Archilla et al., 2001)) and high salinity due to high sulfate concentrations. Although much emphasis has been placed on the extreme acidophiles involved in the iron cycle and the oxidative part of the sulfur cycle, studies of anoxic Tinto River sediments showed the importance of more moderately acidophilic microorganisms, most notably acidophilic sulfate-reducing bacteria (SRB) (Sánchez-Andrea et al., 2011, 2012b). SRB have been shown to have an attenuating effect on the extreme characteristics of the Tinto River through the formation of sulfide (biosulfidogenesis), enabling the precipitation of metals as metal sulfides, and the consumption of protons required for sulfate reduction at low pH, resulting in alkalinization (Sánchez-Andrea et al., 2012a). In specific layers of Tinto River sediments, a higher pH (up to 6.2), a lower redox potential, and lower sulfate and metal concentrations were accompanied by a higher abundance of SRB from the family *Peptococcaceae* (Sánchez-Andrea, *et al*., 2012), representing up to 40 % of the total cell counts in the sediment layers. Geomicrobiological studies of abandoned open pit mines filled with AMD revealed that, similar to observations in AMD sediments, biosulfidogenesis by SRB also had an attenuating effect on acidity and metal concentrations in the water column (Wendt-Potthoff et al., 2012; Santofimia et al., 2013; Falagán et al., 2014; Sánchez-España et al., 2020; van der Graaf et al., 2020).

The in-depth study of the physiology and dominant stress resistance mechanisms of acidophilic SRB requires pure culture isolates. So far, only a few moderately acidophilic or acidotolerant SRB species have been described, *Thermodesulfobium narugense*

(pH 4.0 – 6.5) (Mori et al., 2003) and *Thermodesulfobium acidiphilum* (pH 3.7 – 6.5) (Frolov et al., 2017), both from the genus *Thermodesulfobium* within the family *Thermodesulfobiaceae*; *Desulfothermobacter acidiphilus* (pH 2.9 – 6.5) (Frolov et al., 2018) from the family *Thermoanaerobacteraceae*; and *Desulfosporosinus acididurans* (pH 3.8 – 7.0) (Sánchez-Andrea et al., 2015), *Desulfosporosinus acidiphilus* (pH 3.6 – 5.5) (Alazard et al., 2010), and *Desulfosporosinus metallidurans* (pH 4.0 – 7.0) (Panova et al., 2021) from the genus *Desulfosporosinus* in the family *Peptococcaceae* of the *Clostridia* class in the *Firmicutes* phylum. Here, we report the characterization of a novel moderately acidophilic SRB from a novel genus, *Acididesulfobacillus acetoxydans* strain INE, enriched from Tinto River sediments (Sánchez-Andrea et al., 2013). We use comparative proteomics and cell membrane lipid analysis performed on cells grown at optimum (5.0) and low (3.9) pH of growth to determine the main strategies enabling *A. acetoxydans* to grow at acidic pH.

Materials and Methods

Microorganisms

Strain INE was isolated from an enrichment culture containing acidic sediments from *JL* dam (37.691207N, 6.560587W) in the Tinto River basin (southwestern Spain) by incubation with 5 mM of lactate and 10 mM sulfate at pH 4.5 (Sánchez-Andrea et al., 2013). Detailed physicochemical information on the site has been published previously (Sánchez-Andrea et al., 2012a). For comparison purposes, *Desulfosporosinus orientis* DSM 765^T, *Desulfitobacterium dehalogenans* DSM 9161^T and *Desulfosporosinus acidiphilus* DSM 22704^T were obtained from the DSMZ (Braunschweig, Germany). *Desulfosporosinus acididurans* DSM 27692^T was taken from the laboratory collection.

Phenotypic characterization: morphology and physiology

Cell morphology, motility and spore formation were examined by phase contrast microscopy using a Leica DM2000 microscope (Leica, Hesse, Germany). Cell size was determined by SEM microscopy. To this end, samples were fixed by immersion in glutaraldehyde (2.5 %) for 2 h, and subsequently washed twice in sodium cacodylate buffer (0.2 M, pH 7.1). Samples were dehydrated in a graded series (10, 30, 50, 70, 90, and 100 %) of ethanol/water mixtures, leaving them 20 min in each mixture. After dehydration, samples were critical point dried and mounted on stubs. After gold shadowing, samples were examined in a Phillips XL30 EDAX DX4i SEM (Philips, The Netherlands). The lengths and widths of several cells were measured, and mean

dimensions recorded. Gram staining was performed according to standard procedures (Doetsch, 1981), and Gram-structure was checked by mixing cells with a drop of 3 % (w/v) solution of KOH.

Gram-structure was further checked by TEM microscopy. For this, cells were pelleted, incubated in fixative solution (2.5 % glutaraldehyde, 2 % paraformaldehyde in a 0.1 M phosphate citrate buffer pH 5.0) for 1 h at room temperature, washed twice in 0.1 M phosphate citrate buffer (wash buffer), resuspended in 100 ml 2 % gelatin in 0.1 M phosphate citrate buffer and incubated at 4 °C until gelatin solidified. The gelatin pellet was incubated for 15 min at room temperature in fixative solution, cut into small pieces (maximum 0.5 cm^3), and incubated for 30 min at room temperature. Gelatin sections were washed 6 times with wash buffer, stained and fixed in a 1 % osmium tetroxide solution for 1 h at room temperature. The samples were then washed three times in distilled water, dehydrated in successive ethanol incubations (30, 50, 70, 80, 90, 96 %), with a final dehydration step in 100 % ethanol. Samples were embedded in Spurr epoxy resin as described previously (Spurr, 1969), cut into ultrathin sections with a Leica EM UC7 ultramicrotome (Leica, Wetzlar, Hesse, Germany), and poststained with uranyl-acetate and lead citrate. Samples were imaged using a using a JEOL JEM-1400 series 120kV TEM (JEOL, Tokyo, Japan).

Catalase activity was determined by reaction with 15 % (w/v) solution of H_2O_2. An oxidase test was performed with a filter impregnated in 1 % (w/v) solution of tetramethyl-*p*-phenylenediamine in dimethyl sulfoxide (Sigma-Aldrich, St Louis, MO). Indole and urease formation as well as gelatin and esculin hydrolysis were determined with API® 20A (bioMérieux, France) according to manufacturer´s instructions. Analysis of respiratory quinones of biomass grown on glycerol was carried out by the DSMZ Deutsche Sammlung von Mikroorganismen und Zellkulturen GmbH (Braunschweig, Germany) (Tindall, 1990b, 1990a).

Growth experiments were performed in triplicate, using 120 ml-serum bottles as described elsewhere (Sánchez-Andrea et al., 2013). Growth conditions were pH 5.0 and T_a = 30**°C,** unless indicated otherwise. Growth was monitored by measuring optical density at 600 nm (OD_{600}) with a spectrophotometer (U-1500 Hitachi, Tokyo, Japan). Soluble substrates and intermediates (sugars and volatile fatty acids) were measured using a Thermo Electron spectrasystem High Performance Liquid Chromatography (HPLC) equipped with an Agilent Metacarb 67H column. Gaseous compounds (H_2) were analyzed using a Shimadzu GC-2014 Gas Chromatograph equipped with a Mol sieve 13X column. Sulfide was measured photometrically with the methylene blue method (Cline, 1969). Different electron donors and acceptors were tested at final concentrations of 5 or 10 mM, respectively, except sulfite, which was tested at 5

mM. Electron donors and acceptors were added to the media from sterile 1 M stock solutions. When electron donors were tested, sulfate (10 mM) was used as acceptor and when acceptors were tested, glycerol (5 mM) was used as donor. Growth was also studied at different incubation temperatures (from 10 to 45°C), pH (from 3.0 to 7.5), salinity (up to 0.5 M NaCl), oxygen concentrations, and with different reducing agents: L-cysteine, sodium sulfide, titanium citrate and $FeCl_2$ (2 mM). Sulfate reduction rates were determined during the exponential phase of the cultures grown between pH 4 and 7 at 30°C.

Bioreactor cultivation

Bioreactor cultivation was performed in duplicate in two pH-controlled batch reactors at pH 3.9 and pH 5.0. Basal medium was supplemented with 0.1 g yeast extract L^{-1}, 5 mM glycerol, 10 mM sulfate and 2 mM L-cysteine as reducing agent. Glass reactors (Applikon, The Netherlands) of 5 L volume capacity filled with 4 L of medium were operated with an ADI 1010 Bio-controller and the ADI 1025 Bio-console (Applikon). Autoclavation of the whole system enabled reactor operation under sterile conditions. Stirring speed was 50 rpm, temperature was maintained at 30°C, and pH was maintained at pH 5.0 or pH 3.9 by addition of 0.5 M HCl. The growth rates at pH 3.9 and pH 5.0 were calculated from semi-logarithmic plots of changes in OD_{600} values against time at 30°C. Values were obtained by implementing the modified Gompertz model (Zwietering et al., 1990). Biomass for lipid and proteome analysis was obtained from the reactors at 80 % of maximum OD_{600}.

Membrane lipid analysis

For comparison of the cellular fatty acid (FA) composition all strains were grown at their optimum pH in the medium described elsewhere (Sánchez-Andrea et al., 2013). Bicarbonate buffer was added to the medium for the cultivation of neutrophilic strains. For *A. acetoxydans* strain INE, biomass grown at both pH 3.9 and 5.0 was analyzed. FA analyses were carried out by acid hydrolysis of total cell material with 5 % HCl in methanol by refluxing for 3 h, and analysis by gas chromatography, gas chromatography-mass spectrometry, following procedures described previously (Sinninghe Damsté et al., 2011) and were performed in duplicate. Intact polar lipids (IPLs) were extracted from freeze-dried biomass using a modified Bligh–Dyer procedure and analyzed by ultra-high-pressure liquid chromatography–high resolution mass spectrometry (UHPLC-HRMS) under conditions described previously (Bale et al., 2019).

Phylogenetic analysis

Cloning of the 16S rRNA gene was performed to determine the phylogenetic affiliation of strain INE. Total genomic DNA was extracted using the FastDNA® SPIN Kit for Soil and the FastPrep® Instrument (MP Biomedicals, Santa Ana, CA). The 16S rRNA genes were amplified with the primers set 27F-1492R (T_a = 57°C) for *Bacteria* and cloned in *Escherichia coli* DH5α competent cells by using the pGEM-T vector (Promega, Madison, WI). Sequences were assembled with the DNABaser software 3.5.3 and prior to phylogenetic analysis, vector sequences flanking the 16S rRNA gene inserts were identified using the VecScreen tool (NCBI) (http://www.ncbi.nlm.nih.gov/VecScreen/VecScreen.html) and removed. Clone sequences were checked for chimeras (http://decipher.cee.wisc.edu/FindChimeras.html), aligned with SINA (v1.2.11) (Pruesse et al., 2012), and added to a database of over 230,000 homologous prokaryotic 16S rRNA gene primary structures by using the merging tool of the ARB program package (Ludwig et al., 2004). Sequences were then manually corrected with the alignment tool of the same software and added by parsimony to the tree generated in the *Living Tree Project* (LTP) (Yarza et al., 2008). Phylogenetic reconstruction was performed using the three algorithms as implemented in the ARB package. The maximum-likelihood method was used for the generation of the consensus tree and bootstrap analysis performance. The bar indicates a 10 % estimated sequence divergence. The 16S rRNA gene sequence is available in the EMBL database under accession number LN551924.

Genomic analysis and annotation workflow

Genomic DNA was extracted with the MasterPure™ Gram Positive DNA Purification Kit (Epicentre, Madison, Wisconsin). Pacific Biosciences sequencing was performed on a PacBio RSII at GATC Biotech (Konstanz, Germany), and Illumina sequencing on a MiSeq sequencer (250 bp paired-end with 500 bp insert). The genome was assembled with the smrt analysis pipeline version 2.3.0 and the protocol HGAP version 3. After assembly, the taxonomy of all contigs was determined with megablast (Altschul et al., 1990) and a custom version of the LCA algorithm (Huson et al., 2007). In detail, a blast search was performed against various database of the NCBI (NCBI NT database, the draft bacteria genome database, the human genome, the protozoa database) (NCBI Resource Coordinators, 2013), the Hungate 1000 database (Seshadri et al., 2018) and the human microbiome database (Human Microbiome Project, 2012), using an e value of 0.0001. A custom script with the implementation of the LCA algorithm was used (Huson et al., 2007), with the exception that only the hits exceeding a bitscore of 50 and not deviating >10 % in length from the longest hit were used to determine the taxonomy. After the taxonomy was obtained, all contigs not belonging to the family

Peptococcaceae were discarded as contamination. A correction of the PacBio assembly was performed with Pilon 1.19 (Walker et al., 2014), and the Illumina MiSeq data, which was mapped to the assembly with bowtie2 (Langmead and Salzberg, 2012). The Illumina MiSeq data was additionally used as verification that the discarded contigs of the PacBio assembly were contaminating contigs. Average amino acid identity (AAI) was calculated with compareM v0.1.1 (https://github.com/dparks1134/CompareM).

The annotation of the genome was performed with an early version of SAPP (Koehorst et al., 2018). Gene calling was performed with prodigal 2.6.3 (Hyatt et al., 2010). RNA genes were predicted with RNAmmer 1.2 (Lagesen et al., 2007), Aragorn 1.2.36 (Laslett and Canback, 2004), and the CRISPR Recognition tool version 1.2 (Bland et al., 2007). Protein coding genes were further annotated with InterproScan 5.19-58.0, PRIAM version March 2015 (Claudel-Renard et al., 2003), EnzDP version 1.0 (Nguyen et al., 2015), tmHMM version 2.0c (Krogh et al., 2001) and SignalP 4.1 (Petersen et al., 2011). Additional EC numbers were derived via Gene Ontology terms (Ashburner et al., 2000) predicted by InterproScan. Furthermore blastp searches against the COG database (Galperin et al., 2015) and the Swissprot database (Release 06-Jul-2016) (UniProt, 2014) were performed. The annotations were partially manually curated. To avoid repetition, locus ID are displayed without the locus tag "DEACI_".

Proteomics

Duplicate samples at each pH value of the biomass grown in reactors (pH 3.5 A+B and pH 5.0 A+B) were taken at 80 % of maximum OD_{600}, centrifuged, washed, and transferred to 2 ml low-binding microcentrifuge tubes (Eppendorf, The Netherlands) prior to protein extraction. Around 0.1 g of wet weight pellet was resuspended in 500 ml of 4 % sodium dodecyl sulfate in 100 mM Tris –HCl pH 7.6. Cells were lysed by sonication with a 3 mm tip using a Branson sonifier in 6 pulses of 30 s. Around 40 µg of protein was separated by gel electrophoresis (SDS-PAGE) and cut into 5 slices per sample to fractionate proteins. The gel slices were subjected to in-gel tryptic digestion and peptides were loaded on STAGE-tips (STop And Go Elution, C18-reversed phase SPE) for desalting and concentration.

The resulting purified and concentrated peptide mixtures were analyzed by nanoflow C18 reversed phase HPLC coupled with a maXis 4G ETD ultra-high resolution Qq-TOF mass spectrometer (Bruker Daltonics) with collision-induced dissociation (CID) as fragmentation technique. Chromatographic separation was achieved via a linear gradient of 7 to 32 % acetonitrile in 90 min using 0.1 % formic acid as ion pair reagent. For data analysis a custom *Acididesulfobacillus* database with added sequences for typical contaminant proteins (e.g., skin and hair proteins) was used. For database

searches, validation, and relative quantification the MaxQuant software package was used (version 1.5.0.0, http://www.maxquant.org/). A false discovery rate of 1 % was tolerated at both peptide and protein level.

In total, 1258 *Acididesulfobacillus* proteins were identified. These proteins were quantified in both replicate samples of at least one of the conditions (pH 3.9 or 5.0). Known contaminants like human keratins were excluded from these lists. Please note that no correction for multiple testing has been applied due to the number of replicates (n=2) for each condition.

Data accessibility

All data has been uploaded to the European Nucleotide Archive under bioproject number PRJEB7665 composed by PacBio raw data (ERR3835955), Illumina MiSeq raw data (ERR665276), genome assembly (ERZ1286184). The mass spectrometry proteomics data have been deposited to the ProteomeXchange Consortium (Deutsch et al., 2020) via the PRIDE (Perez-Riverol et al., 2019) partner repository with the dataset identifier PXD022508.

Results and Discussion

Characterization of *Acididesulfobacillus acetoxydans* gen. nov. sp. nov. strain INE

Morphology and physiology. *Acididesulfobacillus acetoxydans* gen. nov. sp. nov. strain INE was isolated previously from enrichment cultures inoculated with Tinto River sediments, supplemented with lactate (5 mM) and sulfate (10 mM) at pH 4.5 (Sánchez-Andrea et al., 2013). Strain INE grew between pH 3.8 and 6.5, with a maximum specific growth rate at pH 5.0 (0.051 h^{-1}). The temperature range of growth was between 25 and 42°C, with an optimum at 30 °C. Growth occurred in the presence of up to 15.3 g L^{-1} of NaCl. Cells of strain INE were single, straight rods, 4-7 µm long and ca. 0.6 µm wide (Figure 1A), with motility associated with observed lateral flagella (Figure 1B). Although strain INE stains Gram-negative, the double membrane characteristic of Gram-negative bacteria is absent (Figure 1C). Its Gram-positive cell wall structure was further supported by the negative KOH test and its susceptibility to vancomycin, as well as the membrane structure observed by TEM (Figure 1C).

Strain INE is a strict anaerobe as it grew only in the presence of L-cysteine, ferrous iron, titanium citrate or sulfide as reducing agents. With sulfate as electron acceptor, strain INE utilized a wide range of compounds as electron donors (Table 1): hydrogen, complex substrates such as yeast extract, carbohydrates such as xylose, glucose,

fructose, maltose, sucrose and raffinose, a variety of C1 - C4 organic acids (formate, acetate, glycolate, pyruvate, lactate, malate, fumarate, butyrate, and succinate), the amino acid L-cysteine, and alcohols, such methanol, ethanol, glycerol and 1- and 2-propanol. Strain INE was capable of the complete oxidation of substrates to CO_2. No growth was observed with propionate, citrate or benzoate as electron donor. With glycerol as electron donor, strain INE used a range of compounds as electron acceptor in addition to sulfate, including elemental sulfur, thiosulfate, arsenate, selenate, nitrate, and DMSO. It could not reduce ferric iron as Fe(III)NTA, sulfite, dithionate, polysulfide, perchlorate, perchloroethylene, fumarate, humic acids, chromate, molybdate, manganese or AQDS. Strain INE was also capable of disproportionation of elemental sulfur and thiosulfate, and of fermentation of cysteine, glucose, pyruvate, and yeast extract. The only detected menaquinone of strain INE was MK-7 (100 %), as also detected for the closely related *Desulfosporosinus* spp., except for *Ds. lacus* which contained up to 36 % MK-5 (Ramamoorthy et al., 2006).

Phylogenetic and genomic analysis. Genome assembly indicated the presence of one chromosome with a size of 4.52 Mbp, with a GC content of 53.65 % and 4104 predicted protein coding sequences, of which 3443 contained at least one protein domain, and 639 were identified as hypothetical proteins. In total 53 tRNAs and 3 full rRNA operons were identified. The phylogenetic position of the complete 16S rRNA gene sequence of strain INE (LN551924) showed that the strain is related to the *Desulfosporosinus* and *Desulfitobacterium* genera (Figure 2): the 16S rRNA gene sequence identity with its closest relatives, *Ds. meridiei* DSM 13257^T, *Ds. auripigmenti* DSM 13351^T and *D.*

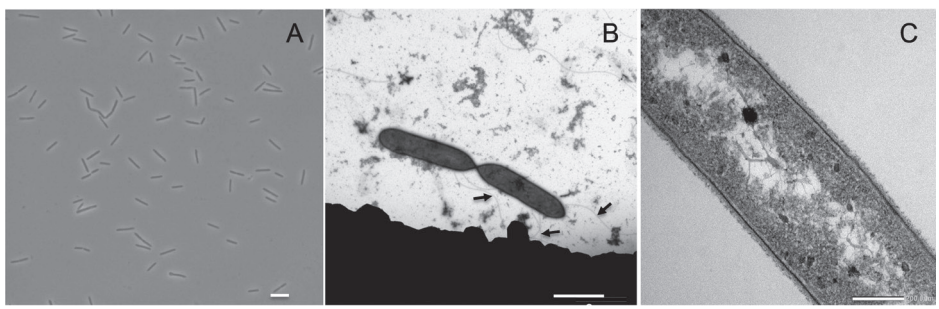

Figure 1 *Acididesulfobacillus acetoxydans* gen. nov. sp. nov. strain INE microscopy images: (A) phase contrast microscopy and (B-C) transmission electron microscopy. Scale bars represent 5 mm, 2 mm and 200 nm, respectively. Arrows in (B) indicate flagella.

Table 1 Main characteristics differentiating strain INE from its closest phylogenetic relatives: *Desulfosporosinus acididurans* (Sánchez-Andrea et al., 2015), *Desulfosporosinus acidiphilus* (Alazard et al., 2010), *Desulfosporosinus metallidurans* (Panova et al., 2021), *Desulfosporosinus orientis* (Adams and Postgate, 1959; Campbell and Postgate, 1965; Klemps et al., 1985; Robertson et al., 2001; Ramamoorthy et al., 2006), *Desulfitobacterium dehalogenans* (Utkin et al., 1994), *Desulfitobacterium metallireducens* (Finneran et al., 2002). +, supported growth; −, did not support growth; (+), weak growth.

	Acididesulfo-bacillus	*Desulfosporosinus*				*Desulfitobacterium*	
Name	*A. acetoxydans* DSM 29876^T	*Ds. acididurans* DSM 27692^T	*Ds. acidiphilus* DSM 22704^T	*Ds. metallidurans* DSM 104464T	*Ds. orientis DSM 765T*	*D. dehalogenans* DSM 9161^T	*D. metallireducens* DSM 15228^T
Type strain	INE	M1^T	SJ4^T	OL^T	Singapore^T	JW/IU-DC1^T	853-15A^T
Isolation source	ARD sediments	AMD/ARD sediments	AMD sediments	AMD microbial mat	Soil	freshwater pond sediment	aquifer sediment (uranium-contaminated)
Cell size (µm)	0.7 x 5.5	0.7 x 3-5	0.8–1 x 4–7	0.5 x 2-3	1.5 x 5	0.5-0.7 x 2.5-4	
DNA G+C mol %	53.7	41.8	42.3		41.7; 42.8[1]; 45.9[2]	45	42
Quinones	MK-7 (100 %)	MK-7 (98 %)			MK-7		
Genome size (Mb)	4.52	4.64	4.99	5.29	5.86	4.32	3.17
Endospore position	Subterminal	Subterminal	Subterminal	Subterminal	Subterminal, paracentral or central	-	-
Motility	+	Variable	−	−	+	+	-
Gram staining	-	−	−	−	−	+	+
T range (°C)	25-42	15–40	25–40	4 - 37	</42		20-37
T opt (°C)	25-35	30	30	28	30–37	38	30
pH range (opt.)	3.8-6.5 (5.0)	3.8–7 (5.5)	3.6–5.6 (5.2)	4.0 - 7.0 (5.5)	5.6–7.4 (6.4-7)	(7.5)	(7.0)
NaCl range (%) (opt)	0.5 - 1.5 (< 0.5)	0–1.5 (0.6)	0–0.6 (1.5)	0–6 (0-0.1)	<4.5		<0.5
Catalase	-	+					
Oxidase	-	−/+	−,+		−,+		
				Electron donors			
H_2	+ (with 0.1 YE)	+	+	+	+	+	+
Formate	+	(+)	−	+	+	+	+
Acetate	+	−	−		−		
Pyruvate	+	+		+	+	+	+
Propionate	-	−	−	+	−		
Lactate	+	+	(+)	+	+	+	+
Malate	+	+	−	+	−		
Fumarate	+	+	−		+		
Butyrate	+	+	−		-[4],+[1]		
Succinate	+	−	−		−		
Methanol	+	(+)	−		+		

Ethanol	+	+	–	+	+		
Glycerol	+	+	+	+	–[1], +[3]		
Xylose	+	+	–		–		
Fructose	+	(+)	+	+	–		
Glucose	+	(+)	(+)	+	–		
			Electron acceptors				
Sulfate	+	+	+	+	+	–	–
Sulfur	+	+	–, +[3]	–	+	+	+
Sulfite	-	–	–	+	+	+	–
Thiosulfate	+	+	+	+	+[3], –[4]	+	+
DMSO	+						
Arsenate	+	+	–		–[1,2,3], +[5]	–	
Fumarate	-	–	–	+	+	+	–
Fe(III) sol./ insol.	-	Variable[3]	–		+	+	+
Nitrate	+	+	(+)[1]	+	–	+	–
PCE	-						
Se(VI)	+					+	–
Mn(IV)	-					+	+

[1](Ramamoorthy et al., 2006); [2](Robertson et al., 2001); [3](Sánchez-Andrea et al., 2015); [4](Adams and Postgate, 1959); [5](Campbell and Postgate, 1965)

metallireducens DSM 15288^T was 93.8 %, 93.5 % and 93.5 %, respectively. This is below the minimum similarity threshold of 94.5 % for genus-delineation (Yarza et al., 2014), indicating that strain INE belongs to a new genus. This is further supported by the average amino acid identity (AAI) derived from the genome comparison of strain INE with *Desulfosporosinus* and *Desulfitobacterium* spp. (Supplementary Table S1). The highest similarity was observed with *Peptococcaceae* bacterium CEB3 (89.3 %) (Ňancucheo and Johnson, 2012b), followed by *Ds. acidiphilus* DSM 22704 (64.4 %). Based on the observed AAI values of more than 96 % in most strains within one species and 62-64 % within the same genus, respectively (Konstantinidis and Tiedje, 2005), AAI values also suggest that *A. acetoxydans* strain INE forms a new genus. Although the AAI with *Ds. acidiphilus* is close to the threshold of 64 %, the 16S rRNA gene similarity is 92.7 %, supporting the separation in a new genus. The 16S rRNA sequence identity further indicates that the novel genus *Acididesulfobacillus* encompasses the isolates CL4 and CEB3 (Jameson et al., 2010; Ňancucheo and Johnson, 2012b). Although strain CL4 was formerly proposed as 'Desulfobacillus acidavidus' (Jameson et al., 2010), it was never formally described, and current nomenclature regulations prevented us from using the proposed name. We therefore hereby propose the alternative name *Acididesulfobacillus*.

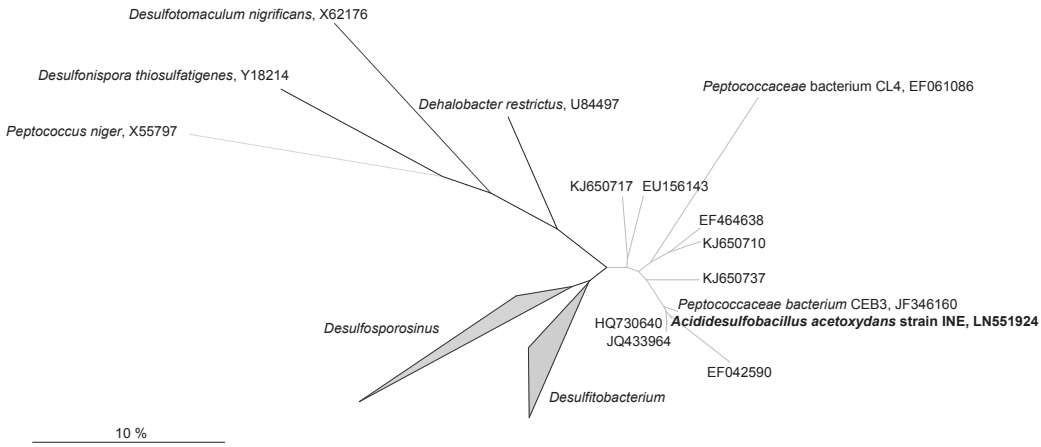

Figure 2 Maximum-likelihood tree showing phylogenetic affiliation of 16S rRNA gene sequences of *Acididesulfobacillus acetoxydans* (in bold) with related environmental sequences found in acidic environments, and closely related species in the *Peptococcaceae* family of the *Firmicutes* phylum. The accession numbers represent sequences retrieved from different acid drainage environments. KJ650710, KJ650737 or KJ650717: sulfidic mine tailings dumps in Botswana; EF042590: an abandoned copper mine in Odiel (Huelva, Spain); HQ730640, JQ433964: Tinto River sediments; EU156143: a thermal spring in Yellowstone National Park (WY, USA); EF464638: acidic enrichment cultures. JF346160 and EF061086: *Peptococcaceae* bacteria CEB3 and CL4. Scalebar indicates a 10 % sequence difference.

The *Desulfosporosinus* and *Desulfitobacterium* genera and the novel genus *Acididesulfobacillus* form a separate cluster from the other recognized genera and species of the family *Peptococcaceae,* order *Clostridiales* of the phylum *Firmicutes*. Members of the *Desulfosporosinus* and *Desulfitobacterium* genera are rod-shaped, Gram-positive, free-living, strictly anaerobic, spore-forming bacteria. They display a diversity of metabolic traits relevant to bioremediation of polluted sites, e.g. reductive dehalogenation and reduction of metals such as arsenic or ferric iron, sulfur compounds or nitrate (Spring and Rosenzweig, 2006; Alazard et al., 2010; Pester et al., 2012; Petzsch et al., 2015; Sánchez-Andrea et al., 2015; Mardanov et al., 2016). Members of *Desulfosporosinus* are known sulfate reducers in AMD environments (Nevin et al., 2003; Petrie et al., 2003; Suzuki et al., 2004; Kimura et al., 2006; Rowe et al., 2007; Cardenas et al., 2008; Lee et al., 2009; Madden et al., 2009; Senko et al., 2009; Ňancucheo and Johnson, 2014), and other low pH ecosystems such as peatlands (Hausmann et al.,

2016, 2019). Three moderately acidophilic or acidotolerant *Desulfosporosinus* species were isolated so far: *Ds. acidiphilus* (pH 3.6 – 5.5, optimum pH 5.2) (Alazard et al., 2010), *Ds. acididurans* (pH 3.8 – 7.0, optimum 5.5) (Sánchez-Andrea et al., 2015) and *Ds. metallidurans* (pH 4.0 – 7.0, optimum 5.5) (Panova et al., 2021).

All 16S rRNA gene amplicon sequences found in the public databases (SILVA and NCBI) that cluster together with *A. acetoxydans* strain INE were identified in AMD or ARD environments (Figure 2): in sulfidic mine tailings dumps in Botswana (pH 3.2 to 3.5) (Korehi et al., 2014), in a stream of an abandoned copper mine in Odiel (Huelva, Spain) (pH 2.5 to 2.75) (Rowe et al., 2007), in Tinto River sediments (pH 5) (Sánchez-Andrea et al., 2011) and in a thermal spring in Yellowstone National Park (pH 5.75 to 6.91) (Hall et al., 2008). In addition, they were detected in enrichment cultures inoculated with samples from acid mine tailings (Winch et al., 2009). The two isolates included in the cluster, *Peptococcaceae* bacteria CL4 and CEB3 (Jameson et al., 2010; Ňancucheo and Johnson, 2012b), were both obtained from reactors treating acid mine waters at a pH of about 2.5. The genome sequence from CEB3 is publicly available, but the two isolates were not characterized further. Interestingly, sequences of CEB3, which according to 16S rRNA gene sequence similarity corresponds to the same species as strain INE, became dominant in a reactor inoculated with an acidophilic consortium when the operating pH of the reactor was lowered, showing their predominance at more acidic conditions over other acidophilic SRB such as *Ds. acididurans* (Ňancucheo and Johnson, 2012b). Its inability to grow at pH 7, combined with the lower pH optimum of strain INE (5.0), compared to *Ds. acididurans* (5.5) and *Ds. acidiphilus* (5.2) (Table 1), this indicates that the SRB in this novel cluster are more acidophilic than the SRB described so far.

Chemotaxonomy. The lipid composition, including FA, of strain INE grown at optimal pH (5.0) was compared with the type strains of the phylogenetically closest genera, *Ds. orientis* (Adams and Postgate, 1959; Stackebrandt et al., 1997) and *D. dehalogenans* (Utkin et al., 1994) (Table 2). As these type strains are neutrophilic, lipid profiles were also compared with two acidophilic/acidotolerant strains from the *Desulfosporosinus* genus: *Ds. acididurans* (Sánchez-Andrea et al., 2015) and *Ds. acidiphilus* (Alazard et al., 2010).

The lipid profile of strain INE was dominated by the *iso*-$C_{15:0}$ FA (representing almost 60 %; Table 2), followed by *iso*-$C_{15:0}$ dimethylacetal (DMA) as the second most abundant lipid. DMAs are formed upon acid hydrolysis from ether lipids containing an alk-1-enyl ether substituent at the sn-1 carbon of glycerol, so called plasmalogens (Jackson et al., 2021). Interestingly, the *iso*-$C_{15:0}$ FA was also abundant in the acidophilic/acidotolerant

strains *Ds. acididurans* (25.8 %) and *Ds. acidiphilus* (16.6 %), but absent in both the neutrophilic strains, *Ds. orientis* and *D. halogenans*. *Iso*-$C_{17:0}$ and 10-methyl *n*-$C_{17:0}$ FA and corresponding DMAs were also present in strain INE. Small amounts (i.e., 5 % of total lipids) of 1-alkyl glycerol ethers with *iso*-C_{15} and 10-methyl *n*-C_{17} groups were also detected in strain INE, but saturated glycerol monoethers were absent in any of the other strains. The two most abundant FAs in *Ds. orientis* were *n*-$C_{16:0}$ FA (35.7 %) and the *n*-$C_{18:1}$ DMA (16.4 %). Both lipids are absent in strain INE and the latter is missing in all three acidophilic strains. Similarly, the abundant FAs *n*-$C_{16:0}$ (23.6 %), *n*-$C_{16:1}$ (15.9 %), and *n*-$C_{14:0}$ (15.8 %) in *D. dehalogenans*, the (neutrophilic) type strain of the second closest phylogenetic genus *Desulfitobacterium*, also showed a negligible presence in strain INE. The saturated branched-chain acid iso-$C_{15:0}$ and the 1-alkyl glycerol ether lipids may therefore be characteristic for acidophilic SRB.

Analysis of the IPL of strain INE showed a high diversity of polar head groups (Supplementary Table S2), including sulfoquinovosyls (SQs), phosphoglycerols (PGs), phosphoethanolamines (PE) and diphosphatidylglycerols (DPG; commonly known as cardiolipins). Additionally, a series of glycolipids with hexosamine moieties were present. The dominant group was tentatively assigned a structure with a hexose group bound to the glycerol backbone and a hexosamine bound to this. The assignment was made based on their MS^2 fragmentation and their accurate masses (Supplementary Figure S1; Supplementary Table S2). The second group also contained a hexosamine head group but the complete structure could not be elucidated (Supplementary Figure S1; Supplementary Table S2). Amino sugars are not routinely reported as components of polar headgroups in bacterial lipids, but have been reported in a range of Archaea (Koga et al., 1993, 1998; Oger and Cario, 2013; Meador et al., 2014). Lipid-A, found in the outer-membrane of most Gram-negative bacteria, consists of two glucosamine moieties. However, the mass spectra of the hexosamine components detected in this study did not agree with published spectra of lipid A (Larrouy-Maumus et al., 2016; Crittenden et al., 2017). The IPL-bound core lipids (Supplementary Table S2) were in agreement with the hydrolysis-derived core lipid analysis (Table 2) and included diacylglycerols (DAGs) and mixed acyl/ether glycerols (AEGs; including plasmalogen lipids).

Table 2 Relative abundance (% of total) of fatty acids and ether lipids of *Acididesulfobacillus acetoxydans* strain INE and its phylogenetically closest relatives grown on glycerol and sulfate. Strains: *Acididesulfobacillus acetoxydan*s strain INE at pH 3.9 and at pH 5.0; *Desulfosporosinus acidiphilus; Desulfosporosinus acididurans; Desulfosporosinus orientis*, and *Desulfitobacterium dehalogenans*. Major lipids (>10 % of total) are indicated in bold.

Lipid			acidophilic/acidotolerant type strains		neutrophilic type strains	
	A. acetoxydans strain INE		*Ds. acidiphilus*	*Ds. acididurans*	*Ds. orientis*	*D. dehalogenans*
	pH 3.9	pH_{opt} 5.0	pH_{opt} 5.2	pH_{opt} 5.5	pH_{opt} 6.8	pH_{opt} 7.5
Fatty acids						
iC_{14}	2.5	1.1				
$C_{14:1}$						1.4
$C_{14:0}$	0.9		**20.4**	7.5	2.0	**15.8**
i$C_{15:1}$	1.5	2.4		1.3		
iC_{15}	**48.0**	**59.5**	**16.6**	**25.8**		
aiC_{15}	6.5	2.4	1.4	1.5		
$C_{15:0}$				2.4		
iC_{16}	1.9		1.1	2.8		
$C_{16:1}$			1.3	1.3	2.2	6.3
$C_{16:1}$			2.6	3.9	6.3	**15.9**
$C_{16:0}$	1.1		**32.3**	**25.9**	**35.7**	**23.6**
diMeC_{15}	1.5					
10MeC_{16}	2.6	1.3				
$C_{17:1}$				3.3		
iC_{17}	1.1	1.3	1.1	2.9		
$C_{17:0}$				1.2		
10MeC_{17}	2.1	2.5				
$C_{18:1}$					2.4	3.8
$C_{18:1}$					8.3	**10.3**
$C_{18:0}$			1.4	1.5	1.1	3.8
Sum	**69.7**	**70.5**	**78.2**	**81.3**	**58**	**80.9**
Sum saturated	**68.2**	**68.1**	**74.3**	**71.5**	**38.8**	**43.2**
Sum unsaturated	**1.5**	**2.4**	**3.9**	**9.8**	**19.2**	**37.7**

β-Hydroxy-fatty acids					
$C_{14:0}$					1.6
$C_{16:1}$					1.0
$C_{16:0}$			1.1		2.0
$C_{18:1}$					1.2
$C_{18:1}$					1.4
Sum	**0**	**0**	**1.1**	**0**	**7.2**
Dimetyl-acetals					
iC_{15}	4.9	**14.7**	1.4		
iC_{16}	3.2	1.9			
$C_{16:1}$			1.3	1.2	3.3
$C_{16:0}$	5.4	2.1	**15.7**	7.5	9.4
$C_{17:1}$				3.8	
iC_{17}	4.1	5.1	1.5	4.3	
$C_{17:0}$				1.9	
$10MeC_{17}$		1.1			
$C_{18:1}$					4.3
$C_{18:1}$					**16.4**
$C_{18:0}$			0.9		1.4
Sum	**17.6**	**24.9**	**20.8**	**18.7**	**34.8**
1-Mono-glycerol ethers					
iC_{15}	2.6	3.5			
iC_{16}	1.1				
$C_{16:0}$	2.5				
$10MeC_{16}$	3.7				
$10MeC_{17}$	2.3	1.5			
$C_{18:1}$	1.0				
Sum	**13.2**	**5.0**	**0**	**0**	**0**

Dominant acid stress resistance mechanisms in *Acididesulfobacillus acetoxydans*

Proton consumption and complete organic acid oxidation at optimum and minimum pH. The pH dependence of growth of *A. acetoxydans* strain INE^T (pH 3.8 to 6.5 with pH optimum at 5.0) indicated that it is moderately acidophilic rather than acid-tolerant, since it is unable to grow at pH 7.0. As aforementioned, members of *Acididesulfobacillus* spp. were found to be more tolerant to low pH than other acidophilic/acidotolerant SRB such as *Desulfosporosinus* spp. The capacity for complete oxidation of organic acids to CO_2 is not common in other acidophilic/acidotolerant SRB described so far (Alazard et al., 2010; Sánchez-Andrea et al., 2013, 2015), and was only recently reported to promote limited growth in *Ds. metallidurans* (Panova et al., 2021). Because of the increasing toxicity of organic acids at pH values below their pK_a, lowering their concentration by complete oxidation likely constituted an important detoxification mechanism for *A. acetoxydans* strain INE. In order to elucidate the main strategies conferring increased robustness at low pH, we investigated this in more detail by monitoring its metabolism through quantifying proton consumption rates, and glycerol, sulfate, and acetic acid concentrations at optimum (5.0) and low (3.9) pH in pH-controlled batch bioreactors fed with glycerol.

By monitoring the acid addition required for pH control, the proton consumption rates could be calculated. A higher net consumption of protons was observed at pH 3.9 than at 5.0 (Table 3): 128 mM H^+ g^{-1} biomass (dry weight) vs. to 58 mM H^+ g^{-1} biomass (dry weight), respectively. Doubling times at pH 3.9 and 5.0 were 17.6 and 13.8 h, respectively. The maximum OD_{600} reached in the late exponential phase after complete oxidation of glycerol was 0.41 at pH 3.9 and 0.44 at pH 5.0, corresponding to a maximum biomass dry weight of 102 and 115 mg L^{-1}, respectively (Table 3). This

Table 3: Summary parameters of bioreactor cultivation of *Acididesulfobacillus acetoxydans* gen. nov. sp. nov. strain INE at pH 3.9 and pH 5.0 when grown on 5 mM glycerol and 10 mM sulfate.

	pH 3.9	pH 5.0
Doubling time t_d (h)	17.6	13.8
Maximum OD_{600}	0.41	0.44
$C_{DW,final}$* (mg·L^{-1})	102	115
H^+ consumption (mM H^+·g_{DW}^{-1})	128	58

*$C_{DW,final}$ was calculated from OD_{600} and ratio c_{DW} (mg·L^{-1})·OD_{600}^{-1}= 254.84

difference likely indicated increased energetic costs for cell maintenance at pH values below the optimum. The increased maintenance energy requirements could have been partly compensated for by the slightly larger theoretical Gibbs free energy change ($\Delta_r G'$) for sulfate reduction with glycerol at pH 3.9 (-1186.7 kJ·mol^{-1}) compared to pH 5.0 (-1142.8 kJ·mol^{-1}), as calculated with Equilibrator (Flamholz et al., 2012) (Table 4).

Consumption of glycerol and sulfate was accompanied by an initial increase of total acetate concentrations to 2.4 mM at pH 3.9 and 2 mM at pH 5.0, followed by its complete removal (Figure 3). Total acetic acid concentrations started to decrease before all glycerol was consumed, indicating a co-consumption phase. Biomass concentrations remained approximately constant once glycerol was completely consumed, while total acetic acid concentrations kept decreasing, indicating that under these conditions, energy derived from acetate degradation was invested in cell maintenance rather than in net growth. This was also reflected in the continued addition of acid (HCl) required to maintain constant pH after the maximum optical density (OD_{600}) was reached. Overall, approximately 30 % of the carbon added as glycerol was not coupled to dissimilatory sulfate reduction but used for anabolism.

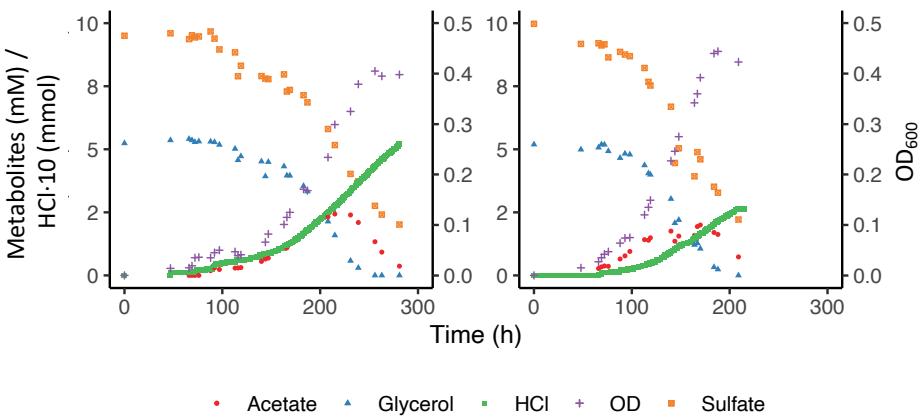

Figure 3. Glycerol, total acetate (undissociated + dissociated) and sulfate concentrations, and OD_{600} of *Acididesulfobacillus acetoxydans* strain INE grown in bioreactors at pH 3.9 (A) and pH 5 (B). Concentration profiles of glycerol, sulfate, acetic acid, as well as OD_{600} and HCl addition are shown for one reactor at each pH value for clarity.

The ability to use acetic acid as electron donor is advantageous in extreme environments such as AMD for several reasons. Firstly, acetic acid is a typical end product of other microorganisms such as fermenters present in AMD sediments (Sánchez-Andrea et al., 2018). The ability to metabolize a variety of organic acids, but especially a metabolic end product such as acetic acid (Table 1) increases the carbon and energy available to strain INE in nutrient-limited AMD/ARD environments. Furthermore, at pH values below their pK_a, organic acids occur in their undissociated (protonated) form and can freely diffuse across the cell membrane, resulting in the acidification of the cytoplasm. Removal of intracellular protons is energetically costly and can be detrimental for growth. Complete oxidation of organic acids to CO_2 prevents their accumulation in the environment, thereby lowering organic acid toxicity. For example, at the pH conditions compared in this study, maximum total extracellular acetic acid (dissociated and undissociated) concentrations reached 2.4 mM at pH 3.9 and 2.0 mM at pH 5.0 removal (Figure 3). Considering the pK_a of acetic acid (4.8), its extracellular concentration (undissociated) at pH 3.9 is 2.1 mM, versus 0.7 mM at pH 5.0. The higher extracellular acetic acid concentration measured at pH 3.9 could correspond to a higher consumption of acetic acid at the optimum pH 5.

Metabolic pathways for complete acetic acid oxidation coupled to sulfate reduction. To enable the more informed prediction of acetotrophic potential in acidophilic SRB from (meta)genomic data, the metabolic pathway for complete oxidation of acetic acid by *A. acetoxydans* was determined through proteome analysis. The Acetyl-CoA pathway seemed to be responsible for the complete oxidation of acetic acid to CO_2, since all of its enzymes were present in the proteome (Figure 4). Additionally, the absence of citrate synthase indicated that acetyl-CoA could not be degraded through the tricarboxylic acid (TCA) cycle, the other potential pathway for acetate oxidation. Two genes encoding bifurcating enzymes related to the reverse Acetyl-CoA pathway were detected, the NADH-dependent reduced ferredoxin:$NADP^+$ oxidoreductase (*nfnAB*, 2795-96), and the cytoplasmic NADH-dependent formate dehydrogenase (*fdh*, 1374-1377). NfnAB catalyses the NAD^+-dependent reduction of ferredoxin by NADPH, acting possibly on the $NADP^+$ generated in the conversion of methylene-THF to methenyl-THF in the Acetyl-coA pathway. The *nfnAB* genes, both encoding iron–sulfur flavoproteins, are present in a diversity of microorganisms (Wang et al., 2010), but often incorrectly annotated as sulfide dehydrogenase. The *nfnAB* genes were detected in the proteome of strain INE and were found in the same operon as two genes encoding methylene-H_4F-DH/methenyl-H_4F cyclohydrolase and the methenyl-H_4F cyclohydrolase (2793-94), both part of the Acetyl-CoA pathway. The second bifurcating enzyme detected in the

proteome of strain INE, the cytoplasmic NADH-dependent formate dehydrogenase (Sebban et al., 1995; Costa et al., 1997), is a selenocysteine-containing Fdh that oxidizes formate while reducing ferredoxin and NAD^+. The Fdh detected in the genome of strain INE resembled the Fdh protein encoded in the genome of *Desulfotomaculum kuznetsovii* (Deasku_2987-2991), and consisted of a catalytic subunit (*fdhA,* 1377), two subunits for oxidoreduction of NADH/NAD^+ (*fdhGH,* 1374), the proton-translocating quinone (*fdhE,* 1375), and the 5-formyltetrahydrofolate cyclo-ligase (*fdhH,* 1373). This Fdh is predicted to act in the Acetyl-CoA pathway (Ragsdale and Pierce, 2008), and it was found next to a gene encoding a histidine kinase (1378), suggesting that it has a regulatory function (Pereira *et al.*, 2011). Although the complete Acetyl-CoA pathway is also present in the genome of sulfate reducers from the genus *Desulfosporosinus* (Alazard et al., 2010; Pester et al., 2012; Sánchez-Andrea et al., 2015), complete oxidation of acetic acid in moderately acidophilic SRB was so far only observed in the recently described *Ds. metallidurans*, where weak growth on acetic acid was reported. However, acetate oxidation was proposed to occur through the TCA cycle instead of the Acetyl-CoA pathway based on genome analysis (Panova et al., 2021).

Enzymes of the metabolic pathways used for oxidation of glycerol coupled to sulfate reduction were also identified in the proteome (Figure 4). Glycerol is taken up by a glycerol transporter (DEACI_1309-DEACI_1310, hereafter "DEACI_" will be omitted for simplicity) and oxidized to dihydroxyacetone-P (DHAP) by glycerol kinase (0310) and glycerol-3-phosphate dehydrogenase (1301-1303). DHAP is converted to pyruvate involving enzymes of the Embden-Meyerhoff pathway (0305-0308, 2591-2592, 3679) and subsequently to acetyl-coA by pyruvate:ferredoxin oxidoreductase (0330, 0621, 1130, 1144, 2105, 2107, 2770). Acetyl-CoA is converted to acetate through P_i acetyltransferase (3443) and acetate kinase (3414), or completely oxidized to CO_2 through the reverse Acetyl-CoA pathway, discussed above. Reducing equivalents are transferred to NAD^+ and oxidized ferredoxin. Electrons flow to sulfate through the respiratory chain, for which the key enzymes were identified. Sulfate is activated with ATP to adenosine-phosphosulfate (APS) and pyrophosphate by ATP sulfurylase (Sat, 0463). Heterodisulfide reductase (HdrF1, 0461) is predicted to receive electrons from the quinone pool and direct them to the cytoplasmic QmoAB/HdrBC complex (0456, 0457, 0470, 0471) (Rabus et al., 2015), reducing APS to sulfite through the AprAB (0464, 0465) complex, as described for other SRB (Ramos et al., 2012). The sulfur in sulfite is then reduced and transferred to DsrC (0677) forming DsrC trisulfide by DsrAB (0668, 0669) (Santos et al., 2015), which is finally reduced to sulfide by electrons received from the DsrMKJOP complex (0672 - 0676) (Pires et al., 2006).

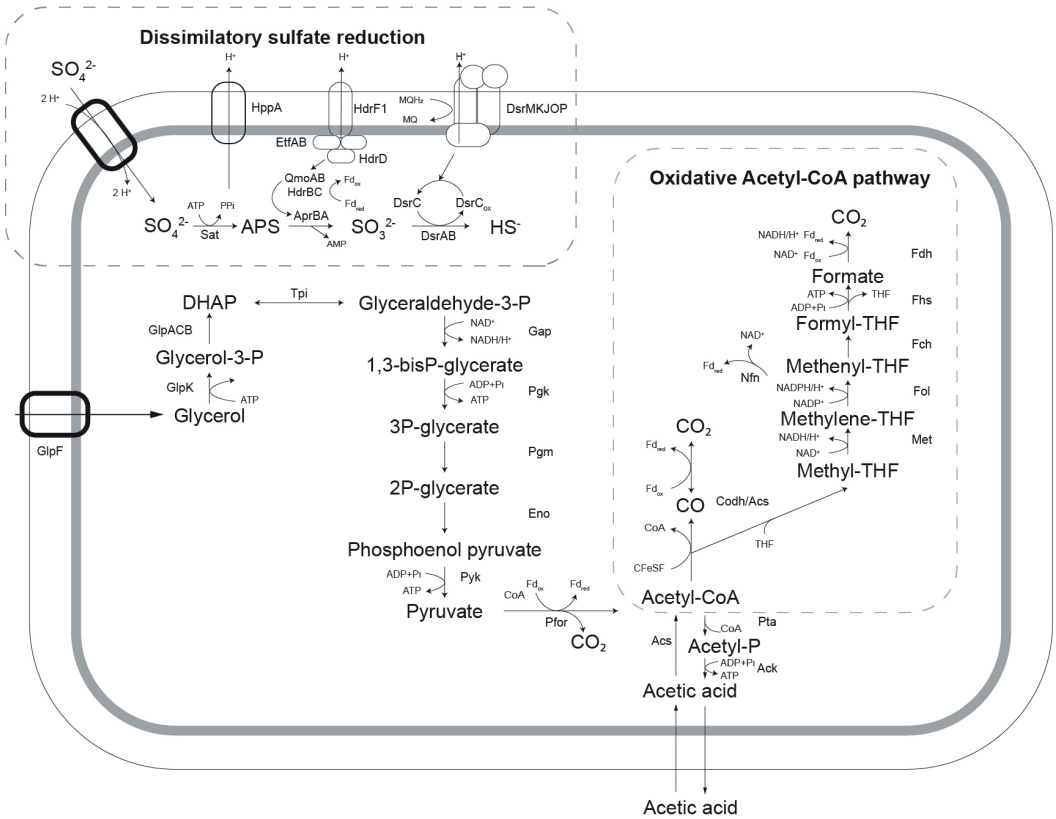

Figure 4. Schematic representation of pathways for glycerol oxidation and sulfate reduction as detected in the genome of *Acididesulfobacillus acetoxydans*. Sat: ATP sulfurylase, Apr: APS reductase, Dsr: dissimilatory sulfite reductase, Qmo: quinone-interacting membrane oxidoreductase complex, Hdr: heterodisulfide reductase, GlpF: glycerol transporter, GlpK: glycerol kinase, Tpi: triose phosphate isomerase, Gap: glyceraldehyde-3-phosphate dehydrogenase, Pgk: phosphoglycerate kinase, Pgm: phosphoglycerate mutase, Eno: phosphoenolpyruvate hydratase, Pyk: pyruvate kinase, Pfor: pyruvate:ferredoxin oxidoreductase, Pta: Phosphate acetyltransferase, Ack: acetate kinase, Acs: acetyl-coA synthase, Codh: carbon monoxide dehydrogenase, Met: methylene-tetrahydrofolate reductase, Fol: methylene-tetrahydrofolate dehydrogenase/methenyl-tetrahydrofolate cyclohydrolase, Fch: 5-formyltetrahydrofolate_cyclo-ligase, Fhs: Formate-tetrahydrofolate ligase/ formyl-H4F synthethase, Fdh: formate dehydrogenase, Nfn: NADH-dependent reduced ferredoxin:$NADP^+$ oxidoreductase.

The increased specific proton consumption rate at pH 3.9 compared to pH 5.0, and the ability to oxidize organic acids to CO_2 has important effects on the biogeochemistry of ARD/AMD environments, as it contributes to the natural attenuation of the extreme conditions. In the Tinto River, for example, the pH values can be as low as 2 in the water column (Sánchez-Andrea *et al.*, 2012; Amils *et al.*, 2014). Consequently, the microbial diversity in the water column of the Tinto River is generally low, and dominated by only a few species belonging to the *Acidithiobacillus*, *Leptospirillum* and *Acidiphilium* genera (López-Archilla et al., 2001). Microbial diversity is higher in the sediments (Sánchez-Andrea et al., 2011), partly due to the wider range of physicochemical characteristics found in the different layers. As strain INE was isolated from Tinto River sediments, its detoxifying characteristics indicate that it could assist in the creation of milder conditions, where less acidophilic microorganisms can thrive. This could facilitate the higher microbial diversity found in the sediments compared to the water column, where the environment is more dynamic due to the water flow.

Additional stress resistance mechanisms at low pH

Other possible pH homeostasis mechanisms enabling *A. acetoxydans* to grow at low pH besides acetate oxidation were also investigated. Protein abundance at optimum and minimum pH were compared to detect increased translation of proteins involved in acid stress response mechanisms at minimum pH. Protein abundances in cultures grown at optimum (5.0) and low (3.9) pH showed 1258 proteins present in at least one of the growth conditions, of which 949 were present in both. Using a p-value cut-off of 0.05 (student t-test), 30 proteins were present in at least two-fold higher abundance at pH 3.9 compared to pH 5.0, with 15 proteins unique for pH 3.9. At pH 5.0, 56 proteins were present in at least two-fold higher abundance, of which 32 were uniquely present at pH 5.0 (Supplementary Table S3*)*.

Donnan potential and transporters. A Donnan potential serves as a chemiosmotic barrier to the influx of protons at low extracellular pH as described for extreme acidophiles (Baker-Austin and Dopson, 2007). A key element in creating a positive membrane potential is the K^+-transporting ATPase, encoded by the *kdpABC* operon, which was indeed detected in the genome of *A. acetoxydans* (3037-39). However, this K^+ ATPase was not detected in the proteome of cells grown at either pH 3.9 or 5.0. Therefore, despite its apparent importance in other acidophiles (Baker-Austin and Dopson, 2007), it did not appear to play an important role in acid stress resistance of *A. acetoxydans*. Although the detection of membrane proteins such as ATPases with standard proteomics methods is difficult, and their presence cannot be completely

dismissed based on these results alone, comparative transcriptomics analysis also verified the absence of the K^+-transporting ATPase from the transcriptome (Sánchez-Andrea, unpublished data).

In addition to K^+-ATPase, genes encoding secondary cation transporters such as Na^+/P_i co-transporters (3752, 0312, 1305) and solute symporters (1779, 2169, 2179, 2830, 3466, 3909) were identified in the genome, and the corresponding proteins (1305, 2179, 3466, and 2830) were present in the proteome. Interestingly, a bile acid:Na^+ symporter (2179) and a transporter from the major facilitator superfamily (0284) were only present at pH 3.9, indicating a potentially important role in ion transport at low pH. Build-up of excess protons in the cytoplasm can be further countered by active H^+ export by ATPase. The proton ATPase found in strain INE (0352-0361) was present in the proteome at both pH values, but not in significantly different abundance at lower pH, suggesting that this system is not upregulated in response to increased acid stress. Antiporters such as the Na^+/H^+ antiporter (2829) or the H^+/Cl^- exchange transporter (*clcA*, 0494) also contribute to H^+ removal. ClcA was detected in the proteome, albeit not in significantly different abundance at lower pH.

Cytoplasmic buffering capacity. The modification of the cytoplasmic buffering capacity through a change in the metabolism of certain amino acids could mitigate acid stress (Baker-Austin and Dopson, 2007; Slonczewski et al., 2009). The decarboxylation of arginine, glutamate and aspartate, for example, releases CO_2 and amines, and consumes protons. (Slonczewski et al., 2009). This would be net H^+ -consuming when the amino acids can be taken up from the environment, and it could be speculated that the yeast extract present in the medium served as an external source of amino acids. L-aspartate decarboxylase (2148) was found in the proteome at pH 5.0, but not at pH 3.9, indicating that this reaction does not contribute to pH homeostasis at increased proton stress. Glutamate decarboxylase (2571), catalyzing the H^+ consuming conversion of glutamate to g-aminobutyrate (GABA) (Castanie-Cornet et al., 1999), and L-arginine decarboxylase (0577), catalyzing the H^+-consuming conversion of L-arginine to agmatine, were detected in the proteome at both conditions, albeit not at a significantly different abundance. Furthermore, glutamate decarboxylase forms the GABA shunt together with GABA aminotransferase and succinate semialdehyde dehydrogenase, which is also proposed to be involved in acid stress resistance in bacteria (Feehily and Karatzas, 2013). Through the GABA shunt, glutamate is converted to GABA by glutamate decarboxylase (2571), consuming a proton, and GABA is converted to succinate semialdehyde (SSA) by GABA aminotransferase (4212, 3258), regenerating the glutamate. Succinate semialdehyde dehydrogenase then

converts SSA to succinate (3872, 3892). Glutamate decarboxylase (2571) and GABA aminotransferase (3258, 4212) were detected in the proteome of strain INE, albeit not at a significantly different abundance at pH 5.0 or 3.9. Succinate semialdehyde dehydrogenase was not detected in the proteome, however, and the role of the GABA shunt in resistance to acid stress in strain INE could, therefore, not be clearly established.

Interestingly, agmatinase (0579), converting agmatine to urea and putrescine, was detected in the proteome at both pH values. Urea may play a role in pH homeostasis through its degradation into two molecules of ammonium and and one CO_2, catalysed by urease. This requires incorporation of 2 H^+, and is known to play a role in acid stress resistance (Young et al., 1996). However, the gene encoding urease was not detected in the genome of strain INE. An alternative route for urea degradation could be through urea amidolyase; genes (0170, 0171) were detected in the genome, but the corresponding proteins were absent in the proteome. Urea does seem to play a role in pH homeostasis of strain INE at low pH—four out of the five enzymes of the urea cycle are present in increased abundance at pH 3.9. A carbamoyl phosphate synthase (0932) was found only at pH 3.9, and ornithine carbamoyltransferase (0934), and argininosuccinate synthase (0935) were present in twofold higher abundance. Argininosuccinate lyase (0936) was present in the proteome at both conditions in similar abundance. Arginase (0853), converting arginine to urea and ornithine and completing the urea cycle, was, however, not detected in the proteome, and the role of the urea cycle in acid stress resistance of strain INE, therefore, remains enigmatic.

DNA, protein, and lipid repair mechanisms. The extreme acidity and high metal concentrations in acid drainage environments increase the risk of damage to DNA, RNA and proteins. A number of DNA, protein and lipid repair systems were present in the proteome of strain INE. Ferroxidase (0081), linked to protection of DNA upon exposure to acid stress in *Helicobacter pylori* (Huang et al., 2010), was present in the proteome at both conditions. Several chaperones involved in protein refolding (0004, 2293, 3249, 0692, 2491, 2469, 1389, 1390) were present in the proteome, and a ferredoxin signature (3253) upstream of a chaperone (3249) was ca. 6-fold more abundant at pH 3.9 than at pH 5.0. An upregulation of chaperones was found to accompany growth at lower pH in many acidophiles (Jerez et al., 1988). Furthermore, 6 peroxiredoxins, potentially involved in lipid repair (Cárdenas et al., 2012), were detected in the proteomes at both conditions (2671, 0858, 0888, 0966, 1064, 2671, 3052). One of these (2671) was ca. twofold more abundant at low pH.

Altered membrane permeability. Comparison of the lipid composition in *A. acetoxydans* strain INE at pH 5.0 and at pH 3.9 showed a transition, with decreasing pH, from acyl/ether glycerol (AEG) lipids with an unsaturated ether moiety (plasmalogens) to AEG lipids with a saturated ether moiety (Table 2). This was evident in the core lipids through an increase in saturated monoalkyl glycerol ether lipids from 5.0 % at pH 5.0 to 13.0 % at pH 3.9 and a concomitant decrease in DMAs (from 24.9 to 17.6 %). The increase in saturated ether moieties may represent an adaptation to maintain membrane homeostasis at lower pH. Increasing saturation of FAs in response to lower pH has been described some in bacterial species, but the opposite effect has been observed in others (Siliakus, van der Oost, and Kengen 2017; Sohlenkamp, 2019). It should be noted that there was no change in the saturation of the diacyl glycerols (DAGs), as seen from the FAs (Table 2). With decreasing growth pH there was also a clear diversification in acyl and ether moieties (Table 2). Bacterial glycerol ether lipids likely play a role in cell resistance or adaptation to adverse environmental conditions (Grossi et al., 2015) since ether linkages are less sensitive to acid hydrolysis than ester bonds. Indeed, AEG lipids are thought to improve cell resistance to extreme external conditions, relative to DAGs (Grossi et al., 2015).

At both pH values, the *A. acetoxydans* FA were dominated by branched-chain FAs (97 % of FAs at pH 3.9, 100 % at pH 5.0), including iso, anti-iso and mid-chain methylated FAs. Similarly, the percentage of FAs that were branch-chained was moderate to high in the other acidophilic strains, *Ds. acididurans* (26 %) and *Ds. acidiphilus* (42 %), while they were absent in both neutrophilic strains *Ds. orientis* and *Ds. halogenans*. In particular, the branched-chain acid iso-$C_{15:0}$ was abundant in strain INE (48.1 % at pH 3.9, 60.7 % at pH 5.0) and in the acidophilic strains *Ds. acididurans* (25.8 %) and *Ds. acidiphilus* (16.6). An increasing proportion of branched-chain FAs is a known adaption to maintain membrane homeostasis under external stress, and a number of extreme acidophilic bacteria have been reported to have high levels of branched-chain FA (Siliakus et al., 2017).

In addition to an altered membrane FA composition, a putative poly-gamma-glutamate (PGA) bacterial capsule synthesis protein CapA (2151) was found in two-fold higher abundance at low pH in the proteome, providing another means to create physical separation between the cell and the acidic environment as a defense mechanism. PGA is a natural polymer that may be involved in avoiding dehydration in high salt concentrations and neutralizing pH in alkaliphiles (Ashiuchi and Misono, 2002) by forming a protective PGA capsule. Furthermore, spermidine is hypothesized to play a role in the protection against acid stress through lowering the permeability of the membrane to protons (Christel et al., 2017). Spermidine synthase (0578) was detected

in both proteome sets at similar abundances, indicating spermidine could play a role in acid stress resistance of *A. acetoxydans* at both pH values tested.

Conclusion

Acididesulfobacillus acetoxydans strain INE, isolated from Tinto River sediments, represents a novel species of a novel genus of moderately acidophilic SRB. The increased specific proton consumption rates at low pH (3.9) compared to optimum pH (5.0) when grown with glycerol and sulfate demonstrated the alkalinizing effect of its metabolism in acidic environments. The capacity for complete oxidation of organic acids to CO_2 can reduce organic acid toxicity and provide increased access to organic carbon compounds in nutrient-limited acid drainage environments. Interestingly, canonical acid stress resistance mechanisms such as an inverted membrane (Donnan) potential, increased abundance of charge transporters, and cytoplasmic buffering capacity were not detected in the proteome during growth at low pH. Instead, an increased fraction of ether-bound FA in the overall membrane lipid composition appeared to be an important acid stress resistance mechanism for *A. acetoxydans* during growth at pH below optimum. In addition, the increased abundance of CapA could suggest that the response to proton stress in *A. acetoxydans* resembles the response to high salinity.

Description of *Acididesulfobacillus* gen. nov.

A.ci.di.de.sul.fo.ba.cil'lus. L. masc. adj. *acidus*, sour; N.L. masc. n. '*Desulfobacillus*', a (not validly published) bacterial genus name; N.L. masc. n. *Acididesulfobacillus*, an acid-loving relative of the genus '*Desulfobacillus*'. Cells present sub-terminal spores and are rod-shaped, strictly anaerobic, motile, and stain Gram-negative, but lack the characteristic double membrane. The genus is closely related to *Desulfosporosinus* and *Desulfitobacterium*. The type species is *Acididesulfobacillus acetoxydans*.

Description of *Acididesulfobacillus acetoxydans* sp. nov.

Acididesulfobacillus acetoxydans: a.cet.o'xy.dans. L. neut. n. *acetum*, vinegar; N.L. v. *oxydo* (from Gr. masc. adj. *oxys*, acid, sour), to oxidize; N.L. part. adj. *acetoxydans*, oxidizing acetate.

Straight single rods are 4-7 µm long and about 0.6 µm wide. Motile in the exponential phase by lateral flagellation. Subterminal, oval endospores are formed in the stationary growth phase. Cells are Gram-positive that stain Gram-negative. The pH range for

growth is pH 3.8-6.5, with an optimum at pH 5.0. The temperature range for growth is 25-42 °C, with an optimum at 30 °C. The upper limit for salt tolerance is 15.3 g L^{-1} NaCl. Strain INE uses a wide range of electron donors in the presence of sulfate such as H_2; organic acids (formate, acetate, pyruvate, lactate, malate, fumarate, butyrate and succinate); alcohols (methanol, ethanol, propanol and glycerol); the amino acid L-cysteine; sugars (xylose, fructose, glucose, maltose, sucrose and raffinose) and yeast extract or starch; but not propionate, citrate or benzoate. Organic substrates are oxidized completely to CO_2. Strain INE uses selenate, arsenate, nitrate, sulfate, elemental sulfur, thiosulfate and DMSO as electron acceptors; but not iron, fumarate, PCE, perchlorate, sulfite, or dithionate. It also ferments some substrates such as cysteine, pyruvate, glucose and yeast extract. It couples the disproportionation of sulfur and thiosulfate to growth, but not sulfite. Strain INE is susceptible to vancomycin. The predominant whole cell membrane lipids of the type strain INE at pH 5 are iso-C15:0 FA (60.7 %), and iso-C15:0 DMA (14.3 %). Its genomic G+C content is 53.65 mol %. Phylogenetically, it is a member of the family *Peptococcaceae*, order *Clostridiales* within the *Firmicutes* phylum. The type strain *Acididesulfobacillus acetoxydans*, strain INE (=DSM 29876^T =JCM 30553^T), was isolated from the Tinto River, Spain.

Acknowledgments

We thank Hans Wessels from Radboud University Nijmegen for the proteomics services, Marcel Giesbers and Jelmer Vroom from the Wageningen Electron Microscopy Center for TEM imaging, and Ellen Hopmans for advice on lipid identification. We thank Aharon Oren for fruitful discussion on nomenclature regulations and Barrie Johnson for his pioneering work on acidophilic SRB.

Supplementary information

Supplementary Table S1.

genome	Desulfitobacterium_dehalogenans_JW_IU-DC1_ATCC_51507.gbk_protein_multifasta	Desulfitobacterium_dichloroeliminans_LM G_P-21439.gbk_protein_multifasta	Desulfitobacterium_hafniense_DCB-2.gbk_protein_multifasta	Desulfitobacterium_metallireducens_853-15A_DSM_15288.gbk_protein_multifasta	Desulfobacillus	desulfosporosinus_acididuransstrain_M1	Desulfosporosinus_acidiphilus_DSM_22704_all	Desulfosporosinus_meridiei_DSM_13257	Desulfosporosinus_orientis_DSM_765	Desulfosporosinus_sp._HMP52.gbk_protein_multifasta	Desulfosporosinus_sp._Tol-M_Ga0063340	Desulfosporosinus_youngiae_DSM_17734	peptococcaceae_bacterium_CEB3
Desulfitobacterium_dehalogenans_JW_IU-DC1_ATCC_51507.gbk_protein_multifasta	100	79.93	87.96	68.4	62.1	63.17	63.5	64.05	63.89	64	63.38	65.09	61.87
Desulfitobacterium_dichloroeliminans_LMG_P-21439.gbk_protein_multifasta	79.93	100	79.25	68.3	62.08	63.13	63.39	63.9	63.34	64.05	63.38	64.84	61.82
Desulfitobacterium_hafniense_DCB-2.gbk_protein_multifasta	87.96	79.25	100	67.98	62.15	63.22	63.31	63.76	63.62	63.69	63.58	65.59	61.52
Desulfitobacterium_metallireducens_853-15A_DSM_15288.gbk_protein_multifasta	68.4	68.3	67.98	100	63.94	64.86	64.9	65.24	65.12	65.19	64.97	65.42	63.67
Desulfobacillus	62.1	62.08	62.15	63.94	100	63.87	64.36	63.07	63.01	63.19	64.21	62.79	89.3
desulfosporosinus_acididuransstrain_M1	63.17	63.13	63.22	64.86	63.87	100	84	72.41	71.99	72.09	71.99	71.99	63.89
Desulfosporosinus_acidiphilus_DSM_22704_all	63.53	63.36	63.33	64.93	64.35	84.03	100	72.18	72.39	72.12	72.09	72.15	64.45
Desulfosporosinus_meridiei_DSM_13257	64.05	63.9	63.76	65.24	63.07	72.41	72.2	100	79.36	94.27	73.81	80.48	63.14
Desulfosporosinus_orientis_DSM_765	63.89	63.34	63.62	65.12	63.01	71.99	72.39	79.36	100	79.34	73.08	78.85	62.86
Desulfosporosinus_sp._HMP52.gbk_protein_multifasta	64	64.05	63.69	65.19	63.19	72.09	72.12	94.27	79.34	100	73.99	80.29	63.04
Desulfosporosinus_sp._Tol-M_Ga0063340	63.38	63.38	63.58	64.97	64.21	71.99	72.11	73.81	73.08	73.99	100	74.59	64.13
Desulfosporosinus_youngiae_DSM_17734	65.09	64.84	65.59	65.42	62.79	71.99	72.06	80.48	78.85	80.29	74.59	100	62.86
peptococcaceae_bacterium_CEB3	61.87	61.82	61.52	63.67	89.3	63.89	64.47	63.14	62.86	63.04	64.13	62.86	100

Supplementary Table S2: The intact polar lipid (IPL) composition of Acididesulfobacillus acetoxydans gen. nov. sp. nov. grown at pH 5.0 (growth optimum) as determined by UHPLC-HRMS analysis.

Polar lipid type	Core lipid	Mass (*m/z*)	AEC	Δ mmu	Relative abundance
SQ	AEG 15:0, O-15:0	770.5437 [a]	$C_{39}H_{80}NO_{11}S^+$	-1.0	3.1 ± 0.2
SQ	AEG 15:0, O-16:0	784.5598 [a]	$C_{40}H_{82}NO_{11}S^+$	-0.5	1.5 ± 0.1
SQ	AEG 15:0, O-17:0	798.5750 [a]	$C_{41}H_{84}NO_{11}S^+$	-0.9	2.6 ± 0.2
SQ	AEG 15:0, O-18:0	812.5908 [a]	$C_{42}H_{86}NO_{11}S^+$	-0.8	0.8 ± 0.1
SQ	DAG 15:0, 15:0	784.5234 [a]	$C_{39}H_{78}NO_{12}S^+$	-0.5	0.9 ± 0.2
SQ	DAG 15:0, 16:0	798.5396 [a]	$C_{40}H_{80}NO_{12}S^+$	-0.1	0.4 ± 0.1
SQ	DAG 15:0, 17:0	812.5545 [a]	$C_{41}H_{82}NO_{12}S^+$	-0.7	0.6 ± 0.1
					9.9 ± 0.9
PG	AEG plasmalogen 15:0, O-15:1	696.5164 [a]	$C_{36}H_{75}NO_9P^+$	-1.0	4.4 ± 0.8
PG	AEG 15:0, O-15:0	698.5320 [a]	$C_{36}H_{77}NO_9P^+$	-1.1	1.6 ± 0.1
PG	AEG plasmalogen 15:0, O-16:1	710.5324 [a]	$C_{37}H_{77}NO_9P^+$	-0.7	1.7 ± 0.1
PG	AEG 15:0, O-16:0	712.5478 [a]	$C_{37}H_{79}NO_9P^+$	-0.9	0.8 ± 0.1
PG	AEG plasmalogen 15:0, O-17:1	724.5473 [a]	$C_{38}H_{79}NO_9P^+$	-1.4	4.2 ± 0.8
PG	AEG 15:0, O-17:0	726.5632 [a]	$C_{38}H_{81}NO_9P^+$	-1.2	1.7 ± 0.1
PG	AEG plasmalogen 15:0, O-18:1	738.5631 [a]	$C_{39}H_{81}NO_9P^+$	-1.3	1.5 ± 0.1
PG	AEG 15:0, O-18:0	740.5787 [a]	$C_{39}H_{83}NO_9P^+$	-1.3	1.6 ± 0.0
PG	DAG 15:0, 15:0	712.5111 [a]	$C_{36}H_{75}NO_{10}P^+$	-1.2	0.3 ± 0.0
PG	DAG 15:0, 16:0	726.5270 [a]	$C_{37}H_{77}NO_{10}P^+$	-0.9	0.3 ± 0.0
PG	DAG 15:0, 17:0	740.5424 [a]	$C_{38}H_{79}NO_{10}P^+$	-1.2	1.3 ± 0.0
					19.3 ± 2.2
PE	AEG plasmalogen 15:0, O-14:1	634.4801 [b]	$C_{34}H_{69}NO_7P^+$	-0.5	0.5 ± 0.0
PE	AEG plasmalogen 15:0, O-15:1	648.4956 [b]	$C_{35}H_{71}NO_7P^+$	-0.7	6.2 ± 0.2
PE	AEG plasmalogen 15:0, O-16:1	662.5110 [b]	$C_{36}H_{73}NO_7P^+$	-0.9	1.5 ± 0.0
PE	AEG plasmalogen 15:0, O-17:1	676.5266 [b]	$C_{37}H_{75}NO_7P^+$	-1.0	1.8 ± 0.1
PE	AEG plasmalogen 15:0, O-18:1	690.5424 [b]	$C_{38}H_{77}NO_7P^+$	-0.8	1.3 ± 0.2
PE	DAG 15:0, 15:0	664.4904 [b]	$C_{35}H_{71}NO_8P^+$	-0.8	3.0 ± 0.1
PE	DAG 15:0, 16:0	678.5062 [b]	$C_{36}H_{73}NO_8P^+$	-0.7	1.2 ± 0.0
PE	DAG 15:0, 17:0	692.5218 [b]	$C_{37}H_{75}NO_8P^+$	-0.7	3.2 ± 0.1
					18.6 ± 0.1
Hexosamine-hexose	AEG plasmalogen 15:0, O-15:1	848.6082 [b]	$C_{45}H_{86}NO_{13}^+$	-1.2	5.4 ± 0.0
Hexosamine-hexose	AEG 15:0, O-15:0	850.6241 [b]	$C_{45}H_{88}NO_{13}^+$	-0.9	4.1 ± 1.2
Hexosamine-hexose	AEG plasmalogen 15:0, O-16:1	862.6239 [b]	$C_{46}H_{88}NO_{13}^+$	-1.1	0.9 ± 0.2
Hexosamine-hexose	AEG 15:0, O-16:0	864.6395 [b]	$C_{46}H_{90}NO_{13}^+$	-1.1	0.7 ± 0.2
Hexosamine-hexose	AEG plasmalogen 15:0, O-17:1	876.6392 [b]	$C_{47}H_{90}NO_{13}^+$	-1.5	1.6 ± 0.4
Hexosamine-hexose	AEG 15:0, O-17:0	878.6552 [b]	$C_{47}H_{92}NO_{13}^+$	-1.1	1.2 ± 0.3
Hexosamine-hexose	AEG plasmalogen 15:0, O-18:1	890.6542 [b]	$C_{48}H_{92}NO_{13}^+$	-2.1	2.1 ± 0.5
Hexosamine-hexose	AEG 15:0, O-18:0	892.3670 [b]	$C_{48}H_{14}NO_{13}^+$	-1.7	2.0 ± 0.3
Hexosamine-hexose	DAG 15:0, 15:1	862.5886 [b]	$C_{45}H_{84}NO_{14}^+$	0.0	0.4 ± 0.1
Hexosamine-hexose	DAG 15:0, 15:0	864.6039 [b]	$C_{45}H_{86}NO_{14}^+$	-0.4	3.1 ± 0.4

Hexosamine-hexose	DAG 15:0, 16:0	878.6194 [b]	$C_{46}H_{88}NO_{14}^+$	-0.6	0.4 ± 0.1
Hexosamine-hexose	DAG 15:0, 17:0	892.6346 [b]	$C_{47}H_{90}NO_{14}^+$	-1.0	0.9 ± 0.1
Hexosamine-hexose	DAG 15:0, 18:1	904.6346 [b]	$C_{48}H_{90}NO_{14}^+$	-0.9	0.9 ± 0.1
					23.7 ± 4.6
Hexosamine unknown		864.6040 [b]	$C_{45}H_{86}NO_{14}^+$	-0.3	1.7 ± 0.3
Hexosamine unknown		878.6199 [b]	$C_{46}H_{88}NO_{14}^+$	0.0	0.2 ± 0.0
Hexosamine unknown		890.6201 [b]	$C_{47}H_{88}NO_{14}^+$	0.1	0.2 ± 0.0
Hexosamine unknown		880.5991 [b]	$C_{45}H_{86}NO_{15}^+$	-0.1	0.9 ± 0.2
Hexosamine unknown		906.6141 [b]	$C_{47}H_{88}NO_{15}^+$	-0.7	0.8 ± 0.2
					3.8 ± 0.7
Lyso-DPG	AEG 15:0, plasmalogen 15:0, O-15:1	1074.7341 [a]	$C_{54}H_{110}NO_{15}P_2^+$	-0.4	2.1 ± 0.2
Lyso-DPG	AEG 15:0, plasmalogen 15:0, O-16:1	1088.7502 [a]	$C_{55}H_{112}NO_{15}P_2^+$	0.0	0.7 ± 0.0
Lyso-DPG	AEG 15:0, plasmalogen 15:0, O-17:1	1102.7661 [a]	$C_{56}H_{114}NO_{15}P_2^+$	0.3	1.0 ± 0.1
					3.8 ± 0.3
DPG	AEG 2x plasmalogens 15:0, O-15:1	1282.9548 [a]	$C_{69}H_{138}NO_{15}P_2^+$	1.1	1.4 ± 0.1
DPG	AEG 2x plasmalogens 15:0, O-15:1, 15:0, O-16:1	1296.9686 [a]	$C_{70}H_{140}NO_{15}P_2^+$	-0.6	0.9 ± 0.0
DPG	AEG 2x plasmalogens 15:0, O-15:1, 15:0, O-17:1	1310.9838 [a]	$C_{71}H_{142}NO_{15}P_2^+$	-1.2	1.4 ± 0.0
DPG	AEG	1325.0011 [a]	$C_{72}H_{144}NO_{15}P_2^+$	0.5	0.5 ± 0.0
					4.6 ± 0.0
Unknowns					**16.4 ± 2.4**

AEC = Assigned elemental composition. mmu = milli mass unit, Δ mmu = (measured mass – calculated mass) x 1000. a = $[M+NH_4]^+$. b = $[M+H]^+$. SQ = sulfoquinovosyl; PG = phosphoglycerol; PE = phosphoethanolamine; DPG diphosphatidylglycerol (commonly known as cardiolipins). DAG = diacylglycerol; AEG = mixed acyl/ether glycerol. XX:Y represent alkyl carbon number : number of double bond equivalents. An alkyl ether linkage is represented by an "O-" prefix.

A. Example spectra of hexosamine-hexose lipid. $[M+H]^+$ of parent ion in MS^1 = 864.60354

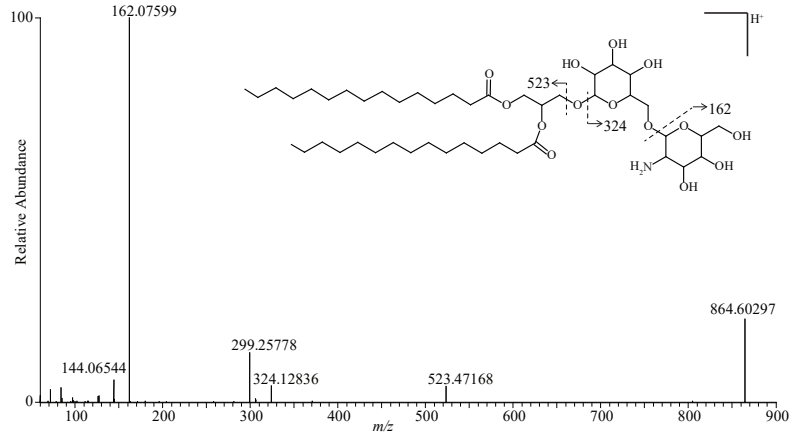

Observed mass $[M+H]^+$	Assigned elemental composition	Calculated mass	Δ mmu	Assignment
864.60354 (parent from MS^1)	$C_{45}H_{86}NO_{14}^+$	864.60428	0.7	Hexosamine-hexose-DAG
523.47168	$C_{33}H_{63}O_4^+$	523.47209	0.4	C_{30} DAG core
324.12836	$C_{12}H_{22}NO_9^+$	324.12891	0.6	Hexose-hexosamine
299.25778	$C_{18}H_{35}O_3^+$	299.25807	0.3	C_{15} fatty acid
162.07599	$C_6H_{12}NO_4^+$	162.07608	0.1	Hexosamine
144.06544	$C_6H_{10}NO_3^+$	144.06552	0.2	Hexosamine fragment (loss of H_2O)

B. Example spectra of unknown hexosamine. $[M+H]^+$ of parent ion in MS^1 = 880.5991

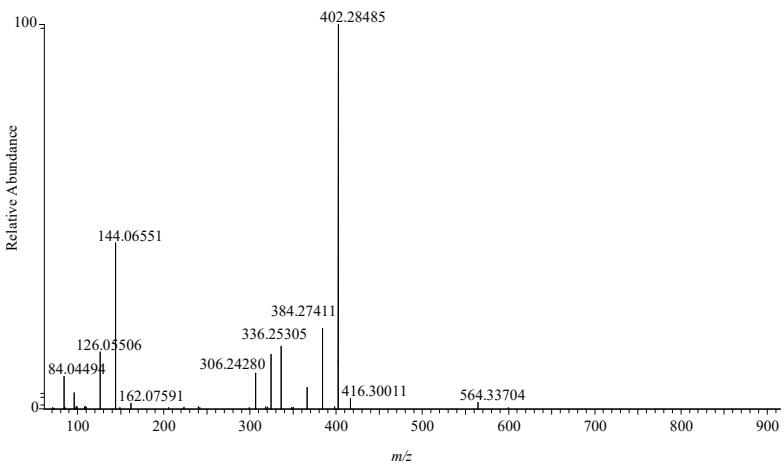

Supplementary Figure S1 (A) Example MS^2 spectra of a hexosamine-hexose lipid. $[M+H]^+$ of parent ion in MS^1 = 864.604. Placement of amine group in structure is tentative. Table insert of ion assignments, mmu = milli mass unit, Δ mmu = (measured mass – calculated mass) x 1000. (B) Example MS^2 spectra of one of the unknown hexosamine-containing lipids. $[M+H]^+$ of parent ion in MS^1 = 880.599.

Supplementary Table S3 Proteins detected at 2-fold or higher increased abundance at pH 3.9 or pH 5.0 (p-value < 0.05, student t-test). Locus tag DEACI_**** is followed by the annotation. U: unique at this condition.

Locus ID | Annotation	Ratio
Up at pH 3.9 (p < 0.05)	
DEACI_3808 | Amidohydrolase family	U
DEACI_1219 | YopX-like domain, beta barrel type	U
DEACI_2957 | Aminotransferase class I and II	U
DEACI_3393 | UPF0109 protein <locus_tag>	U
DEACI_0929 | acetylglutamate kinase	U
DEACI_0150 | Hypothetical protein	U
DEACI_0043 | Two component system, signal transduction histidine kinase	U
DEACI_0431 | Putative ABC transporter	U
DEACI_0616 | Glutamate/leucine/phenylalanine/valine dehydrogenase signature	U
DEACI_1273 | Alcohol dehydrogenase, iron-type, conserved site	U
DEACI_2503 | diaminohydroxyphosphoribosylaminopyrimidine deaminase/glucuronate reductase	U
DEACI_0284 | Major facilitator superfamily transporter	U
DEACI_3079 | Imidazole glycerol phosphate synthase subunit HisF [hisF]	U
DEACI_0932 | Carbamoyl-phosphate synthase (glutamine-hydrolysing)	U
DEACI_2179 | arsenical-resistance protein	U
DEACI_1267 | Methyltransferase cognate corrinoid protein	14.8
DEACI_0220 | Putative cell wall binding repeat 2	8.4
DEACI_3253 | 3Fe-4S ferredoxin signature	6.3
DEACI_1268 | trimethylamine-corrinoid protein Co-methyltransferase	3.4
DEACI_1848 | Periplasmic binding protein-like I	3.1
DEACI_3294 | 2-dehydro-3-deoxy-phosphogluconate aldolase	3.0
DEACI_3321 | Serine dehydratase-like, alpha subunit	2.9
DEACI_3250 | Domain of unknown function DUF815	2.4
DEACI_0935 | Argininosuccinate synthase	2.3
DEACI_2359 | Bacterial translocase SecF protein signature	2.3
DEACI_1260 | Leu/Ile/Val-binding protein family signature	2.3
DEACI_1137 | Methyl-accepting chemotaxis protein (MCP) signalling domain	2.2
DEACI_0934 | ornithine carbamoyltransferase	2.2
DEACI_0227 | Putative cell wall binding repeat 2	2.1
DEACI_0923 | Ferritin- like diiron domain protein	2.1
Up at pH 5.0	
DEACI_2761 | purine-nucleoside phosphorylase	2.0
DEACI_0532 | stage V sporulation protein T	2.0
DEACI_1328 | Uncharacterised ArCR, COG2043	2.0
DEACI_1622 | Lipoprotein localisation LolA/LolB/LppX	2.0
DEACI_2229 | prepilin-type N-terminal cleavage/methylation domain protein	2.1
DEACI_3701 | sporulation protein, YlmC/YmxH family	2.1
DEACI_3671 | dihydroorotase	2.2
DEACI_3723 | Periplasmic binding protein domain	2.3
DEACI_2529 | Succinate dehydrogenase/Fumarate reductase transmembrane subunit	2.3
DEACI_0527 | PRC-barrel-like	2.4
DEACI_2466 | Flavin reductase like domain protein	2.5

DEACI_3992 | Putative cell wall binding repeat 2	2.8
DEACI_4292 | UBA-like	3.2
DEACI_0833 | ferredoxin hydrogenase	3.3
DEACI_1144 | pyruvate flavodoxin/ferredoxin oxidoreductase	3.8
DEACI_4004 | Flagellar protein FliS	4.0
DEACI_4008 | Bacterial flagellin C-terminal helical region	4.8
DEACI_3249 | Hsp20/alpha crystallin family	4.8
DEACI_2496 | Hypothetical protein	6.3
DEACI_2870 | Spore coat protein CotF-like	9.7
DEACI_1833 | Hypothetical protein	11.4
DEACI_3202 | Dipicolinic acid synthetase, subunit B	16.4
DEACI_3203 | dipicolinic acid synthetase, A subunit	17.5
DEACI_0510 | Glycoside hydrolase superfamily	34.6
DEACI_2148 | aspartate 1-decarboxylase	U
DEACI_2885 | 4Fe4S-binding SPASM domain protein	U
DEACI_1633 | amidophosphoribosyltransferase	U
DEACI_3784 | Flagellar motor switch protein FliM signature	U
DEACI_3666 | Orotidine-5'-phosphate decarboxylase	U
DEACI_0130|Protein MutL	U
DEACI_2759 | serine-type D-Ala-D-Ala carboxypeptidase	U
DEACI_0552 | 6-phosphogluconate dehydrogenase C-terminal domain-like	U
DEACI_4003 | Hypothetical protein	U
DEACI_3804 | CO dehydrogenase flavoprotein C-terminal domain	U
DEACI_0841 | N-acetylmuramoyl-L-alanine amidase	U
DEACI_4010 | NAD dependent epimerase/dehydratase, LLPSF_EDH_00030 family	U
DEACI_2569 | ATPase, AAA-type, core	U
DEACI_1838 | Gcn5-related N-acetyltransferase (GNAT) domain protein	U
DEACI_0871 | glutamate formimidoyltransferase	U
DEACI_1114 | Hypothetical protein	U
DEACI_0365 | uracil phosphoribosyltransferase	U
DEACI_1339 | Alanine racemase	U
DEACI_4072 | 5-dehydro-4-deoxy-D-glucuronate isomerase	U
DEACI_2311 | SHOCT domain protein	U
DEACI_0982 | 6-phosphogluconolactonase	U
DEACI_3823 | Methyl-accepting chemotaxis protein (MCP) signalling domain	U
DEACI_2460 | Asparagine synthase (glutamine-hydrolysing)	U
DEACI_1574 | acetaldehyde dehydrogenase (acetylating)	U
DEACI_0071 | Ferritin-related protein	U
DEACI_4307 | HIT-like domain protein	U
DEACI_0144 | Control of competence regulator ComK, YlbF/YmcA	U
DEACI_0416 | Ribosomal protein S18 family signature	U
DEACI_4066 | mannitol-1-phosphate 5-dehydrogenase	U
DEACI_1315 | Hypothetical protein	U
DEACI_0104 | RNA polymerase sigma factor 54 interaction domain protein	U
DEACI_2368 | Hypothetical protein	U

General Discussion

Expanding the operating conditions for sulfidogenesis from elemental sulfur

One of the aims of this thesis was to achieve (bio)sulfidogenesis from S_8^0 at higher temperatures and more acidic pH than the neutral pH and moderate temperatures currently used in the industrial BioSulphide and THIOTEQ® Metal processes (Huisman et al., 2006; Adams et al., 2008). This would improve process economics by enabling integration of sulfidogenesis and metal precipitation in a single reactor, incentivizing implementation of this technology for metal recovery and recycling from (hot) acidic, metalliferous waste streams such as AMD and metallurgy process waters. In **chapter 2**, sulfidogenesis at high temperature and low pH was investigated, whereas **chapter 3** addressed sulfidogenesis at mesophilic temperatures at neutral and acidic pH.

Sulfidogenesis from S_8^0 at high T and low pH – an unexpected role for pyrite

As described in **chapter 2**, a process for sulfidogenesis at high temperature (80 °C) and acidic pH (<4.5) was developed, albeit in an unforeseen way. Instead of biological S_8^0 reduction by thermoacidophilic S_8^0-reducing microbial communities—which we aimed to enrich from samples from acidic, volcanic hot pools—a novel chemical process for sulfidogenesis was discovered. This involved the formation of micrometer-sized pyrite spheroids, which subsequently catalyzed the chemical reduction of S_8^0 by H_2. The reduction of S_8^0 required the presence of pyrite, likely because it functioned as electrocatalyst. Although it was initially hypothesized that the catalytic properties of the pyrite spheroids were related to their surface structure, and that this was governed by the physicochemical conditions in the incubations, this was disproven by the finding that commercially sourced, milled pyrite (< 50 μm) also catalyzed S_8^0 reduction. Although not microbial, this chemical process is of great interest both from a fundamental scientific perspective, and for potential technological applications, which will be discussed below.

Environmental implications of pyrite-catalyzed S_8^0 reduction with H_2

The temperature and pH at which chemical S_8^0 reduction by H_2 was observed in **chapter 2** resemble those found in certain Earth environments such as acidic hydrothermal vents and acidic geothermal pools. In addition, both types of environments can have inputs of H_2S and H_2 gas from e.g. volcanic sources, and contain significant deposits

of S_8^0 and nano- to microparticulate pyrite particles, as shown for hydrothermal plumes (Yücel et al., 2011; Gartman et al., 2014), and chimneys (Nakamura et al., 2010). Furthermore, as mentioned in **chapter 2**, the minerals in hydrothermal vent chimney walls were shown to have conductive properties, which was proposed to result from the presence of pyrite and pyrite-type minerals (Nakamura et al., 2010; Yamamoto et al., 2018). These studies focused on H_2 or S_8^0 oxidation coupled to O_2 reduction, and did not investigate the reaction described here, H_2 oxidation coupled to S_8^0 reduction. However, given the similarity of the geochemical conditions, and the observation in **chapter 2** that increased salinity did not significantly impact the timeframe within which S_8^0 is reduced (**chapter 2**, Supplementary Figure 12B), it can be expected that pyrite-catalyzed S_8^0 reduction with H_2 occurs in (deep-sea) hydrothermal environments. Subsequent studies are needed to investigate the effect of lower H_2 partial pressures on the process, more closely mimicking those found in natural environments (Truche and Bazarkina, 2019; Zgonnik, 2020). If pyrite-catalyzed S_8^0 reduction is indeed found to occur in natural environments, it would nuance the generally held assumption that sulfide production in moderate temperature environments is the result of dissimilatory microbial metabolism of sulfur compounds, which could have consequences for the interpretation of sulfur isotope data.

Do sulfidogenic microorganisms accelerate pyrite formation by creating favorable conditions for the polysulfide pathway?

As described in **chapter 2**, our results suggest that pyrite formation occurred through the polysulfide (Bunsen) pathway, and that this was related to the presence of S_8^0, enabling formation of polysulfides (equation 1). The shorter lag phase observed in incubations at pH 6 (chapter 2, Figure 3E, F), could further support this, as more neutral pH favored higher polysulfide concentrations.

$$\frac{n-1}{8}S_8^0 + HS^- \rightarrow S_n^{2-} + H^+ \qquad (1)$$

S_8^0 furthermore could have provided a nucleation site for pyrite crystallization, related in part to enhanced polysulfide concentrations at the S_8^0 surface as proposed previously (Graham and Ohmoto, 1994; Ohfuji and Rickard, 2005). Recent work proposed that increased S_n^{2-} concentrations at the surface of S_8^0 could occur when the nucleophilic attack of sulfide on S_8^0 rings takes place on the surface of S_8^0 particles, forming a polysulfide chain that is then released into solution (Kafantaris and Druschel, 2020).

Even though pyrite formation has been studied for decades (Roberts et al., 1969; Rickard, 1975, 1997; Schoonen and Barnes, 1991; Graham and Ohmoto, 1994; Wang

and Morse, 1996; Wilkin and Barnes, 1997; Gartman and Luther, 2013), intriguing questions remain regarding the factors determining whether the sulfide (equation 2) or polysulfide (equation 3) pathway is the preferred mechanism of pyrite formation under different conditions.

$$Fe^{2+} + 2H_2S \rightarrow FeS_2 + H_2 + 2H^+ \qquad (2)$$

$$Fe^{2+} + H_2S + \tfrac{1}{8}S_8^0 \rightarrow FeS_2 + 2H^+ \qquad (3)$$

For example, multiple studies showed that the rate and mechanism of pyrite formation are strongly influenced by the presence of SO_4^{2-}-reducing (Thiel et al., 2019; Berg et al., 2020; Duverger et al., 2020), S_8^0-reducing (Berg et al., 2020), and S_8^0-disproportionating (Canfield et al., 1998) microorganisms, but the exact mechanisms through which these microorganisms influence (accelerate) pyrite formation have not yet been elucidated. The abovementioned studies provide indications that the sulfidogenic microorganisms influence pyrite formation by increasing the availability of S_8^0 and consequently of polysulfides (as long as sulfide is available) enabling FeS_2 formation through the polysulfide pathway. For example, in a pure culture of *Desulfovibrio desulfuricans*, pyrite formed when ferric phosphate ($FePO_4$) was supplemented as Fe source, but not with $FeCl_2$ (Duverger et al., 2020). In the presence of sulfide, the Fe^{3+} from $FePO_4$ is reduced to Fe^{2+} according to (equation 4), resulting in the formation of S_8^0. Therefore, supplementation of Fe^{3+} to sulfidogenic incubations also implies the formation of polysulfides, if free sulfide remains available (equation 1).

$$2FePO_4 + HS^- + 3H^+ \rightarrow \tfrac{1}{8}S_8^0 + 2Fe^{2+} + 2H_2PO_4 \qquad (4)$$

This reaction could also have played a role in the formation of pyrite in a mixed culture of SRB and S_8^0-reducing bacteria enriched with $FePO_4$ and SO_4^{2-} as Fe- and S-source (Berg et al., 2020). In that study, pyrite formation was observed in the enrichment cultures after 3 weeks, while in a sterile control intermittently supplemented with sterile sulfide this was not observed after 3 weeks, but took up to two months. The presence of sulfidogenic microorganisms could have accelerated pyrite formation by increasing H_2S availability, and consequently S_8^0 formation through equation 2, increasing polysulfide availability (equation 1). The presence of S_8^0 in that study was further supported by the microbial community composition—although the SRB genus *Desulfovibrio* was the dominant community member according 16S rRNA gene amplicon sequencing (80 ± 0.3 %), the genus *Sulfurospirilllum* accounted for 6 ± 1.1 % of sequenced reads (Berg et al., 2020).

As also discussed in **chapter 3**, *Sulfurospirillum* species use S_8^0, thiosulfate ($S_2O_3^{2-}$) and sulfite (SO_3^{2-}) as electron acceptor, but not SO_4^{2-} (Wolfe and Pfennig, 1977; Schumacher et al., 1992; Finster et al., 1997), supporting the presence of S_8^0 in these incubations.

An increased importance of the polysulfide pathway over the sulfide pathway for pyrite formation in the presence of microorganisms was supported by the observation that S_8^0 was required for pyrite formation in incubations with the thermophilic S_8^0-reducing species *Thermococcus kodakarensis* (Gorlas et al., 2022). Although that study suggested a key role for intracellular S_8^0 vesicles produced by the *T. kodakarensis* cells (Gorlas et al., 2022), additional abiotic controls with higher amounts of Na_2S, more closely mimicking the conditions created by actively S_8^0-reducing microorganisms, were not performed. The abiotic controls performed in that study were supplemented with 0.05 wt% Na_2S (2 mM total sulfide) (Gorlas et al., 2022), which can be expected to have precipitated immediately as FeS, making H_2S unavailable for subsequent pyrite formation. Abiotic controls with excess of H_2S, would have helped to assess whether the S_8^0 vesicles indeed have a so far undefined beneficial property to induce pyrite formation, or whether pyrite formation in the microbial cultures is enabled by the higher H_2S concentrations, regardless of the form of S_8^0 in the medium (bulk or biologically produced vesicles).

Pyrite formation through the sulfide pathway was recently proposed to underpin a syntrophic community enriched using only FeS, H_2S and CO_2 as electron donors/acceptors, producing methane (CH_4) and pyrite (Thiel et al., 2019). The dominant taxa detected in the enriched microbial community were related to the hydrogenotrophic methanogen *Methanospirillum stamsii*, explaining methanogenesis, but also to the SO_4^{2-}-reducing *Desulfomicrobium baculatum*, and the SO_4^{2-}-reducing, and $S_2O_3^{2-}$- and SO_3^{2-}-disproportionating *Desulfovibrio sulfodismutans*, later reclassified as *Desulfolutivibrio sulfodismutans* comb. nov (Thiel et al., 2020). The enrichment cultures were not supplemented with a sulfur compound other than FeS, suggesting that these species were gaining energy through pyrite formation from FeS and H_2S, producing the H_2 that supported growth of *M. stamsii*. Interestingly, abiotic controls with FeS and H_2S showed no pyrite formation (Thiel et al., 2019), suggesting that pyrite formation through the sulfide pathway was inhibited in the absence of the enriched microorganisms mentioned above. However, as also discussed in that study, although pyrite formation and concomitant H_2 production through the sulfide pathway would agree with FeS and H_2S as sole substrates and the enrichment of methanogens using the H_2 as energy source, an alternative explanation involving the polysulfide pathway cannot be excluded. In that scenario, as detailed by the authors, H_2S would be converted to H_2 and S_8^0. The S_8^0 would enable subsequent polysulfide formation (equation 1), and pyrite formation through the polysulfide pathway (equation 3). The disproportionation of H_2S to S_8^0 and

H_2 is endergonic under biological standard conditions, but becomes thermodynamically feasible if H_2 and S_8^0 concentrations are kept below 10^{-4} atm and 1 mM, respectively (Thiel et al., 2019), which would be enabled by H_2 consumption for methanogenesis and S_8^0 consumption for pyrite formation.

Technological application of pyrite-catalyzed S_8^0 reduction with H_2

Although the initial aim of this project was to develop a process for microbial S_8^0 reduction at thermoacidophilic conditions, from a technological perspective, pyrite-catalyzed S_8^0 reduction as described in **chapter 2** has similar benefits. As with microbial S_8^0 reduction, this chemical process would enable on-site sulfidogenesis, at high temperature and acidic pH, and could be tailored to meet process demands by regulating the supply of H_2 and S_8^0. An important driver for developing a process for sulfidogenesis at hot, acidic conditions is the opportunity to combine sulfidogenesis and metal sulfide precipitation from hot, acidic metallurgy process waters in one reactor. For this purpose, it therefore needs to be investigated whether *in situ* pyrite formation and subsequent S_8^0 reduction (Figure 1A) is affected by the presence of the high amounts of dissolved metals such as Cu^{2+} and Zn^{2+} typical for such streams. As Cu^{2+} precipitates with sulfide at lower pH than Fe^{2+} (Lewis, 2010), this could for example limit the availability of H_2S for the formation of FeS_2, inhibiting the process. To circumvent this potential issue, externally sourced pyrite could be used (Figure 1B) instead of *in situ* formation of catalytic pyrite, as this was also shown to enable S_8^0 reduction. However, as with *in situ* FeS_2 formation, additional research is required to assess the effect of the presence of other dissolved metals on the process.

Alternatively, a process scheme could be considered where sulfidogenesis still occurs in a separate reactor (Figure 1C). As rates were higher at higher temperatures (80°C), this reactor would need to be heated. To mitigate the associated increased energy requirements, process heat from e.g. onsite metallurgy operations could be used. To assess the competitiveness of this configuration with the current technologies for biosulfidogenesis on the market, future research needs to address the upper limits of sulfide production rates that can be achieved, and how rates are affected by temperature and pH. Preliminary results obtained during the experimental part of this thesis indicated that a VSPR of 0.4 – 0.6 g $S^{2-} \cdot L^{-1} \cdot day^{-1}$ could be achieved in a H_2-fed batch reactor operated at 80°C and pH 4 (data not shown). This is 5 to 10 times higher than rates observed in a semi-batch bioreactor operated at 80 °C, pH 3.5 (Hidalgo-Ulloa et al., 2020). In the operation of that reactor no attempts were made to further optimize the VSPR, and higher rates could likely be reached

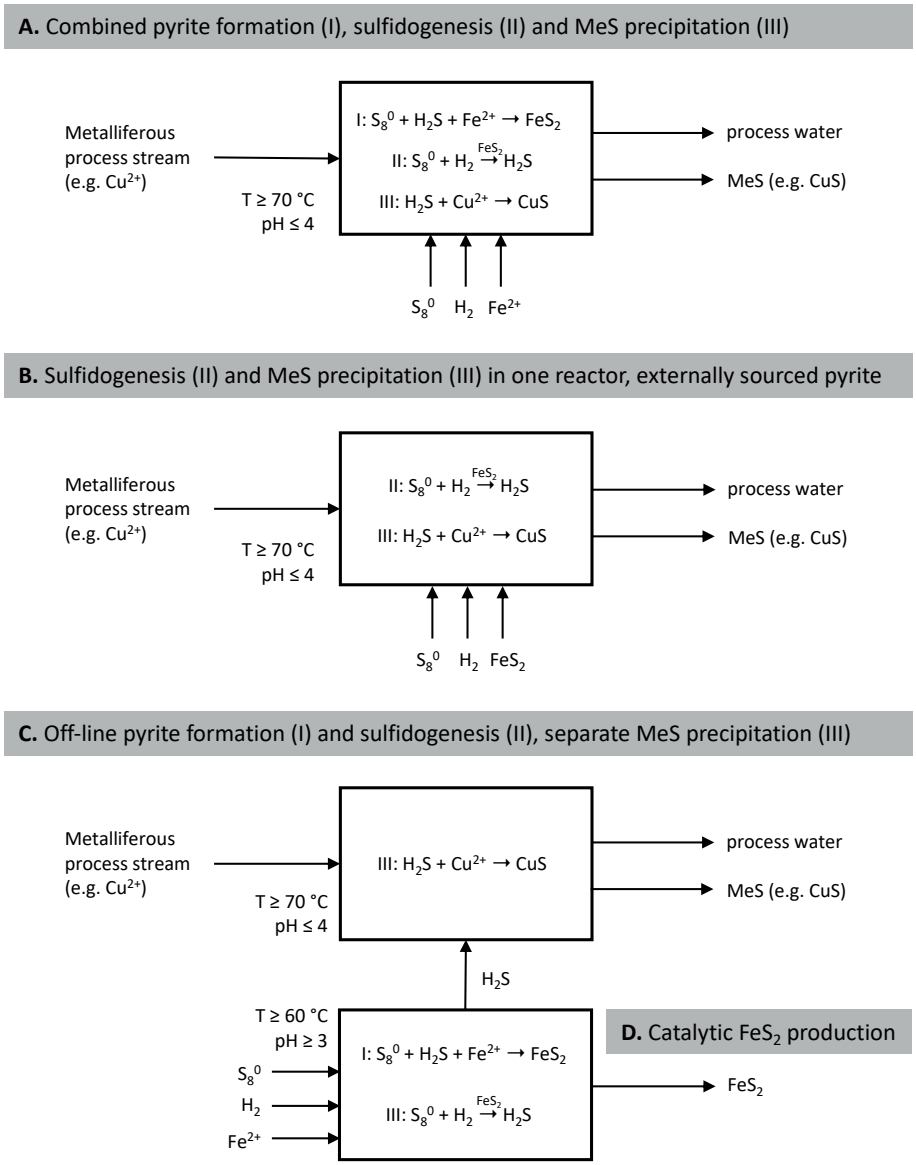

Figure 1: Proposed simplified process schemes for metal recovery from metalliferous process streams containing elevated Cu^{2+} concentrations using pyrite-catalyzed sulfidogenesis from H_2 and S_8^0. (A) Combined pyrite formation from Fe^{2+}, H_2S and S_8^0, sulfidogenesis from S_8^0 and H_2 and metal recovery as MeS in one unit, (B) externally sourced, milled pyrite is added, and sulfidogenesis from S_8^0 and H_2 and metal recovery as MeS occur in one unit, (C) pyrite formation from S_8^0, H_2S and Fe^{2+} and sulfidogenesis from S_8^0 and H_2 occur in a separate unit (off line), and H_2S is transported to the metal sulfide precipitation unit via a carrier gas, (D) production of catalytic pyrite crystals as final product.

If, as hypothesized in **chapter 2**, the electron acceptor reduced by H_2 via pyrite is not S_8^0, but polysulfide, and the low polysulfide concentrations at acidic pH are an important rate-limiting factor, higher rates could be achieved at more neutral pH. This is also in line with the higher rates observed at pH 6, as reported in **chapter 2**. In that case, separation of sulfidogenesis and metal sulfide precipitation would be beneficial, as the pH of the two steps does not have to overlap. It could even be argued that this chemical process is potentially more reliable and easier to operate than microbial S_8^0 reduction, especially at thermoacidophilic conditions. Only three main substrates are required (S_8^0, H_2, Fe^{2+}), as opposed to the range of substrates needed for microbial growth, and the start-up of the process is rapidly achieved by dosing H_2S, after which it is autocatalytic as long as sufficient H_2 and S_8^0 are supplied. The chemical nature of the process furthermore avoids the fluctuations in performance that can occur when using a microbial community as catalyst, or the need to pre-adapt the inoculum before seeding the bioreactor.

Technological application of pyrite as 'greener' electrocatalyst

Apart from the catalysis of S_8^0 reduction by H_2, the pyrite particles described in **chapter 2** have a broader potential range of application as more sustainable electrocatalysts. Renewable energy technologies such as photovoltaic cells and water electrolyzers for H_2 production rely on electrocatalysts for transformation of solar energy into electrical and chemical energy. Currently electrocatalysts consist almost exclusively of (rare) noble metals such as platinum (Pt) and palladium (Pd), and the scarcity of these elements means that they are not well suited for scaling up production of solar cells and electrolyzers to the levels needed to meet future energy demands (Faber and Jin, 2014). It is therefore crucial to develop catalysts from easily accessible, Earth-abundant elements. Promising alternatives are metal sulfides such as pyrite (FeS_2) and pyrite-type materials (CoS_2, NiS_2, MoS_2, CuS_2) (Faber et al., 2014; Heift, 2019). The catalytic performance of these metal sulfides is highly dependent on the crystal size, however. For example, bulk pyrite is considered a bad conductor, while nano- to micrometer-sized crystals are electrochemically active (Nakamura et al., 2010; Yamamoto et al., 2018). The crystal size can be controlled via the physicochemical conditions (temperature, pH, pressure) and reagents used during chemical synthesis, and current chemical synthesis methods for catalytic pyrite(-type) crystals typically use high temperatures and pressures, as well as additional (toxic) solvents and reactants (Faber et al., 2014; Khalid et al., 2018). The catalytic pyrite particles described in **chapter 2** were synthesized at milder temperatures (80°C) and pressure (<2 atm), without the use of additional solvents, providing a potentially more environmentally benign synthesis method. It

would therefore be important to investigate how the electroactive properties and catalytic performance of the crystals synthesized via this method compare to those obtained through other methods. If this comparison is favourable, one could envision a process scheme as shown in (Figure 1C), but where part of the FeS_2 synthesized in the separate reactor is harvested for application as electrocatalyst, providing a (significant) additional source of revenue (Figure 1D).

In light of its potential for application, a patent application was filed pertaining to the results described in **chapter 2**.

Biosulfidogenesis from S_8^0 at mesophilic conditions and neutral to acidic pH

In addition to the development of sulfidogenic processes at high temperature and acidic pH, biosulfidogenesis from S_8^0 at lower temperatures (30°C) at neutral and acidic pH was investigated. 16S rRNA gene amplicon sequencing studies of S_8^0-reducing bioreactors using organic carbon and energy sources such as glucose and acetate indicated a high relative abundance of fermentative taxa, such as *Paludibacter* and *Treponema* (Qiu et al., 2017; Guo et al., 2019; Sun et al., 2019). Even though certain fermentation products such as organic acids can be utilized as carbon source by S_8^0-reducing microorganisms which, as described in **chapter 3,** likely supported growth of the heterotrophic *Sulfurospirillum*, the partial redirection of organic substrates to microbial processes other than S_8^0 reduction lowers the C/S efficiency of the process. We therefore investigated the performance of an autotrophic S_8^0-reducing bioreactor. Our results could indicate that at neutral pH, higher volumetric sulfide production rates (VSPR) are enabled by heterotrophic S_8^0-reduction, as higher VSPR were observed when the heterotrophic genus *Sulfurospirillum* was dominant, likely supported by the production of acetic acid by *Acetobacterium*. However, these higher VSPR were obtained when the system was not yet in steady state, and this remains speculative. At low pH (3.8), S_8^0 reduction was likely autotrophic, performed by *Desulfurella*, and measured VSPR were comparable to the VSPR achieved in a heterotrophic reactor operated at pH 3.8 (Guo et al., 2021), indicating that the low pH was the main factor controlling the VSPR, and not the carbon source. here

In **chapter 3** it was observed that a decrease in pH from pH 6.9 to pH 3.9 lowered VSPR 2.5 times, from 1.79 ± 0.18 to 0.71 ± 0.07 g $S^{2-}{\cdot}L^{-1}{\cdot}day^{-1}$. Using total organic carbon content as a proxy for biomass concentrations in the reactor, the biomass specific sulfide production rates (SSPR) were calculated to be 38.9 and 22.0 g $S^{2-}{\cdot}g_X^{-1}{\cdot}day^{-1}$ at pH 6.9 and pH 3.9, respectively, indicating that SSPR also decreased at lower pH. However, biomass concentrations were only estimated indirectly. Direct cell counting could have supported conclusions based on TOC measurements. In addition, although inspection

of reactor contents during operation using light microscopy gave no clear indication of cell attachment to S_8^0 particles, it cannot be excluded that cells were lost with S_8^0 particles before TOC determination, affecting the final measured values. Loss of cells through attachment to S_8^0 could play a more important role at acidic pH than at neutral pH, if cells utilize (solid) S_8^0 directly (instead of soluble polysulfides) and accessed this substrate through direct attachment.

The decrease in VSPR upon a switch to acidic pH agrees with other studies of continuously operated S_8^0-reducing bioreactors at mesophilic temperatures (Sun et al., 2020b; Guo et al., 2021). For example, in a continuous bioreactor fed with synthetic wastewater with acetic acid and glucose, VSPR dropped from 1.34 ± 0.19 at pH 6.5 to 0.89 ± 0.19 g $S^{2-}{\cdot}L^{-1}{\cdot}day^{-1}$ at pH 3.8 (Guo et al., 2021). This could point to a more general trend of lower VSPR at lower pH, most likely related to decreased bioavailability of S_8^0 at acidic pH as described in the introduction (1.5), and not to limitations imposed by reactor configurations. Interestingly, the VSPR obtained at acidic pH in **chapter 3**, 0.71 ± 0.07 g $S^{2-}{\cdot}L^{-1}{\cdot}day^{-1}$ was higher than obtained in a S_8^0-reducing, H_2/CO_2-fed (semi-)batch bioreactor operated at 80 °C, pH 3.5: 0.06 – 0.08 mg $S^{2-}{\cdot}L^{-1}{\cdot}day^{-1}$ (Hidalgo-Ulloa et al., 2020). This was surprising, as it could be expected that higher operating temperatures would enable higher reaction rates (Amend and Shock, 2001) due to the dependence of the rate constant on temperature according to the Arrhenius equation (equation 5).

$$k = Ae^{\frac{Ea}{RT}} \qquad (5)$$

In this equation k is the rate constant, A is a reaction specific constant, E_a is the activation energy and R and T are the gas constant and temperature, respectively. However, in biological systems this temperature-dependence will only hold if the microorganisms carrying out a specific metabolism can rapidly adapt to higher temperatures. It is very well possible that the microbial community enriched in the thermophilic S_8^0-reducing reactor did not contain (hyper)thermophilic species, and instead mostly consisted of moderately thermophilic species that were growing close to their upper temperature limit. This is likely, given that the inoculum used to seed this reactor was obtained from Emmtec, a mesophilic industrial (sulfate-reducing) bioreactor. Research is needed to investigate whether higher rates of sulfide production can be achieved with (hyper)thermoacidophilic S_8^0-reducing species, either using pure cultures of known S_8^0 reducers such as *Acidianus ambivalens* (Zillig et al., 1986), or microbial communities enriched from natural hot, acidic environments as attempted in **chapter 2**.

Biosulfidogenesis in AMD at increased exposure to extreme conditions

The conditions encountered in AMD/ARD can be considered poly-extreme, as they are often a combination of extreme acidity, high metal concentrations, and high salinity (Nordstrom et al., 2015). While AMD sediments could provide protection to these extreme conditions through the formation of micro-environments, this is less likely to occur in the water column, and biosulfidogenic microorganisms thriving there are likely more poly-extremophilic than those described so far. This thesis therefore investigated biosulfidogenesis in the water column of two previously microbiologically unexplored acidic pit lakes (APL), Filón Centro (FC) and La Zarza (LZ), as sites potentially harboring more (poly-)extremophilic SRB (**chapter 4**).

In FC we observed a high relative abundance of reads assigned to *Desulfomonile* in the water column at pH 4.3. Sequences assigned to this genus were previously detected in the Brunita (Sánchez-España et al., 2020) and Cueva de la Mora pit lakes (Falagán et al., 2014; Ayala-Muñoz et al., 2020), as well as in sulfidogenic bioreactors treating AMD (Sánchez-Andrea et al., 2012c). However, so far no acidotolerant or acidophilic *Desulfomonile* species have been described or even isolated (to the best of our knowledge). Because microorganisms growing at pH 4.3 are not considered (extreme) acidophiles, the *Desulfomonile* taxa detected in FC are not necessarily more acidophilic than the SRB isolated to date. However, its high abundance (18 % of total reads) in the chemocline of the APL Cueva de la Mora at pH 3.95 (Falagán et al., 2014; Ayala-Muñoz et al., 2020), suggests it could tolerate increasing acidity. In addition, it was detected in high abundance (12.3 %) in the monimolimnion of Brunita pit lake, one of the most extreme pit lakes in terms of salinity and dissolved metal concentrations (Fe^{2+}, Zn^{2+}, Mn^{2+}). The *Desulfomonile* species detected in these APL could be more tolerant to the poly-extreme conditions of AMD due to the greater exposure to the high metal concentrations, acidity, and salinity in the water column than in sediments. This makes them interesting candidates for application in bioreactors for acidophilic biosulfidogenesis with elevated metal concentrations.

From 16S to '-omics'

In **chapter 4,** 16S rRNA gene amplicon sequencing is used to explore the microbial community composition along the water column of two APL. Although this technology

has drastically increased our knowledge of the extent of microbial diversity (Yarza et al., 2014), it has several limitations. Only information on the taxonomic diversity of the microbial community is obtained, and the use of PCR amplification imposes an inherent bias on the detected diversity. Although extensive efforts are made to design 16S rRNA gene primers that cover as much of the tree of life as possible (Thompson et al., 2017), they do not cover all diversity (Tahon et al., 2021).

For taxa assigned to the genus level, potentially active metabolic pathways can be suggested based on the physiological traits shared by all isolated representative species from that genus, as done for example for *Desulfomonile* (DeWeerd et al., 1990; Tiedje et al., 2015). However, this is limited by the small percentage of microorganisms with cultured representatives (Hug et al., 2016). Even though isolation and cultivation are required to confirm a species' physiological capabilities, this is notoriously difficult and likely requires modifications of existing cultivation methods and development of novel innovative techniques (Lewis et al., 2021). Independent of cultivation, metagenomics can provide a more detailed picture of the genetic potential in a microbial community, which can be partly verified by combining it with metatranscriptomics in order to identify actively transcribed genes. For example, metagenomics assembled genomes (MAGs) obtained from an AMD site in the USA indicated the importance of previously unrecognized taxa in the cycling of iron (Grettenberger and Hamilton, 2021), and combined metagenomics and metatranscriptomics studies were used to investigate active metal resistance strategies employed by microorganisms in the water column of the APL Cueva de la Mora (IPB) (Ayala-Muñoz et al., 2020).

In a broader context, metagenomics approaches were used to investigate the extent to which dissimilatory sulfate reduction might be carried out by so far uncultivated microorganisms, indicating that this capacity is more widespread among the tree of life than previously thought (Anantharaman et al., 2018). Combined metagenomics and metatranscriptomics of moderately acidic peatland mesocosms furthermore indicated that putative genera from the *Acidobacteria* phylum play an important role in dissimilatory sulfur metabolism in acidic environments (Hausmann et al., 2018). *Acidobacteria* are also found in AMD environments, as shown for example in sediments from Tinto river (Sánchez-Andrea et al., 2011). *Acidobacteria* were also detected in the monimolimnion of both FC and LZ (**chapter 4**), which could suggest that the associated microorganisms contributed to biosulfidogenesis. It is therefore of great interest to perform combined metagenomics and metatranscriptomics studies of the APL described in this thesis, focusing specifically on dissimilatory sulfur metabolism, similar to the studies of other APL described above (Ayala-Muñoz et al., 2020; Grettenberger and Hamilton, 2021).

Establishment of biosulfidogenesis in AMD: does S_8^0 reduction precede SO_4^{2-} reduction?

Although the remediating effect of biosulfidogenesis, especially by SRB, on the acidity and metal concentrations in AMD environments is well-recognized (Sánchez-Andrea et al., 2014a; Johnson and Sánchez-Andrea, 2019), it remains to be elucidated whether SRB are active from the onset of alkalinization, or whether their establishment is preceded by other (H^+-consuming) (bio)geochemical processes. In environments with abundant carbonate minerals, chemical alkalinization can occur rapidly due to carbonate dissolution, as occurred for example in the Brunita pit lake in SW Spain (Sánchez-España et al., 2020). However, carbonate minerals are scarce in the IPB (Sánchez-España et al., 2013), and this plays little to no role in initial alkalinization of APL there.

In **chapter 4** we proposed that the two APL LZ and FC are examples of 'young' (LZ, flooding since the 1990's) and 'mature' (FC, flooding since the 1960's) APLs undergoing bioremediation through biosulfidogenesis. In the younger LZ, biosulfidogenesis in the monimolimnion (pH 2.6 – 3.0) was attributed to *Acidianus*, *Desulfocapsa* and *Thermoplasma*, taxa known for S_8^0 reduction and/or S_8^0 disproportionation, while in the monimolimnion of the more mature FC, where the pH had increased to 4.5 and all dissolved Cu had been removed from the water column, the putative SRB *Desulfomonile* dominated the microbial community. This could suggest pH as a main factor for the establishment of SRB, which was also proposed as one of the explanations for the absence of SRB in the APL Peña de Hierro (IPB), with and even lower pH than in LZ, 2.4 in the mixolimnion and 2.1 in the monimolimnion (Grettenberger et al., 2020).

Based on these results we hypothesized that at the onset of natural remediation mediated by biosulfidogenesis, S_8^0, and not SO_4^{2-}, is the dominant electron acceptor. If this is the case, it remains to be clarified which processes contribute to initial pH alkalinization. Although biosulfidogenesis from S_8^0 mediates metal removal through H_2S production, it is not H^+-consuming. A possible microbial metabolism contributing to initial pH increase could be the reduction of ferric iron (Fe^{3+}) (Diez-Ercilla et al., 2014, 2019) in the form of ferric hydroxides such as goethite (α-FeO(OH)) (equation 6) or ferrihydrite ($Fe(OH)_3$) (equation 7), both proton consuming.

$$FeOOH + \frac{1}{2}H_2 + 2H^+ \rightarrow 2H_2O + Fe^{2+} \qquad (6)$$

$$Fe(OH)_3 + \frac{1}{2}H_2 + 2H^+ \rightarrow 3H_2O + Fe^{2+} \qquad (7)$$

In the monimolimnion of LZ this might be catalyzed by *Acidibacillus*, detected at both 30 m and 70 m and capable of ferric iron reduction with e.g. organic carbon compounds as electron donor (Holanda et al., 2016). To gain a better understanding of the sequence of (bio)geochemical processes involved in the establishment of biosulfidogenesis and the transition from S_8^0 reduction to SO_4^{2-} reduction, as hypothesized in **chapter 4**, this process could be mimicked in Winogradsky-type incubation columns, as also used in e.g. (Diez-Ercilla et al., 2019), enabling the close monitoring of geochemical and microbiological developments at different stages.

Acetotrophic sulfate reduction at low pH

In **chapter 5** a novel species of SRB from a novel genus was described, *Acidisedisulfobacillus acetoxydans*. Although its optimum pH of growth (5.0) still classifies it as moderately acidophilic, not being able to grow at pH 7, its ability to oxidize organic acids, especially acetic acid, completely to CO_2 distinguishes it from the other moderately acidophilic SRB isolated to date. Complete oxidation of acetic acid was so far only reported in low amounts for *Desulfosporosinus metallidurans* (Panova et al., 2021), and we hypothesize that for *A. acetoxydans* this ability is an important acid stress resistance mechanism, as it reduces acetic acid concentrations, and provides a strategy for increased access to organic carbon compounds as energy sources. AMD environments are commonly oligotrophic, with primary production limited largely by low phosphate concentrations (Falagán et al., 2014; Johnson and Aguilera, 2015) due to its precipitation as ferric phosphate, and coprecipitation with other ferric minerals. Algae are an important main source of organic carbon through excretion of exudates (Ňancucheo and Johnson, 2012a), and production of lysates from decaying biomass. These can then be degraded by fermenters, resulting in fermentation products such as acetic acid (Méndez-García et al., 2015) which can serve as energy source for complete oxidizers.

The sequential degradation of organic carbon was used to develop a co-culture carrying out the complete oxidation of glycerol coupled to S_8^0 reduction by the fermenter *Lucifera butyrica* and the acetic acid-oxidizing, S_8^0-reducing *Desulfurella amilsii* (Sánchez-Andrea et al., 2018), both isolated from the Tinto river. Because glycerol is a relatively cheap electron donor, its utilization for biosulfidogenesis is interesting for application in metal recovery processes. *A. acetoxydans* can completely oxidize glycerol, avoiding the need for such a co-culture. However, it would be an interesting candidate for designing a co- or mixed culture where more complex substrates are fermented to intermediate fermentation products by one or several acidophilic species, which are subsequently oxidized to CO_2 coupled to SO_4^{2-} reduction by *A.*

acetoxydans. This avoids the accumulation of acetic acid in bioreactors operated with SRB in other studies (Ňancucheo and Johnson, 2012b; Hedrich and Johnson, 2014; Santos and Johnson, 2018), improving the carbon efficiency of sulfate reduction.

(Bio)sulfidogenesis in the context of increasing metal demands

The transition from fossil fuels to renewable energy sources such as solar and wind implies an increased reliance on the metals and minerals needed to build the technologies for harvesting these forms of energy (The World Bank Group, 2020). For example, photovoltaic cells for harvesting solar energy require large amounts of aluminum, copper and silicon, as well as rare earth elements (REE); conversion of wind to electrical energy requires REEs for the magnets driving wind turbines, as well as other metals such as copper, nickel, manganese, chromium and molybdenum; electrolysis of water to produce hydrogen (H_2) as a fuel relies on electro- or photocatalysts, which currently require noble metals such as platinum; and electric vehicles driven by lithium-ion batteries require copper, aluminum, lithium, nickel, cobalt, manganese and graphite, as well as REEs for the magnets driving the electromotors (European Commission, 2020; The World Bank Group, 2020; International Energy Agency (IEA), 2021). Projected scenarios by institutes like the International Energy Agency (IEA) and the World Bank should be interpreted with care because they rely on assumptions about technological developments (e.g. the dominant battery chemistry that will be adopted) and the specifics and implementation of climate policies. Still, it is clear that metal and mineral demands will strongly increase (The World Bank Group, 2020; International Energy Agency (IEA), 2021), and with it the requirement for mining to ensure sufficient supply.

Increased mining activities, combined with the decreasing ore grade of reserves that are being mined (Calvo et al., 2016), can be expected to result in increasing volumetric production of solid and liquid wastes such as AMD and tailings from mineral processing (Lottermoser, 2010; Hudson-Edwards et al., 2011), with the associated environmental and social issues (Franks et al., 2021). Published data on mineral resources and reserves do not represent the absolute availability of minerals in

the crust but merely the publicly reported amount that is deemed to be of economic interest, and we are not expected to 'run out of' metals in a geological sense in the near future (Jowitt et al., 2020). Rather, the main problems with securing sufficient supply will likely be associated with environmental, social, and governance (ESG) factors, as shown for example for undeveloped copper ores (Valenta et al., 2019). It is therefore of paramount importance to design new mining projects in such a way that these impacts are minimized as much as possible (Pell et al., 2021). Minimization and improved treatment of waste streams is an integral part of this. Although newer approaches, such as deep *in situ* mining combined with bioleaching should result in less solid and liquid waste (Johnson, 2015; Levett et al., 2021), solid and liquid mine waste will remain a major issue. The increased focus on these aspects, combined with increasing demand for metals such as Cu, Co and Zn can be expected to result in an increased interest from the mining and metals sector in (bio)sulfidogenesis for metal recovery, which is a proven technology (Huisman et al., 2006; Adams et al., 2008). In addition, it could be expected that historic mine wastes, such as the APL discussed in this thesis, will in the future increasingly be considered as secondary mines instead of merely wastes, for which (bio)sulfidogenesis can be an attractive technology.

Conclusions

The results presented in this thesis contribute to the development of (bio)sulfidogenesis for metal recovery at more acidic pH and higher temperatures than those currently used in industry. The function of pyrite as catalyst for reduction of S_8^0 by H_2 to H_2S has not been described previously and expands both our fundamental understanding of the (abiotic) sulfur cycle in the environment, and the operating parameters at which sulfidogenesis can be applied for metal recovery and recycling. Future work should address the rate-limiting factors controlling pyrite formation and sulfidogenesis, in order to optimize process design for achieving maximum H_2S production rates. (Bio) sulfidogenesis for metal recovery should be adopted by the metal & mining sector on a larger scale, as it contributes to waste reduction as well as increased metal recovery. For biosulfidogenesis from S_8^0, the bioavailability of S_8^0 at acidic pH likely is a limiting factor. The mechanism(s) enabling use of S_8^0 as electron acceptor at acidic pH remains an important question in the study of acidophilic S_8^0-reducing microorganisms, and requires further investigation.

In AMD-impacted environments showing natural attenuation of extreme conditions due to biosulfidogenesis, it remains to be determined which (microbial) processes

are responsible for the initial alkalinization. Our study of two APL indicate that biosulfidogenesis initially originates from S_8^0 reduction and disproportionation, contributing to metal precipitation but not alkalinization. The water column of APL, where microorganisms are more exposed the poly-extreme conditions of AMD, likely harbor novel species of more acidophilic SRB, as shown by the abundance of *Desulfomonile*, a putative SRB for which no acidophilic species have been isolated yet. Our in-depth study of the physiology and acid stress resistance mechanisms of a novel species of moderately acidophilic SRB from the novel genus *Acididesulfobacillus*, *A. acetoxydans*, indicate that this species adapts to grow at low pH (3.8) by modifying its membrane lipid composition and detoxifying its environment by complete oxidation of organic acids.

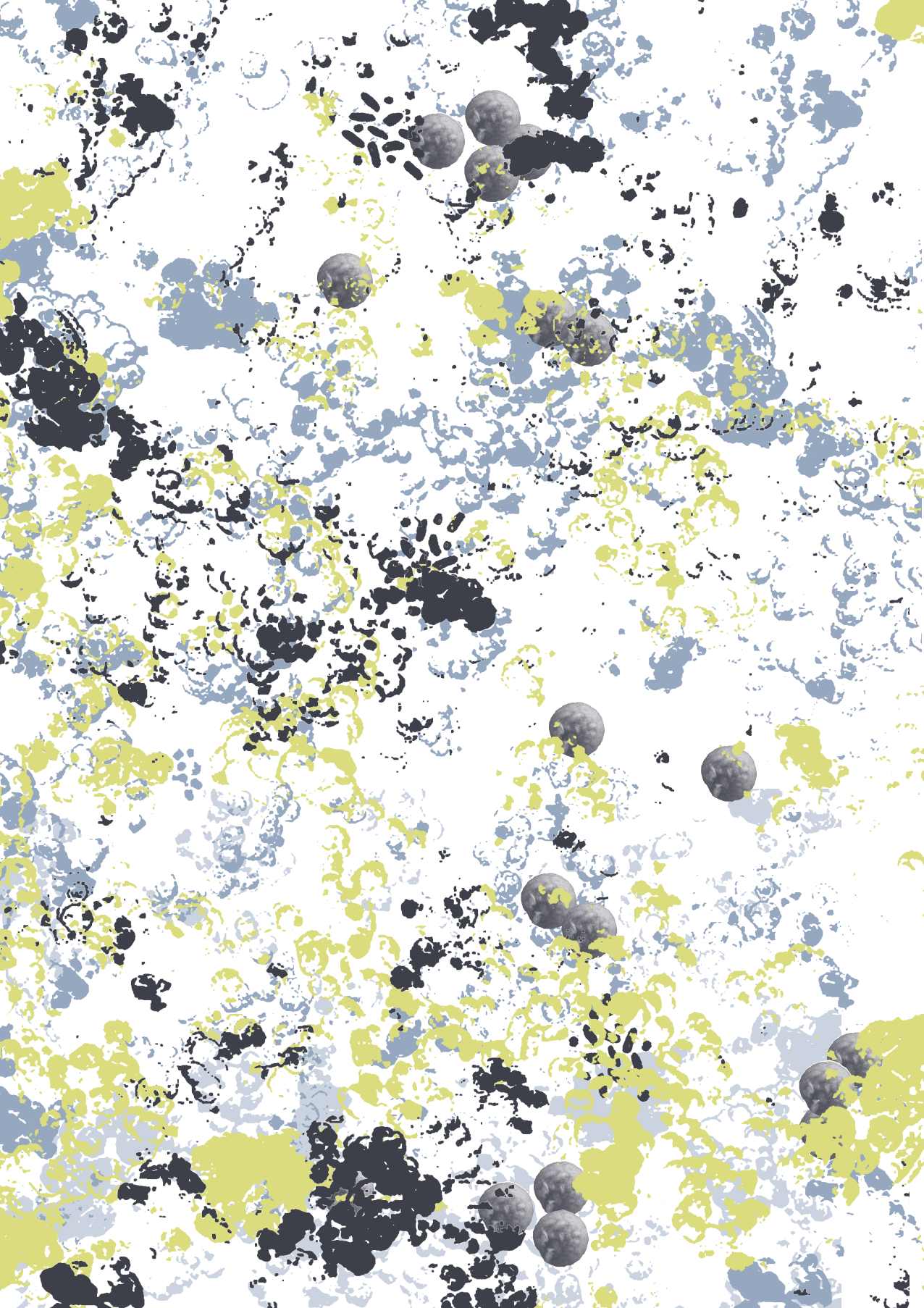

References

Abbott, B. J., and Clamen, A. (1973). The relationship of substrate, growth rate, and maintenance coefficient to single cell protein production. *Biotechnol. Bioeng.* 15, 117–127. doi:10.1002/bit.260150109.

Adams, M. E., and Postgate, J. R. (1959). A New Sulphate-Reducing Vibrio. *J. Gen. Microbiol.* 20, 252–257. doi:10.1099/00221287-20-2-252.

Adams, M., Lawrence, R., and Bratty, M. (2008). Biogenic sulphide for cyanide recycle and copper recovery in gold-copper ore processing. *Miner. Eng.* 21, 509–517. doi:10.1016/j.mineng.2008.02.001.

Akob, D. M., Hallenbeck, M., Beulig, F., Fabisch, M., Küsel, K., Keffer, J. L., et al. (2020). Mixotrophic Iron-Oxidizing *Thiomonas* Isolates from an Acid Mine Drainage-Affected Creek. *Appl. Environ. Microbiol.* 86. doi:10.1128/AEM.01424-20.

Alazard, D., Joseph, M., Battaglia-Brunet, F., Cayol, J. L., and Ollivier, B. (2010). *Desulfosporosinus acidiphilus* sp. nov.: a moderately acidophilic sulfate-reducing bacterium isolated from acid mining drainage sediments. *Extremophiles* 14, 305–312. doi:10.1007/s00792-010-0309-4.

Allison, J. D., Brown, D. S., and Novo-Gradac, K. J. (1991). MINTEQA2/PRODEFA2, a geochemical assessment model for environmental systems. Environmental Research Laboratory, Office of Research and Development, U.S. Environmental Protection Agency.

Altschul, S. F., Gish, W., Miller, W., Myers, E. W., and Lipman, D. J. (1990). Basic Local Alignment Search Tool. *J Mol Biol* 215, 403–410. doi:10.1016/S0022-2836(05)80360-2.

Amenabar, M. J., and Boyd, E. S. (2018). Mechanisms of mineral substrate acquisition in a thermoacidophile. *Appl. Environ. Microbiol.* 84, 1–18. doi:10.1128/AEM.00334-18.

Amenabar, M. J., and Boyd, E. S. (2019). A review of the mechanisms of mineral-based metabolism in early Earth analog rock-hosted hydrothermal ecosystems. *World J. Microbiol. Biotechnol.* 0, 0. doi:10.1007/s11274-019-2604-2.

Amend, J. P., and Shock, E. L. (2001). Energetics of overall metabolic reaction of thermophilic and hyperthermophylic Archaea and Bacteria. *FEMS Microb. Revs.* 25, 175–243.

Amils, R., Fernández-Remolar, D., and IPBSL Team (2014). Río Tinto: a geochemical and mineralogical terrestrial analogue of Mars. *Life* 4, 511–534. doi:10.3390/life4030511.

Amils, R., González-Toril, E., Aguilera, A., Rodríguez, N., Fernández-Remolar, D., Gómez, F., et al. (2011). From Río Tinto to Mars: the terrestrial and extraterrestrial ecology of acidophiles. *Adv. Appl. Microbiol.* 77, 41–70. doi:10.1016/B978-0-12-387044-5.00002-9.

Anantharaman, K., Hausmann, B., Jungbluth, S. P., Kantor, R. S., Lavy, A., Warren, L. A., et al. (2018). Expanded diversity of microbial groups that shape the dissimilatory sulfur cycle. *ISME J.* doi:10.1038/s41396-018-0078-0.

Ashburner, M., Ball, C. A., Blake, J. A., Botstein, D., Butler, H., Cherry, J. M., et al. (2000). Gene Ontology: tool for the unification of biology. *Nat. Genet.* 25, 25–29. doi:10.1038/75556.

Ashiuchi, M., and Misono, H. (2002). Biochemistry and molecular genetics of poly-γ-glutamate synthesis. *Appl. Microbiol. Biotechnol.* 59, 9–14. doi:10.1007/s00253-002-0984-x.

Auld, R. R., Myre, M., Mykytczuk, N. C. S., Leduc, L. G., and Merritt, T. J. S. (2013). Characterization of the microbial acid mine drainage microbial community using culturing and direct sequencing techniques. *J. Microbiol. Methods* 93, 108–115. doi:10.1016/j.mimet.2013.01.023.

Aussignargues, C., Giuliani, M.-C., Infossi, P., Lojou, E., Guiral, M., Giudici-Orticoni, M.-T., et al. (2012). Rhodanese Functions as Sulfur Supplier for Key Enzymes in Sulfur Energy Metabolism. *J. Biol. Chem.* 287, 19936–19948. doi:10.1074/jbc.M111.324863.

Avetisyan, K., Buchshtav, T., and Kamyshny, A. (2019). Kinetics and mechanism of polysulfides formation by a reaction between hydrogen sulfide and orthorhombic cyclooctasulfur. *Geochim. Cosmochim. Acta* 247, 96–105. doi:10.1016/j.gca.2018.12.030.

Ayala-Muñoz, D., Burgos, W. D., Sánchez-España, J., Couradeau, E., Falagán, C., and Macalady, J. L. (2020). Metagenomic and metatranscriptomic study of microbial metal resistance in an acidic pit lake. *Microorganisms* 8, 1–271350. doi:10.3390/microorganisms8091350.

Baker-Austin, C., and Dopson, M. (2007). Life in acid: pH homeostasis in acidophiles. *Trends Microbiol.* 15, 165–171. doi:10.1016/j.tim.2007.02.005.

Balch, W. E., Schoberth, S., Tanner, R. S., and Wolfe, R. S. (1977). *Acetobacterium*, a new genus of hydrogen-oxidizing, carbon dioxide-reducing, anaerobic bacteria. *Int. J. Syst. Bacteriol.* 27, 355–361. doi:10.1099/00207713-27-4-355.

Bale, N. J., Hopmans, E. C., Schoon, P. L., de Kluijver, A., Downing, J. A., Middelburg, J. J., et al. (2016). Impact of trophic state on the distribution of intact polar lipids in surface waters of lakes. *Limnol. Oceanogr.* 61, 1065–1077. doi:10.1002/lno.10274.

Bale, N. J., Sorokin, D. Y., Hopmans, E. C., Koenen, M., Irene Rijpstra, W. C., Villanueva, L., et al. (2019). New insights into the polar lipid composition of extremely halo(alkali) philic euryarchaea from hypersaline lakes. *Front. Microbiol.* 10, 1–24. doi:10.3389/fmicb.2019.00377.

Batty, J. D., and Rorke, G. V. (2006). Development and commercial demonstration of the BioCOP™ thermophile process. *Hydrometallurgy* 83, 83–89. doi:10.1016/j.hydromet.2006.03.049.

Belkin, S., Wirsen, C. O., and Jannasch, H. W. (1985). Biological and Abiological Sulfur Reduction at High Temperatures. *Appl. Environ. Microbiol.* 49, 1057–1061. doi:10.1128/aem.49.5.1057-1061.1985.

Benthaus, F. C., Totsche, O., and Luckner, L. (2020). In-lake Neutralization of East German Lignite Pit Lakes: Technical History and New Approaches from LMBV. *Mine Water Environ.* 39, 603–617. doi:10.1007/s10230-020-00707-5.

Berg, J. S., Duverger, A., Cordier, L., Christel, L., Guyot, F., and Miot, J. (2020). Rapid pyritization in the presence of a sulfur/sulfate-reducing bacterial consortium. 1–13. doi:10.1038/s41598-020-64990-6.

Berner, R. A. (1969). The synthesis of framboidal pyrite. *Econ. Geol.* 64, 383–384. doi:10.2113/gsecongeo.64.4.383.

Berner, R. A. (1984). Sedimentary pyrite formation: An update. *Geochim. Cosmochim. Acta* 48, 605–615. doi:10.1016/0016-7037(84)90089-9.

Biebl, H., and Pfennig, N. (1977). Growth of sulfate-reducing bacteria with sulfur as electron acceptor. *Arch. Microbiol.* 112, 115–117. doi:10.1007/BF00446664.

Blanchette, M. L., and Lund, M. A. (2016). Pit lakes are a global legacy of mining: an integrated approach to achieving sustainable ecosystems and value for communities. *Curr. Opin. Environ. Sustain.* 23, 28–34. doi:10.1016/j.cosust.2016.11.012.

Bland, C., Ramsey, T. L., Sabree, F., Lowe, M., Brown, K., Kyrpides, N. C., et al. (2007). CRISPR Recognition Tool (CRT): a tool for automatic detection of clustered regularly interspaced palindromic repeats. *BMC Bioinformatics* 8, 209. doi:10.1186/1471-2105-8-209.

Bonch-Osmolovskaya, E. A., Sokolova, T. G., Kostrikina, N. A., and Zavarzin, G. A. (1990). *Desulfurella acetivorans* gen. nov. and sp. nov. —a new thermophilic sulfur-reducing eubacterium. *Arch. Microbiol.* 153, 151–155. doi:10.1007/BF00247813.

Bond, P. L., Druschel, G. K., and Banfield, J. F. (2000a). Comparison of acid mine drainage microbial communities in physically and geochemically distinct ecosystems. *Appl. Environ. Microbiol.* 66, 4962–4971.

Bond, P. L., Smriga, S. P., and Banfield, J. F. (2000b). Phylogeny of microorganisms populating a thick, subaerial, predominantly lithotrophic biofilm at an extreme acid mine drainage site. *Appl. Environ. Microbiol.* 66, 3842–3849. doi:10.1128/AEM.66.9.3842-3849.2000.

Boyd, E. S., and Druschel, G. K. (2013). Involvement of intermediate sulfur species in biological reduction of elemental sulfur under acidic, hydrothermal conditions. *Appl. Environ. Microbiol.* 79, 2061–2068. doi:10.1128/AEM.03160-12.

Boyd, E. S., Jackson, R. A., Encarnacion, G., Zahn, J. A., Beard, T., Leavitt, W. D., et al. (2007). Isolation, characterization, and ecology of sulfur-respiring Crenarchaea inhabiting acid-sulfate-chloride-containing geothermal springs in Yellowstone National Park. *Appl. Environ. Microbiol.* 73, 6669–6677. doi:10.1128/AEM.01321-07.

Brandsma, J., Hopmans, E. C., Brussaard, C. P. D., Witte, H. J., Schouten, S., and Damsté, J. S. S. (2012). Spatial distribution of intact polar lipids in North Sea surface waters: Relationship with environmental conditions and microbial community composition. *Limnol. Oceanogr.* 57, 959–973. doi:10.4319/lo.2012.57.4.0959.

Bräuer, S. L., Cadillo-Quiroz, H., Ward, R. J., Yavitt, J. B., and Zinder, S. H. (2011). *Methanoregula boonei* gen. nov., sp. nov., an acidiphilic methanogen isolated from an acidic peat bog. *Int. J. Syst. Evol. Microbiol.* 61, 45–52. doi:10.1099/ijs.0.021782-0.

Burggraf, S., Jannasch, H. W., Nicolaus, B., and Stetter, K. O. (1990). *Archaeoglobus profundus* sp. nov., Represents a New Species within the Sulfate-reducing Archaebacteria. *Syst. Appl. Microbiol.* 13, 24–28. doi:10.1016/S0723-2020(11)80176-1.

Butler, I. B., Böttcher, M. E., Rickard, D., and Oldroyd, A. (2004). Sulfur isotope partitioning during experimental formation of pyrite via the polysulfide and hydrogen sulfide pathways: Implications for the interpretation of sedimentary and hydrothermal pyrite isotope records. *Earth Planet. Sci. Lett.* 228, 495–509. doi:10.1016/j.epsl.2004.10.005.

Calvo, G., Mudd, G., Valero, A., and Valero, A. (2016). Decreasing ore grades in global metallic mining: A theoretical issue or a global reality? *Resources* 5. doi:10.3390/resources5040036.

Campbell, L. L., and Postgate, J. R. (1965). Classification of the spore-forming sulfate-reducing bacteria. *Microbiol. Mol. Biol. Rev. 29*, 359–362. doi:10.1128/br.29.3.359-363.1965.

Canfield, D. E. (2004). The evolution of the Earth surface sulfur reservoir. *Am. J. Sci.* 304, 839–861. doi:10.2475/ajs.304.10.839.

Canfield, D. E., and Farquhar, J. (2012). "The Global Sulfur Cycle," in *Fundamentals of Geobiology* (Chichester, UK: John Wiley & Sons, Ltd), 49–64. doi:10.1002/9781118280874.ch5.

Canfield, D. E., and Raiswell, R. (1999). The evolution of the sulfur cycle. *Am. J. Sci. 299*, 697–723. doi:10.2475/ajs.299.7-9.697.

Canfield, D. E., Thamdrup, B., and Fleischer, S. (1998). Isotope fractionation and sulfur metabolism by pure and enrichment cultures of elemental sulfur-disproportionating bacteria. *Limnol. Oceanogr.* 43, 253–264. doi:10.4319/lo.1998.43.2.0253.

Cardenas, E., Wu, W. M., Leigh, M. B., Carley, J., Carroll, S., Gentry, T., et al. (2008). Microbial communities in contaminated sediments, associated with bioremediation of uranium to submicromolar levels. *Appl. Environ. Microbiol.* 74, 3718–3729. doi:10.1128/AEM.02308-07.

Cárdenas, J. P., Moya, F., Covarrubias, P., Shmaryahu, A., Levicán, G., Holmes, D. S., et al. (2012). Comparative genomics of the oxidative stress response in bioleaching microorganisms. *Hydrometallurgy* 127–128, 162–167. doi:10.1016/j.hydromet.2012.07.014.

Castanie-Cornet, M.-P., Penfound, T. A., Smith, D., Elliott, J. F., and Foster, J. W. (1999). Control of Acid Resistance in *Escherichia coli*. *J. Bacteriol.* 181, 3525–3535. doi:10.1128/JB.181.11.3525-3535.1999.

Castro, J. M., and Moore, J. N. (2000). Pit lakes: Their characteristics and the potential for their remediation. *Environ. Geol.* 39, 1254–1260. doi:10.1007/s002549900100.

Checa Espinosa, M., Carrasco Martiañez, I., and Muñoz López-Astilleros, A., Gómez Delgado, B. (2000). Minería y actualidad en la Faja Pirítica Ibérica. *Bocamina* 5, 62–92.

Chernyh, N. A., Neukirchen, S., Frolov, E. N., Sousa, F. L., Miroshnichenko, M. L., Merkel, A. Y., et al. (2020). Dissimilatory sulfate reduction in the archaeon 'Candidatus Vulcanisaeta moutnovskia' sheds light on the evolution of sulfur metabolism. *Nat. Microbiol.* 5, 1428–1438. doi:10.1038/s41564-020-0776-z.

Christel, S., Herold, M., Bellenberg, S., El Hajjami, M., Buetti-Dinh, A., Pivkin, I. V., et al. (2017). Multi-omics reveals the lifestyle of the acidophilic, mineral-oxidizing model species *Leptospirillum ferriphilum*. *Appl. Environ. Microbiol.* 84, e02091-17. doi:10.1128/AEM.02091-17.

Christensen, B., Laake, M., and Lien, T. (1996). Treatment of acid mine water by sulfate-reducing bacteria; results from a bench scale experiment. *Water Res.* 30, 1617–1624.

Church, C. D., Wilkin, R. T., Alpers, C. N., Rye, R. O., and Blaine, R. B. (2007). Microbial sulfate reduction and metal attenuation in pH 4 acid mine water. *Geochem. Trans.* 8, 1–14. doi:10.1186/1467-4866-8-10.

Claudel-Renard, C., Chevalet, C., Faraut, T., and Khan, D. (2003). Enzyme-specific profiles for genome annotation - PRIAM. *Nucleic Acids Reseach* 31, 6633–6639. doi:10.1093/nar/gkg847.

Cline, J. (1969). Spectrophotometric Determination of Hydrogen Sulfide in Natural Waters. *Limnol. Oceanogr.* 14, 454–458. doi:10.4319/lo.1969.14.3.0454.

Colman, D. R., Lindsay, M. R., Amenabar, M. J., and Boyd, E. S. (2019). The Intersection of Geology, Geochemistry, and Microbiology in Continental Hydrothermal Systems. *Astrobiology* 19, 1–18. doi:10.1089/ast.2018.2016.

Core Team, R. (2021). R: A lanuguage and environment for statistical computing.

Costa, C., Teixeira, M., LeGall, J., Moura, J. J. G., and Moura, I. (1997). Formate dehydrogenase from *Desulfovibrio desulfuricans* ATCC 27774: Isolation and spectroscopic characterization of the active sites (heme, iron- sulfur centers and molybdenum). *J. Biol. Inorg. Chem.* 2, 198–208. doi:10.1007/s007750050125.

Crittenden, C. M., Akin, L. D., Morrison, L. J., Trent, M. S., and Brodbelt, J. S. (2017). Characterization of lipid A variants by energy-resolved mass spectrometry: impact of acyl chains. *J. Am. Soc. Mass Spectrom.* 28, 1118–1126. doi:10.1007/s13361-016-1542-6.

Dann, A. L., Cooper, R. S., and Bowman, J. P. (2009). Investigation and optimization of a passively operated compost-based system for remediation of acidic, highly iron- and sulfate-rich industrial waste water. *Water Res.* 43, 2302–2316.

Davison, W. (1991). The solubility of iron sulphides in synthetic and natural waters at ambient temperature. *Aquat. Sci.* 53, 309–329. doi:10.1007/BF00877139.

Deutsch, E. W., Bandeira, N., Sharma, V., Perez-Riverol, Y., Carver, J. J., Kundu, D. J., et al. (2020). The ProteomeXchange consortium in 2020: Enabling "big data" approaches in proteomics. *Nucleic Acids Res.* 48, D1145–D1152. doi:10.1093/nar/gkz984.

DeWeerd, K. A., Mandelco, L., Tanner, R. S., Woese, C. R., and Suflita, J. M. (1990). *Desulfomonile tiedjei* gen. nov. and sp. nov., a novel anaerobic, dehalogenating, sulfate-reducing bacterium. *Arch. Microbiol.* 154, 23–30. doi:10.1007/BF00249173.

Dick, G. J. (2019). The microbiomes of deep-sea hydrothermal vents: distributed globally, shaped locally. *Nat. Rev. Microbiol.* 17, 271–283. doi:10.1038/s41579-019-0160-2.

Diez-Ercilla, M., Falagán, C., Yusta, I., and Sánchez-España, J. (2019). Metal mobility and mineral transformations driven by bacterial activity in acidic pit lake sediments: evidence from column experiments and sequential extraction. *J. Soils Sediments* 19, 1527–1542. doi:10.1007/s11368-018-2112-2.

Diez-Ercilla, M., Sánchez-España, J., Yusta, I., Wendt-Potthoff, K., and Koschorreck, M. (2014). Formation of biogenic sulphides in the water column of an acidic pit lake: biogeochemical controls and effects on trace metal dynamics. *Biogeochemistry* 121, 519–536. doi:10.1007/s10533-014-0020-0.

Ding, J., Zhang, R., Yu, Y., Jin, D., Liang, C., Yi, Y., et al. (2011). A novel acidophilic, thermophilic iron and sulfur-oxidizing archaeon isolated from a hot spring of Tengchong, Yunnan, China. *Brazilian J. Microbiol.* 42, 514–525. doi:10.1590/S1517-83822011000200016.

Doetsch, R. N. (1981). "Determinative methods of light microscopy," in *Manual of Methods for General Bacteriology.* (Washington, D.C.: American Society for Microbiology,), 21–33.

Doukas, M., and Gerlach, T. (1995). "Sulfur dioxide scrubbing during the 1992 eruptions of Crater Peak, Mount Spurr Volcano, Alaska," in *The 1992 eruptions of Crater Peak vent, Mount Spurr Volcano, Alaska*, ed. T. E. C. Keith (U.S. Geological Survey), 47–57.

Druschel, G. K., Baker, B. J., Gihring, T. M., and Banfield, J. F. (2004). Acid mine drainage biogeochemistry at Iron Mountain, California. *Geochem. Trans.* 5, 13. doi:10.1186/1467-4866-5-13.

Dubilier, N., Bergin, C., and Lott, C. (2008). Symbiotic diversity in marine animals: The art of harnessing chemosynthesis. *Nat. Rev. Microbiol.* 6, 725–740. doi:10.1038/nrmicro1992.

Duverger, A., Berg, J. S., Busigny, V., Guyot, F., Bernard, S., and Miot, J. (2020). Mechanisms of Pyrite Formation Promoted by Sulfate-Reducing Bacteria in Pure Culture. *Front. Earth Sci.* 8, 1–15. doi:10.3389/feart.2020.588310.

Duverger, A., Bernard, S., Viennet, J., Miot, J., and Busigny, V. (2021). Formation of Pyrite Spherules From Mixtures of Biogenic FeS and Organic Compounds During Experimental Diagenesis. *Geochemistry, Geophys. Geosystems* 22, 1–16. doi:10.1029/2021gc010056.

Eow, J. S. (2002). Recovery of Sulfur from Sour Acid Gas : A Review of the Technology. 143–162.

Ertefai, T. F., Fisher, M. C., Fredricks, H. F., Lipp, J. S., Pearson, A., Birgel, D., et al. (2008). Vertical distribution of microbial lipids and functional genes in chemically distinct layers of a highly polluted meromictic lake. *Org. Geochem.* 39, 1572–1588. doi:10.1016/j.orggeochem.2008.07.009.

European Commission (2020). European Commission, Critical Materials for Strategic Technologies and Sectors in the EU - a Foresight Study, 2020. doi:10.2873/58081.

Faber, M. S., and Jin, S. (2014). Earth-abundant inorganic electrocatalysts and their nanostructures for energy conversion applications. *Energy Environ. Sci.* 7, 3519–3542. doi:10.1039/c4ee01760a.

Faber, M. S., Lukowski, M. A., Ding, Q., Kaiser, N. S., and Jin, S. (2014). Earth-Abundant Metal Pyrites (FeS 2 , CoS 2 , NiS 2 , and Their Alloys) for Highly Efficient Hydrogen Evolution and Polysulfide Reduction Electrocatalysis. *J. ofc Phys. Chem. C* 118, 21347–21356. doi:10.1021/jp506288w.

Falagán, C., and Johnson, D. B. (2014). *Acidibacter ferrireducens* gen. nov., sp. nov.: an acidophilic ferric iron-reducing gammaproteobacterium. *Extremophiles* 18, 1067–1073. doi:10.1007/s00792-014-0684-3.

Falagán, C., Sánchez-España, F. J., and Johnson, D. B. (2013). Microbiological Communities in Two Acidic Mine Pit Lakes in the Iberian Pyrite Belt (IPB), Spain. *Adv. Mater. Res.* 825, 19–22. doi:10.4028/www.scientific.net/AMR.825.19.

Falagán, C., Sánchez-España, F. J., Yusta, I., and Johnson, D. B. (2015). Microbial Communities in Sediments in Acidic, Metal-Rich Mine Lakes: Results from a Study in South-West Spain. *Adv. Mater. Res.* 1130, 7–10. doi:10.4028/www.scientific.net/AMR.1130.7.

Falagán, C., Sánchez-España, J., and Johnson, D. B. (2014). New insights into the biogeochemistry of extremely acidic environments revealed by a combined cultivation-based and culture-independent study of two stratified pit lakes. *FEMS Microbiol. Ecol.* 87, 231–243. doi:10.1111/1574-6941.12218.

Feehily, C., and Karatzas, K. A. G. (2013). Role of glutamate metabolism in bacterial responses towards acid and other stresses. *J. Appl. Microbiol.* 114, 11–24. doi:10.1111/j.1365-2672.2012.05434.x.

Fike, D. A., Bradley, A. S., and Rose, C. V (2015). Rethinking the ancient sulfur cycle. *Annu. Rev. Earth Planet. Sci.* 43, 593–622. doi:10.1146/annurev-earth-060313-054802.

Finneran, K. T., Forbush, H. M., VanPraagh, C. V, and Lovley, D. R. (2002). *Desulfitobacterium metallireducens* sp. nov., an anaerobic bacterium that couples growth to the reduction of metals and humic acids as well as chlorinated compounds. *Int. J. Syst. Evol. Microbiol.* 52, 1929–1935. doi:10.1099/ijs.0.02121-0.

Finster, K. (2008). Microbiological disproportionation of inorganic sulfur compounds. *J. Sulfur Chem.* 29, 281–292. doi:10.1080/17415990802105770.

Finster, K., Liesack, W., and Thamdrup, B. (1998). Elemental sulfur and thiosulfate disproportionation by *Desulfocapsa sulfoexigens* sp. nov., a new anaerobic bacterium isolated from marine surface sediment. *Appl. Environ. Microbiol.* 64, 119–125.

Finster, K., Liesack, W., and Tindall, B. J. (1997). *Sulfurospirillum arcachonense* sp. nov., a new microaerophilic sulfur- reducing bacterium. *Int. J. Syst. Bacteriol.* 47, 1212–1217. doi:10.1099/00207713-47-4-1212.

Flamholz, A., Noor, E., Bar-Even, A., and Milo, R. (2012). EQuilibrator - The biochemical thermodynamics calculator. *Nucleic Acids Res.* 40, 770–775. doi:10.1093/nar/gkr874.

Florentino, A. P., Brienza, C., Stams, A. J. M., and Sánchez-Andrea, I. (2016a). *Desulfurella amilsii* sp. nov., a novel acidotolerant sulfur-respiring bacterium isolated from acidic river sediments. *Int. J. Syst. Evol. Microbiol.* doi:10.1099/ijsem.0.000866.

Florentino, A. P., Pereira, I. A. C., Boeren, S., van den Born, M., Stams, A. J. M., and Sánchez-Andrea, I. (2019). Insight into the sulfur metabolism of *Desulfurella amilsii* by differential proteomics. *Environ. Microbiol.* 21, 209–225. doi:10.1111/1462-2920.14442.

Florentino, A. P., Weijma, J., Stams, A. J. M., and Sánchez-Andrea, I. (2015). Sulfur Reduction in Acid Rock Drainage Environments. *Environ. Sci. Technol.* 49, 11746–11755. doi:10.1021/acs.est.5b03346.

Florentino, A. P., Weijma, J., Stams, A. J. M., and Sánchez-Andrea, I. (2016b). "Ecophysiology and Application of Acidophilic Sulfur-Reducing Microorganisms," in *Biotechnology of Extremophiles Grand Challenges in Biology and Biotechnology* (Springer International Publishing Switzerland), 141–175. doi:10.1007/978-3-319-13521-2_5.

Franks, D. M., Stringer, M., Cruz, L. A. T., Baker, E., Valenta, R., Thygesen, K., et al. (2021). Tailings facility disclosures reveal stability risks. *Sci. Rep.*, 1–7. doi:10.1038/s41598-021-84897-0.

Franz, B., Lichtenberg, H., Hormes, J., Modrow, H., Dahl, C., and Prange, A. (2007). Utilization of solid "elemental" sulfur by the phototrophic purple sulfur bacterium *Allochromatium vinosum*: A sulfur K-edge X-ray absorption spectroscopy study. *Microbiology* 153, 1268–1274. doi:10.1099/mic.0.2006/003954-0.

Frolov, E. N., Kublanov, I. V., Toshchakov, S. V., Samarov, N. I., Novikov, A. A., Lebedinsky, A. V., et al. (2017). *Thermodesulfobium acidiphilum* sp. nov., a thermoacidophilic, sulfate-reducing, chemoautotrophic bacterium from a thermal site. *Int. J. Syst. Evol. Microbiol.* 67, 1482–1485. doi:10.1099/ijsem.0.001745.

Frolov, E. N., Zayulina, K. S., Kopitsyn, D. S., Kublanov, I. V., Bonch-Osmolovskaya, E. A., and Chernyh, N. A. (2018). *Desulfothermobacter acidiphilus* gen. Nov., sp. nov., a thermoacidophilic sulfate-reducing bacterium isolated from a terrestrial hot spring. *Int. J. Syst. Evol. Microbiol.* 68, 871–875. doi:10.1099/ijsem.0.002599.

Gaidos, E., Marteinsson, V., Thorsteinsson, T., Jóhannesson, T., Rúnarsson, Á. R., Stefansson, A., et al. (2009). An oligarchic microbial assemblage in the anoxic bottom waters of a volcanic subglacial lake. *ISME J.* 3, 486–497. doi:10.1038/ismej.2008.124.

Galperin, M. Y., Makarova, K. S., Wolf, Y. I., and Koonin, E. V (2015). Expanded microbial genome coverage and improved protein family annotation in the COG database. *Nucleic Acids Res* 43, D261-9. doi:10.1093/nar/gku1223.

Gammons, C. H., and Icopini, G. A. (2020). Improvements to the Water Quality of the Acidic Berkeley Pit Lake due to Copper Recovery and Sludge Disposal. *Mine Water Environ.* 39, 427–439. doi:10.1007/s10230-019-00648-8.

García-Moyano, A., González-Toril, E., Aguilera, Á., and Amils, R. (2012). Comparative microbial ecology study of the sediments and the water column of the Río Tinto, an extreme acidic environment. *FEMS Microbiol. Ecol.* 81, 303–314. doi:10.1111/j.1574-6941.2012.01346.x.

Gartman, A., Findlay, A. J., and Luther, G. W. (2014). Nanoparticulate pyrite and other nanoparticles are a widespread component of hydrothermal vent black smoker emissions. *Chem. Geol.* 366, 32–41. doi:10.1016/j.chemgeo.2013.12.013.

Gartman, A., and Luther, G. W. (2013). Comparison of pyrite (FeS_2) synthesis mechanisms to reproduce natural FeS_2 nanoparticles found at hydrothermal vents. *Geochim. Cosmochim. Acta* 120, 447–458. doi:10.1016/j.gca.2013.06.016.

Geller, W., Schultze, M., Kleinmann, R., and Wolkersdorfer, C. (2013). "Case Studies and Regional Surveys," in *Acidic pit lakes: The legacy of coal and metal surface mines*, eds. W. Geller, M. Schultze, R. Kleinmann, and C. Wolkersdorfer (Berlin, Heidelberg: Springer Verlag), 265–435. doi:10.1007/978-3-642-29384-9.

González-Toril, E., Aguilera, A., Rodriguez, N., Fernández-Remolar, D., Gómez, F., Diaz, E., et al. (2010). Microbial ecology of Río Tinto, a natural extreme acidic environment of biohydrometallurgical interest. *Hydrometallurgy* 104, 329–333. doi:10.1016/j.hydromet.2010.01.011.

González-Toril, E., Águilera, Á., Souza-Egipsy, V., Pamo, E. L., Sánchez-España, J., and Amils, R. (2011). Geomicrobiology of La Zarza-Perrunal acid mine effluent (Iberian Pyritic Belt, Spain). *Appl. Environ. Microbiol.* 77, 2685–2694. doi:10.1128/AEM.02459-10.

Gonzalez-Toril, E., Gómez, F., Rodríguez, N., Fernández-Remolar, D., Zuluaga, J., Marín, I., et al. (2003). Geomicrobiology of the Tinto River, a model of interest for biohydrometallurgy. *Hydrometallurgy* 71, 301–309. doi:10.1016/S0304-386X(03)00169-5.

González-Toril, E., Llobet-Brossa, E., Casamayor, E. O., Amann, R., and Amils, R. (2003). Microbial Ecology of an Extreme Acidic Environment, the Tinto River. *Appl. Environ. Microbiol.* 69, 4853–4865. doi:10.1128/AEM.69.8.4853.

Gorlas, A., Mariotte, T., Morey, L., Truong, C., Bernard, S., Guigner, J. -M., et al. (2022). Precipitation of greigite and pyrite induced by *Thermococcales*: an advantage to live in Fe- and S-rich environments? *Environ. Microbiol.* 24, 626–642. doi:10.1111/1462-2920.15915.

Graham, U. M., and Ohmoto, H. (1994). Experimental study of formation mechanisms of hydrothermal pyrite. *Geochim. Cosmochim. Acta* 58, 2187–2202. doi:10.1016/0016-7037(94)90004-3.

Grettenberger, C. L., and Hamilton, T. L. (2021). Metagenome-Assembled Genomes of Novel Taxa from an Acid Mine Drainage Environment. *Appl. Environ. Microbiol.* 87, 1–17. doi:10.1128/aem.00772-21.

Grettenberger, C. L., Mccauley Rench, R. L., Gruen, D. S., Mills, D. B., Carney, C., Brainard, J., et al. (2020). Microbial population structure in a stratified, acidic pit lake in the Iberian Pyrite Belt. *Geomicrobiol. J.* 0, 1–12. doi:10.1080/01490451.2020.1751748.

Grossi, V., Mollex, D., Vinçon-Laugier, A., Hakil, F., Pacton, M., and Cravo-Laureau, C. (2015). Mono- and dialkyl glycerol ether lipids in anaerobic bacteria: biosynthetic insights from the mesophilic sulfate reducer *Desulfatibacillum alkenivorans* PF2803 T. *Appl. Environ. Microbiol.* 81, 3157–3168. doi:10.1128/AEM.03794-14.

Guo, J., Li, Y., Sun, J., Sun, R., Zhou, S., Duan, J., et al. (2021). pH-dependent biological sulfidogenic processes for metal-laden wastewater treatment: Sulfate reduction or sulfur reduction? *Water Res.* 204, 117628. doi:10.1016/j.watres.2021.117628.

Guo, J., Wang, J., Qiu, Y., Sun, J., and Jiang, F. (2019). Realizing a high-rate sulfidogenic reactor driven by sulfur-reducing bacteria with organic substrate dosage minimization and cost-effectiveness maximization. *Chemosphere* 236, 124381. doi:10.1016/j.chemosphere.2019.124381.

Hall, J. R., Mitchell, K. R., Jackson-Weaver, O., Kooser, A. S., Cron, B. R., Crossey, L. J., et al. (2008). Molecular characterization of the diversity and distribution of a thermal spring microbial community by using rRNA and metabolic genes. *Appl. Environ. Microbiol.* 74, 4910–4922. doi:10.1128/AEM.00233-08 [doi].

Hamilton-Brehm, S. D., Gibson, R. A., Green, S. J., Hopmans, E. C., Schouten, S., van der Meer, M. T. J., et al. (2013). *Thermodesulfobacterium geofontis* sp. nov., a hyperthermophilic, sulfate-reducing bacterium isolated from Obsidian Pool, Yellowstone National Park. *Extremophiles* 17, 251–263. doi:10.1007/s00792-013-0512-1.

Hassannayebi, N., Azizmohammadi, S., De Lucia, M., and Ott, H. (2019). Underground hydrogen storage: application of geochemical modelling in a case study in the Molasse Basin, Upper Austria. *Environ. Earth Sci.* 78, 1–14. doi:10.1007/s12665-019-8184-5.

Hausmann, B., Knorr, K. H., Schreck, K., Tringe, S. G., Glavina Del Rio, T., Loy, A., et al. (2016). Consortia of low-abundance bacteria drive sulfate reduction-dependent degradation of fermentation products in peat soil microcosms. *ISME J.* 10, 2365–2375. doi:10.1038/ismej.2016.42.

Hausmann, B., Pelikan, C., Herbold, C. W., Köstlbacher, S., Albertsen, M., Eichorst, S. A., et al. (2018). Peatland *Acidobacteria* with a dissimilatory sulfur metabolism. *ISME J.*, 1–14. doi:10.1038/s41396-018-0077-1.

Hausmann, B., Pelikan, C., Rattei, T., Loy, A., and Pester, M. (2019). Long-Term Transcriptional Activity at Zero Growth of a Cosmopolitan Rare Biosphere Member. *MBio* 10, 1–16. doi:10.1128/mBio.02189-18.

Hedderich, R., Klimmek, O., Kröger, A., Dirmeier, R., Keller, M., and Stetter, K. O. (1998). Anaerobic respiration with elemental sulfur and with disulfides. *FEMS Microbiol. Rev.* 22, 353–381. doi:10.1111/j.1574-6976.1998.tb00376.x.

Hedrich, S., and Johnson, D. B. (2014). Remediation and selective recovery of metals from acidic mine waters using novel modular bioreactors. *Environ. Sci. Technol.* 48, 12206–12212. doi:10.1021/es5030367.

Hedrich, S., Joulian, C., Graupner, T., Schippers, A., and Guézennec, A. G. (2018). Enhanced chalcopyrite dissolution in stirred tank reactors by temperature increase during bioleaching. *Hydrometallurgy* 179, 125–131. doi:10.1016/j.hydromet.2018.05.018.

Heift, D. (2019). Iron Sulfide Materials: Catalysts for Electrochemical Hydrogen Evolution. *Inorganics* 7, 75. doi:10.3390/inorganics7060075.

Herrington, R. (2021). Mining our green future. *Nat. Rev. Mater.* 0123456789. doi:10.1038/s41578-021-00325-9.

Hidalgo-Ulloa, A., Sánchez-Andrea, I., Buisman, C., and Weijma, J. (2020). Sulfur Reduction at Hyperthermoacidophilic Conditions with Mesophilic Anaerobic Sludge as the Inoculum. *Environ. Sci. Technol.* 54, 14656–14663. doi:10.1021/acs.est.0c02557.

Hiibel, S. R., Pereyra, L. P., Breazeal, M. V. R., Reisman, D. J., Reardon, K. F., and Pruden, A. (2011). Effect of organic substrate on the microbial community structure in pilot-scale sulfate-reducing biochemical reactors treating mine drainage. *Environ. Eng. Sci.* 28, 563–572.

Hippe, H. (2000). *Leptospirillum* gen. nov. (ex Markosyan 1972), nom. rev., including *Leptospirillum ferrooxidans* sp. nov. (ex Markosyan 1972), nom. rev. and *Leptospirillum thermoferrooxidans* sp. nov. (Golovacheva et al. 1992). *Int. J. Syst. Evol. Microbiol.* 50, 501–503. doi:10.1099/00207713-50-2-501.

Hiraishi, A., Nagashima, K. V. P., Matsuura, K., Shimada, K., Takaichi, S., Wakao, N., et al. (1998). Phylogeny and photosynthetic features of *Thiobacillus acidophilus* and related acidophilic bacteria: Its transfer to the genus *Acidiphilium* as *Acidiphilium acidophilum* comb. nov. *Int. J. Syst. Bacteriol.* 48, 1389–1398. doi:10.1099/00207713-48-4-1389.

Hochella, M. F., Lower, S. K., Maurice, P. A., Penn, R. L., Sahai, N., Sparks, D. L., et al. (2008). Nanominerals, Mineral Nanoparticles, and Earth Systems. *Science (80-.).* 319, 1631–1635. doi:10.1126/science.1141134.

Holanda, R., Hedrich, S., Ňancucheo, I., Oliveira, G., Grail, B. M., and Johnson, D. B. (2016). Isolation and characterisation of mineral-oxidising "Acidibacillus" spp. from mine sites and geothermal environments in different global locations. *Res. Microbiol.* 167, 613–623. doi:10.1016/j.resmic.2016.04.008.

Huang, C. H., Lee, I. L., Yeh, I. J., Liao, J. H., Ni, C. L., Wu, S. H., et al. (2010). Upregulation of a non-heme iron-containing ferritin with dual ferroxidase and DNA-binding activities in *Helicobacter pylori* under acid stress. *J. Biochem.* 147, 535–543. doi:10.1093/jb/mvp200.

Hudson-Edwards, K. A., Jamieson, H. E., and Lottermoser, B. G. (2011). Mine wastes: Past, present, future. *Elements* 7, 375–380. doi:10.2113/gselements.7.6.375.

Hug, L. A., Baker, B. J., Anantharaman, K., Brown, C. T., Probst, A. J., Castelle, C. J., et al. (2016). A new view of the tree of life. *Nat. Microbiol.* 1, 1–6. doi:10.1038/nmicrobiol.2016.48.

Huisman, J. L., Schouten, G., and Schultz, C. (2006). Biologically produced sulphide for purification of process streams, effluent treatment and recovery of metals in the metal and mining industry. *Hydrometallurgy* 83, 106–113. doi:10.1016/j.hydromet.2006.03.017.

Hulshoff Pol, L. W., Lens, P. N. L., Weijma, J., and Stams, A. J. M. (2001). New developments in reactor and process technology for sulfate reduction. *Water Sci. Technol.* 44, 67–76. doi:10.2166/wst.2001.0467.

Human Microbiome Project, C. (2012). Structure, function and diversity of the healthy human microbiome. *Nature* 486, 207–214. doi:10.1038/nature11234.

Huson, D. H., Auch, A. F., Qi, J., and Schuster, S. C. (2007). MEGAN analysis of metagenomic data. *Genome Res* 17, 377–386. doi:10.1101/gr.5969107.

Hyatt, D., Chen, G. L., Locascio, P. F., Land, M. L., Larimer, F. W., and Hauser, L. J. (2010). Prodigal: prokaryotic gene recognition and translation initiation site identification. *BMC Bioinformatics* 11, 119. doi:10.1186/1471-2105-11-119.

Inagaki, F., Takai, K., Nealson, K. H., and Horikoshi, K. (2004). *Sulfurovum lithotrophicum* gen. nov., sp. nov., a novel sulfur-oxidizing chemolithoautotroph within the *E-Proteobacteria* isolated from Okinawa Trough hydrothermal sediments. *Int. J. Syst. Evol. Microbiol.* 54, 1477–1482. doi:10.1099/ijs.0.03042-0.

International Energy Agency (IEA) (2021). The Role of Critical Minerals in Clean Energy Transitions. Paris Available at: https://www.iea.org/reports/the-role-of-critical-minerals-in-clean-energy-transitions.

Itoh, T. (2002). *Vulcanisaeta distributa* gen. nov., sp. nov., and *Vulcanisaeta souniana* sp. nov., novel hyperthermophilic, rod-shaped crenarchaeotes isolated from hot springs in Japan. *Int. J. Syst. Evol. Microbiol.* 52, 1097–1104. doi:10.1099/ijs.0.02152-0.

Itoh, T., Suzuki, K., Sanchez, P. C., and Nakase, T. (1999). *Caldivirga maquilingensis* gen. nov., sp. nov., a new genus of rod-shaped crenarchaeote isolated from a hot spring in the Philippines. *Int. J. Syst. Evol. Microbiol.* 49, 1157–1163. doi:10.1099/00207713-49-3-1157.

Jackson, D. R., Cassilly, C. D., Plichta, D. R., Vlamakis, H., Liu, H., Melville, S. B., et al. (2021). Plasmalogen Biosynthesis by Anaerobic Bacteria: Identification of a Two-Gene Operon Responsible for Plasmalogen Production in *Clostridium perfringens*. *ACS Chem. Biol.* 16, 6–13. doi:10.1021/acschembio.0c00673.

Jameson, E., Rowe, O. F., Hallberg, K. B., and Johnson, D. B. (2010). Sulfidogenesis and selective precipitation of metals at low pH mediated by *Acidithiobacillus* spp. and acidophilic sulfate-reducing bacteria. *Hydrometallurgy* 104, 488–493. doi:10.1016/j.hydromet.2010.03.029.

Janssen, P. H., Schuhmann, A., Bak, F., and Liesack, W. (1996). Disproportionation of inorganic sulfur compounds by the sulfate-reducing bacterium *Desulfocapsa thiozymogenes* gen, nov., sp. nov. *Arch. Microbiol.* 166, 184–192. doi:10.1007/s002030050374.

Jelen, B., Giovannelli, D., Falkowski, P. G., and Vetriani, C. (2018). Elemental sulfur reduction in the deep-sea vent thermophile, *Thermovibrio ammonificans*. *Environ. Microbiol.* 20, 2301–2316. doi:10.1111/1462-2920.14280.

Jerez, C., Chamorro, D., Peirano, I., and Toledo, H. (1988). Studies of the stress response in chemolithotrophic acidophilic bacteria. *Biochem. Int.* 17, 989–999.

Johnson, D. B. (2015). Biomining goes underground. *Nat. Geosci.* 8, 165–166. doi:10.1038/ngeo2384.

Johnson, D. B., and Aguilera, A. (2015). "The Microbiology of Extremely Acidic Environments," in *Manual of Environmental Microbiology*, eds. M. Yates, C. Nakatsu, R. Miller, and S. Pillai (Washington, DC, USA: ASM Press), 4.3.1-1-4.3.1-24. doi:10.1128/9781555818821.ch4.3.1.

Johnson, D. B., and Hallberg, K. B. (2003). The microbiology of acidic mine waters. *Res. Microbiol.* 154, 466–473. doi:10.1016/S0923-2508(03)00114-1.

Johnson, D. B., and Hallberg, K. B. (2005). Acid mine drainage remediation options: A review. *Sci. Total Environ.* 338, 3–14. doi:10.1016/j.scitotenv.2004.09.002.

Johnson, D. B., and Hallberg, K. B. (2008). Carbon, iron and sulfur metabolism in acidophilic micro-organisms. *Adv. Microb. Physiol.* 54, 201–255.

Johnson, D. B., and Sánchez-Andrea, I. (2019). Dissimilatory reduction of sulfate and zero-valent sulfur at low pH and its significance for bioremediation and metal recovery. *Adv. Microb. Physiol.* 75, 205–231. doi:10.1016/bs.ampbs.2019.07.002.

Jones, R. M., Hedrich, S., and Johnson, D. B. (2013). *Acidocella aromatica* sp. nov.: an acidophilic heterotrophic alphaproteobacterium with unusual phenotypic traits. *Extremophiles* 17, 841–850. doi:10.1007/s00792-013-0566-0.

Jørgensen, B. B. (1982). Mineralization of organic matter in the sea bed – the role of sulphate reduction. *Nature* 296, 643–645. doi:10.1038/296643a0.

Jørgensen, B. B. (2021). Sulfur Biogeochemical Cycle of Marine Sediments. *Geochemical Perspect.* 10, 145–307. doi:10.7185/geochempersp.10.2.

Jørgensen, B. B., Findlay, A. J., and Pellerin, A. (2019). The Biogeochemical Sulfur Cycle of Marine Sediments. 10, 1–27. doi:10.3389/fmicb.2019.00849.

Jowitt, S. M., Mudd, G. M., and Thompson, J. F. H. (2020). Future availability of non-renewable metal resources and the influence of environmental, social, and governance conflicts on metal production. *Commun. Earth Environ.* 1, 1–8. doi:10.1038/s43247-020-0011-0.

Kafantaris, F. C. A., and Druschel, G. K. (2020). Kinetics of the nucleophilic dissolution of hydrophobic and hydrophilic elemental sulfur sols by sulfide. *Geochim. Cosmochim. Acta* 269, 554–565. doi:10.1016/j.gca.2019.11.010.

Kamyshny, A. (2009). Solubility of cyclooctasulfur in pure water and sea water at different temperatures. *Geochim. Cosmochim. Acta* 73, 6022–6028. doi:10.1016/j.gca.2009.07.003.

Kamyshny, A., Borkenstein, C. G., and Ferdelman, T. G. (2009). Protocol for quantitative detection of elemental sulfur and polysulfide zero-valent sulfur distribution in natural aquatic samples. *Geostand. Geoanalytical Res.* 33, 415–435. doi:10.1111/j.1751-908X.2009.00907.x.

Kamyshny, A., Goifman, A., Gun, J., Rizkov, D., and Lev, O. (2004). Equilibrium distribution of polysulfide ions in aqueous solutions at 25°C: A new approach for the study of polysulfides' equilibria. *Environ. Sci. Technol.* 38, 6633–6644. doi:10.1021/es049514e.

Kamyshny, A., Gun, J., Rizkov, D., Voitsekovski, T., and Lev, O. (2007). Equilibrium distribution of polysulfide ions in aqueous solutions at different temperatures by rapid single phase derivatization. *Environ. Sci. Technol.* 41, 2395–2400. doi:10.1021/es062637+.

Kassambara, A. (2020). ggpubr:"ggplot2" based publication ready plots. Available at: https://cran.r-project.org/web/packages/ggpubr/index.html.

Kelly, D. P., and Wood, A. P. (2000). Reclassification of some species of *Thiobacillus* to the newly designated genera *Acidithiobacillus* gen. nov., *Halothiobacillus* gen. nov. and *Thermithiobacillus* gen. nov. *Int. J. Syst. Evol. Microbiol.* 50, 511–516. doi:10.1099/00207713-50-2-511.

Khalid, S., Ahmed, E., Khan, Y., Riaz, K. N., and Malik, M. A. (2018). Nanocrystalline Pyrite for Photovoltaic Applications. *ChemistrySelect* 3, 6488–6524. doi:10.1002/slct.201800405.

Kimura, S., Hallberg, K. B., and Johnson, D. B. (2006). Sulfidogenesis in low pH (3.8-4.2) media by a mixed population of acidophilic bacteria. *Biodegradation* 17, 159–167. doi:10.1007/s10532-005-3050-4.

Kleinjan, W. E., de Keizer, A., and Janssen, A. J. H. (2005). Kinetics of the Reaction between Dissolved Sodium Sulfide and Biologically Produced Sulfur. *Ind. Eng. Chem. Res.* 44, 309–317. doi:10.1021/ie049579q.

Klemps, R., Cypionka, H., Widdel, F., and Pfennig, N. (1985). Growth with hydrogen, and further physiological characteristics of *Desulfotomaculum* species. *Arch. Microbiol.* 143, 203–208. doi:10.1007/BF00411048.

Kletzin, A. (2006). Metabolism of inorganic sulfur compounds in archaea. *Archaea. Evolution, Physiol. Mol. Biol. Garrett H.-P.Klenk.Blackwell Publ. Oxford*, 261–274.

Kletzin, A. (2007). "Oxidation of sulfur and inorganic sulfur compounds in *Acidianus ambivalens*," in *Microbial Sulfur Metabolism*, 184–201. doi:10.1007/978-3-540-72682-1_15.

Kletzin, A., Urich, T., Müller, F., Bandeiras, T. M., and Gomes, C. M. (2004). Dissimilatory oxidation and reduction of elemental sulfur in thermophilic Archaea. *J. Bioenerg. Biomembr.* 36, 77–91. doi:10.1023/B:JOBB.0000019600.36757.8c.

Klimmek, O., Kröger, A., Steudel, R., and Holdt, G. (1991). Growth of *Wolinella succinogenes* with polysulphide as terminal acceptor of phosphorylative electron transport. *Arch. Microbiol.* 155, 177–182. doi:10.1007/BF00248614.

Klinger, M. (2017). More features, more tools, more CrysTBox. *J. Appl. Crystallogr.* 50, 1226–1234. doi:10.1107/S1600576717006793.

Koehorst, J. J., van Dam, J. C. J., Saccenti, E., Martins Dos Santos, V. A. P., Suarez-Diez, M., and Schaap, P. J. (2018). SAPP: functional genome annotation and analysis through a semantic framework using FAIR principles. *Bioinformatics* 34, 1401–1403. doi:10.1093/bioinformatics/btx767.

Koga, Y., Morn, H., Akagawa-Matsushita, M., and Ohga, M. (1998). Correlation of polar lipid composition with 16S rRNA phylogeny in methanogens. further analysis of lipid component parts. *Biosci. Biotechnol. Biochem.* 62, 230–236. doi:10.1271/bbb.62.230.

Koga, Y., Nishihara, M., Morii, H., and Akagawa-Matsushita, M. (1993). Ether polar lipids of methanogenic bacteria: Structures, comparative aspects, and biosyntheses. *Microbiol. Rev.* 57, 164–182. doi:10.1128/mmbr.57.1.164-182.1993.

Konstantinidis, K. T., and Tiedje, J. M. (2005). Towards a genome-based taxonomy for prokaryotes. *J. Bacteriol.* 187, 6258–6264. doi:10.1128/JB.187.18.6258-6264.2005.

Korehi, H., Blöthe, M., and Schippers, A. (2014). Microbial diversity at the moderate acidic stage in three different sulfidic mine tailings dumps generating acid mine drainage. *Res. Microbiol.* 165, 713–718. doi:10.1016/j.resmic.2014.08.007.

Koschorreck, M. (2008). Microbial sulphate reduction at a low pH. *FEMS Microbiol. Ecol.* 64, 329–342. doi:10.1111/j.1574-6941.2008.00482.x.

Krogh, A., Larsson, B., Von Heijne, G., and Sonnhammer, E. L. L. (2001). Predicting transmembrane protein topology with a hidden Markov model: Application to complete genomes. *J. Mol. Biol.* 305, 567–580. doi:10.1006/jmbi.2000.4315.

Kumar, M., Nandi, M., and Pakshirajan, K. (2021). Recent advances in heavy metal recovery from wastewater by biogenic sulfide precipitation. *J. Environ. Manage.* 278, 111555. doi:10.1016/j.jenvman.2020.111555.

Kumar, R. N., McCullough, C. D., Lund, M. A., and Newport, M. (2011). Sourcing Organic Materials for Pit Lake Bioremediation in Remote Mining Regions. *Mine Water Environ.* 30, 296–301. doi:10.1007/s10230-011-0144-6.

Lagesen, K., Hallin, P., Rodland, E. A., Staerfeldt, H. H., Rognes, T., and Ussery, D. W. (2007). RNAmmer: consistent and rapid annotation of ribosomal RNA genes. *Nucleic Acids Res* 35, 3100–3108. doi:10.1093/nar/gkm160.

Lahti, L., and Shetty, S. (2017). Tools for microbiome analysis in R. Available at: https://bioconductor.org/packages/release/bioc/html/microbiome.html.

Langmead, B., and Salzberg, S. L. (2012). Fast gapped-read alignment with Bowtie 2. *Nat Methods* 9, 357–359. doi:10.1038/nmeth.1923.

Larrouy-Maumus, G., Clements, A., Filloux, A., McCarthy, R. R., and Mostowy, S. (2016). Direct detection of lipid A on intact Gram-negative bacteria by MALDI-TOF mass spectrometry. *J. Microbiol. Methods* 120, 68–71. doi:10.1016/j.mimet.2015.12.004.

Laska, S., Lottspeich, F., and Kletzin, A. (2003). Membrane-bound hydrogenase and sulfur reductase of the hyperthermophilic and acidophilic archaeon *Acidianus ambivalens*. *Microbiology* 149, 2357–2371. doi:10.1099/mic.0.26455-0.

Laslett, D., and Canback, B. (2004). ARAGORN, a program to detect tRNA genes and tmRNA genes in nucleotide sequences. *Nucleic Acids Res* 32, 11–16. doi:10.1093/nar/gkh152.

Lee, Y. J., Romanek, C. S., and Wiegel, J. (2009). *Desulfosporosinus youngiae* sp. nov., a spore-forming, sulfate-reducing bacterium isolated from a constructed wetland treating acid mine drainage. *Int. J. Syst. Evol. Microbiol.* 59, 2743–2746.

Leistel, J. M., Marcoux, E., Thiéblemont, D., Quesada, C., Sánchez, A., Almodóvar, G. R., et al. (1997). The volcanic-hosted massive sulphide deposits of the Iberian Pyrite Belt: review and preface to the thematic Issue. *Miner. Depos.* 33, 2–30. doi:10.1007/s001260050130.

Levett, A., Gleeson, S. A., and Kallmeyer, J. (2021). From exploration to remediation: A microbial perspective for innovation in mining. *Earth-Science Rev.* 216, 103563. doi:10.1016/j.earscirev.2021.103563.

Lewis, A. E. (2010). Review of metal sulphide precipitation. *Hydrometallurgy* 104, 222–234. doi:10.1016/j.hydromet.2010.06.010.

Lewis, W. H., Tahon, G., Geesink, P., Sousa, D. Z., and Ettema, T. J. G. (2021). Innovations to culturing the uncultured microbial majority. *Nat. Rev. Microbiol.* 19, 225–240. doi:10.1038/s41579-020-00458-8.

Lindsay, M. B. J., Wakeman, K. D., Rowe, O. F., Grail, B. M., Ptacek, C. J., Blowes, D. W., et al. (2011). Microbiology and geochemistry of mine tailings amended with organic carbon for passive treatment of pore water. *Geomicrobiol. J.* 28, 229–241.

López-Archilla, A. I., Marin, I., and Amils, R. (2001). Microbial community composition and ecology of an acidic aquatic environment: the Tinto River, Spain. *Microb. Ecol.* 41, 20–35. doi:10.1007/s002480000044.

López-Pamo, E., Sánchez-España, J., Diez, M., Santofimia, E., and Reyes, J. (2009). *Cortas mineras inundadas de la Faja Pirítica: inventario e hidroquímica*. Spain: Instituto Geológico y Minero de España.

Lottermoser, B. (2010). *Mine Wastes*. Berlin, Heidelberg: Springer Berlin Heidelberg doi:10.1007/978-3-642-12419-8.

Ludwig, W., Strunk, O., Westram, R., Richter, L., and Meier, H. (2004). ARB: a software environment for sequence data. *Nucleic Acids Res.* 32, 1363–1371. doi:10.1093/nar/gkh293.

Machel, H. G. (2001). Bacterial and thermochemical sulfate reduction in diagenetic settings - old and new insights. *Sediment. Geol.* 140, 143–175. doi:10.1016/S0037-0738(00)00176-7.

Madden, A. S., Palumbo, A. V., Ravel, B., Vishnivetskaya, T. A., Phelps, T. J., Schadt, C. W., et al. (2009). Donor-dependent extent of uranium reduction for bioremediation of contaminated sediment microcosms. *J. Environ. Qual.* 38, 53–60. doi:10.2134/jeq2008.0071.

Mardanov, A. V., Panova, I. A., Beletsky, A. V., Avakyan, M. R., Kadnikov, V. V., Antsiferov, D. V., et al. (2016). Genomic insights into a new acidophilic, copper-resistant *Desulfosporosinus* isolate from the oxidized tailings area of an abandoned gold mine. *FEMS Microbiol. Ecol.* 92, 1–14. doi:10.1093/femsec/fiw111.

Matamoros-Veloza, A., Cespedes, O., Johnson, B. R. G., Stawski, T. M., Terranova, U., de Leeuw, N. H., et al. (2018). A highly reactive precursor in the iron sulfide system. *Nat. Commun.* 9. doi:10.1038/s41467-018-05493-x.

McCleskey, B., Ball, J. W., Nordstrom, D. K., Holloway, J. M., and Taylor, H. E. (2005). Water-Chemistry Data for Selected Hot Springs, Geysers, and Streams in Yellowstone National Park, Wyoming, 2001-2002. doi:10.3133/ofr20041316.

McCullough, C. D., and Lund, M. A. (2011). Bioremediation of Acidic and Metalliferous Drainage (AMD) through organic carbon amendment by municipal sewage and green waste. *J. Environ. Manage.* 92, 2419–2426. doi:10.1016/j.jenvman.2011.04.011.

McDonough, W. F., and Sun, S. s. (1995). The composition of the Earth. *Chem. Geol.* 120, 223–253. doi:10.1016/0009-2541(94)00140-4.

McMurdie, P. J., and Holmes, S. (2013). Phyloseq: An R Package for Reproducible Interactive Analysis and Graphics of Microbiome Census Data. *PLoS One* 8, 1–11. doi:10.1371/journal.pone.0061217.

McNaughton, S. J., and Wolf, L. L. (1970). Dominance and the Niche in Ecological Systems. *Science (80-.).* 167, 131–139. doi:10.1126/science.167.3915.131.

Meador, T. B., Gagen, E. J., Loscar, M. E., Goldhammer, T., Yoshinaga, M. Y., Wendt, J., et al. (2014). *Thermococcus kodakarensis* modulates its polar membrane lipids and elemental composition according to growth stage and phosphate availability. *Front. Microbiol.* 5, 1–13. doi:10.3389/fmicb.2014.00010.

Méndez-García, C., Peláez, A. I., Mesa, V., Sánchez, J., Golyshina, O. V., and Ferrer, M. (2015). Microbial diversity and metabolic networks in acid mine drainage habitats. *Front. Microbiol.* 6, 1–17. doi:10.3389/fmicb.2015.00475.

Mino, S., Kudo, H., Arai, T., Sawabe, T., Takai, K., and Nakagawa, S. (2014). *Sulfurovum aggregans* sp. nov., a hydrogen-oxidizing, thiosulfate-reducing chemolithoautotroph within the Epsilonproteobacteria isolated from a deep-sea hydrothermal vent chimney, and an emended description of the genus *Sulfurovum*. *Int. J. Syst. Evol. Microbiol.* 64, 3195–3201. doi:10.1099/ijs.0.065094-0.

Miroshnichenko, M. L., Gongadze, G. A., Lysenko, A. M., and Bonch-Osmolovskaya, E. A. (1994). *Desulfurella multipotens* sp. nov., a new sulfur-respiring thermophilic eubacterium from Raoul Island (Kermadec archipelago, New Zealand). *Arch. Microbiol.* 161, 88–93. doi:10.1007/BF00248898.

Miroshnichenko, M. L., Rainey, F. A., Hippe, H., Chernyh, N. A., Kostrikina, N. A., and Bonch-Osmolovskaya, E. A. (1998). *Desulfurella kamchatkensis* sp. nov. and *Desulfurella propionica* sp. nov., new sulfur-respiring thermophilic bacteria from Kamchatka thermal environments. *Int. J. Syst. Bacteriol.* 48, 475–479. doi:10.1099/00207713-48-2-475.

Moore, E. K., Hopmans, E. C., Rijpstra, W. I. C., Villanueva, L., and Sinninghe Damsté, J. S. (2016). Elucidation and identification of amino acid containing membrane lipids using liquid chromatography/high-resolution mass spectrometry. *Rapid Commun. Mass Spectrom.* 30, 739–750. doi:10.1002/rcm.7503.

Mori, K., Kim, H., Kakegawa, T., and Hanada, S. (2003). A novel lineage of sulfate-reducing microorganisms: *Thermodesulfobiaceae* fam. nov., *Thermodesulfobium narugense*, gen. nov., sp. nov., a new thermophilic isolate from a hot spring. *Extremophiles* 7, 283–290. doi:10.1007/s00792-003-0320-0.

Morse, J. W., and Wang, Q. (1997). Pyrite formation under conditions approximating those in anoxic sediments: II. Influence of precursor iron minerals and organic matter. *Mar. Chem.* 57, 187–193. doi:10.1016/S0304-4203(97)00050-9.

Muyzer, G., and Stams, A. J. M. (2008). The ecology and biotechnology of sulphate-reducing bacteria. *Nat. Rev. Microbiol.* 45, 187–192. doi:10.1038/nrmicro1892.

Nakagawa, S., Takai, K., Inagaki, F., Hirayama, H., Nunoura, T., Horikoshi, K., et al. (2005). Distribution, phylogenetic diversity and physiological characteristics of epsilon-Proteobacteria in a deep-sea hydrothermal field. *Environ. Microbiol.* 7, 1619–1632. doi:10.1111/j.1462-2920.2005.00856.x.

Nakamura, R., Takashima, T., Kato, S., Takai, K., Yamamoto, M., and Hashimoto, K. (2010). Electrical current generation across a black smoker chimney. *Angew. Chemie - Int. Ed.* 49, 7692–7694. doi:10.1002/anie.201003311.

Ňancucheo, I., Bitencourt, J. A. P., Sahoo, P. K., Alves, J. O., Siqueira, J. O., and Oliveira, G. (2017). Recent Developments for Remediating Acidic Mine Waters Using Sulfidogenic Bacteria. *Biomed Res. Int.* 2017, 1–17. doi:10.1155/2017/7256582.

Ňancucheo, I., and Johnson, D. B. (2012a). Acidophilic algae isolated from mine-impacted environments and their roles in sustaining heterotrophic acidophiles. *Front. Microbiol.* 3, 1–8. doi:10.3389/fmicb.2012.00325.

Ňancucheo, I., and Johnson, D. B. (2012b). Selective removal of transition metals from acidic mine waters by novel consortia of acidophilic sulfidogenic bacteria. *Microb. Biotechnol.* 5, 34–44. doi:10.1111/j.1751-7915.2011.00285.x.

Ňancucheo, I., and Johnson, D. B. (2014). Removal of sulfate from extremely acidic mine waters using low pH sulfidogenic bioreactors. *Hydrometallurgy* 150, 222–226. doi:10.1016/j.hydromet.2014.04.025.

NCBI Resource Coordinators (2013). Database resources of the National Center for Biotechnology Information. *Nucleic Acids Res* 41, D8–D20. doi:10.1093/nar/gks1189.

Nevin, K. P., Finneran, K. T., and Lovley, D. R. (2003). Microorganisms associated with uranium bioremediation in a high-salinity subsurface sediment. *Appl. Environ. Microbiol.* 69, 3672–3675. doi:10.1128/AEM.69.6.3672-3675.2003.

Nguyen, N.-N., Srihari, S., Leong, H. W., and Chong, K.-F. (2015). EnzDP: Improved enzyme annotation for metabolic network reconstruction based on domain composition profiles. *J. Bioinform. Comput. Biol.* 13, 1543003. doi:10.1142/S0219720015430039.

Nielsen, L. P., Risgaard-Petersen, N., Fossing, H., Christensen, P. B., and Sayama, M. (2010). Electric currents couple spatially separated biogeochemical processes in marine sediment. *Nature* 463, 1071–1074. doi:10.1038/nature08790.

Nordstrom, D. K. (2000). Advances in the hydrogeochemistry and microbiology of acid mine waters. *Int. Geol. Rev.* 42, 499–515. doi:10.1080/00206810009465095.

Nordstrom, D. K., and Alpers, C. N. (1999). "Geochemistry of acid mine waters," in *The environmental geochemistry of mineral deposits: Part A: Processes, methods and health issues*, eds. G. S. Plumlee and M. J. Logsdon (Society of Economic Geologists), 133–160.

Nordstrom, D. K., Ball, J. W., and McCleskey, R. B. (2005). "Ground water to surface Water: Chemistry of thermal outflows in Yellowstone National Park," in *Geothermal Biology and Geochemistry in Yellowstone National Park*, eds. W. P. Inskeep and T. R. McDermott (Bozeman, Montana: Montana State University), 73–94.

Nordstrom, D. K., Blowes, D. W., and Ptacek, C. J. (2015). Hydrogeochemistry and microbiology of mine drainage: An update. *Appl. Geochemistry* 57, 3–16. doi:10.1016/j.apgeochem.2015.02.008.

Nordstrom, D. K., Mccleskey, R. B., and Ball, J. W. (2009). Sulfur geochemistry of hydrothermal waters in Yellowstone National Park : IV Acid – sulfate waters. *Appl. Geochemistry* 24, 191–207. doi:10.1016/j.apgeochem.2008.11.019.

Ntagia, E., Chatzigiannidou, I., Williamson, A. J., Arends, J. B. A., and Rabaey, K. (2020). Homoacetogenesis and microbial community composition are shaped by pH and total sulfide concentration. *Microb. Biotechnol.* 13, 1026–1038. doi:10.1111/1751-7915.13546.

Oger, P. M., and Cario, A. (2013). Adaptation of the membrane in Archaea. *Biophys. Chem.* 183, 42–56. doi:10.1016/j.bpc.2013.06.020.

Ohfuji, H., and Rickard, D. (2005). Experimental syntheses of framboids - A review. *Earth-Science Rev.* 71, 147–170. doi:10.1016/j.earscirev.2005.02.001.

Okamura, K., Kawai, A., Wakao, N., Yamada, T., and Hiraishi, A. (2015). *Acidiphilium iwatense* sp. nov., isolated from an acid mine drainage treatment plant, and emendation of the genus Acidiphilium. *Int. J. Syst. Evol. Microbiol.* 65, 42–48. doi:10.1099/ijs.0.065052-0.

Olsen, I., and Jantzen, E. (2001). Sphingolipids in bacteria and fungi. *Anaerobe* 7, 103–112. doi:10.1006/anae.2001.0376.

Panda, S. K., Jyoti, V., Bhadra, B., Nayak, K. C., Shivaji, S., Rainey, F. A., et al. (2009). *Thiomonas bhubaneswarensis* sp. nov., an obligately mixotrophic, moderately thermophilic, thiosulfate-oxidizing bacterium. *Int. J. Syst. Evol. Microbiol.* 59, 2171–2175. doi:10.1099/ijs.0.007120-0.

Panevska, A., Skočaj, M., Križaj, I., Maček, P., and Sepčić, K. (2019). Ceramide phosphoethanolamine, an enigmatic cellular membrane sphingolipid. *Biochim. Biophys. Acta - Biomembr.* 1861, 1284–1292. doi:10.1016/j.bbamem.2019.05.001.

Panova, I. A., Ikkert, O., Avakyan, M. R., Kopitsyn, D. S., Mardanov, A. V., Pimenov, N. V., et al. (2021). *Desulfosporosinus metallidurans* sp. nov., an acidophilic, metal-resistant sulfate-reducing bacterium from acid mine drainage. *Int. J. Syst. Evol. Microbiol.* 71. doi:10.1099/ijsem.0.004876.

Parkhurst, D. L., and Appelo, C. A. J. (1999). User's guide to PHREEQC (Version 2): A computer program for speciation, batch-reaction, one-dimensional transport, and inverse geochemical calculations. doi:10.3133/wri994259.

Patel, G. B., Sprott, G. D., and Fein, J. E. (1990). Isolation and characterization of *Methanobacterium espanolae* sp. nov., a mesophilic, moderately acidiphilic methanogen. *Int. J. Syst. Bacteriol.* 40, 12–18. doi:10.1099/00207713-40-1-12.

Payne, D., Spietz, R. L., and Boyd, E. S. (2021). Reductive dissolution of pyrite by methanogenic archaea. *ISME J.* 15, 3498–3507. doi:10.1038/s41396-021-01028-3.

Pell, R., Tijsseling, L., Goodenough, K., Wall, F., Dehaine, Q., Grant, A., et al. (2021). Towards sustainable extraction of technology materials through integrated approaches. *Nat. Rev. Earth Environ.* 0123456789. doi:10.1038/s43017-021-00211-6.

Perez-Riverol, Y., Csordas, A., Bai, J., Bernal-Llinares, M., Hewapathirana, S., Kundu, D. J., et al. (2019). The PRIDE database and related tools and resources in 2019: Improving support for quantification data. *Nucleic Acids Res.* 47, D442–D450. doi:10.1093/nar/gky1106.

Pester, M., Brambilla, E., Alazard, D., Rattei, T., Weinmaier, T., Han, J., et al. (2012). Complete genome sequences of *Desulfosporosinus orientis* DSM765T, *Desulfosporosinus youngiae* DSM17734T, *Desulfosporosinus meridiei* DSM13257T, and *Desulfosporosinus acidiphilus* DSM22704T. *J. Bacteriol.* 194, 6300–6301. doi:10.1128/JB.01392-12.

Petersen, T. N., Brunak, S., von Heijne, G., and Nielsen, H. (2011). SignalP 4.0: discriminating signal peptides from transmembrane regions. *Nat Methods* 8, 785–786. doi:10.1038/nmeth.1701.

Petrie, L., North, N. N., Dollhopf, S. L., Balkwill, D. L., and Kostka, J. E. (2003). Enumeration and characterization of Iron(III)-reducing microbial communities from acidic subsurface sediments contaminated with uranium(VI). *Appl. Environ. Microbiol.* 69, 7467–7479. doi:10.1128/AEM.69.12.7467-7479.2003.

Petzsch, P., Johnson, D. B., Daniel, R., and Schlömann, M. (2015). Genome sequence of the moderately acidophilic sulfate-reducing firmicute *Desulfosporosinus acididurans* (Strain M1T). *Genome Announc.* 3, 5–6. doi:10.1128/genomeA.00881-15.Copyright.

Pinedo Vara, I. (1963). *Piritas De Huelva: Su Historia, Minería Y Aprovechamiento*. Madrid: Editorial Summa.

Pires, R. H., Venceslau, S. S., Morais, F., Teixeira, M., Xavier, A. V., and Pereira, I. A. C. (2006). Characterization of the *Desulfovibrio desulfuricans* ATCC 27774 DsrMKJOP complex - A membrane-bound redox complex involved in the sulfate respiratory pathway. *Biochemistry* 45, 249–262. doi:10.1021/bi0515265.

Plumb, J. J., Haddad, C. M., Gibson, J. A. E., and Franzmann, P. D. (2007). *Acidianus sulfidivorans* sp. nov., an extremely acidophilic, thermophilic archaeon isolated from a solfatara on Lihir Island, Papua New Guinea, and emendation of the genus description. *Int. J. Syst. Evol. Microbiol.* 57, 1418–1423. doi:10.1099/ijs.0.64846-0.

Poncheewin, W., Hermes, G. D. A., van Dam, J. C. J., Koehorst, J. J., Smidt, H., and Schaap, P. J. (2020). NG-Tax 2.0: A semantic framework for high-throughput amplicon analysis. *Front. Genet.* 10, 1–12. doi:10.3389/fgene.2019.01366.

Pruesse, E., Peplies, J., and Glöckner, F. O. (2012). SINA: Accurate high-throughput multiple sequence alignment of ribosomal RNA genes. *Bioinformatics* 28, 1823–1829. doi:10.1093/bioinformatics/bts252.

Qiu, Y. Y., Guo, J. H., Zhang, L., Chen, G. H., and Jiang, F. (2017). A high-rate sulfidogenic process based on elemental sulfur reduction: Cost-effectiveness evaluation and microbial community analysis. *Biochem. Eng. J.* 128, 26–32. doi:10.1016/j.bej.2017.09.001.

Quast, C., Klindworth, A., Pruesse, E., Schweer, T., Horn, M., and Glo, F. O. (2013a). Evaluation of general 16S ribosomal RNA gene PCR primers for classical and next-generation sequencing-based diversity studies. *Nucleic Acids Reseach* 41, 1–11. doi:10.1093/nar/gks808.

Quast, C., Pruesse, E., Yilmaz, P., Gerken, J., Schweer, T., Yarza, P., et al. (2013b). The SILVA ribosomal RNA gene database project: Improved data processing and web-based tools. *Nucleic Acids Res.* 41, 590–596. doi:10.1093/nar/gks1219.

Rabus, R., Hansen, T. A., and Widdel, F. (2006a). Dissimilatory sulfate- and sulfur-reducing prokaryotes. *The prokaryotes* 2, 659–768.

Rabus, R., Hansen, T. A., and Widdel, F. (2006b). "Dissimilatory Sulfate- and Sulfur-Reducing Prokaryotes," in *The Prokaryotes* (New York, NY: Springer New York), 659–768. doi:10.1007/978-3-642-30141-4_70.

Rabus, R., Venceslau, S. S., Wöhlbrand, L., Voordouw, G., Wall, J. D., and Pereira, I. A. C. (2015). A post-genomic view of the ecophysiology, catabolism and biotechnological relevance of sulphate-reducing prokaryotes. *Adv. Microb. Physiol.* 66, 55–321. doi:10.1016/bs.ampbs.2015.05.002.

Ragsdale, S. W., and Pierce, E. (2008). Acetogenesis and the Wood-Ljungdahl pathway of CO_2 fixation. *Biochim. Biophys. Acta - Proteins Proteomics* 1784, 1873–1898. doi:10.1016/j.bbapap.2008.08.012.

Ramamoorthy, S., Sass, H., Langner, H., Schumann, P., Kroppenstedt, R. M., Spring, S., et al. (2006). *Desulfosporosinus lacus* sp. nov., a sulfate-reducing bacterium isolated from pristine freshwater lake sediments. *Int. J. Syst. Evol. Microbiol.* 56, 2729–2736. doi:10.1099/ijs.0.63610-0.

Ramos, A. R., Keller, K. L., Wall, J. D., and Pereira, I. A. (2012). The membrane QmoABC complex interacts directly with the dissimilatory adenosine 5'-phosphosulfate reductase in sulfate reducing bacteria. *Front. Microbiol.* 3, 137. doi:10.3389/fmicb.2012.00137 [doi].

Rickard, D. (1997). Kinetics of pyrite formation by the H_2S oxidation of iron (II) monosulfide in aqueous solutions between 25 and 125°C: The rate equation. *Geochim. Cosmochim. Acta* 61, 115–134. doi:10.1016/s0016-7037(96)00321-3.

Rickard, D., and Luther, G. W. (1997). Kinetics of pyrite formation by the H_2S oxidation of iron (II) monosulfide in aqueous solutions between 25 and 125°C: The mechanism. *Geochim. Cosmochim. Acta* 61, 135–147. doi:10.1016/S0016-7037(96)00322-5.

Rickard, D., and Luther, G. W. (2007). Chemistry of Iron Sulfides. *Chem. Rev.* 107, 514–562. doi:10.1021/cr0503658.

Rickard, D., and Morse, J. W. (2005). Acid volatile sulfide (AVS). *Mar. Chem.* 97, 141–197. doi:10.1016/j.marchem.2005.08.004.

Rickard, D. T. (1975). Kinetics and Mechanism of Pyrite Formation At Low Temperatures. *Am J Sci* 275, 636–652. doi:10.2475/ajs.275.6.636.

Robert T Downs, and Hall-Wallace, M. (2003). The American Mineralogist crystal structure database. *Am. Mineral.* 88, 247–250. doi:0003-004X/03/0001–247$05.00.

Roberts, W. M. B., Walker, A. L., and Buchanan, A. S. (1969). The chemistry of pyrite formation in aqueous solution and its relation to the depositional environment. *Miner. Depos.* 4, 18–29. doi:10.1007/BF00206645.

Robertson, W. J., Bowman, J. P., Franzmann, P. D., and Mee, B. J. (2001). *Desulfosporosinus meridiei* sp. nov., a spore-forming sulfate-reducing bacterium isolated from gasolene-contaminated groundwater. *Int. J. Syst. Evol. Microbiol.* 51, 133–140. doi:10.1099/00207713-51-1-133.

Rohwerder, T., and Sand, W. (2003). The sulfane sulfur of persulfides is the actual substrate of the sulfur-oxidizing enzymes from *Acidithiobacillus* and *Acidiphilium* spp. *Microbiology* 149, 1699–1709. doi:10.1099/mic.0.26212-0.

Ross, D. E., Marshall, C. W., May, H. D., and Norman, R. S. (2016). Comparative genomic analysis of *Sulfurospirillum cavolei* MES reconstructed from the metagenome of an electrosynthetic microbiome. *PLoS One* 11, e0151214. doi:10.1371/journal.pone.0151214.

Rowe, O. F., Sánchez-España, J., Hallberg, K. B., and Johnson, D. B. (2007). Microbial communities and geochemical dynamics in an extremely acidic, metal-rich stream at an abandoned sulfide mine (Huelva, Spain) underpinned by two functional primary production systems. *Environ. Microbiol.* 9, 1761–1771. doi:10.1111/j.1462-2920.2007.01294.x.

Rütters, H., Sass, H., Cypionka, H., and Rullkötter, J. (2001). Monoalkylether phospholipids in the sulfate-reducing bacteria *Desulfosarcina variabilis* and *Desulforhabdus amnigenus*. *Arch. Microbiol.* 176, 435–442. doi:10.1007/s002030100343.

Sánchez-Andrea, I., Florentino, A. P., Semerel, J., Strepis, N., Sousa, D. Z., and Stams, A. J. M. (2018). Co-culture of a novel fermentative bacterium, *Lucifera butyrica* gen. nov. sp. nov., with the sulfur reducer *Desulfurella amilsii* for enhanced sulfidogenesis. *Front. Microbiol.* 9, 1–13. doi:10.3389/fmicb.2018.03108.

Sánchez-Andrea, I., Guedes, I. A., Hornung, B., Boeren, S., Lawson, C. E., Sousa, D. Z., et al. (2020). The reductive glycine pathway allows autotrophic growth of *Desulfovibrio desulfuricans*. *Nat. Commun.* 11, 1–12. doi:10.1038/s41467-020-18906-7.

Sánchez-Andrea, I., Knittel, K., Amann, R., Amils, R., and Sanz, J. L. (2012a). Quantification of Tinto River sediment microbial communities: importance of sulfate-reducing bacteria and their role in attenuating acid mine drainage. *Appl. Environ. Microbiol.* 78, 4638–4645. doi:10.1128/AEM.00848-12.

Sánchez-Andrea, I., Rodriguez, N., Amils, R., and Sanz, J. L. (2011). Microbial diversity in anaerobic sediments at Rio Tinto, a naturally acidic environment with a high heavy metal content. *Appl. Environ. Microbiol.* 77, 6085–6093. doi:10.1128/AEM.00654-11.

Sánchez-Andrea, I., Rojas-Ojeda, P., Amils, R., and Sanz, J. L. (2012b). Screening of anaerobic activities in sediments of an acidic environment: Tinto River. *Extremophiles* 16, 829–839. doi:10.1007/s00792-012-0478-4.

Sánchez-Andrea, I., Sanz, J. L. L., Bijmans, M. F. M., and Stams, A. J. M. (2014a). Sulfate reduction at low pH to remediate acid mine drainage. *J. Hazard. Mater.* 269, 98–109. doi:10.1016/j.jhazmat.2013.12.032.

Sánchez-Andrea, I., Sanz, J. L., and Stams, A. J. M. (2014b). *Microbacter margulisiae* gen. nov., sp. nov., a novel propionigenic bacterium isolated from sediments of an acid rock drainage pond. *Int. J. Syst. Evol. Microbiol.*, ijs.0.066241-0-. doi:10.1099/ijs.0.066241-0.

Sánchez-Andrea, I., Stams, A. J. M., Amils, R., and Sanz, J. L. (2013). Enrichment and isolation of acidophilic sulfate-reducing bacteria from Tinto River sediments. *Environ. Microbiol. Rep.* 5, 672–678. doi:10.1111/1758-2229.12066.

Sánchez-Andrea, I., Stams, A. J. M., Hedrich, S., Ňancucheo, I., and Johnson, D. B. (2015). *Desulfosporosinus acididurans* sp. nov.: an acidophilic sulfate-reducing bacterium isolated from acidic sediments. *Extremophiles* 19, 39–47. doi:10.1007/s00792-014-0701-6.

Sánchez-Andrea, I., Stams, A. J. M., Weijma, J., Contreras, P. G., Dijkman, H., Rozendal, R. A., et al. (2016). A case in support of implementing innovative bio-processes in the metal mining industry. *FEMS Microbiol. Lett.* doi:10.1093/femsle/fnw106.

Sánchez-Andrea, I., Triana, D., and Sanz, J. L. (2012c). Bioremediation of acid mine drainage coupled with domestic wastewater treatment. *Water Sci. Technol.* 66, 2425–2431. doi:10.2166/wst.2012.477.

Sánchez-Andrea, I., van der Graaf, C. M., Hornung, B., Bale, N. J., Jarzembowska, M., Sousa, D. Z., et al. (2022). Acetate Degradation at Low pH by the Moderately Acidophilic Sulfate Reducer *Acididesulfobacillus acetoxydans* gen. nov. sp. nov. *Front. Microbiol.* 13. doi:10.3389/fmicb.2022.816605.

Sánchez-España, J. (2017). "Crystallization in acidic media: from nanoparticles to macrocrystals," in *Crystallization under extreme conditions*, eds. A. Jiménez, M. Prieto, and Á. Fernández-González (Madrid: Sociedad Española de Mineralogía), 15–34.

Sánchez-España, J., Diez-Ercilla, M., and Santofimia, E. (2013). "Mine pit lakes of the Iberian Pyrite Belt: some basic limnological, hydrogeochemical and microbiologica considerations," in *Acidic Pit Lakes: The Legacy of Coal and Metal Surface Mines*, eds. W. Geller, M. Schultze, B. Kleinmann, and C. Wolkersdorfer (Berlin: Springer-Verlag), 315–342.

Sánchez-España, J., López Pamo, E., Santofimia Pastor, E., Reyes Andrés, J., and Martín Rubí, J. A. (2006). The impact of acid mine drainage on the water quality of the Odiel river (Huelva, Spain): Evolution of precipitate mineralogy and aqueous geochemistry along the Concepción-Tintillo segment. *Water. Air. Soil Pollut.* 173, 121–149. doi:10.1007/s11270-005-9033-6.

Sánchez-España, J., Yusta, I., and Diez-Ercilla, M. (2011). Schwertmannite and hydrobasaluminite: A re-evaluation of their solubility and control on the iron and aluminium concentration in acidic pit lakes. *Appl. Geochemistry* 26, 1752–1774. doi:10.1016/j.apgeochem.2011.06.020.

Sánchez-España, J., Yusta, I., Gray, J., and Burgos, W. D. (2016). Geochemistry of dissolved aluminum at low pH: Extent and significance of Al–Fe(III) coprecipitation below pH 4.0. *Geochim. Cosmochim. Acta* 175, 128–149. doi:10.1016/j.gca.2015.10.035.

Sánchez-España, J., Yusta, I., Ilin, A., van der Graaf, C. M., and Sánchez-Andrea, I. (2020). Microbial geochemistry of the acidic saline pit lake of Brunita Mine (La Unión, SE Spain). *Mine Water Environ.* 39, 535–555. doi:10.1007/s10230-020-00655-0.

Sánchez-España, J., López-Pamo, E., Diez-Ercilla, M., and Santofimia, E. (2009). Physico-chemical gradients and meromictic stratification in Cueva de la Mora and other acidic pit lakes of the Iberian Pyrite Belt. *Mine Water Environ.* 28, 15–29. doi:10.1007/s10230-008-0059-z.

Sánchez-España, J., López Pamo, E., Santofimia, E., Aduvire, O., Reyes, J., and Barettino, D. (2005). Acid mine drainage in the Iberian Pyrite Belt (Odiel river watershed, Huelva, SW Spain): Geochemistry, mineralogy and environmental implications. *Appl. Geochemistry* 20, 1320–1356. doi:10.1016/j.apgeochem.2005.01.011.

Sánchez-España, J., Pamo, E. L., Pastor, E. S., and Ercilla, M. D. (2008). The acidic mine pit lakes of the Iberian Pyrite Belt: an approach to their physical limnology and hydrogeochemistry. *Appl. Geochemistry* 23, 1260–1287. doi:10.1016/j.apgeochem.2007.12.036.

Sand, W., Gehrke, T., Jozsa, P.-G., and Schippers, A. (2001). (Bio)chemistry of bacterial leaching—direct vs. indirect bioleaching. *Hydrometallurgy* 59, 159–175. doi:10.1016/S0304-386X(00)00180-8.

Sand, W., Gerke, T., Hallmann, R., and Schippers, A. (1995). Sulfur chemistry, biofilm, and the (in)direct attack mechanism — a critical evaluation of bacterial leaching. *Appl. Microbiol. Biotechnol.* 43, 961–966. doi:10.1007/BF00166909.

Sander, R. (2021). "NIST Chemistry WebBook, NIST Standard Reference Database Number 69," in, ed. P.J. Linstrom and W.G. Mallard (Gaithersburg MD, 20899: National Institute of Standards and Technology). doi:https://doi.org/10.18434/T4D303.

Santofimia, E., González-Toril, E., López-Pamo, E., Gomariz, M., Amils, R., and Aguilera, Á. (2013). Microbial diversity and Its relationship to physicochemical characteristics of the water in two extreme acidic pit lakes from the Iberian Pyrite Belt (SW Spain). *PLoS One* 8, 1–12. doi:10.1371/journal.pone.0066746.

Santos, A. A., Venceslau, S. S., Grein, F., Leavitt, W. D., Dahl, C., Johnston, D. T., et al. (2015). A protein trisulfide couples dissimilatory sulfate reduction to energy conservation. *Science (80-.).* 350, 1541–1545. doi:10.1126/science.aad3558.

Santos, A. L., and Johnson, D. B. (2018). Design and application of a low pH upflow biofilm sulfidogenic bioreactor for recovering transition metals from synthetic waste water at a Brazilian copper mine. *Front. Microbiol.* 9, 1–11. doi:10.3389/fmicb.2018.02051.

Sanz, J. L., Rodríguez, N., Díaz, E. E., and Amils, R. (2011). Methanogenesis in the sediments of Rio Tinto, an extreme acidic river. *Environ. Microbiol.* 13, 2336–2341. doi:10.1111/j.1462-2920.2011.02504.x.

Savant, D. V, Shouche, Y. S., Prakash, S., and Ranade, D. R. (2002). *Methanobrevibacter acididurans* sp. nov., a novel methanogen from a sour anaerobic digester. *Int. J. Syst. Evol. Microbiol.* 52, 1081–1087. doi:10.1099/00207713-52-4-1081.

Schauder, R., and Müller, E. (1993). Polysulfide as a possible substrate for sulfur-reducing bacteria. *Arch. Microbiol.* 160, 377–382. doi:10.1007/BF00252224.

Schippers, A., and Sand, W. (1999). Bacterial leaching of metal sulfides proceeds by two indirect mechanisms via thiosulfate or via polysulfides and sulfur. *Appl. Environ. Microbiol.* 65, 319–321. doi:10.1128/aem.65.1.319-321.1999.

Schoonen, M. A. A., and Barnes, H. L. (1991). Reactions forming pyrite and marcasite from solution: I. Nucleation of FeS2 below 100°C. *Geochim. Cosmochim. Acta* 55, 1495–1504. doi:10.1016/0016-7037(91)90122-L.

Schultze, M., Boehrer, B., Wendt-Potthoff, K., Sánchez-España, J., and Castendyk, D. (2017). "Meromictic Pit Lakes: Case Studies from Spain, Germany and Canada and General Aspects of Management and Modelling," in *Ecology of Meromictic Lakes*, eds. R. D. Gulati, E. S. Zadereev, and A. G. Degermendzhi (Cham: Springer International Publishing), 235–275. doi:10.1007/978-3-319-49143-1_9.

Schumacher, W., Kroneck, P. M. H., and Pfennig, N. (1992). Comparative systematic study on "Spirillum" 5175, Campylobacter and *Wolinella* species. *Arch. Microbiol.* 158, 287–293. doi:10.1007/bf00245247.

Sebban, C., Blanchard, L., Bruschi, M., and Guerlesquin, F. (1995). Purification and characterization of the formate dehydrogenase from *Desulfovibrio vulgaris* Hildenborough. *FEMS Microbiol. Lett.* 133, 143–149. doi:10.1016/0378-1097(95)00339-7.

Segerer, A. H., Trincone, A., Gahrtz, M., and Stetter, K. O. (1991). *Stygiolobus azoricus* gen. nov., sp. nov. Represents a Novel Genus of Anaerobic, Extremely Thermoacidophilic Archaebacteria of the Order *Sulfolobales*. *Int. J. Syst. Bacteriol.* 41, 495–501. doi:10.1099/00207713-41-4-495.

Segerer, A., Langworthy, T. A., and Stetter, K. O. (1988). *Thermoplasma acidophilum* and *Thermoplasma volcanium* sp. nov. from Solfatara Fields. *Syst. Appl. Microbiol.* 10, 161–171. doi:10.1016/S0723-2020(88)80031-6.

Segerer, A., Neuner, A., Kristjansson, J. K., and Stetter, K. O. (1986). *Acidianus infernus* gen. nov., sp. nov., and *Acidianus brierleyi* Comb. nov.: Facultatively Aerobic, Extremely Acidophilic Thermophilic Sulfur-Metabolizing *Archaebacteria*. *Int. J. Syst. Bacteriol.* 36, 559–564. doi:10.1099/00207713-36-4-559.

Senko, J. M., Zhang, G., McDonough, J. T., Bruns, M. A., and Burgos, W. D. (2009). Metal Reduction at Low pH by a *Desulfosporosinus* species: Implications for the Biological Treatment of Acidic Mine Drainage. *Geomicrobiol. J.* 26, 71–82. doi:10.1080/01490450802660193.

Seshadri, R., Leahy, S. C., Attwood, G. T., Teh, K. H., Lambie, S. C., Cookson, A. L., et al. (2018). Cultivation and sequencing of rumen microbiome members from the Hungate1000 Collection. *Nat. Biotechnol.* 36, 359–367. doi:10.1038/nbt.4110.

Siliakus, M. F., van der Oost, J., and Kengen, S. W. M. (2017). Adaptations of archaeal and bacterial membranes to variations in temperature, pH and pressure. *Extremophiles* 21, 651–670. doi:10.1007/s00792-017-0939-x.

Sinninghe Damsté, J., Rijpstra, W. I., Hopmans, E. C., Weijers, J. W., Foesel, B. U., Overmann, J., et al. (2011). 13,16-Dimethyl octacosanedioic acid (iso-diabolic acid), a common membrane-spanning lipid of Acidobacteria subdivisions 1 and 3. *Appl. Environ. Microbiol.* 77, 4147–4154. doi:10.1128/AEM.00466-11; 10.1128/AEM.00466-11.

Slonczewski, J. L., Fujisawa, M., Dopson, M., and Krulwich, T. A. (2009). "Cytoplasmic pH Measurement and Homeostasis in Bacteria and Archaea," in *Advances in Microbial Physiology* (Elsevier), 1–317. doi:10.1016/S0065-2911(09)05501-5.

Spiteri, C., Cappellen, P. Van, and Regnier, P. (2008). Surface complexation effects on phosphate adsorption to ferric iron oxyhydroxides along pH and salinity gradients in estuaries and coastal aquifers. *Geochim. Cosmochim. Acta* 72, 3431–3445. doi:10.1016/j.gca.2008.05.003.

Spring, S., and Rosenzweig, F. (2006). "The Genera *Desulfitobacterium* and *Desulfosporosinus*: Taxonomy," in *The Prokaryotes* doi:10.1007/0-387-30744-3_24.

Spurr, A. R. (1969). A low-viscosity epoxy resin embedding medium for electron microscopy. *J. Ultrastruct. Res.* 26, 31–43. doi:10.1016/S0022-5320(69)90033-1.

Stackebrandt, E., Sproer, C., Rainey, F. A., Burghardt, J., Pauker, O., and Hippe, H. (1997). Phylogenetic analysis of the genus *Desulfotomaculum*: evidence for the misclassification of *Desulfotomaculum guttoideum* and description of *Desulfotomaculum orientis* as *Desulfosporosinus orientis* gen. nov., comb. nov. *Int. J. Syst. Evol. Microbiol.* 47, 1134–1139. doi:10.1099/00207713-47-4-1134.

Stams, A. J. M., Van Dijk, J. B., Dijkema, C., and Plugge, C. M. (1993). Growth of syntrophic propionate-oxidizing bacteria with fumarate in the absence of methanogenic bacteria. *Appl. Environ. Microbiol.* 59, 1114–1119.

Stetter, K. O., and Gaag, G. (1983). Reduction of molecular sulphur by methanogenic bacteria. *Nature* 305, 309–311. doi:10.1038/305309a0.

Steudel, R. (2020a). "Sulfur, Selenium and Tellurium," in *Chemistry of the Non-Metals*, eds. R. Steudel and D. Scheschkewitz (Berlin/Munich/Boston: De Gruyter), 521–598. doi:10.1515/9783110578065-013.

Steudel, R. (2020b). "The chemical sulfur cycle," in *Environmental Technologies to Treat Sulphur Pollution: Principles and Engineering* (IWA Publishing), 11–53. doi:10.2166/9781789060966_0011.

Steudel, R., and Eckert, B. (2003). Solid Sulfur Allotropes Sulfur Allotropes. *Elem. Sulfur Sulfur-Rich Compd. I*, 1–80. doi:10.1007/b12110.

Stolz, J. F., Ellis, D. J., Blum, J. S., Ahmann, D., Lovley, D. R., and Oremland, R. S. (1999). *Sulfurospirillum barnesii* sp. nov. and *Sulfurospirillum arsenophilum* sp. nov., new members of the *Sulfurospirillum* clade of the ε-*Proteobacteria*. *Int. J. Syst. Evol. Microbiol.* 49, 1177–1180. doi:10.1099/00207713-49-3-1177.

Stookey, L. L. (1970). Ferrozine-A New Spectrophotometric Reagent for Iron. *Anal. Chem.* 42, 779–781. doi:10.1021/ac60289a016.

Sturt, H. F., Summons, R. E., Smith, K., Elvert, M., and Hinrichs, K. U. (2004). Intact polar membrane lipids in prokaryotes and sediments deciphered by high-performance liquid chromatography/electrospray ionization multistage mass spectrometry - New biomarkers for biogeochemistry and microbial ecology. *Rapid Commun. Mass Spectrom.* 18, 617–628. doi:10.1002/rcm.1378.

Sun, J., Hong, Y., Guo, J., Yang, J., Huang, D., Lin, Z., et al. (2019). Arsenite removal without thioarsenite formation in a sulfidogenic system driven by sulfur reducing bacteria under acidic conditions. *Water Res.* 151, 362–370. doi:10.1016/j.watres.2018.12.027.

Sun, R., Li, Y., Lin, N., Ou, C., Wang, X., Zhang, L., et al. (2020a). Removal of heavy metals using a novel sulfidogenic AMD treatment system with sulfur reduction: Configuration, performance, critical parameters and economic analysis. *Environ. Int.* 136. doi:10.1016/j.envint.2019.105457.

Sun, R., Zhang, L., Wang, X., Ou, C., Lin, N., Xu, S., et al. (2020b). Elemental sulfur-driven sulfidogenic process under highly acidic conditions for sulfate-rich acid mine drainage treatment: Performance and microbial community analysis. *Water Res.* 185, 116230. doi:10.1016/j.watres.2020.116230.

Sun, R., Zhang, L., Zhang, Z., Chen, G.-H., and Jiang, F. (2018). Realizing high-rate sulfur reduction under sulfate-rich conditions in a biological sulfide production system to treat metal-laden wastewater deficient in organic matter. *Water Res.* 131, 239–245. doi:10.1016/j.watres.2017.12.039.

Suzuki, Y., Kelly, S. D., Kemner, K. M., and Banfield, J. F. (2004). Enzymatic U(VI) reduction by Desulfosporosinus species. *Radiochim. Acta* 92, 11–16. doi:10.1524/ract.92.1.11.25404.

Tabatabaei, M., Rahim, R. A., Abdullah, N., Wright, A. D. G., Shirai, Y., Sakai, K., et al. (2010). Importance of the methanogenic archaea populations in anaerobic wastewater treatments. *Process Biochem.* 45, 1214–1225. doi:10.1016/j.procbio.2010.05.017.

Tahon, G., Geesink, P., and Ettema, T. J. G. (2021). Expanding Archaeal Diversity and Phylogeny: Past, Present, and Future. *Annu. Rev. Microbiol.* 75, 359–381. doi:10.1146/annurev-micro-040921-050212.

Thabet, O. B. D., Wafa, T., Eltaief, K., Cayol, J. L., Hamdi, M., Fauque, G., et al. (2011). *Desulfovibrio legallis* sp. nov.: A moderately halophilic, sulfate-reducing bacterium isolated from a wastewater digestor in Tunisia. *Curr. Microbiol.* 62, 486–491. doi:10.1007/s00284-010-9733-z.

The World Bank Group (2020). Minerals for Climate Action: The Mineral Intensity of the Clean Energy Transition. Available at: http://pubdocs.worldbank.org/en/961711588875536384/Minerals-for-Climate-Action-The-Mineral-Intensity-of-the-Clean-Energy-Transition.pdf.

Thiel, J., Byrne, J. M., Kappler, A., Schink, B., and Pester, M. (2019). Pyrite formation from FeS and H_2S is mediated through microbial redox activity. *Proc. Natl. Acad. Sci. U. S. A.* 116, 6897–6902. doi:10.1073/pnas.1814412116.

Thiel, J., Spring, S., Tindall, B. J., Spröer, C., Bunk, B., Koeksoy, E., et al. (2020). *Desulfolutivibrio sulfoxidireducens* gen. nov., sp. nov., isolated from a pyrite-forming enrichment culture and reclassification of *Desulfovibrio sulfodismutans* as *Desulfolutivibrio sulfodismutans* comb. nov. *Syst. Appl. Microbiol.* 43, 126105. doi:10.1016/j.syapm.2020.126105.

Thompson, L. R., Sanders, J. G., McDonald, D., Amir, A., Ladau, J., Locey, K. J., et al. (2017). A communal catalogue reveals Earth's multiscale microbial diversity. *Nature* 551, 457–463. doi:10.1038/nature24621.

Tiedje, J. M., Cole, J. R., and Sun, B. (2015). *Desulfomonile limimaris* sp. nov., an anaerobic dehalogenating bacterium from marine sediments. *Int. J. Syst. Evol. Microbiol.* 51, 365–371. doi:10.1099/00207713-51-2-365.

Tindall, B. J. (1990a). A Comparative Study of the Lipid Composition of *Halobacterium saccharovorum* from Various Sources. *Syst. Appl. Microbiol.* 13, 128–130. doi:10.1016/S0723-2020(11)80158-X.

Tindall, B. J. (1990b). Lipid composition of *Halobacterium lacusprofundi*. *FEMS Microbiol. Lett.* 66, 199–202.

Tornos, F. (2008). La Geología y Metalogenia de la Faja Pirítica Ibérica. *Macla* 23, 10–13.

Tornos, F., González Clavijo, E., and Spiro, B. (1997). The Filon Norte orebody (Tharsis, Iberian Pyrite Belt): A proximal low-temperature shale-hosted massive sulphide in a thin-skinned tectonic belt. *Miner. Depos.* 33, 150–169. doi:10.1007/s001260050138.

Truche, L., and Bazarkina, E. F. (2019). Natural hydrogen the fuel of the 21st century. *E3S Web Conf.* 98, 2–6. doi:10.1051/e3sconf/20199803006.

Truche, L., Berger, G., Destrigneville, C., Guillaume, D., and Giffaut, E. (2010). Kinetics of pyrite to pyrrhotite reduction by hydrogen in calcite buffered solutions between 90 and 180°C: Implications for nuclear waste disposal. *Geochim. Cosmochim. Acta* 74, 2894–2914. doi:10.1016/j.gca.2010.02.027.

Truche, L., Jodin-Caumon, M. C., Lerouge, C., Berger, G., Mosser-Ruck, R., Giffaut, E., et al. (2013). Sulphide mineral reactions in clay-rich rock induced by high hydrogen pressure. Application to disturbed or natural settings up to 250°C and 30bar. *Chem. Geol.* 351, 217–228. doi:10.1016/j.chemgeo.2013.05.025.

Tucci, N. J., and Gammons, C. H. (2015). Influence of copper recovery on the water quality of the acidic Berkeley pit lake, Montana, U.S.A. *Environ. Sci. Technol.* 49, 4081–4088. doi:10.1021/es504916n.

Tuttle, J. H., Dugan, P. R., and Randles, C. I. (1969). Microbial sulfate reduction and its potential utility as an acid mine water pollution abatement procedure. *Appl. Microbiol.* 17, 297–302. doi:10.1128/aem.17.2.297-302.1969.

UniProt, C. (2014). Activities at the Universal Protein Resource (UniProt). *Nucleic Acids Res* 42, D191-8. doi:10.1093/nar/gkt1140.

Utkin, I., Woese, C. R., and Wiegel, J. (1994). Isolation and characterization of *Desulfitobacterium dehalogenans* gen. nov., sp. nov., an anaerobic bacterium which reductively dechlorinates chlorophenolic compounds. *Int. J. Syst. Bacteriol.* 44, 612–619. doi:10.1099/00207713-44-4-612.

Valenta, R. K., Kemp, D., Owen, J. R., Corder, G. D., and Lèbre (2019). Re-thinking complex orebodies: Consequences for the future world supply of copper. *J. Clean. Prod.* 220, 816–826. doi:10.1016/j.jclepro.2019.02.146.

Valkanas, M. M., Rosso, T., Packard, J. E., and Trun, N. J. (2021). Limited carbon sources prevent sulfate remediation in circumneutral abandoned mine drainage. *FEMS Microbiol. Ecol.* 97, 1–14. doi:10.1093/femsec/fiaa262.

van der Graaf, C. M., Sánchez-España, J., Yusta, I., Ilin, A., Shetty, S. A., Bale, N. J., et al. (2020). Biosulfidogenesis mediates natural attenuation in acidic mine pit lakes. *Microorganisms* 8, 1–26. doi:10.3390/microorganisms8091275.

Vésteinsdóttir, H., Reynisdóttir, D. B., and Örlygsson, J. (2011). *Thiomonas islandica* sp. nov., a moderately thermophilic, hydrogen- and sulfur-oxidizing betaproteobacterium isolated from a hot spring. *Int. J. Syst. Evol. Microbiol.* 61, 132–137. doi:10.1099/ijs.0.015511-0.

Wächtershäuser, G. (1988). Pyrite Formation, the First Energy Source for Life: a Hypothesis. *Syst. Appl. Microbiol.* 10, 207–210. doi:10.1016/S0723-2020(88)80001-8.

Walker, B. J., Abeel, T., Shea, T., Priest, M., Abouelliel, A., Sakthikumar, S., et al. (2014). Pilon: An Integrated Tool for Comprehensive Microbial Variant Detection and Genome Assembly Improvement. *PLoS One* 9, e112963. doi:10.1371/journal.pone.0112963.

Wang, Q., and Morse, J. W. (1996). Pyrite formation under conditions approximating those in anoxic sediments: I. Pathway and morphology. *Mar. Chem.* 52, 99–121. doi:10.1016/0304-4203(95)00082-8.

Wang, S., Huang, H., Moll, J., and Thauer, R. K. (2010). $NADP^+$ reduction with reduced ferredoxin and $NADP^+$ reduction with NADH are coupled via an electron-bifurcating enzyme complex in *Clostridium kluyveri*. *J. Bacteriol.* 192, 5115–5123. doi:10.1128/JB.00612-10.

Weijma, J., Copini, C. F. M., Buisman, C. J. N., and Schultz, C. E. (2002). "Biological recovery of metals, sulfur and water in the mining and metallurgical industy," in *Water Recycling and Recovery in Industry*, eds. P. N. L. Lens, L. W. H. Pol, P. Wilderer, and T. Asano (London: IWA Publishing), 605–622.

Wendt-Potthoff, K., Koschorreck, M., Diez Ercilla, M., and Sánchez-España, J. (2012). Microbial activity and biogeochemical cycling in a nutrient-rich meromictic acid pit lake. *Limnologica* 42, 175–188. doi:10.1016/j.limno.2011.10.004.

Wetzel, R. G. (2001). *Limnology: Lake and River Ecosystems*. 3rd ed. Elsevier Academic Press.

Wickham, H. (2008). *Elegant Graphics for Data Analysis: ggplot2*.

Wickham, H., Averick, M., Bryan, J., Chang, W., McGowan, L., François, R., et al. (2019). Welcome to the Tidyverse. *J. Open Source Softw.* 4, 1686. doi:10.21105/joss.01686.

Wilkin, R. T., and Barnes, H. L. (1997). Formation processes of framboidal pyrite. *Geochim. Cosmochim. Acta* 61, 323–339. doi:10.1016/S0016-7037(96)00320-1.

Winch, S., Mills, H. J., Kostka, J. E., Fortin, D., and Lean, D. R. S. (2009). Identification of sulfate-reducing bacteria in methylmercury-contaminated mine tailings by analysis of SSU rRNA genes. *FEMS Microbiol. Ecol.* 68, 94–107. doi:10.1111/j.1574-6941.2009.00658.x.

Wolfe, R. S., and Pfennig, N. (1977). Reduction of sulfur by Spirillum 5175 and syntrophism with *Chlorobium*. *Appl. Environ. Microbiol.* 33, 427–433. doi:10.1128/aem.33.2.427-433.1977.

Yamamoto, M., Nakagawa, S., Shimamura, S., Takai, K., and Horikoshi, K. (2010). Molecular characterization of inorganic sulfur-compound metabolism in the deep-sea epsilonproteobacterium *Sulfurovum* sp. NBC37-1. *Environ. Microbiol.* 12, 1144–1153. doi:10.1111/j.1462-2920.2010.02155.x.

Yamamoto, M., Nakamura, R., Kasaya, T., Kumagai, H., Suzuki, K., and Takai, K. (2017). Spontaneous and Widespread Electricity Generation in Natural Deep-Sea Hydrothermal Fields. *Angew. Chemie* 129, 5819–5822. doi:10.1002/ange.201701768.

Yamamoto, M., Nakamura, R., and Takai, K. (2018). Deep-Sea Hydrothermal Fields as Natural Power Plants. *ChemElectroChem* 5, 2162–2166. doi:10.1002/celc.201800394.

Yarza, P., Richter, M., Peplies, J., Euzeby, J., Amann, R., Schleifer, K.-H., et al. (2008). The All-Species Living Tree project: A 16S rRNA-based phylogenetic tree of all sequenced type strains. *Syst. Appl. Microbiol.* 31, 241–250. doi:10.1016/j.syapm.2008.07.001.

Yarza, P., Yilmaz, P., Pruesse, E., Glöckner, F. O., Ludwig, W., Schleifer, K. H., et al. (2014). Uniting the classification of cultured and uncultured bacteria and archaea using 16S rRNA gene sequences. *Nat. Rev. Microbiol.* 12, 635–645. doi:10.1038/nrmicro3330.

Yilmaz, P., Parfrey, L. W., Yarza, P., Gerken, J., Pruesse, E., Quast, C., et al. (2014). The SILVA and "all-species Living Tree Project (LTP)" taxonomic frameworks. *Nucleic Acids Res.* 42, 643–648. doi:10.1093/nar/gkt1209.

Yim, K. J., Song, H. S., Choi, J. S., and Roh, S. W. (2015). Thermoproteus thermophilus sp. nov., a hyperthermophilic crenarchaeon isolated from solfataric soil. *Int. J. Syst. Evol. Microbiol.* 65, 2507–2510. doi:10.1099/ijs.0.000293.

Young, G. M., Amid, D., and Miller, V. L. (1996). A bifunctional urease enhances survival of pathogenic Yersinia enterocolitica and Morganella morganii at low pH. *J. Bacteriol.* 178, 6487–6495. doi:10.1128/jb.178.22.6487-6495.1996.

Yücel, M., Gartman, A., Chan, C. S., and Luther, G. W. (2011). Hydrothermal vents as a kinetically stable source of iron-sulphide-bearing nanoparticles to the ocean. *Nat. Geosci.* 4, 367–371. doi:10.1038/ngeo1148.

Zeikus, J. G., Dawson, M. A., and Thompson, T. E. (1983). Microbial ecology of volcanic sulphidogenesis: Isolation and characterization of Thermodesulfobacterium commune gen. nov. and sp. nov. *J. Gen. Microbiol.* 129, 1159–1169. doi:10.1099/00221287-129-4-1159.

Zellner, G., Stackerbrandt, E., Kneifel, H., Messner, P., Sleytr, U. B., Conway de Macario, E., et al. (1989). Isolation and characterization of a thermophilic, sulfate reducing archaebacterium, Archaeoglobus fulgidus strain Z. *Syst. Appl. Microbiol.* 11, 151–160.

Zgonnik, V. (2020). The occurrence and geoscience of natural hydrogen: A comprehensive review. *Earth-Science Rev.* 203, 103140. doi:10.1016/j.earscirev.2020.103140.

Zhang, L., Qiu, Y. Y., Zhou, Y., Chen, G. H., van Loosdrecht, M. C. M., and Jiang, F. (2021). Elemental sulfur as electron donor and/or acceptor: Mechanisms, applications and perspectives for biological water and wastewater treatment. *Water Res.* 202, 117373. doi:10.1016/j.watres.2021.117373.

Zhang, L., Zhang, Z., Sun, R., Liang, S., Chen, G. H., and Jiang, F. (2018). Self-accelerating sulfur reduction via polysulfide to realize a high-rate sulfidogenic reactor for wastewater treatment. *Water Res.* 130, 161–167. doi:10.1016/j.watres.2017.11.062.

Zhou, X., Liu, L., Chen, C., Ren, N., Wang, A., and Lee, D. J. (2011). Reduction of produced elementary sulfur in denitrifying sulfide removal process. *Appl. Microbiol. Biotechnol.* 90, 1129–1136. doi:10.1007/s00253-011-3087-8.

Ziegler, S., Waidner, B., Itoh, T., Schumann, P., Spring, S., and Gescher, J. (2013). *Metallibacterium scheffleri* gen. nov., sp. nov., an alkalinizing gammaproteobacterium isolated from an acidic biofilm. *Int. J. Syst. Evol. Microbiol.* 63, 1499–1504. doi:10.1099/ijs.0.042986-0.

Zillig, W., Yeats, S., Holz, I., Böck, A., Rettenberger, M., Gropp, F., et al. (1986). *Desulfurolobus ambivalens*, gen. nov., sp. nov., an autotrophic archaebacterium facultatively oxidizing or reducing sulfur. *Syst. Appl. Microbiol.* 8, 197–203. doi:10.1016/S0723-2020(86)80077-7.

Zwietering, M. H., Jongenburger, I., Rombouts, F. M., and van 't Riet, K. (1990). Modeling of the bacterial growth curve. *Appl. Environ. Microbiol.* 56, 1875–1881. doi:10.1128/aem.56.6.1875-1881.1990.

Summary

The microbial sulfur cycle plays an important role in acidic environments such as acid mine drainage (AMD) and acidic volcanic hot pools. The reduction of inorganic sulfur compounds such as sulfate (SO_4^{2-}) and elemental sulfur (S_8^0) results in the production of sulfide (H_2S) (biosulfidogenesis). H_2S reacts with dissolved metals to form metal sulfides, which precipitate out of solution and thereby lower metal concentrations in AMD environments. In addition, at low pH biosulfidogenesis from SO_4^{2-} is proton-consuming, mitigating the acidity. (Bio)sulfidogenesis furthermore is an attractive technology for selective recovery of metals as metal sulfides from mining and metallurgy process waters. In industry this has been applied predominantly with neutrophilic sulfate-reducing bacteria (SRB). Process economics can be improved, however, by using S_8^0 instead of SO_4^{2-} as electron acceptor, as this enables a fourfold decrease in electron donor requirements. The use of S_8^0 could also enable operation at more acidic pH and higher temperatures, as so far no extremely acidophilic (pH_{opt} < 3.0) SRB are known, while multiple (thermo)acidophilic S_8^0-reducing bacteria and archaea have been described. Biosulfidogenesis at (thermo)acidophilic conditions can further reduce process costs by enabling the combination of sulfidogenesis and metal precipitation from AMD or hot acidic metallurgy process waters in one reactor. In this thesis we investigated sulfidogenesis from S_8^0 and SO_4^{2-} at acidic pH and low to high temperature, focusing on laboratory-scale processes for application (**chapter 2** and **3**), and bioremediation of AMD-impacted environments (**chapter 4** and **5)**—acidic mine pit lakes and AMD sediments.

In **chapter 2** we describe a novel abiotic process for sulfidogenesis from S_8^0 and H_2, mediated by catalytic pyrite. The catalytic properties of pyrite likely are related to their size, since both pyrite formed *in situ* from the S_8^0, H_2S and Fe^{2+} present in the medium, and externally sourced, milled pyrite mediated sulfidogenesis from H_2 and S_8^0. The process was investigated in detail at pH 4, 80°C, but also occurred at lower temperatures (40 °C) and higher pH (pH 6). Analysis of the mineral precipitates from the incubations using a combination of mineralogical techniques showed spherical pyrite particles composed of acicular pyrite nanocrystals. The identification of pyrrhotite nanocrystals suggested this was an intermediate in pyrite formation in these incubations. Yeast extract (YE) lengthened the lag phase preceding sulfidogenesis, likely through limiting pyrite formation, and appeared to result in less organized FeS_2 nanocrystals on the surface of the pyrite spheroids. Spherical pyrite particles formed both in the presence and absence of YE, countering the hypothesis that spherical pyrite is a proxy for the presence of organic matter. Based on the absence of H_2 production

during pyrite formation, the presence of excess S_8^0 and geochemical modeling, we propose that pyrite formation in our incubations occurs via the polysulfide pathway, which was unexpected at acidic pH.

In **chapter 3** we investigated S_8^0 reduction at lower temperatures (30°C) at neutral (6.9) and acidic (3.8) pH in a continuous laboratory-scale process, using H_2/CO_2 as electron donor and carbon source, and industrial mesophilic granular sludge as inoculum (Emmtec, The Netherlands). We assessed the effect of pH on VSPR and the microbial community composition. The steady-state VSPR dropped 2.3-fold upon transition to acidic pH, from 1.79 ± 0.18 to 0.71 ± 0.07 g $S^{2-}{\cdot}L^{-1}{\cdot}d^{-1}$. Similar VSPR were obtained in another study using different system configurations, suggesting that VSPR from S_8^0 at acidic pH are limited by S_8^0 bioavailability rather than system limitations. With regards to temperature, VSPR achieved in chapter 3 at acidic pH were higher than those obtained with a similar system configuration at higher temperatures and acidic pH (pH 3.5, 60 °C) (Hidalgo-Ulloa, personal communication), suggesting that the inoculum used in our study is not suitable for high temperature processes. Microbial community analysis of the reactor at neutral and acidic pH via 16S rRNA gene amplicon sequencing showed that at pH 6.9, *Sulfurospirillum, Sulfurovum* and *Desulfurella* were the most abundant S_8^0-reducers, while at pH 3.9, *Desulfurella* dominated the sequenced reads. The detection of acetic acid and the abundance of *Acetobacterium* at pH 6.9 pointed towards acetogenesis, explaining the dominance of the heterotrophic genus *Sulfurospirillum* in this H_2 and CO_2–fed bioreactor.

In **chapter 4** we investigated biosulfidogenesis in the water column of two acidic pit lakes (APL) in the Iberian Pyrite Belt (IPB), Filón Centro (Tharsis) (FC) and La Zarza (LZ). In both APL a natural attenuation of acidity and toxic metal concentrations occurred towards the lake bottom, which was more pronounced in FC. The detection of Cu and Zn sulfides in the monimolimnion of FC indicated the presence of biogenic sulfide. This was supported by the detection of sulfidogenic taxa in the 16S rRNA gene amplicon sequence reads from the monimolimnion of both APL. Metal sulfide precipitation was likely mediated by biosulfidogenesis from S_8^0 reduction and disproportionation in the younger APL (LZ), as indicated by the abundance of S_8^0-reducing *Acidianus* and -disproportionating *Desulfocapsa* in the sequenced reads. In the older APL (FC), SO_4^{2-} reduction became dominant, indicated by the abundance of reads assigned to the putative SRB *Desulfomonile* (58 %). The water columns of these APL provide fewer opportunities for the formation of protective microenvironments than AMD sediments, and the species detected in these APL are therefore likely more resistant to the poly-extreme conditions, making them of great interest for application in bioremediation technologies.

In **chapter 5** we describe a novel species from a novel genus of acidotolerant SRB, *Acididesulfobacillus acetoxydans*, that was previously isolated from AMD sediment. We investigated the dominant acid stress resistance mechanisms enabling this species to grow at low pH. Of great interest was the capacity of this species to completely oxidize organic acids to CO_2. This is uncommon among the moderately acidophilic SRB described so far, and likely provides an important mechanism to cope with acid stress. Comparative proteogenomic and membrane lipid analysis further indicated that the presence of saturated ether-bound lipids in the membrane, and their relative increase at lower pH, could be a protection mechanism against acid stress, while a canonical acid stress resistance mechanisms such as a Donnan potential and increased active charge transport did not appear to be active.

Finally, in **chapter 6**, the results of the chapters were discussed in light of the overarching aim of the thesis, and their potential application for bioremediation and metal recovery.

Samenvatting

De microbiële zwavelcyclus speelt een belangrijke rol in milieus met lage pH (zuur), zoals beschreven in **hoofdstuk 1**. Voorbeelden van zulke omgevingen zijn zuur metaalhoudend afvalwater uit de mijnbouw, ook bekend als '*acid mine drainage*' (AMD), en zure vulkanische heetwaterbronnen. De microbiële reductie van anorganische zwavelverbindingen zoals sulfaat (SO_4^{2-}) en elementair zwavel (S_8^0) leidt tot de vorming van (di)waterstofsulfide (H_2S), ook wel biosulfidogenese genoemd. Biosulfidogenese is interessant voor het behandelen van AMD en afvalstromen uit de metallurgische industrie, omdat het gebruikt kan worden om opgeloste metalen selectief terug te winnen voor hergebruik. In metaalhoudend afvalwater reageert H_2S met opgeloste metalen en vormt het metaalsulfiden, die vervolgens neerslaan en daarmee de metaalconcentraties in het water verlagen. Daarnaast gaat biosulfidogenese uit SO_4^{2-} bij lage pH gepaard met de consumptie van protonen, hetgeen kan bijdragen aan het verminderen van de zuurgraad van het water.

Bij industriële toepassingen van biosulfidogenese worden tot nu toe vooral neutrofiele, SO_4^{2-}-reducerende bacteriën (SRB) gebruikt. Het proces kan echter verbeterd worden door S_8^0 in plaats van SO_4^{2-} te gebruiken, omdat reductie van S_8^0 tot H_2S slechts twee elektronen vereist, vergeleken met acht elektronen voor SO_4^{2-} reductie. Dit vermindert de benodigde hoeveelheid elektrondonor met een factor vier, en daarmee ook de operationele kosten. Biosulfidogenese uit S_8^0 in plaats van SO_4^{2-} kan daarnaast worden toegepast bij hogere temperatuur en lagere pH dan de huidige industriële processen, dit omdat er tot nu toe geen extreem acidofiele ($pH_{opt} < 3.0$) SRB bekend zijn, maar er wel meerdere extreem (thermo)acidofiele S_8^0-reducerende bacteriën en archaea zijn beschreven. Biosulfidogenese uit S_8^0 bij deze extremere condities kan de proceskosten verder verlagen doordat het gecombineerd kan worden met metaalsulfideprecipitatie uit zure (hete) metaalvervuilde afvalstromen in één processtap. In dit proefschrift onderzoeken we (bio)sulfidogenese uit S_8^0 en SO_4^{2-} bij lage pH en lage tot hoge temperatuur. Ons overkoepelende doel is om de condities te verruimen waaronder (bio)sulfidogenese kan worden toegepast in de industrie (**hoofdstuk 2** en **3**), en waaronder het is aangetoond in AMD milieus (**hoofdstuk 4** en **5**).

In **hoofdstuk 2** beschrijven we de ontdekking van een nieuw, abiotisch proces voor sulfidogenese uit S_8^0 en waterstof (H_2), mogelijk gemaakt door de katalytische werking van pyriet. Uit ons onderzoek blijkt dat de katalytische eigenschappen van de pyrietdeeltjes waarschijnlijk gerelateerd zijn aan hun grootte, en niet aan de specifieke condities waaronder de deeltjes vormden. We hebben het proces vooral

bestudeerd bij pH 4 en 80 °C, maar observeerden dat het ook plaatsvond bij lagere temperatuur (40 °C) en hogere pH (pH 6). Analyse van de gevormde deeltjes middels een combinatie van mineralogische technieken liet bolvormige pyrietdeeltjes zien, die waren opgebouwd uit naaldvormige pyriet-nanokristallen. We namen daarnaast pyrrhotiet-nanokristallen waar, wat erop zou kunnen wijzen dat dit mineraal een tussenvorm is bij pyrietvorming. Toevoeging van gistextract (een mix van organische verbindingen) vertraagde het begin van sulfidogenese, waarschijnlijk omdat het de pyrietvorming hinderde. Gistextract leek er verder voor te zorgen dat het oppervlak van de bolvormige pyrietdeeltjes een minder georganiseerde structuur had. Op basis van de afwezigheid van H_2-productie in de experimenten, de aanwezigheid van een overmaat aan S_8^0 en geologische modellen, leidden we af dat pyrietvorming in deze experimenten plaatsvindt via de polysulfide-route, hetgeen onverwacht is door de instabiliteit van polysulfide bij lage pH.

In **hoofdstuk 3** beschrijven we ons onderzoek naar S_8^0 reductie bij lagere temperatuur (30 °C), bij neutrale (6.9) en lage (3.8) pH in een continue reactor op laboratoriumschaal. Hierbij hebben we H_2/CO_2 als elektrondonor en koolstofbron, en industrieel mesofiel granulair slib als entmateriaal (Emmtec, Emmen, Nederland) gebruikt. We hebben onderzocht wat het effect is van de pH op de volumetrische sulfide-productiesnelheid (VSPR) en de samenstelling van de microbiële gemeenschap. Verlaging van de pH van 6.9 naar 3.8 zorgde voor een 2.3-voudige verlaging van de VSPR tijdens stabiele operatie, van 1.79 ± 0.18 naar 0.71 ± 0.07 g $S^{2-}\cdot L^{-1}\cdot d^{-1}$. In een eerdere studie met een andere systeemconfiguratie werd een vergelijkbare VSPR gemeten, wat kan betekenen dat de VSPR uit S_8^0 bij lage pH gelimiteerd worden door de biologische beschikbaarheid van S_8^0 en niet door beperkingen van het reactorsysteem. Verder zagen we dat de VSPR die werd behaald in **hoofdstuk 3** bij lage pH en lage temperatuur (pH 3.8, 30°C) hoger waren dan de VSPR die werd behaald in een andere studie met dezelfde reactoropzet, maar hogere temperatuur (pH 3.5, 60 °C), wat kan betekenen dat het gebruikte entmateriaal niet geschikt is voor processen bij hogere temperatuur. Analyse van de microbiële gemeenschap middels moleculaire technieken (16S rRNA gen amplificatie en *sequencing*) liet zien dat bij pH 6.9 bacteriën van de genera *Sulfurospirillum*, *Sulfurovum*, en *Desulfurella* de meest voorkomende S_8^0-reduceerders waren, terwijl bij pH 3.8 het genus *Desulfurella* dominant was. De aanwezigheid van acetaat en van *Acetobacterium* bij pH 6.9 wijst op acetogenese, wat de dominantie van het heterotrofe geslacht *Sulfurospirillum* in deze H_2/CO_2 gevoede (autotrofe) reactor verklaart.

In **hoofdstuk 4** hebben we biosulfidogenese onderzocht in de waterkolom van twee mijnmeren in de *Iberian Pyrite Belt*, Filón Centro (FC) en La Zarza (LZ). In beide

meren zagen we een natuurlijke vermindering van de zuurgraad en verlaging van metaalconcentraties naarmate we dieper in het meer metingen verrichtten. Dit was het duidelijkst zichtbaar in FC. De detectie van koper- (Cu) en zink (Zn)-sulfide in het diepere anoxische deel van FC wees op biosulfidogenese, wat werd ondersteund door de detectie van sulfidogene taxa in de diepere lagen van beide meren middels 16S rRNA gen amplificatie en *sequencing*. In het meer dat later gevormd is (LZ), werd neerslag van metaalsulfiden naar alle waarschijnlijkheid mogelijk gemaakt door biosulfidogenese uit S_8^0-reductie en S_8^0-dismutatie. Dit leidden we af uit de aanwezigheid van de S_8^0-reducerende *Acidianus* en S_8^0-dismuterende *Desulfocapsa*. In het meer dat al eerder gevormd is (FC) was biosulfidogenese hoogstwaarschijnlijk toe te schrijven aan SO_4^{2-}-reductie, wat we afleidden uit de dominantie van een bacterie uit het SRB genus *Desulfomonile*. Omdat de waterkolom van deze twee meren nauwelijks bescherming biedt aan micro-organismen tegen de extreme condities (lage pH, hoge metaalconcentraties), zoals waarschijnlijk wel het geval is in AMD-vervuild slib, zijn de micro-organismen die in deze meren leven vermoedelijk nóg resistenter tegen deze poly-extreme omstandigheden. Dit maakt ze relevant voor toepassing in biozuiveringstechnologieën.

In **hoofdstuk 5** beschrijven we een nieuwe soort van een nieuw geslacht van zuurtolerante SRB, *Acididesulfobacillus acetoxydans*, die eerder werd geïsoleerd uit AMD-vervuild slib. We onderzochten de belangrijkste resistentiemechanismen die het deze bacteriesoort mogelijk maken te overleven bij lage pH. Deze nieuwe soort was in staat acetaat volledig te oxideren naar CO_2. Dit is niet het geval bij de tot nu toe geïsoleerde zuurtolerante SRB, en is waarschijnlijk een belangrijk resistentiemechanisme tegen zuurstress. Vergelijkende analyse van het proteoom en de celmembraanlipiden bij optimale en lage groei pH toonde aan dat de toegenomen hoeveelheid van bepaalde celmembraanlipiden bij lagere pH een ander belangrijk resistentiemechanisme zou kunnen zijn. Bekende zuurstress-resistentiemechanismen zoals de Donnan-potentiaal en toegenomen actieve export van kationen leken niet belangrijk te zijn.

Tenslotte worden in **hoofdstuk 6** de resultaten van de verschillende hoofdstukken besproken in de context van het overkoepelende doel van dit proef-schrift, en hun potentiële belang voor toepassing in (bio)zuiverings- en metaalterugwinningstechnologieën.

List of Publications

Sánchez-Andrea, I., **van der Graaf, C. M.**, Hornung, B., Bale, N. J., Jarzembowska, M., Sousa, D. Z., et al. (2022). Acetate Degradation at Low pH by the Moderately Acidophilic Sulfate Reducer *Acididesulfobacillus acetoxydans* gen. nov. sp. nov. *Front. Microbiol.* 13. doi:10.3389/fmicb.2022.816605.

Sánchez-España, J., Yusta, I., Ilin, A., **van der Graaf, C. M.**, and Sánchez-Andrea, I. (2020). Microbial geochemistry of the acidic saline pit lake of Brunita Mine (La Unión, SE Spain). *Mine Water Environ.* 39, 535–555. doi:10.1007/s10230-020-00655-0.

van der Graaf, C. M., Sánchez-España, J., Yusta, I., Ilin, A., Shetty, S. A., Bale, N. J., et al. (2020). Biosulfidogenesis mediates natural attenuation in acidic mine pit lakes. *Microorganisms* 8, 1–26. doi:10.3390/microorganisms8091275.

In preparation:

Hidalgo-Ulloa, A., **van der Graaf, C.M.**, Buisman, C.J.N., Sánchez-Andrea, I., Weijma, J. Biological sulfur reduction in a H_2/CO_2-fed bioreactor operated at neutral (pH 6.9) and acidic (pH 3.8) conditions using neutrophilic industrial sludge as inoculum.

Ilin, A., **van der Graaf, C.M.**, Yusta, I., Sorrentino, A., Sánchez-Andrea, I., Sánchez-España. J. Organic carbon amendment enhances biosulfidogenesis in Acid Mine Drainage affected areas: incubation column experiment assessment.

van der Graaf, C. M., Sánchez-España, J., Ilin, A., Yusta, I., Stams, A.J.M., Sánchez-Andrea, I. Pyrite formation at acidothermal conditions and its catalytic role in sulfidogenesis from elemental sulfur and hydrogen.

About the author

Lot was born on February 10, 1989 in The Hague, The Netherlands. She attended the *Erasmiaans Gymnasium* in Rotterdam for her pre-university education, and took a gap year before starting the BSc track in philosophy at the Erasmus University in Rotterdam 2007. After completing the first year, Lot switched to the BSc track Life Science & Technology, taught jointly at Delft University of Technology and Leiden University 2008. During her BSc she paused her studies for one year to join the full-time student board of the StuD student job agency in Delft. Lot completed her BSc in 2013, with a BSc thesis at the Industrial Microbiology group of Jack T. Pronk in Delft, where she focused on the evolutionary engineering of *Saccharomyces cerevisiae* for increased osmotic stress resistance. She continued with the MSc program Life Science & Technology at Delft University of Technology, for which she again did her master thesis research project at the Industrial Microbiology group, this time focusing on the metabolic engineering of nitrogen assimilation in *Saccharomyces cerevisiae* with the CRISPR/Cas9 genome editing tool. Lot then moved to Missoula (Montana, USA) for one year to do an academic research internship at the University of Montana, followed by an industrial internship at the biotechnology company Blue Marble Biomaterials. After completing her MSc program in 2016, Lot started her PhD research project in 2017 at the Microbial Physiology group in the Laboratory of Microbiology at Wageningen University & Research, to follow her interest in microbial diversity and physiology. She carried out her PhD research under supervision of prof. Alfons JM Stams, dr. Irene Sánchez-Andrea, and dr. Javier Sánchez-España, of which the results are presented in this thesis.

Acknowledgements

Doing a PhD at times felt like making an extremely long solo hike in the mountains, where the peaks are reached in the first 1-2.5 years, and the remainder of the time is dedicated to carefully descending, trying to keep your footing while already being tired and mildly injured, your gear is starting to wear out, and the weather is unpredictable. But I was not really alone of course, and I am deeply grateful for the support I received from so many people.

Dear **Irene**, thank you for your faith in me five years ago, when you chose me as your PhD student for this project. I still vividly remember our first meeting, and the warmth and enthusiasm you emanated. What a journey it has been, from excitement to bewilderment back to excitement. I am very grateful for your positive, curious and generous nature, and your constructive, truly scientific attitude. I have learned a lot from you, muchas gracias for your big heart and introducing me to the wondrous world of acid drainage together with Javi.

Dear **Javi**, your geological expertise, your tireless (near immediate, and elaborate) answering of all my questions, and the shared excitement about the experiments have been absolutely invaluable, not least in solving 'the pyrite mystery'. But above all for me, your trust and support, and your motivating words at key moments have been one of the single most important factors helping me reach the finish line. I cannot thank you enough.

Dear **Fons**, thank you for your guidance in the past 4.5 years. I think you really 'see' people, and that you had me figured out quite well. Your clear, no-nonsense feedback and advise on important decisions always helped me feel more grounded and calmer. After a meeting with you I would be back to 'Ah yes, I can do this, step by step'. Thank you, Fons.

Dear **Adrian**, I am very happy we managed to collaborate on part of this challenging project. Our shared first-author paper really felt like teamwork, because we were both committed to helping each other. Your tenacity and grit inspired me, thank you for all your help and support. **Andrey**, you made a big contribution to my thesis. Thank you for your positive mindset, unfailing support and sincere helpfulness. **Iñaki** thank you very much for sharing your electron microscopy expertise, and always patiently answering all my questions. Your contribution has been very important.

Thank you **Jan (Weijma)** and **Henk** for the many update meetings we had, and your insightful questions. Henk, I enjoyed thinking through possible process configurations together, and am grateful for your feedback on part of my discussion. **Jan (Klok)**, thanks for your never-ending enthusiasm and ideas, your input on the complex chemistry of polysulfides, and your motivational words every once in a while. Much appreciated. **Cees**, thank you for your enthusiasm and out-of-the-box thinking. **Annemerel**, nice to have some of the last project meetings with you on board. And of course many thanks for your sulfur-enthusiasm. Thank you also to the other members of the user committee of this TTW project: **Dries**, **Elise** and **Dieuwke. Dieuwke**, I really enjoyed interacting with you, thank you for all your help and support. **Marina**, thank you for the administrative work behind the scenes.

Nicole thank you for contributing your expertise on membrane lipids, to both chapter 4 and 5, and always being so friendly, patient and helpful. **Jaap**, thank you for the collaboration on chapter 5. **Laura**, thank you for sharing your expertise and contributing to chapter 4.

Jack, your guidance and mentorship during my BSc and MSc thesis continues to be an inspiration, and I would not be where I am today without it. Thank you. **Ton**, together with Jack you kindled my fascination for microbial diversity and physiology in your BSc course at TU Delft, thank you very much.

From day one I felt very fortunate to have landed in MicPhys for my PhD. Fons, Diana, Irene, and Caroline, I haven't fully figured out how you managed to create a group with such a good atmosphere, but you did. It could be a coincidence, but rather I think it reflects what you value most as leaders. **Diana**, I am very grateful for your support and positive input. It has been a great learning experience to teach in part of your Microbial Physiology Course, and especially to see how dedicated you are not just to teaching, but to inspiring and motivating students. Your care and focus on our wellbeing during the COVID lockdowns helped all of us cope better as a group. **Caroline**, we had several reflective conversations during my PhD that helped me see things from a different perspective, thank you. You are a teacher and mentor pur sang, a real role model. **Ton**, one of the backbones of MicPhys. I was lucky enough to get a desk next to you (and next to the window, we had the prime location), and pre-COVID we had many early morning conversations about a range of topics: history, travel, clouds, and more personal things. I am glad we had at least a few more of them between the end of the lockdown(s) and the end of my contract. I might not become a weather amateur

like you, but looking at clouds has gotten a new dimension. **Iame**, we started on the TTW project together, and you helped me out in the lab several times when I had overbooked my schedule (or maybe felt overbooked, there is a difference..). You have a way of exuding calm and no-problem-we-will-manage, a lifeline in the lab. Thank you for your friendship and the warm, happy lunches, dinners, and drinks at your place with Fran and Martín.

Dear **Daan**, when I started my PhD you quickly took me under your wing, helping me (attempt to) prepare for my sampling trip and navigate the responsibilities of early PhD life. Over the years you became an allround support and friend, and in the last phase of my PhD our coffee breaks helped me a lot. I still think the two of us were incorrectly labeled hipsters by certain individuals, and I consider this matter not settled. I was honored to be your paranimf, and am honored that you agreed to be mine!

Dear **Reinier**, you are a force of nature. While your stamina and positive attitude are amazing, your baritone voice might be an even bigger asset. Friday afternoons in the lab with you doing karaoke to the crème de la crème of Dutch music were a treat that is not easy to surpass. I highly valued our conversations on a range of topics, and am inspired by your attitude to work and life. I also very much appreciated that you always pretended to be impressed by my new PRs with the barbell. Thank you for everything Reinier, I am honored that you agreed to be my paranimf.

Dear **Sara**, you taught me the art of the stroll, or better, the paseo, and especially during the lockdowns these were social highlights of my week. Your friendship and support made a big difference. I look forward to seeing you in Valladolid, in Cádiz, or somewhere in the middle! **Jarrett**, thanks for your patience, listening ear, and humor.

Dear **Wen**, you weren't in MicPhys, but that's ok, we still hit it off. Thank you for our big friendship, your unwavering support, your enthusiasm and limitless energy, and sharing your driven, focused, curious, dedicated, honest self. We made some great memories, from pancakes to weightlifting contests. I cherish them and look forward to making new ones.

Ivetsita, the lady in control, with a big love for fun, drinks and party. It is always great to sail along on your vibes, very contagious. Thank you for the love, support and friendship these past years. Dear **Martijn**, you have a combination of qualities that make you a natural scientist, mentor and teacher. It has been very uplifting and

inspiring to be around you, and I am happy we got to share an office. Our conversations touched many topics, and I am grateful for your trust in me and your listening ear when I needed one. Dear **Peter**, supplier of books to read and even operas to listen to. Your diverse interests, omnivorous mind, and dedication to contributing to a more just society sets a bright example. Thank you for our conversations, and for being so caring and thoughtful. Dear **Nico**, we started our PhDs at the same time, and I'm glad we connected over the years. Your outspokenness and strong ideas about right and wrong always give food for thought. You have a big and kind heart, thank you for always being ready to help. Dear **James**, thanks for the fun and serious conversations we had, and always being interested in my endeavors. Dear **Anna (F.)**, your thesis was my bright(yellow) shining sulfur example when I started my PhD. I am glad we got to spend time together when you returned as a Postdoc. Thank you for our open and honest conversations and your sincere support. **Anna (D.)**, I remember very well when you left after your first stay with us, and was very happy to see you back. I deeply admire your strength and kindness.

Cristina, thank you for welcoming me into the group so enthusiastically when I started. **Yuan**, you were my first desk neighbor, thank you for all our conversations and the great hot pot. **Nohemi**, I was lucky to be there for two of your longer stays, thank you for your kind heart. And for teaching me the ONLY way to make guacamole. **Bruna**, it was great to spend time with you while you were here. **Eva**, thank you for your help and good advice. **Nam**, thank you for the great Vietnamese lunches, and our fun conversations. **Susakul**, thank you for your friendly presence, and your attempts to teach me to cook Thai dishes. I never managed to match you. Thank you **Cata** for bringing life to the party. **Anastasia**, **Keija**, **Timon**, **Marten**, **Maaike**, **Maryse**, **Lukas**, **Eric**, thank you for all the good times! Thank you **Jingjie**, **Teja**, and **Jurgen** for having me as your thesis supervisor. Your projects were challenging, and I admired your positive attitudes.

MicPhys was part of the big MIB family, of which many people played an important role in my PhD journey. I learned a lot from being part of the Daily Board for 2 years, if only that it takes a lot of management to do science. Thank you, **Wen**, **Gerben**, **Thijs**, **Diana**, **Hauke**, **Serve**, **John**, **Erwin**, **Anja** and **Willem** for the many meetings and the fun we had organizing the strategy days. **Anja**, **Heidi** and **Hannie**, thank you very much for all the hard work you put into making MIB run smoothly. **Anja**, you always had something uplifting to say to me, thank you so much. **Heidi**, it was always fun to see you.

I was happy to be a part of the organizing committee of the 2019 PhD trip, with **Giannis**, **Ivette**, **Ran**, **Caifang**, **Costas**, **Enrique**, **Catarina**, and **Nong**. I learned from our experiences together and I think we can proudly look back on a successful trip. **Giannis**, you were a great team captain, supporting and guiding us, thank you very much! **Patsy**, **Dani**, **Jolanda**, **Felix**, **Burak**, **Guillaume**, **Hans**, **Eva** thanks for the fun you brought to MIB as the new MicEvo group. I enjoyed our lunches, drinks, and the laughs in the lab. **Patsy**, **Guillaume** and **Thijs** thank you for taking the time to help me troubleshoot my experiments. **Sudarshan**, thank you for your guidance and sharing your expertise. I'm glad we got to collaborate. **Bastian**, it was great working with you, thank you! **Prokopis** and **Nancy,** thank you for thinking along with me when I had doubts about my experimental design and data analysis. **Menia**, we shared some of the experiences of the final stage of the PhD in our random encounters on the 5th floor. You are a great person! **Taojun**, we spent many weeks writing our thesis chapters in the same office, thank you for your positive spirit. **Ineke** and **Laura**, thank you for the fun, laughs, and of course your help in the lab. **Laura**, my life was never the same after you introduced me to the multichannel pipettor. **Merlijn**, thank you for always being ready to help. **Steven**, you combine having fun with being professional, a very good combination. Thank you for your help. **Philippe**, thank you for all the efforts you put into making the lab a safe and organized place. **Jannie**, **Carrie**, **Marie-Luise**, **Jeroen**, **Emmy**, **Nico**, **Max**, **Costas**, **Catarina**, **Caifang**, **Ran**, **Chen**, **Giannis**, **Janneke** (thanks for organizing the Veluweloop!), thank you for making MIB a great place to work.

In the Summer of 2019, I was lucky enough to be part of the Microbial Diversity Sumer School in Woods Hole (MA, USA). For 6 weeks we got the rare opportunity to explore and discover the microbial world around us, guided by a team of great teachers and scientists. This was one of the highlights of my PhD, not in the least thanks to the great Pantano Metano team. **Lymarie**, **Natalia**, **Pedro** and **Sheila**, thanks for all the time we spent together, we created a very special bond. Stranger Things will never be the same without you. **Kurt**, your deep passion for teaching and mentoring was very inspiring and has stayed with me to this day.

Many friends and family have patiently supported me over the past 4.5 years. **Eva**, thank you for all our conversations ever since we became friends in Delft. Your thoughtfulness and your support always warm my heart. Hopefully there are more cycling trips in our future. **Hester**, our friendship means a lot to me, going strong since StuD. Our trip to the Alps was a big highlight, and I look forward to many more. Thank you for your warm, generous heart, unceasing interest in my project, and even helping me in my

work planning endeavors. To the boys of StuD13, **Hans**, **Rik** and **Clint**, thank you for being there for me when I needed it, and for your interest and support. **Elise**, thank you for your sense of wonder, and the good times we spent together.

My dear Erasmiani **Fre**, **Juud**, **Juul**, **Em**, **Fen**, **Lot** and **Ca**, we have known each other for more than half our lives. I find that a remarkable thought. Each of us is on our own paths, but we still manage to find one another. I look forward to seeing what the future has in store for all of us.

I was lucky enough to have warm and open-hearted neighbors, where there was always a light on. Dear **Hanneke**, thank you for your loving presence and real support. **Mira**, thank you for sprinkling life, joy and playfulness around while you are on you adventures. **Monique**, thank you for your warm presence. **Stefan**, thank you for sharing some of your birding enthusiasm.

A big factor in keeping me sane and grounded, especially during the COVID lockdowns, were the workouts at CrossFit Ede. Many thanks for your expert coaching, **Rutger**, **Luuk**, **Iris**, **Sven**, **Jip**, and **Jan-Willem**. Above all the Wednesday evening sessions with the Olympic Weightlifting group were a highlight of my week. **Rutger**, thanks for your very down-to-earth, dedicated, focused, and patient coaching. 'Trust and enjoy the process' captures it all. **Nick**, **Davy**, **Robbin**, **Siemen** and **Charlotte** thanks for all the hours we spent together at the barbell. I won't get started on how training for better snatches and clean & jerks changed my approach to life in general, but let's just say it did.

Dear **Jan**, thank you from the bottom of my heart for your wise guidance, for so many years already. Our conversations are an anchor for me.

They say you don't choose your family, but I couldn't have chosen a better one anyway. **Onne** and **Willem**, best brothers in the universe, front row seats in my heart, the guys in my corner. **Willem**, you deeply care for my well-being and happiness and help me see the important things I sometimes lose sight of. **Onne**, you help me gather my thoughts when I am stuck, and give me your honest perspective when I need it. **Marein**, I can't tell you what a gift it is to have you as extended family. Your interest and support, your patience, and your grounding comments are priceless. **Minne**, I am very happy that you are included in the bunch, thanks for your advice, and for listening and reflecting with me. **Pomme**, thank you for your upbeat, down-to-earth presence, it is great having

you with us. **Bub** & **Mint**, your love and open arms have played a very important role in my life, and have shaped me in many ways, big and small. Thank you for everything. **Monique** & **Robert**, thank you for your support and your way of so naturally being there for me. **Miel & Melissa,** thank you for always receiving me with open arms.

Then, my dear **papa** & **mama**, you continue to give me the gift of unconditional love and trust, the biggest gift of all. You believe in me, even when I don't. You are a harbor, a rock, and a pillar of strength. Your arms and hearts are always open. In so many ways I would not be here without you. **Papa**, you help me become my own captain. **Mama**, you help me stop and remember how far I have come. I love you both to the moon and back. A big bear hug.

Netherlands Research School for the
Socio-Economic and Natural Sciences of the Environment

D I P L O M A

for specialised PhD training

The Netherlands research school for the
Socio-Economic and Natural Sciences of the Environment
(SENSE) declares that

Charlotte Monique van der Graaf

born on 10th February 1989 in The Hague, The Netherlands

has successfully fulfilled all requirements of the
educational PhD programme of SENSE.

Wageningen, 5th July 2022

Chair of the SENSE board

Prof. dr. Martin Wassen

The SENSE Director

Prof. Philipp Pattberg

The SENSE Research School has been accredited by the Royal Netherlands Academy of Arts and Sciences (KNAW)

KONINKLIJKE NEDERLANDSE
AKADEMIE VAN WETENSCHAPPEN

The SENSE Research School declares that **Charlotte Monique van der Graaf** has successfully fulfilled all requirements of the educational PhD programme of SENSE with a work load of 47.7 EC, including the following activities:

SENSE PhD Courses

- Environmental research in context (2017)
- Research in context activity: 'Organizational committee PhD study trip' (2019)

Other PhD and Advanced MSc Courses

- Open & Reproducible Microbiome Analysis, VLAG (2018)
- Adobe Illustrator for Scientists, WIMEK (2018)
- Microbial Diversity Summer School, Marine Biology laboratory Woods Hole & University of Chicago (2019)
- Presenting with Impact, Wageningen Graduate Schools (2019)
- Scientific Writing, Wageningen Graduate Schools (2019)
- Advances in (Bio)hydrometallurgy and Application, Federal Institute for Geosciences and Natural Resources (2019)
- Bioinformatics with Linux and Python, WIMEK (2020)
- Tidy Data Transformation & Visualization with R, PE&RC (2021)

Management and Didactic Skills Training

- PhD representative Daily Board, Laboratory of Microbiology (2018-2019)
- Supervision of two MSc students with thesis (2019-2020), a Bachelor student with thesis (2020)
- Teaching in the BSc course 'Microbial Physiology' (2017-2020)

Oral Presentations

- *Geomicrobiological factors influencing metal attenuation in extremely acidic and metal-rich mine pit lakes*. Scientific Spring Meeting KNVM and NVMM, 26-27 March 2019, Arnhem, The Netherlands
- *Biosulfidogenesis in acidic mine pit lakes mediates natural attenuation of extreme conditions*. Scientific Spring Meeting KNVM and NVMM, 30-31 March 2021, The Netherlands (Online)
- *Studying the response of sulfidogenic microorganisms to nutrient availability in acid mine drainage*. Goldschmidt Virtual, 4-9 July 2021 (Online)

SENSE coordinator PhD education

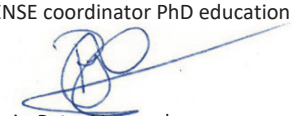

Dr. ir. Peter Vermeulen

The research described in this thesis is part of the project 'Extremophilic Bioreduction of Elemental Sulfur for Recovery of Valuable Metals' (with project number 14979) of the research programme TTW which is (partly) financed by the Dutch Research Council (NWO), and was supported by Paques Global B.V., Fertipaq and Emmtec Services.

Financial support from Wageningen University for printing this thesis is gratefully acknowledged.

Cover design and illustration & layout: Esther Beekman (www.estherontwerpt.nl)
Printed by: Ipskamp printing, Enschede